Terms and Conditions of Use of Digitised Theses from Trinity College Library Dublin

Copyright statement

All material supplied by Trinity College Library is protected by copyright (under the Copyright and Related Rights Act, 2000 as amended) and other relevant Intellectual Property Rights. By accessing and using a Digitised Thesis from Trinity College Library you acknowledge that all Intellectual Property Rights in any Works supplied are the sole and exclusive property of the copyright and/or other IPR holder. Specific copyright holders may not be explicitly identified. Use of materials from other sources within a thesis should not be construed as a claim over them.

A non-exclusive, non-transferable licence is hereby granted to those using or reproducing, in whole or in part, the material for valid purposes, providing the copyright owners are acknowledged using the normal conventions. Where specific permission to use material is required, this is identified and such permission must be sought from the copyright holder or agency cited.

Liability statement

By using a Digitised Thesis, I accept that Trinity College Dublin bears no legal responsibility for the accuracy, legality or comprehensiveness of materials contained within the thesis, and that Trinity College Dublin accepts no liability for indirect, consequential, or incidental, damages or losses arising from use of the thesis for whatever reason. Information located in a thesis may be subject to specific use constraints, details of which may not be explicitly described. It is the responsibility of potential and actual users to be aware of such constraints and to abide by them. By making use of material from a digitised thesis, you accept these copyright and disclaimer provisions. Where it is brought to the attention of Trinity College Library that there may be a breach of copyright or other restraint, it is the policy to withdraw or take down access to a thesis while the issue is being resolved.

Access Agreement

By using a Digitised Thesis from Trinity College Library you are bound by the following Terms & Conditions. Please read them carefully.

I have read and I understand the following statement: All material supplied via a Digitised Thesis from Trinity College Library is protected by copyright and other intellectual property rights, and duplication or sale of all or part of any of a thesis is not permitted, except that material may be duplicated by you for your research use or for educational purposes in electronic or print form providing the copyright owners are acknowledged using the normal conventions. You must obtain permission for any other use. Electronic or print copies may not be offered, whether for sale or otherwise to anyone. This copy has been supplied on the understanding that it is copyright material and that no quotation from the thesis may be published without proper acknowledgement.

Nitrogen isotopes in the palynomorph *Tasmanites,* as an indicator of climate change

Abigail Rooney

A thesis in partial fulfilment of the regulations for the degree of Doctor of Philosophy submitted to the University of Dublin, Trinity College

May **2014**

I declare that this thesis has not been submitted as an exercise for a degree at this or any other university and it is entirely my own work.

I agree to deposit this thesis in the University's open access institutional repository or allow the library to do so on my behalf, subject to Irish Copyright Legislation and Trinity College Library conditions of use and acknowledgement.

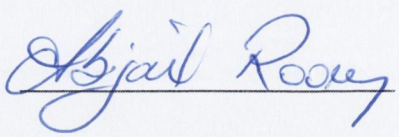

Abigail Rooney

SUMMARY

The stable nitrogen isotope signature ($\delta^{15}N$) of plants and animals preserved in sedimentary rocks retain a record of past oceanic and atmospheric chemical changes. The majority of modern nitrogen isotope studies focus primarily on the interpretation of total nitrogen from bulk sedimentary marine samples. This technique is fraught with uncertainty because bulk samples often contain large quantities of inorganic nitrogen and considerable variation in the organic fraction. Furthermore, diagenesis can have a greater impact on the sinking flux of organic material in different areas of the ocean, leading to additional uncertainty in the data extracted from bulk samples.

As the precision of modern equipment has improved, it has become possible to analyse extracted sedimentary N fractions, reducing some of the inconsistencies associated with analysing bulk samples. This study investigates the $\delta^{15}N$ value of bulk organic residues and the extracted palynomorph, *Tasmanites*, from Kentucky shales, to gain a greater understanding of baseline $\delta^{15}N$ changes within documented Late Devonian – Early Carboniferous glacial / interglacial cycles.

Preliminary chemical and thermal maturation tests were carried out on samples of *Tasmanites* to assess their influence on $\delta^{15}N$ and $\delta^{13}C$ values. These tests found no significant change in $\delta^{15}N$ and $\delta^{13}C$, brought about by experimental laboratory heating up to 170 °C, in order to replicate natural thermal maturation. Treatment with HCl, hot and cold HF and a combination of NaClO, sodium-citrate solution, sodium-bicarbonate solution and sodium-dithionite, led to no discernable change in $\delta^{15}N_{Tas}$ and proved to be the most effective chemical treatment for the removal of unwanted material and the extraction of *Tasmanites*.

Both the post-HF bulk organic residues and the post clay treatment residue were mounted onto glass slides for palynological investigation. These slides assisted in the identification of productive samples, the palynological determination of the age of the sections, and in establishing a new species of miospore (*Retusotriletes loboziakii*), liberated from the *Protosalvinia* thalli.

In order to attain on-scale peaks on a low volume configuration of the Elemental Analyser – Isotope Ratio Mass Spectrometer (EA - IRMS), between 2,500 and 4,000 specimens of *Tasmanites*, extracted from the Kentucky shales, would be required per sample for a single N_2 analysis. To reduce the number of specimens required, a nano-EA, based on Polissar *et al.* (2008), was built and attached to the existing system, leading to a dramatic reduction in sample size, down to approximately 60 – 120 specimens of *Tasmanites* per sample.

The majority of the variation recorded in $\delta^{15}N_{bulk}$ closely mirrors the variation recorded in $\delta^{15}N_{Tas}$, although, occassionally it was observed that the $\delta^{15}N_{bulk}$ and $\delta^{15}N_{Tas}$ trends were opposing. Increases and decreases in the growth of cyanobacteria is suggested to be one of the main factors controlling the observed changes in the $\delta^{15}N_{bulk}$ signal through the succession. Observed differences in $\delta^{15}N_{bulk}$ and $\delta^{15}N_{Tas}$ trends are considered to provide a greater understanding of the dominant processes (N-Fixation, denitrification) taking place within the Appalachian Basin during the time

period studied, and thus, may be used to assess basinal, environmental and climatic conditions at the time of deposition.

$\delta^{15}N_{bulk}$ and $\delta^{15}N_{Tas}$ values remained relatively steady through the depositon of the Huron Member, with slight variation recorded within the Three Lick Bed. Variation in the $\delta^{15}N_{bulk}$ and $\delta^{15}N_{Tas}$ of the Cleveland Member, observed between the two sections studied, led to inconclusive interpretations of this interval. The upper Cleveland Member may correspond to either the Hangenberg Black Shale trangression, or the Hangenberg Shale and Sandstone regression of the Rhenish Massif, which was brought about by documented glacial events. Increased sampling resolution and further palynological interpretation of the Cleveland Member is required to fully interpret this interval. The Bedford Shale was deposited during a known glacial period, and it is therefore suggested that the $\delta^{15}N_{bulk}$ and $\delta^{15}N_{Tas}$ values observed through the Bedford Shale may imply a lower average Late Devonian marine $\delta^{15}NO_3^-$ value (2 – 3.5 ‰) than the modern marine average $\delta^{15}NO_3^-$ (5 – 6 ‰). The slight $\delta^{15}N_{bulk}$ and $\delta^{15}N_{Tas}$ changes within the Bedford Shale may correspond to the C isotope excursion that has been recorded towards the top of the LN Miospore Biozone at other localities, or may be due to the waxing and waning of polar glaciers, as well as alpine glaciers on the adjacent Acadian highlands.

The Sunbury Shale records abrupt and coeval changes in both $\delta^{15}N_{bulk}$ and $\delta^{15}N_{Tas}$, possibly brought about by undocumented glacial events, eustatic sealevel changes within the VI Miospore Biozone, or increased loading during the onset of the fourth tectophase of the Acadian orogen (Ettensohn and Pashin, 1997; Sandberg *et al.*, 1986). If increased loading led to these changes, it may have consequences for future study of nitrogen isotopes, as basinal changes could lead to abrupt variation in sedimentary $\delta^{15}N$ values.

The $\delta^{15}N$ values obtained from *Protosalvinia* samples from the Appalachian, Illinois and Michigan basins within North America, show very little variation between and within basins, suggesting similar nutrient dynamics throughout the region. The *Protosalvinia* thalli recorded lighter $\delta^{15}N$ values than the *Tasmanites*, perhaps due to differences in their location within the euphotic zone. The Brazilian sample of *Protosalvinia* recorded a heavier $\delta^{15}N$ value than those from North America, likely due to decreased N-fixation at higher palaeo-latitudes (Brazil).

Explorative research was also carried out on the trace element ratios of the palynomorph *Tasmanites,* to support the main body of research examining the palaeoenvironmental conditions within the Late Devonian Appalachian Basin. The variation observed is most likely due to a combination of benthic redox conditions and pelagic nutrient conditions, where increases in V/Cr_{Tas}, $V/(V+Ni)_{Tas}$ and V/Mo_{Tas} tentatively indicate increased oxic conditions, and increases in Fe/Ni_{Tas} and Zn/Co_{Tas} possibly indicate increased nutrient conditions. Any conclusions drawn from these ratios require further testing, as this work was purely explorative.

ACKNOWLEDGMENTS

This project was carried out with the financial support of Science Foundation Ireland (Research Frontiers Program Grant GEOF152) and Trinity College Dublin (TCD Studentship).

I would like to extend my sincere thanks to the best project supervisors I could have asked for: Prof. Geoff Clayton and Dr. Robbie Goodhue. Their constant and unwavering support throughout this process has been central to the completion of the project, and to my development as a geologist, and a researcher.

Countless thanks must go to Mr. Francis Hendron, not only for his technical abilities and his guidance through the palynological process, but for his friendship and encouragement throughout the journey.

A huge thanks to Prof. Reed Wicander and Prof. Chris Nicholas, for being so helpful in their comments and revision of this thesis. Their expert input and advice extends beyond this thesis, for which I am very grateful.

To Prof. Balz Kamber, Prof. Dave Chew, Michael Babechuk and Meabh Gallagher, thank you for guiding me through the wonderful world of trace elements, and to Michael for providing me with an endless supply of clean lab water.

Many thanks to Prof. Carlos Rocha, for the generousity of his time and his advice.

To Dr. Mags Duncan, for her astute knowledge of how to navigate the complex network of the Trinity College Dublin Graduate Studies Program, and our coffee room chats.

To all the staff of the Department of Geology, for their continual encouragement and warm hospitality throughout my project.

To Neil Kearney, Noel McGinley and Maura Morgan, thank you for your endless assistance and your constant optimistic encouragement.

To all the postgraduate students of the Department of Geology, thank you so much for your friendship and all the banter, and a special thanks to my office companions, Dr. Alastair Haddow, Allyson Smith and Luca Mancinelli, for always having an open ear and sound advice.

A sincere thanks to Dr. Cortland Eble at the Kentucky Geological Survey, Prof. Thomas Lierman at Eastern Kentucky University, Prof. Charles Mason at Morehead State University, Prof. Frank Ettensohn at the University of Kentucky, and Prof. Jen O'Keefe at Morehead State University for their invaluable help with sample localities, collection and stratigraphy, and their tremendous hospitality during our time in Kentucky.

I must acknowledge and send many thanks to Prof. Kate Freeman at Pennsylvania State University, Dr. Pratigya Polissar at Columbia University, Prof. Christopher Junium at Syracuse University, Mr. Denny Walizer and Mr. Laurence Bird at Pennsylvania State University, for the generosity of their

time and access to their lab, and their hugely significant contribution to the completion of this project.

To Mr. Pete Smith, a sincere thanks for his invaluable technical input and advice while building the nano-EA.

To Derek Armstrong at the Ontario Geological Survey and Prof. Jeff Over at the State University of New York, many thanks for their generosity in locating and shipping North American samples of *Protosalvinia* spp.

To our colleagues in Brazil, José Henrique Goncalves de Melo, Luciane Moutinho and Sara Nascimento, many thanks for their help and kindness in locating and sending Brazilian samples of *Protosalvinia* spp.

A big thanks to Dr. Clive Burnett at the University of Tasmania for supplying samples of the Tasmanite Oil Shale.

Many thanks to Mr.Barry Moran, for very kindly helping to run investigative samples on the Flow Cytometer in TCD.

To the Cushman Foundation, the American Association of Stratigraphic Palynologists, the Irish Geological Association, the TCD Student Travel Grant Program, the John Boldy Bursary and the Dave Johnston Memorial Fund for their financial support towards field trips, conferences and training programs, all of which have contributed towards the completion of this thesis.

I would also like to thank my family and friends, their continuous support helps to make everything in life that much easier.

I must acknowledge my wonderful new daughter, Fern, who was considerate enough to arrive a week after I handed in the initial copy of this thesis, the idea of holding her in my arms on graduation day pulled me through the final few hurdles.

Lastly, I would like to thank my wonderful husband, Owen, for his endless support, encouragement and assistance in every way possible. It is difficult to quantify or measure the enormity of his contribution to the completion of this thesis, but needless to say, he has been instrumental in my own development throughout this project.

TABLE OF CONTENTS

TABLE OF FIGURES

Chapter 1

Introduction

1.1 OVERVIEW

Ocean and atmospheric chemical changes can be recorded in the nitrogen ($\delta^{15}N$) and carbon ($\delta^{13}C$) isotopes preserved in the tissues of plants and animals in sedimentary rocks. These organisms have their own distinctive isotopic signal as a product of their surrounding environment, their trophic level within an ecosystem, and the biochemical pathway used to synthesize nutrients. As conditions and nutrient availability vary over geologic time, organisms record these changes in their stable isotope ratios ($\delta^{15}N$ and $\delta^{13}C$). As nitrogen is typically the limiting factor for growth in natural ecosystems, it can be a reliable indicator of change within a biological system. Bulk samples, containing a mixture of inorganic and organic N, are commonly used in stable isotope studies to infer climate changes. However, due to uncertainties in the composition of the bulk samples, and the inconsistency of diagenetic alteration throughout the ocean, the isolation of specific sedimentary N fractions has become more significant as research on nitrogen isotopes progresses. Because the detection limits of modern equipment has improved in recent years, it has become possible to analyse the modest quantity (often <1% by weight) of nitrogen found within independent organisms, rather than bulk samples. The aim of this research was to investigate climate changes that took place during the Late Devonian, and to explore the value of analysing the stable nitrogen isotope signature of specific palynomorphs, such as *Tasmanites* spp., to further our understanding of such past climate changes. Upper Devonian to Lower Carboniferous shale sequences from Kentucky, USA, were chosen for this study as they were deposited during documented glacial / deglacial cycles, have not undergone extensive thermal maturation and are well exposed. Several considerations following the collection of these shales have also been investigated in detail, as outlined in Chapter 3.

1.2 BACKGROUND

A brief overview of the palaeogeographic setting, palaeoclimate and Late Devonian events are described below. A comprehensive review of Late Devonian – Early Carboniferous geology is beyond the scope of this project, however, the regional geological setting is discussed in more detail in Chapter 2.

1.2.1 Palaeogeography

The Appalachian Basin is thought to represent a retro-arc foreland basin, brought about by lithospheric flexure during the Taconic, Acadian and Alleghenian orogenies (Quinlan and Beaumont, 1984). Sedimentation within the basin began during the mid-Ordovician and continued to the end of the Palaeozoic, corresponding to the loading phases of the respective orogenies. Sedimentation during the Acadian orogeny is thought to have occurred over four foreland basin

tectophase cycles, which migrated southward in time and space due to the dextral accretion of the Carolina and Avalonian terranes along the eastern margin of Euramerica (Ettensohn, 1985, 1994, 1998). The third and fourth tectophase of the Acadian orogeny is thought to be representative of Late Devonian – Early Mississippian deposition within the Appalachian Basin, during which time the Euramerican continent straddled the equator (Figure 1.1).

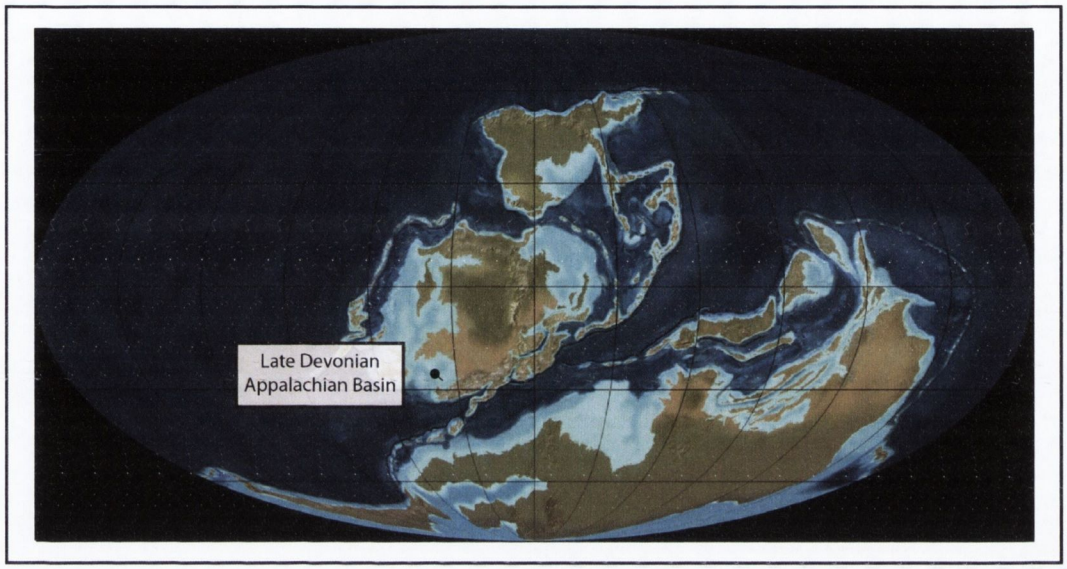

Figure 1.1. Palaeogeography of the Late Devonian, with the Appalachian Basin located approxiamately 25° to 30° S. Modified from Blakey (2011).

The Appalachian Basin is separated from the Illinois and Michigan basins by topographic highs such as the Cincinnati, Findlay and Algonquin arches, located to the west of the basin (Colton, 1970) (Figure 1.2). To the northeast /east, the Appalachian Basin is bordered by the Appalachian Mountains, which formed as a result of the various orogenic events referred to above and its southern boundary is transitional into the Black Warrior Basin (Ettensohn, 2008). Basinal black and grey shales, deposited in the Late Devonian – Early Mississippian age Appalachian Basin, are preserved in the state of Kentucky, USA, which was located approximately 25° to 30° south of the equator in Late Devonian time (Figure 1.1). Samples of these basinal black and grey shales were collected from Kentucky for this project.

1.2.2 Palaeoclimate

Well documented evidence for a Late Devonian / Early Carboniferous global climatic cooling event has been recorded in the form of glacial deposits in South America, North Africa, and more recently, eastern North America (Brezinski *et al.*, 2008; Caputo and Crowell, 1985; Isaacson *et al.*, 2008; Streel *et al.*, 2012; Veevers and Powell, 1987; Wicander *et al.*, 2011).

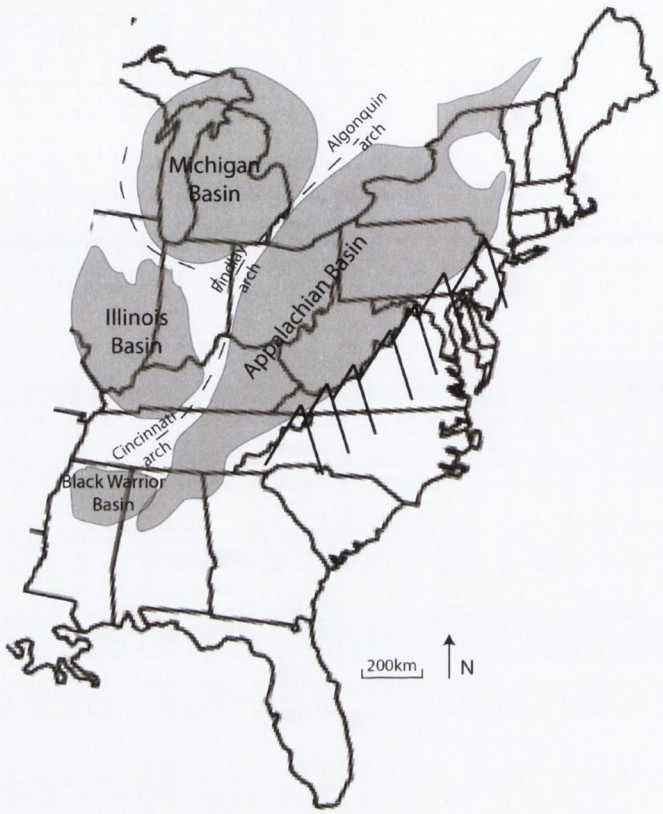

Figure 1.2. Approximate outline of the Appalachian, Michigan, Illinois and Black Warrior sedimentary basins within eastern North America during the Late Devonian. Topographic highs, such as the Algonquin, Cincinnati and Findlay arches, often separated the basins. Acadian orogenic uplift is shown along the eastern margin of North America. Modified from Ettensohn (2008).

The glacial deposits of South America and North Africa were located at relatively high latitudes during the Late Devonian, between 45°and 60°S (Blakey, 2011; Scotese, 2001; Veevers and Powell, 1987), whereas the equivalent glacial deposits found in eastern North America were located between 25°-30°S, within the subtropical trade wind belt (Ettensohn *et al.*, 2009). This climatic episode is considered to have taken place within the Appalachian Basin over one glacial advance and retreat cycle during the latest Famennian LN Miospore Biozone (Brezinski *et al.*, 2010) (Figure 1.3).

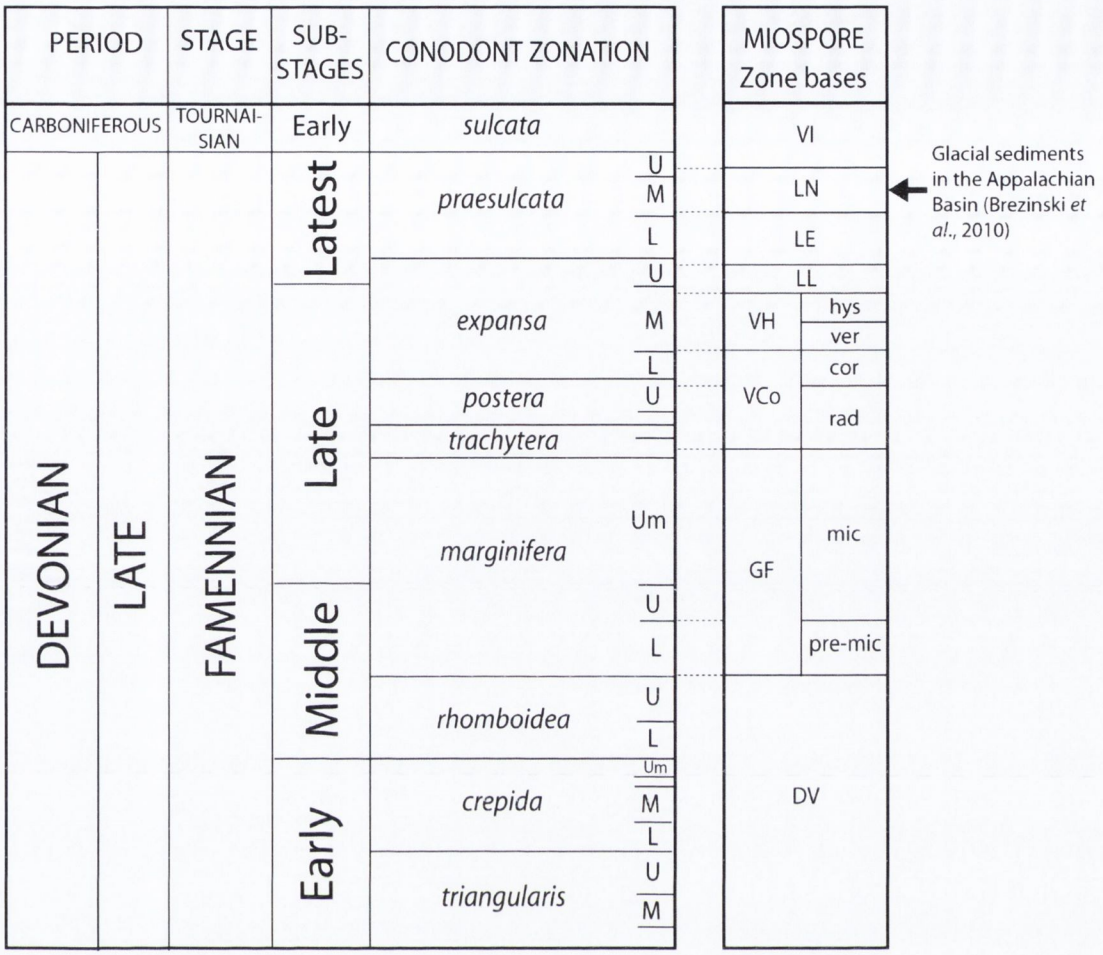

Figure 1.3. Correlation of the conodont and miospore zonations of the Famennian Stage of the Late Devonian, based on Streel (1999), Kaufmann (2006) and Streel (2009), Higgs *et al.* (2013).

Deposits of diamictite accumulated between the Acadian highlands and the shores of the Appalachian Basin (Figure 1.4), and were subsequently overlain by glacio-lacustrine varves containing dropstones (Brezinski *et al.*, 2008). These units are contemporaneous with South American glacial deposits (Isaacson *et al.*, 2008) and equivalent to regressive marine strata within the Appalachian Basin, thought to be related to glacioeustatic events (Streel *et al.*,2000). The explanation for such low latitude glaciation is partly due to Acadian orogenic events taking place on the eastern coast of Euramerica, where increased tectonic loading may have led to the development of high altitude alpine glaciers. However, near-shore glacial deposits and dropstones found in distal marine sediments suggest that glaciers were present at, or at least near, sea level (Brezinski *et al.*, 2009). This low-latitude glaciation is therefore thought to be due to a combination of alpine glaciation brought about by Acadian uplift, global cooling and southern polar glaciation.

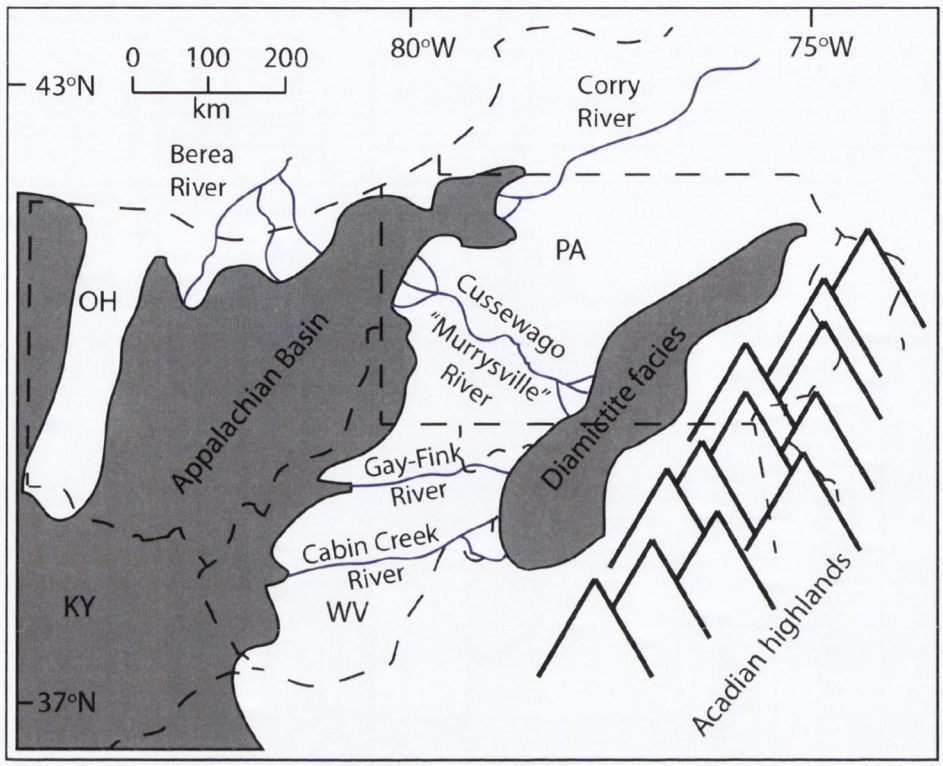

Figure 1.4. The approximate extent of Late Devonian glacial facies, river systems and the Appalachian Basin. Modified from Brezinski *et al.* (2010). Acadian orogenic uplift is depicted to the right, along the eastern margin of North America.

1.2.3 Late Devonian events

This section presents the current understanding of the Late Devonian environment and the changes and events that are thought to have taken place during this time period. As with many geological events, differing opinions and interpretations exist on the timing, causes, extent and severity of the events that took place during the Late Devonian.

The Late Devonian was a time dominated by change. Arborescent plants and multi-storied forests began colonising the land for the first time, which possibly led to increased O_2 concentrations in the atmosphere, and a concomitant drawdown of atmospheric CO_2 (Algeo and Scheckler, 2010). Increased weathering rates and enhanced organic carbon burial in anoxic oceanic basins contributed to this rapid drawdown of CO_2, changing the climate from equitable to cool (Algeo and Scheckler, 1998). This led to the development of southern polar continental glaciers by the end of the Devonian, and at least two extinction events which are recorded in Upper Devonian sediments (Streel *et al.*, 2000). This research is concerned with the latter of these two events; however, they are both briefly discussed below.

1.2.3.1 The Kellwasser and Hangenberg events

Two main pulses of extinction have been recognised within the Late Devonian. The first event at the Frasnian / Famennian boundary is referred to as the Kellwasser Event. It lasted approximately 0.3 million years (Streel *et al.*, 2000) and documents the greatest extinction phase within the prolonged, approximately three million years of the Late Frasnian Crisis (McGhee, 1996). The second extinction event, designated the Hangenberg Event, took place in the latest Famennian, corresponding to the LN Miospore Biozone (Higgs and Streel, 1994), and coeval with the deposition of the shales studied within this thesis. The Late Frasnian Crisis is often referred to as one of the Earths 'big 5' biotic crises, where more than 29 % of marine genera and 17 % of families became extinct (Sepkoski, 1996); however, up to 21 % of marine genera and 16 % of families became extinct as a result of the Hangenberg Event (Simakov, 1993; Sepkoski, 1996), which possibly took place over a much shorter time period (~0.1 Ma) (Sandberg and Ziegler, 1996). The Hangenberg Event is named after the Hangenberg Shale of Germany, the base of which coincides with the base of the LN Miospore Biozone (Higgs and Streel, 1994). Although the Hangenberg Event may not yet be considered one of the five greatest extinction events within the Phanerozoic, it has been recognised as a relatively severe bio-event (McGhee *et al.*, 2012) which led to lasting changes in vertebrate evolution (Sallan and Coates, 2010) and phytoplankton dynamics (Riegel, 2008).

The Hangenberg Event comprises two main extinction phases. The first phase is associated with the global migration of anoxic waters onto the palaeocontinental shelf during transgression, and recognised by low-latitude black shale deposits in Europe, China and North America (Walliser, 1996). This led to the reduced availability of marine ecological niches, overcrowding and the death of sessile benthic and nektobenthic organisms (McGhee, 1996). The second phase of extinction is associated with a eustatic regression, recognised in the global stratigraphy by grey silty mudrocks overlying the black shale deposits (Caplan and Bustin, 1999). This sea-level fall led to declines in acritarchs (Riegel, 2008) and abrupt changes in the miospore assemblages (Higgs and Streel, 1994).

The Hangenberg Event resulted in the extinction of chitinozoans and placoderms, and an abrupt decline in the diversity of ammonoids, trilobites and conodonts (Walliser 1996; Caplan and Bustin, 1999, Sallans and Coates, 2010). The event also led to more gradual declines in acritarchs, foraminifera, corals, blastoids, stromatoporoids, ostracods, brachiopods and cystoids (Simakov, 1993; Walliser, 1996; Caplan and Bustin, 1999; Sandberg *et al.*, 2002b). Sallin and Coates (2010) noted that the Hangenberg extinction was a global phenomenon which had an effect on all ecosystems, whether marine or terrestrial.

Terrestrial flora may have appeared as early as the mid-Ordovician, however, it was not until the Devonian Period that the evolution of trees and multi-storied forests took place (Algeo and

Scheckler, 1998). A sudden increase in arborescence and the expansion of trees from the equator to boreal latitudes appears to have taken place between the Givetian and Frasnian ages (Algeo and Scheckler, 2010). Seed plants also first appeared in the late Middle Devonian (Marshall and Hemsley, 2003), an innovation that would have allowed for the exploitation of a broader range of environments beyond that of coastal or lacustrine environments. This expansion of forests and the increasing depth of root systems may have intensified weathering rates and led to a drawdown of atmospheric CO_2 (Algeo and Scheckler, 1998), coinciding with climatic cooling in the Late Devonian. During the latest Famennian, a cosmopolitan coastal plant community (*lepidophya* complex) flourished, but by the end of the LN Miospore Biozone it was dramatically reduced (Streel, 1986; Caplan and Bustin, 1999; Streel *et al.*, 2000). Therefore, it appears that coastal plant communities were substantially reduced at the end of the Famennian, but, inland plant communities seem to be less affected as environments changed during the Hangenberg Event (Caplan and Bustin, 1999).

1.2.3.2 Climate changes (Figure 1.5)

The late Frasnian may have seen a short glacial phase, followed by a cold, non-glacial phase from the early to middle Famennian, with a strong climatic gradient from a warm equator to a cool pole (Streel *et al.*, 2000). The late Famennian is considered to have been less cold at high latitudes than the middle Famennian, but wetter, allowing the development of alpine glaciers, possibly corresponding to a global regression (Johnston *et al.*, 1985). A widespread transgression in the late Famennian VH Miospore Biozone may correspond to the melting of these alpine glaciers (Streel *et al.*, 2000). Glacio-marine sediments in Brazil and Bolivia are considered to correspond to a global regression during the subsequent latest Famennian LL, LE and LN miospore biozones (Melo *et al.*, 1999; Wicander *et al.*, 2011). This lowstand appears to correspond to a wetter climate in the tropical regions (Streel *et al.*, 2000), which may have contributed to the build up of low latitude alpine glaciers. This wet climate at low latitudes may have been replaced by a colder climate during the earliest Carboniferous (Brand, 1993), possibly contributing to the disappearance of the *lepidophyta* complex.

Johnston *et al.* (1985) describe Devonian sea level fluctuations in terms of eustatic transgressive-regressive cycles (T-R), where T-R cycles IIe and IIf are recorded as taking place during the Famennian. These cycles are generally regressive, and interrupted by periods of transgression. It is suggested that high latitude continental glaciation, extending from southern polar regions, may have lowered sea levels which are recorded as background regressive phases within these cycles.

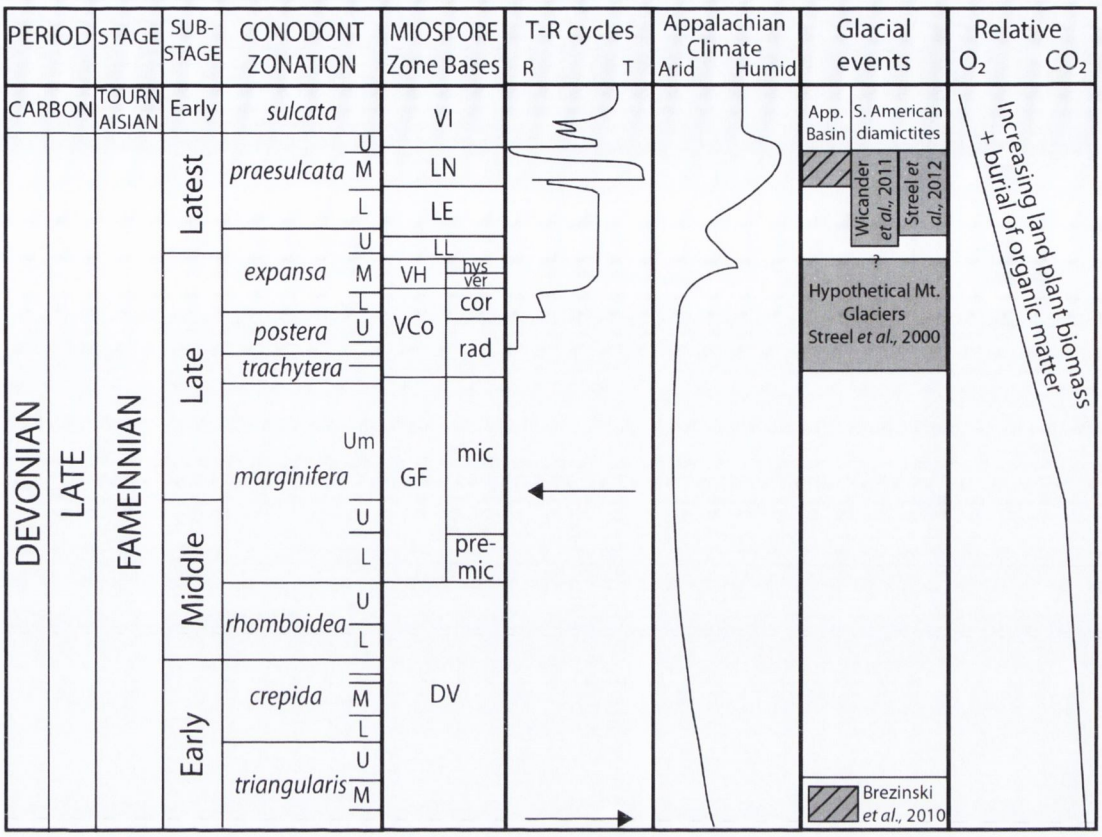

Figure 1.5. Summary of the timing of trangressive-regressive events (Johnson *et al.*, 1985; Streel *et al.*, 2000; Kaiser *et al.*, 2008), Appalachian Basin climate events (Brezinski *et al.*, 2009), global glaciation events (Streel *et al.*, 2000; Brezinski *et al.*, 2010, Wicander *et al.*, 2011; Streel *et al.*, 2012) and variation in atmospheric CO_2 and O_2 levels (Algeo *et al.*, 1995; Algeo and Scheckler, 1998; Marynowski and Filipiak, 2007).

Recent palynological interpretations of the South American, latest Famennian, diamictite sections (the Iquiri and Itaqua formations, Peruvian-Argentinian Basin, Bolivia, and the Cabeças Formation, Parnaíba Basin, Brazil) have led to varying interpretations of the timing and extent of latest Famennian glaciation, ranging from 100,000 years up to 3 million years (Streel *et al.*, 2012; Wicander *et al.*, 2011). Wicander *et al.* (2011) have proposed that multiple glacial / deglacial events may have taken place during the deposition of the Bolivian diamictite sections, which they interpreted to include the LL, LE and LN Western European miospore biozones. From this, it was suggested that the section may have been deposited over a period of up to 3 million years, as these three miospore biozones represent the Strunian substage, with an estimated duration of 3 million years (Trapp *et al.*, 2004; Streel *et al.*, 2006). Streel *et al.* (2012) argue for a brief glacial event during the LE and LN miospore biozones, proposing that glaciation may have occurred over a period as short as 100,000 years, based on the time required for accumulation of the Hangenberg section in Germany (Sandberg and Ziegler, 1996) (discussed in more detail in Chapter 2).

A sharp fall in atmospheric CO_2 takes place from the Middle Devonian to the Early Carboniferous (Algeo *et al.*, 1995), possibly as a result of the increase in land plant biomass (Algeo and Scheckler, 1998; Berner, 1999), and the global deposition of anoxic, organic-rich muds during transgressive phases, leading to the sequestration of atmospheric CO_2. This may have instigated or contributed to global cooling and glaciation in the Late Devonian. Atmospheric O_2 levels increased to over 13 % in the latest Famennian, as evidenced by an increase in fossil charcoal, which Marynowski and Filipiak (2007) have argued is an indication of global wildfires. This was possibly brought about as a result of the increase in photosynthesizing terrestrial plants, producing oxygen as a by-product.

1.2.3.3 Phytoplankton changes

Acritarchs and prasinophytes mostly constitute the marine phytoplankton during the Palaeozoic (Tappan, 1980; Colbath and Grenfell, 1995; Strother, 1996; Le Hérissé *et al.*, 2009). The Devonian / Carboniferous boundary has been noted as the beginning of the "Phytoplankton Blackout" (Riegel, 2008), where the demise of the acritarchs led to a prolonged reduction in the fossil phytoplankton record, covering approximately 130 million years during the assembly of the Pangaea Supercontinent.

Prasinophytes often formed blooms during black shale events, and have therefore been referred to as "opportunistic," whereas acritarchs are recorded as declining or disappearing under the same conditions, perhaps due to the effective uptake of ammonium (the reduced form of nitrogen), by prasinophytes (Prauss, 2007). Ammonium may be a more widely available form of nitrogen in areas of high denitrification, where nitrate and nitrite are reduced to unusable forms (N_2 and N_2O) for uptake by many phytoplankton. Denitrification is likely to have expanded and intensified under the reducing conditions in which black shale formation takes place. Plankton diversity appears to be highest in oligotrophic waters (Martin, 1995, 1996), and therefore it has been considered that eutrophication may have also contributed to the demise of the acritarchs at the end of the Devonian. Eutrophication may have arisen through the expansion of terrestrial vegetation from Middle to Late Devonian time, leading to increased nutrient input to the marine environment (Algeo *et al.*, 1995; Algeo and Scheckler, 1998). Increased upwelling and oceanic overturn may have also taken place during the Late Devonian due to altered thermohaline circulation brought about by global cooling and glaciation (Frakes *et al.*, 1992). It is suggested that this would have brought large volumes of nutrients and trace elements to the ocean surface, leading to eutrophication, increased marine primary productivity and possible decreased overall phytoplankton diversity (Caplan and Bustin, 1999).

1.2.3.4 Variation in stable isotopes

Positive shifts in the carbon isotope signature of brachiopods, ooids, micritic limestones and bulk organic carbon have been recorded within the Middle and Upper *praesulcata* conodont Zone of the latest Famennian (Brand *et al.*, 2004; Buggisch and Joachimski, 2006; Kaiser *et al.*, 2006) (Figure 1.6). The Hangenberg marine extinction event takes place at the base of the Hangenberg Black Shale (referred to by Myrow *et al.*, 2011 as the Hangenberg Extinction Event, or HEE), within the lower Middle *praesulcata* Conodont Zone. The positive $\delta^{13}C_{carb}$ shift appears to be recorded in carbonates deposited subsequent to the faunal extinction. The C isotope excursion is assigned to the upper Middle *praesulcata* Conodont Zone, possibly coinciding with the latter part of the Hangenberg Event that led to the demise of coastal plant communities and a decline in acritarchs. Myrow *et al.* (2011) referred to this as the Hangenberg Isotopic Excursion (HIE). These isotopic excursions have been suggested to be related to a drawdown in atmospheric CO_2, possibly brought about by the increasing terrestrial biomass and arborescent forests, increased weathering rates related to orogenic events and tectonic activity, and the burial of organic rich black shales during the Late Devonian (Kaiser *et al.*, 2006).

Analysis of the oxygen isotope signature recorded in conodonts suggest that temperatures were low during the Lower *expansa* Conodont Zone, increased in the Middle *expansa* Conodont Zone and remained relatively high from the Upper *expansa* Conodont Zone to the Lower *praesulcata* Conodont Zone (Kaiser *et al.*, 2006). A subsequent short decrease in temperature during the Lower *praesulcata* Conodont Zone was followed again by higher temperatures. Lower temperatures return and intensify into the lower Middle *praesulcata* Conodont Zone, coeval with the deposition of the Drewer Sandstone within the Rhenish Massif stratigraphy in Germany (Figure 1.6). An increase in temperature is recorded during the deposition of the Hangenberg Black Shale and associated marine faunal extinction (Kaiser *et al.*, 2006). The upper Middle *praesulcata* Conodont Zone records a shift to heavier oxygen isotope values, suggesting a shift to colder temperatures which correspond to the recorded glacial episode and the regressive phase of the Hangenberg Event that took place in the latest Famennian. A reversal then occurs just before the Devonian-Carboniferous boundary at the top of the Upper *praesulcata* Zone, where conditions return to more equitable temperatures (Brand *et al.*, 2004).

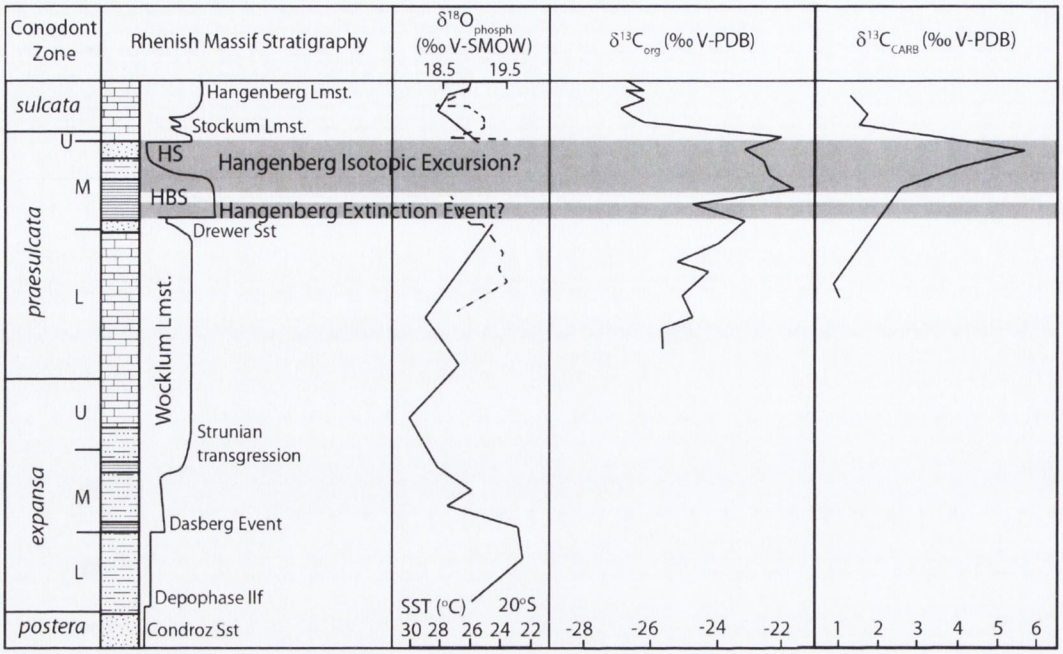

Figure 1.6. Correlation and timing of recorded Late Devonian geochemical changes set against the Rhenish Massif stratigraphy (Kaiser *et al.*, 2008). Oxygen isotope data is based on conodont apatite and is modified from Kaiser *et al.*, (2006) (dashed line) and (2008) (solid line). C_{org} isotope data is modified from Kaiser *et al.* (2006). C_{carb} isotopic data is modified from Brand *et al.* (2004). The Hangenberg Isotopic Event and Hangenberg Extinction Event timings are based on Myrow *et al.*, (2011).

1.3 NITROGEN ISOTOPES

Nitrogen exists in the form of two stable isotopes, ^{14}N and ^{15}N, where the lighter isotope (^{14}N) is much more abundant (99.64 %) than the heavier isotope (0.36 %) (Sharp, 2007). Isotopic fractionation can cause the enrichment of one isotope relative to the other in biological, chemical or physical processes. This fractionation occurs because ^{15}N has greater mass and higher binding energy than ^{14}N. Molecular bonds containing the heavier isotope require more energy to break than bonds containing the lighter isotope; therefore certain processes will discriminate between these isotopes.

1.3.1 Diagenesis and bulk material

By compiling the research that has been carried out on modern sediments, Robinson *et al.* (2012) observed that significant diagenetic alteration can occur at the sediment-water interface during early burial, specifically in areas that record low sediment accumulation rates, whereas areas of high sediment accumulation rates, such as continental margins, appear to record negligible change between the sinking flux $\delta^{15}N$ and sedimentary $\delta^{15}N$. Significant differences in $\delta^{15}N$ (> 2 ‰) have also been found within sedimentary downcore records located a mere 15 km apart from each other

in the South China Sea (Kienast *et al.*, 2005). Due to the concern that bulk sediments can record varying $\delta^{15}N$ signals that are susceptible to change based on the type of organic matter being supplied, and the rate of sediment accumulation at the time of deposition, targeted sedimentary N fractions are being analysed more routinely, in the hope that they will provide a better overall sedimentary $\delta^{15}N$ record of past changes. The $\delta^{15}N$ of N bound in diatoms (e.g. Crosta and Shemesh, 2002; Robinson *et al.*, 2004; Sigman *et al.*, 1999), foraminifera (e.g. Altabet and Curry, 1989, Ren *et al.*, 2009) and chlorophyll degradation products (e.g. Ohkouchi *et al.*, 2006; Sachs and Repeta, 1999) have all been analysed as a means of overcoming some of the concerns related to bulk sedimentary $\delta^{15}N$.

The extraction and analysis of a specific N fraction of sedimentary bulk material requires an understanding of how different N fractions relate to each other within a trophic system. Trophic enrichment occurs within food-webs as organisms preferentially excrete the lighter ^{14}N and retain the heavier ^{15}N (Kling *et al.*, 1992). This typically leads to a 3-4 ‰ enrichment in $\delta^{15}N$ for each trophic step up the food chain, making it a useful tool in food-web reconstructions (DeNiro and Epstein, 1981; Minagawa and Wada, 1984). The trophic enrichment factor of an ecosystem is assumed to stay constant through time, but the isotopic base-line does not. This thesis is mainly concerned with base-line isotopic variation induced by environmental change. Therefore the focus of this study will be to analyse the isotopic signature of marine primary producers, which record the first initial stage of nutrient N uptake within the marine trophic system.

1.3.2 The nitrogen cycle

Based on computer models of the evolution of the atmosphere, atmospheric N_2 had built up to near modern day levels by two billion years ago, although it accounted for a larger fraction of atmospheric gases (up to 96 %) due to the lack of free O_2 in the early atmosphere (Hart, 1978). As gases such as O_2 increased over time, the overall fraction of N_2 in the atmosphere decreased, but with increasing atmospheric volume (Hart, 1978). By the Late Devonian, atmospheric N_2 had most likely reached similar concentrations to the modern atmosphere, while at the same time O_2 levels increased to over 13 % as forests began to flourish (Marynowski and Filipiak, 2007). Although the Earth's atmosphere is composed mainly of nitrogen (N_2), this reservoir of unreactive nitrogen is not available to the majority of primary producers, which require a fixed form of nitrogen, such as ammonium (NH_4^+), nitrite (NO_2^-) and nitrate (NO_3^-), as well as urea and other organic N compounds. The marine nitrogen budget is balanced between the addition of new nitrogen via fixation from the atmosphere, and the removal of nitrogen through sedimentary and water column denitrification. Each process is dictated by its own set of environmental parameters, making them regionally distinct from each other (Figure 1.7) and imperfectly coupled, where N-fixation lags behind denitrification (Galbraith *et al.*, 2004).

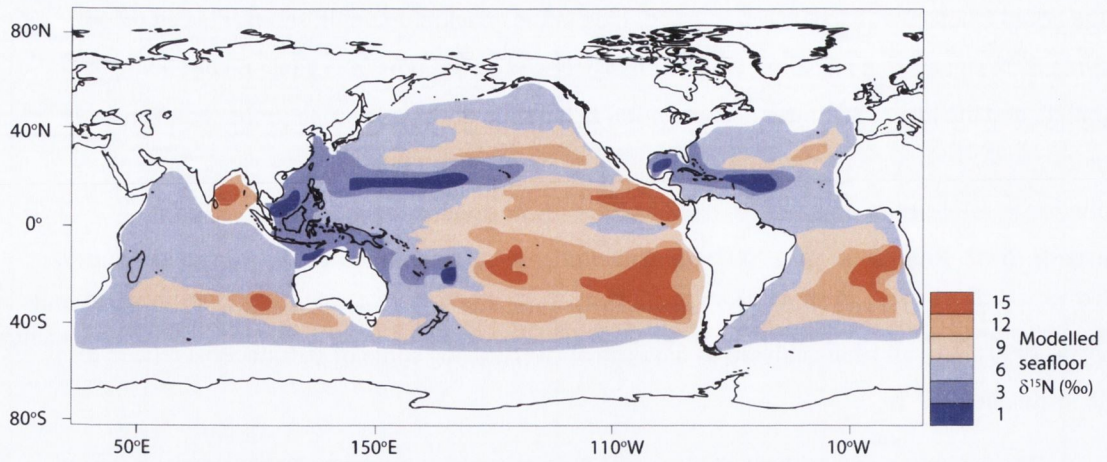

Figure 1.7. Modelled low latitude seafloor $\delta^{15}N$ (‰). Modified from Galbraith *et al.* (2013). The model overestimated denitrification within the southern Atlantic and placed a denitrification zone in the Bay of Bengal instead of the Arabian Sea. Regions in red denote areas likely influenced by denitrification, whereas regions in dark blue denote areas likely influenced by N-fixation.

Diazotrophic bacteria, such as cyanobacteria, are specialised organisms that can utilise nitrogen directly from the atmosphere (N_2). This process is the primary method of transforming atmospheric nitrogen into reactive nitrogen, which increases the nitrogen budget of the ocean. Very little isotopic fractionation is associated with this process, such that these organisms record a very similar $\delta^{15}N$ to that of atmospheric nitrogen (present N_2, ~ 0 ‰). After the death of these organisms, or through grazing, nitrogen remains in the marine environment, where it can be taken up by other primary producers, leading to the first fractionation step within the food-web.

In contrast, water column and sedimentary denitrification remove fixed nitrogen from the marine environment. Sedimentary denitrification occurs within sediment pore waters, where the near complete consumption of nitrate at the site of denitrification does not lead to any discernible enrichment in ^{15}N in the nitrate escaping to the water column (Brandes and Devol, 2002; Deutsch *et al.*, 2004; Sigman *et al.*, 2003). Water column denitrification (WCD) commonly occurs between 150-500 m water depth, and is confined to areas where oxygen concentrations are below 5 µmol/kg (Sigman *et al.*, 2009). Denitrifying bacteria preferentially reduce lighter nitrate ($^{14}NO_3^-$) to unreactive N_2 or N_2O (nitrous oxide), leaving the residual marine nitrate enriched in ^{15}N (+9 to +18 ‰). This heavier nitrate is upwelled to the ocean surface and assimilated by organisms which contribute to the sedimentary record (Figure 1.8). However, the upwelled waters from denitrification zones are relatively nitrate poor, recording a low N:P ratio. These N-limited waters lead to the export of excess phosphorus to nearby oceanic regions, prompting an increase in N-fixation in areas of the ocean proximal to denitrification zones (Deutsch *et al.*, 2007). Cyanobacteria use this excess P, while fixing their own nitrogen directly from the atmosphere.

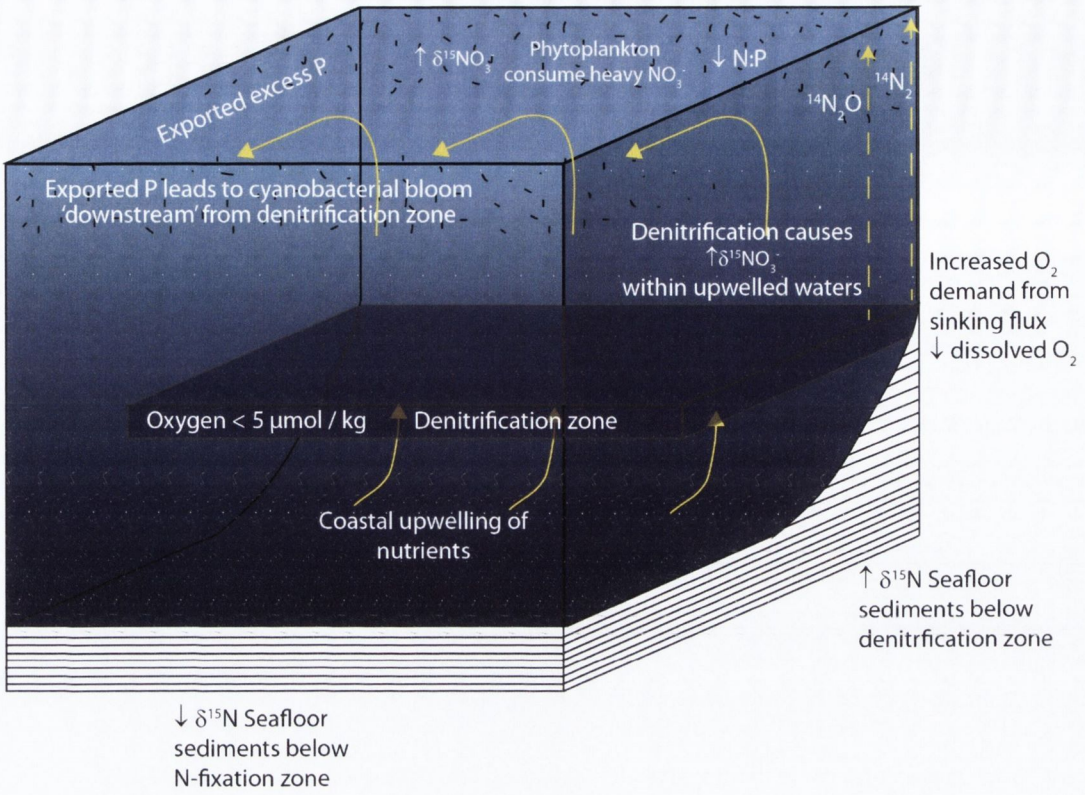

Figure 1.8. Box model depicting coastal upwelling, denitrification within the oxygen minimum zone, leading to exported P and increased sedimentary $\delta^{15}N$ beneath the coastal denitrification zone.

This process has been found to be closely tied to the development of N-deficient waters from denitrification zones. As N-fixation requires more energy than nitrate assimilation, cyanobacteria lose their competitive edge to other non-N-fixing phytoplankton once nitrogen conditions improve.

Another form of fixed N loss is due to anaerobic ammonium oxidation, more commonly known as 'annamox,' where nitrite is used to oxidise ammonium to N_2 (Thamdrup and Dalsgaard, 2002; Dalsgaard *et al.*, 2003). This process occurs under low oxygen conditions within sediments and the water column, however, its effect on isotopic distribution within the ocean is unknown (Sigman *et al.*, 2009). For the purposes of this thesis, the annamox reaction will be included as part of WCD. Denitrification zones are commonly confined to small areas of the ocean (currently limited to less than 0.2 % of the modern ocean volume), leading to highly elevated $\delta^{15}N$ values in localised sedimentary records. Whereas nitrogen fixation takes place over larger expanses of water, within tropical or subtropical basins; consequently, the effect of lowering the $\delta^{15}N$ signal of organic matter, by the addition of fixed nitrogen (~ 0 ‰) to the ecosystem, is diluted over such large areas. These two processes interact to produce an average modern marine nitrate $\delta^{15}N$ value of ~ 5 ‰, however, regionally the $\delta^{15}N$ of nitrate can range from 2 - 20 ‰ due to the changing influence of N_2 fixation, denitrification and nitrate assimilation (Sigman *et al.*, 2009) (Figure 1.7).

Nitrate assimilation can have an effect on the isotopic signature of organic matter as phytoplankton will preferentially consume nitrate containing the lighter ^{14}N over the heavier ^{15}N, leading to an isotope effect of approximately 5 ‰. However, fixed N is relatively scarce in the surface ocean, especially within low latitudinal areas, therefore this isotope effect is often minimised (Sigman *et al.*, 2009).

Because little to no isotopic fractionation takes place through N-fixation, it has been suggested that variations in the intensity of WCD essentially controls the nitrogen isotope composition of the oceans. WCD only occurs where there are low levels of oxygen in the upper kilometre of the water column. Therefore, if redox conditions control the extent of denitrification, this indicates that the global $\delta^{15}N$ of living organic matter is dependent upon redox conditions within the water column. Consequently, the nitrogen isotope composition of sedimentary organic matter can be used as a marker of major changes in the nitrogen cycle, which should in turn provide valuable information on past environmental changes.

1.3.3 Modern analogues and climatic implications

The majority of nitrogen isotope studies have focused on modern sediments and the palaeo-environments of the recent ice ages and interglacials, whereas only a few have tried to use nitrogen isotopes to reconstruct the palaeo-environments of the distant past (e.g. Beaumont and Robert, 1999; Fennel *et al.*, 2005; Jenkyns *et al.*, 2001; Kuypers *et al.*, 2004; Rau *et al.*, 1987; Saltzman, 2005). Galbraith *et al.* (2004) compiled information from various sediment cores throughout the modern ocean to compare the most recent glacial-interglacial changes in $\delta^{15}N$. The approach focussed on the co-variation of denitrification and N-fixation, where both processes were found to increase during warmer, interglacial periods, when sluggish circulation leads to the expansion of anoxia and therefore, the expansion of denitrification. A heavier $\delta^{15}N$ is evident in the interglacial sedimentary record located near oxygen minimum zones as a result of increasing WCD, and a lighter $\delta^{15}N$ value is recorded below N-fixation zones during interglacial periods. However, the coupling of denitrification and N-fixation is imperfect as the two processes are spatially distinct (Codispoti *et al.*, 2001).

N-fixation increases as a result of increased water column denitrification (Deutsch *et al.*, 2007), thereby lagging behind the initial deglacial increase in denitrification. This may lead to a deglacial maximum $\delta^{15}N$ recorded beneath denitrification zones, followed by a slight decrease in $\delta^{15}N$ subsequent to deglaciation, as N-fixation and sedimentary denitrification (the decrease in O_2 in the water column precedes the flooding of the continental shelves) catch up to the initial increases in WCD, diluting the increase in $\delta^{15}N$ produced by WCD.

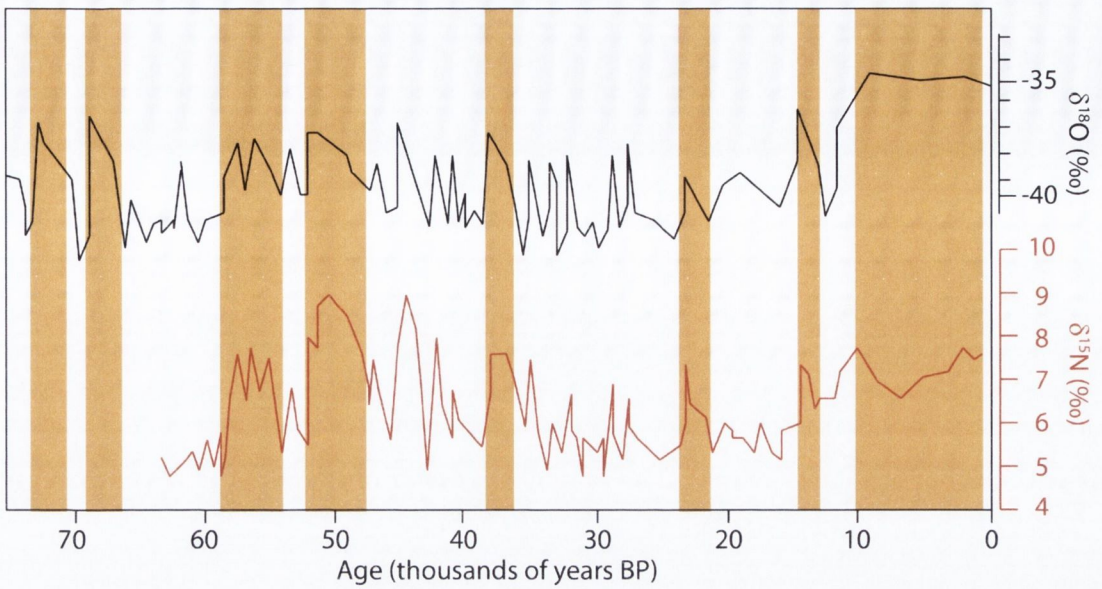

Figure 1.9. Changes in $\delta^{18}O$ (proxy for past temperature changes) recorded within a Greenland ice-core is shown in black, compared against a downcore record of sedimentary $\delta^{15}N$ in the Arabian Sea, shown in red (proxy for regional changes in denitrification). The orange panels denote interglacial periods, where increases in $\delta^{18}O$ suggest warming, coinciding with increases in $\delta^{15}N$, brought about by increased denitrification rates. Modified from Gruber and Galloway (2008).

The increase in N-fixation, brought about by the excess P exported from WCD zones, will record a decrease in the $\delta^{15}N$ of sedimentary organic matter within N-fixation zones, thus balancing the changes to the nitrogen budget and the nitrogen isotope signature of the ocean brought about by increased WCD.

Both N-fixation and WCD have been found to decrease during glacial periods (Galbraith *et al.*, 2013). As the water temperature approaches freezing point, the solubility of O_2 in seawater increases rapidly. Increased high latitude winds during glacial periods also leads to increased thermocline ventilation, which decreases the extent and intensity of denitrification in the ocean. Subsequently, a higher N:P ratio is likely to be recorded in glacial-stage upwelled waters, leading to lower rates of P export, and lower rates of N-fixation. By analysing $\delta^{15}N$ records, this glacial / interglacial trend can be used as a tracer of past climatic variation, once it is established that the sedimentary record observes changes in either WCD or N-fixation. In Figure 1.9, the sedimentary downcore $\delta^{15}N$ record from the Arabian Sea is shown alongside changes recorded in the $\delta^{18}O$ record from a Greenland ice-core. Oxygen isotopes have been used by researchers as a reliable proxy for changes in global temperature, where increases in $\delta^{18}O$ in high latitude ice-cores corresponds to higher average global temperatures (Bradley, 1999). Increases in $\delta^{18}O$ appear to be synchronised with the changes recorded in the downcore $\delta^{15}N$ value from a known WCD zone (the Arabian Sea).

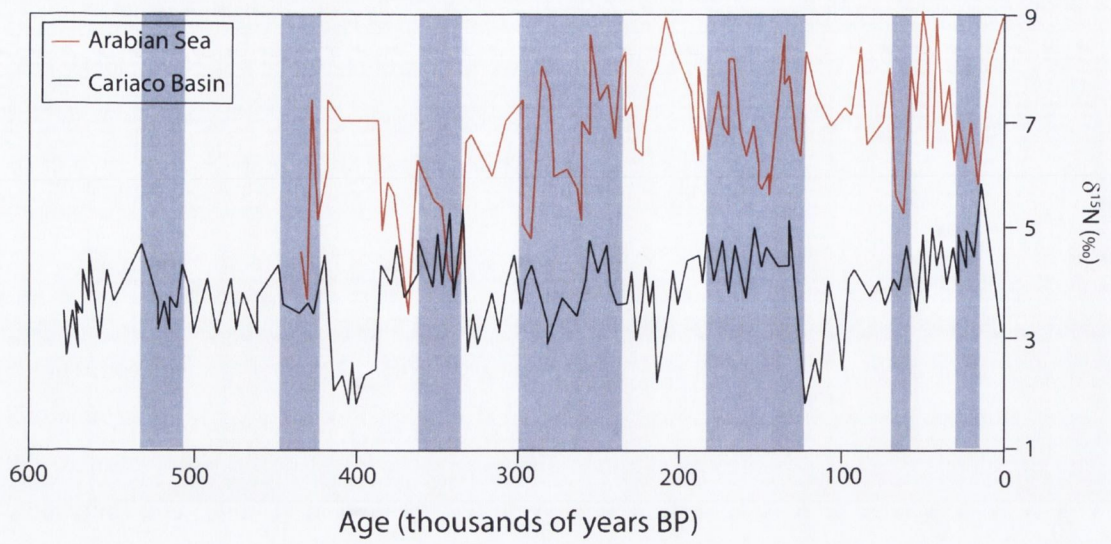

Figure 1.10. Downcore $\delta^{15}N$ records from the Cariaco Basin (Haug *et al.*, 1998) and the Arabian Sea (Altabet *et al.*, 1995). Blue panels denote glacial periods. Opposing $\delta^{15}N$ trends are recorded at each locality due to differences in the dominant processes at each site. Denitrification rates decrease in the Arabian Sea and N-fixation rates decrease in the Cariaco Basin during these glacial intervals, produing $\delta^{15}N$ values similar to the modern average marine $\delta^{15}NO_3^-$.

The increases in $\delta^{15}N$ correspond to periods of intensified denitrification, most likely brought about due to higher temperatures and increased anoxia, recorded as an increase in $\delta^{18}O$ in the Greenland ice-core.

The glacial / interglacial transition is recorded as opposing $\delta^{15}N$ trends between denitrification and N-fixation zones (Figure 1.10). During glacial periods both of these oceanic regions will record a return to $\delta^{15}N$ values similar to that of average marine $\delta^{15}NO_3^-$ (~ 5 ‰). However, following the transition from a glacial to an interglacial period, the sedimentary organic matter accumulating under a denitrification zone will record an increase in $\delta^{15}N$, whereas the organic matter accumulating beneath a N-fixation zone will record a decrease in $\delta^{15}N$.

Denitrification occurs in the modern ocean in three major regions; continental margin sediments, mainly along the eastern North and South Pacific continental margins; areas of restricted circulation, such as fjords; and oxygen minima zones of perennially stratified seas, such as the Arabian Sea, and the Black Sea. N-fixation appears to be strongest in oligotrophic subtropical regions, often 'downstream' from tropical upwelling zones and proximal to denitrification zones (Deutsch *et al.*, 2007). By comparing the modern glacial / interglacial downcore $\delta^{15}N$ records of two distinct regions, the Cariaco Basin and the Arabian Sea, a pattern of opposing $\delta^{15}N$ trends can be observed (Figure 1.10). The interglacial sediments of the Cariaco Basin record increased rates of N-fixation whereas the Arabian Sea records increased interglacial

rates of denitrification. The glacial sediments of both regions record a return to values similar to average marine $\delta^{15}NO_3^-$ (~ 5 ‰). These trends will be discussed in more detail in Chapter 5.

Based on modern analyses of the nitrogen cycle, sedimentary $\delta^{15}N$ can be used as a proxy for past changes in denitrification and N-fixation, brought about by changes in oxic conditions within the water column. Climate change is a likely candidate for changes in oceanic oxic conditions, however, other factors may contribute to oceanic anoxic events, as will be discussed in more detail in Chapter 5. Nitrogen isotopes spanning oceanic anoxic events have been analysed by various researchers from the Late Ordovician (Melchin *et al.*, 2013), the Jurassic (early Toarcian) (Jenkyns *et al.*, 2001), the Cretaceous (Junium and Arthur, 2007; Kuypers *et al.*, 2004; Ohkouchi *et al.*, 2006; Rau *et al.*, 1987), and the Cenozoic Mediterranean sapropels (Arnaboldi and Meyers, 2006; Calvert *et al.*, 1992; Emeis and Weissert, 2009; Sachs and Repeta, 1999). All of these studies, with the exception of the Jurassic (Jenkyns *et al.*, 2001), record very light $\delta^{15}N$ values during the supposed oceanic anoxic events, possibly indicating increased N-fixation during the deposition of the organic-rich facies. This hypothesis will be discussed in more detail, alongside the results of this research in Chapter 5.

1.4 TRACE ELEMENTS

Explorative research was carried out, as part of this project, into the trace element ratios of the palynomorph, *Tasmanites*. This work was carried out in order to support the main body of research examining the palaeoenvironmental conditions of the Late Devonian Appalachian Basin.

Trace elements are fundamental to phytoplanktonic life as they take part in major element assimilation, biological energy capture, information transfer and control, and the development of shape (Whitfield, 2001). The abundance and ratios of specific elements have been used as tracers of past environments to predict nutrient balance and oxic conditions within palaeo-marine settings. Dust fluxes during glacial periods may have led to increased trace elements, such as Fe, transported to the oceans during these times (Galbraith *et al.*, 2008), and increased Fe availability is known to increase marine primary production under Fe-deficient conditions (Martin *et al.*, 1994). Fe is required for the process of nitrogen fixation by diazotrophs and nitrate assimilation by phytoplankton. Algae grown on nitrate are estimated to require 60 % more Fe than algae grown on ammonium or urea (Raven *et al.*, 1992), whereas a dramatic increase in Ni is recorded if grown on urea rather than nitrate (Price and Morel, 1991). Therefore, higher Ni and lower Fe concentrations in phytoplankton, such as *Tasmanites*, may indicate N-limited, oligotrophic conditions.

Mo is involved in the major biogeochemical cycles of particle formation and destruction and exhibits fairly uniform distribution in the ocean (Bruland and Lohan, 2006). Mo tends to be enriched in anoxic-euxinic environments, and can therefore be used as a proxy for redox conditions

(Perkins *et al.*, 2008; Tribovillard *et al.*, 2006).Vanadium and Ni are thought to occur in tetrapyrrole structures which are involved in photosynthesis and respiration. These structures are preferentially preserved under anoxic conditions, consequently, the increased presence of V and Ni (taking into account TOC) in sediments has been used as a proxy for bottom water anoxia (Rimmer, 2004). It is thought that Cr is unaffected by redox conditions, and it is therefore used in conjunction with V as a redox indicator (V/Cr). The Ni/Co ratio has been utilised alongside V/Cr, U/Th and the degree of pyritisation as an internally consistent set of reliable indicators of redox conditions (Jones and Manning, 1994). However, both Ni and Co concentrations can vary according to other parameters, such as nutrient conditions, as outlined for Ni, above.

Cobalt can replace Zn in open waters where Zn concentrations may be low (Whitfield, 2001). Therefore increases in Co found in phytoplankton may indicate an open water environment, rather than forming a reliable ratio with Ni to predict redox conditions. Cadmium can partially replace Co and Zn when one or more are depleted. A high Cd/Co ratio can signify open ocean conditions, where uptake rates of Cd can be much higher than in coastal waters due to aeolian input (Whitfield, 2001). Cadmium and Zn have also been used as proxies for nutrient input as they are strongly correlated with phosphate and nitrate. Therefore increases in these elements may provide information on nitrate availability.

Barium has been used to assess paleoproductivity, where increases in Ba are associated with high productivity. However, Ba is usually found as barite and forms as a result of the decay of organic matter (Dymond *et al.*, 1992). Increases in Ba therefore relate to particulate fluxes of organic matter rather than increased nutrient conditions in the upper ocean. Barium concentration in algal cysts, such as *Tasmanites,* could possibly indicate their state of decomposition, rather than productivity levels. However, this is a very tentative association that would require further testing.

Chapter 2

Geological Setting

2.1 OVERVIEW

In order to test the hypothesis outlined in Chapter 1, a number of considerations were made before suitable samples could be collected for this project. The hypothesis sets out to investigate whether the nitrogen isotope ratio recorded in genus-specific marine palynomorphs (*Tasmanites* spp.) can be used to trace palaeo-climate changes. Therefore, it was important to consider samples with continuous deposition over a glaciation / deglaciation cycle, such as the Upper Devonian – Lower Carboniferous shales deposited in the Appalachian Basin. These shales are exposed at roadcuts throughout northeastern Kentucky, ensuring ease of access to samples throughout the stratigraphy. There has also been very little faulting or intrusive igneous activity in the area, such that the tectonic and thermal history of the area is quite straightforward, with peak palaeotemperatures of approximately 80°C recorded from the interpretation of vitrinite reflectance values (0.61-0.64 % R_o, Mason *et al.*, 2012). Upon palynological investigation of these shales, a continuous record of the alga, *Tasmanites,* is evident throughout the stratigraphic interval. The decision to analyse this particular palynomorph is discussed in more detail in Chapter 3. Based upon conodont work carried out by Over (2002) and Over *et al.* (2009), the age of the section ranges from the Uppermost *marginifera* Zone (early late Famennian) to the *sulcata* Zone (early Kinderhookian), which correlates approximately to the GF Miospore Biozone and the VI Miospore Biozone (Higgs *et al.*, 2013). The lithologies consist of predominantly black shales interbedded with grey shale deposits, each containing various mixtures of clay minerals, marine and terrestrial organic components.

A note on nomenclature: *Tasmanites* and *Protosalvinia* refer to *Tasmanites* spp. and *Protosalvinia* spp., respectively, throughout this thesis.

2.2 LITHOSTRATIGRAPHY

Shallow water carbonates and clastics dominated most of what is now the central United States, during the Early Palaeozoic (Ettensohn *et al.*, 2009). Due to rapid deformational loading in the Acadian orogen, subsidence in the adjacent Appalachian Basin exceeded sedimentation, leading to the development of basinal black shales (Ettensohn, 1991). A series of sea level lowstands are interpreted from the periodic deposition of grey shales within the Upper Devonian deep marine stratigraphic sequence found in northeastern Kentucky (Figure 2.1).

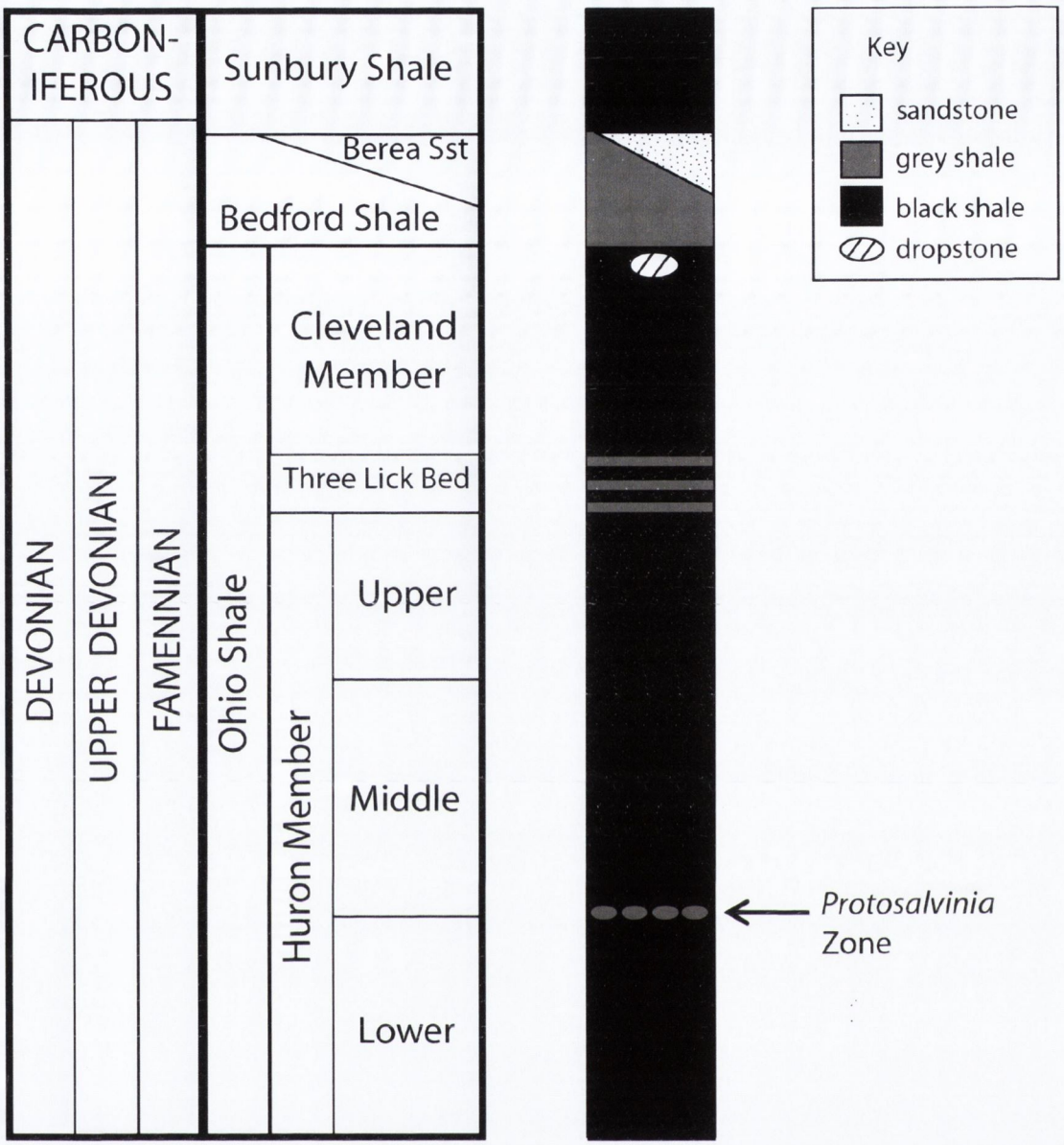

Figure 2.1. Generalised Famennian stratigraphy from northeastern Kentucky. The *Protosalvinia* Zone is located within interbedded grey shales located at the base of the Middle Huron Member. Modified from Provo *et al.* (1978).

2.2.1 Ohio Shale

The Ohio Shale consists of the lower, middle and upper Huron Members, the Three Lick Bed and the Cleveland Member. In northeastern Kentucky, the Ohio Shale is up to 100 m thick (Mason *et al.*, 2012). It is suggested that the Catskill Delta Complex, located to the east, grades westwardly into the Ohio Shale, northwestwardly into the New Albany Shale, and into the Chattanooga Shale to the south (Ettensohn *et al.*, 1988). The Ohio Shale is mainly composed of silt (quartz, feldspar,

chlorite, and mica), clay (mostly illite and some kaolinite), carbonaceous matter, and minor amounts of carbonate and pyrite (Schwietering, 1979).

2.2.1.1 Huron Member

The lower and upper Huron Members are organic-rich black shales, with the base of the lower Huron Member containing interbedded greenish-grey shale (Ettensohn *et al.*, 1988). The middle Huron Member is a black shale containing more clastic constituents and less organic matter than the lower and upper members, and includes interbedded grey shales near the base of the unit, which also contains the enigmatic late Devonian fossil, *Protosalvinia*. This fossil is found over a relatively short stratigraphic interval, making it a useful stratigraphic marker throughout the Appalachian, Illinois and Michigan basins. *Protosalvinia* will be discussed in more detail in Chapter 3. The combined thickness of the Huron Members is 38 m in the sections studied. They are interpreted as recording a transgressive-regressive sequence (Ettensohn, 1992).

2.2.1.2 Three Lick Bed

The Three Lick Bed conformably overlies the upper Huron Member and consists of three thin beds of greenish-grey shale, separated by two beds of ribbed, fissile black shales. The Three Lick Bed represents the distal most tongues of delta progradation from the north and east and can be followed to the west and south where it pinches out into bioturbated black shales (Provo *et al.*, 1978). Within the sampled horizons in northeastern Kentucky (Rowan and Lewis counties), the Three Lick Bed measures between 0.5 m and 3 m in thickness from the bottom grey shale to the top grey shale (inclusive). However, its thickness varies from nearly 40 m in eastern Kentucky to just a few centimetres in central Kentucky (Ettensohn *et al.*, 1988).

2.2.1.3 Cleveland Member

The Cleveland Member is a black, fissile, organic-rich, silty shale with a ribbed appearance. The ribbed appearance is associated with changes in organic content, where the sections containing less organic matter tend to weather more easily and therefore appear recessed in comparison to the more organic-rich layers. Pyrite is found throughout the unit, as well as an occasional siderite or phosphate nodule.

The Cleveland Member can be differentiated into lower and upper units, where the lower unit contains beds of grey shale and several thin beds of siliceous limestones, and the upper unit is characterised by its rusty brown appearance following weathering (Pepper *et al.*, 1954). Rimmer (2004) separated the Cleveland Member into two subunits based on total organic carbon content; the lower subunit typically has a lower organic carbon content than the upper subunit. The

Cleveland Member thins to the east and is conformably overlain by the Bedford Shale (Schwietering, 1979). Within the study area of northeastern Kentucky, the Cleveland Member is between 8 and 20 m thick. A granitic dropstone ('Robinson Dropstone'), estimated to weigh approximately three tonnes, is located at the top of the upper Cleveland Member, and is interpreted to be the product of alpine glaciation on the adjacent Acadian Mountains (Lierman and Mason, 2007; Clayton *et al.*, 2010).

2.2.2 Bedford Shale and Berea Sandstone

The Bedford Shale is a poorly fissile, non-calcareous, olive grey mud shale which conformably overlies the Ohio Shale in eastern Kentucky (Pepper *et al.*, 1954). The olive grey colour is mainly due to the presence of illite and chlorite. The Bedford Shale largely consists of silt and clay particles with small, fine, framboidal crystals of pyrite. Very thin, discontinuous beds of argillaceous siltstone, containing siderite nodules and irregularly shaped pyrite, are scattered throughout the formation (Mason *et al.*, 2012). The Bedford Shale is overlain by the Berea Sandstone in Ohio.

Two tongues of the Berea Sandstone are evident in northeastern Kentucky, separated by a northeastwardly thinning wedge of the Bedford Shale (Pashin and Ettensohn, 1992a). However, the Berea Sandstone is not present in the studied sections. Throughout much of eastern Kentucky, a black shale equivalent to the Bedford Shale has been recognised and comprises the entire Bedford Shale south of where the olive grey mud shale pinches out (Swager, 1978; Elam, 1981; Ettensohn and Elam, 1985; Pashin and Ettensohn, 1987). The contact between the Bedford Shale and the Sunbury Shale defines a regional unconformity, where a well developed cone-in-cone limestone layer is evident at the top of the Bedford Shale, just below a lag deposit at the base of the Sunbury Shale. The cone-in-cone limestone is possibly the result of burial induced pressure at the peak of orogenic activity during the deposition of the Sunbury Shale (Ettensohn *et al.*, 2009) and the lag deposit defines the beginning of the fourth tectophase cycle in the Acadian orogeny (Ettensohn, 1994; Ettensohn and Pashin, 1997). Within the sampled sections of northeastern Kentucky, the Bedford Shale attains a thickness of between 3 and 10 m.

2.2.3 Sunbury Shale

The Sunbury Shale consists of fissile, organic-rich black shales, with similar lithologies to the Huron and Cleveland Members of the Ohio Shale, and a similar ribbed appearance to the Cleveland Member. Within the sampled area of northeastern Kentucky, its thickness ranges from 2 - 8 m. The contact between the Bedford and Sunbury shales is represented by a lag deposit, overlying the cone-in-cone limestone at the top of the Bedford Shale. This basal lag deposit is

recognised throughout the outcrop area of the Sunbury Shale (Pepper *et al.*, 1954). The sharp contact between the lag deposit and the cone-in-cone limestone possibly defines a regional unconformity, and is thought to represent the division of the Devonian and Mississippian systems (Ettensohn, 1994). The unit contains small pyritic nodules and pyrite crystals.

Unlike the underlying transgressive black shales that seem to have migrated westward during deformational loading, it has been suggested that the Sunbury Shale migrated eastward, possibly reflecting the beginning of a more proximal 'Neo-Acadian' event, or the fourth tectophase of the Acadian orogen, to the east (Ettensohn, 1985; Ettensohn *et al.*, 1988). Additional information and interpretations regarding the Sunbury Shale can be found in papers by Chaplin and Mason (1979, 1985), Ettensohn and Elam (1985), Mason and Lierman (1985), Ettensohn *et al.* (1988), and Lierman *et al.* (1992).

2.3 BIOSTRATIGRAPHY

As the shallow-water, carbonate-dominated environment of the Middle Devonian was replaced by deeper water basinal sediments in the Late Devonian, the biota dramatically changed. Shallow water benthic biotas were replaced by a restrictive, commonly planktonic, depauperate biota in the basinal sediments.

2.3.1 Ohio Shale with miospore zonation after Clayton *et al.* (2012), Heal (2009), Rooney *et al.* (2013)

Conodonts, radiolaria (Foreman, 1959, 1963), inarticulate and articulate brachiopods, crinoids (Wells, 1941), fish, spores, algae, logs of land plants (Wells, 1947), and trace fossils have all been reported from the Ohio Shale. Petrographic profiles of the black shales have shown a general increase in the quantity of terrestrial organic components (vitrinite and inertinite) from the base to the top of the Ohio Shale (Eble *et al.*, 2010; Nuttall *et al.*, 2005; Rimmer *et al.*, 2004). This may reflect the expansion of terrestrial flora at the end of the Devonian, termed the "Devonian Explosion" by Algeo *et al.* (1995), or possibly the development of delta complexes that carried the terrestrial flora further into the basin as the adjacent Acadian Mountains advanced and matured.

2.3.1.1 Huron Member

The enigmatic and widespread fossil, *Protosalvinia*, is found within approximately 3 m of interbedded grey and black shales at the boundary between the lower and middle Huron members. This zone is often referred to as the *Protosalvinia* Zone as it has become a useful stratigraphic

marker throughout the Appalachian, Illinois and Michigan Basins (Matthews, 1983; Over *et al.*, 2009; Schopf and Schwietering, 1970). More detail will be provided on this fossil in Chapter 3.

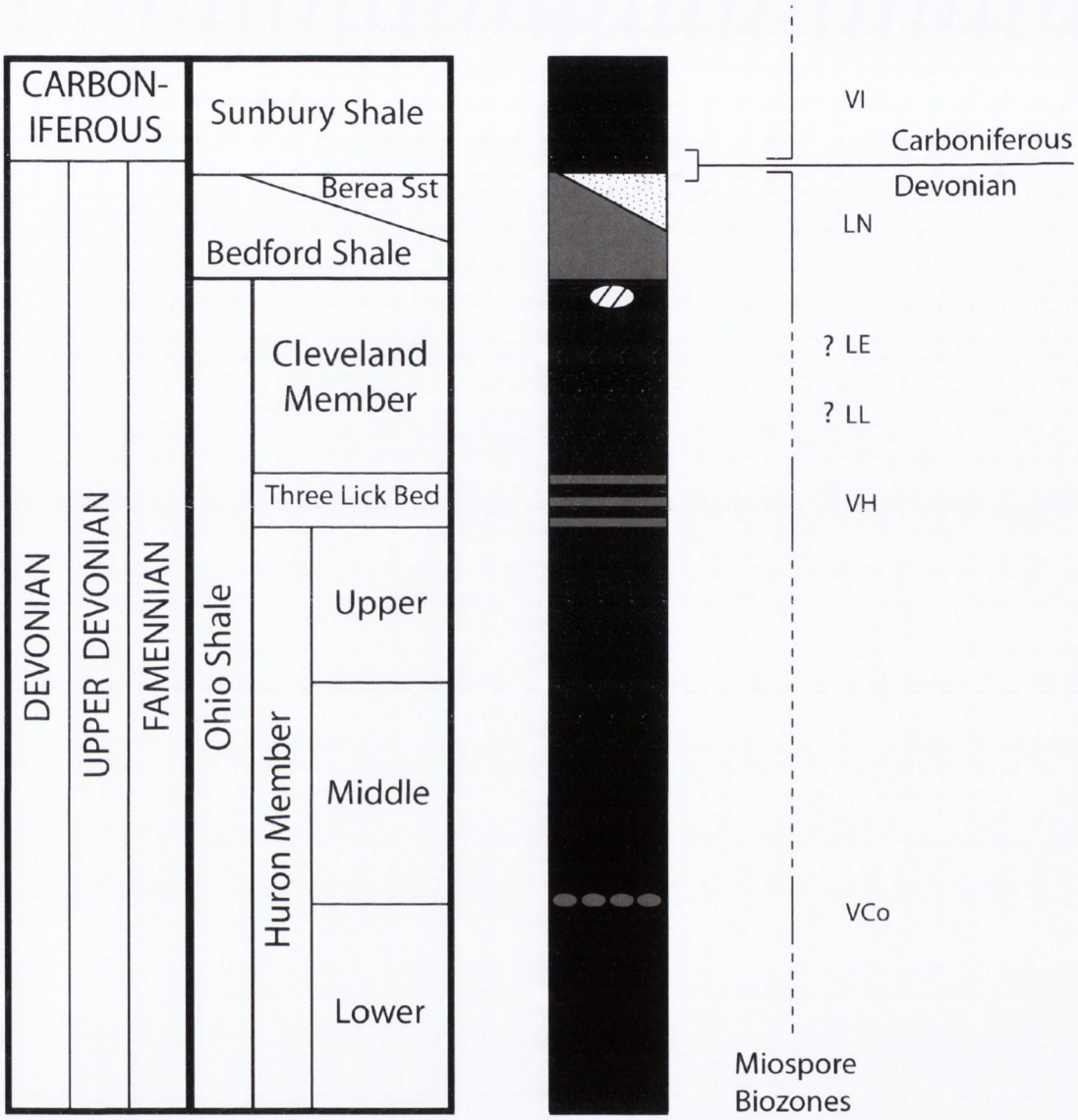

Figure 2.2. Generalised Famennian stratigraphy in northeastern Kentucky alongside known associated Miospore biozones. Question marks denote the speculative location of the LE and LL Misospore biozones.

The interbedded grey shales of the *Protosalvinia* Zone, found in northeastern Kentucky, have been placed within the VCo Miospore Biozone (Rooney *et al.*, 2013) (Figure 2.2) and contain trace fossils that include *Zoophycos, Planolites, Phycodes, Chrondites, Teichichnus*, and *Rhizocorallium* (Griffith, 1977; Jordan, 1980). Fossils are relatively rare throughout the rest of the Huron Member, with benthic forms being especially rare. However, plankton (spores, chitinozoans, algae, and radiolarians), nektoplankton (ostracods, conodonts), epiplankton

(brachiopods, bivalves, crinoids, and graptolites that attached to floating logs), and nekton (fish remains and cephalopods) have been locally reported (Barron and Ettensohn, 1981).

The proportion of terrestrially derived inertinite and vitrinite relative to the marine derived liptinite increases through the Huron Member: the trangressive Lower Huron Member > 5 %, the regressive Middle Huron Member 15 %, and the transgressive Upper Huron Member 23 % (Rimmer *et al.*, 2004). Since the proportion of terrestrially derived inertinite and vitrinite increases upsection, regardless of transgressive or regressive facies, it is unlikely that the increase in terrestrial material is due to an increase in proximity to the shoreline brought about by sea level fluctuation. As mentioned above, this increase in terrestrial organic matter may be due to the expansion of terrestrial ecological niches in the Late Devonian, described by Algeo *et al.* (1995) as the "Devonian Explosion."

2.3.1.2 Three Lick Bed

The grey shale units of the Three Lick Bed contain less organic matter than the intervening black shales and may be intensely bioturbated. They also contain burrows and some *Lingula*-like inarticulate brachiopods, agglutinated foraminifera, ostracods and palynomorphs (Barron and Ettensohn, 1981). Based on the palynomorph assemblage and the absence of *Retispora lepidophyta*, the Three Lick Bed has been assigned to the Late Devonian VH Miospore Biozone (Clayton *et al.*, 2012) (Figure 2.2). The proportion of terrestrially derived inertinite and vitrinite relative to the marine derived liptinite increases again, up to 30 %, in the Three Lick Bed, and remains at this proportion through the Cleveland Member and the Sunbury Shale (Rimmer *et al.*, 2004).

2.3.1.3 Cleveland Member

Body fossils and trace fossils are rare in the Cleveland Member, with the complete absence of benthic forms (Mason *et al.*, 2012). Instead, fossils within this unit represent organisms that maintain a nektic or planktic lifestyle, and mainly consist of fish remains (teeth, scales and bones), conodonts, palynomorphs and the occasional linguloid brachiopod (Ettensohn *et al.*, 2009). The palynomorphs found in the Cleveland Member are of low taxonomic diversity making it difficult to assign the entire unit to a particular miospore biozone. However, the top of the section has been assigned to the latest Famennian LN Miospore Biozone (Heal, 2009).

The Cleveland Member of the Ohio Shale might be the first unit in this stratigraphic sequence associated with the Hangenberg Event. The Hangenberg Event is defined at the base of the Hangenberg Black Shale in Germany, which corresponds to the base of the LN Miospore Biozone (Higgs and Streel, 1994). The base of the Hangenberg Black Shale corresponds to faunal

extinction, which is the first phase of extinction recognised within the Hangenberg Event (Myrow *et al.*, 2011). Therefore, the top of the Cleveland Member may also correlate with the onset of faunal extinction at the base of the LN Miospore Biozone (Figure 2.2). As previously mentioned in Chapter 1, the LL Miospore Biozone corresponds to widespread transgression and the LE and LN miospore biozones relate to the beginning of global regression and the onset of latest Famennian glaciation (Kaiser *et al.*, 2008; Streel *et al.*, 2012; Wicander *et al.*, 2011). Due to the low taxonomic diversity encountered in the Cleveland Member, the boundaries between these biozones have not been located. If continuous depositon took place from the top of the Three Lick Bed (VH Miopore Biozone) through to the base of the Bedford Shale, it can be suggested that the VH-LL, LL-LE and LE-LN miospore biozone boundaries are likely to exist within the Cleveland Member. However, their identification has not yet been made.

The ribbed character of the Cleveland Member represents changes in organic carbon content within the shales (Ettensohn *et al.*, 2009). This may have been due to periodic increases and decreases in phytoplankton productivity, changes in the amount of fine-grained mud reaching the basin or cyclic variations in the amount of terrigenous detrital plant matter reaching the basin (Mason *et al.*, 2012).

2.3.2 Bedford Shale with miospore zonation after Coleman and Clayton (1987)

Fossils within the Bedford Shale are generally preserved as casts, molds or through pyritic replacement, and typically occur in patchy deposits of both articulated and disarticulated shells (Pashin and Ettensohn, 1992a). The fauna is generally most abundant immediately above the black shale of the Cleveland Member, and is dominated by infaunal brachiopods, such as *Lingula* and similar to the Three Lick Bed. Horizontal burrows filled with pyrite are common within the formation and bioturbation is often found within the siltstone layers of the Bedford Shale in northeastern Kentucky. Palynomorphs within the Bedford Shale are of higher taxonomic diversity in comparison to the underlying Ohio Shale, permitting the assignment of the entire Bedford Shale to the latest Famennian LN Miospore Biozone (Coleman and Clayton, 1987) (Figure 2.2). This stratigraphic age indicates that the deposition of the Bedford Shale was during the Hangenberg Event, possibly coinciding with the second phase of extinction that led to the disappearance of the *lepidophyta* complex (Streel, 1986). The last recorded LN miospore assemblage, containing non-reworked *Retispora lepidophyta*, has been located approximately 10 cm from the top of the Bedford Shale in northeastern Kentucky (Coleman and Clayton, 1987).

2.3.3 Sunbury Shale with miospore zonation after Coleman and Clayton (1987) and Heal (2009)

The uppermost part of the Sunbury Shale is bioturbated. Fossils are generally rare throughout the rest of the unit, with the occasional appearance of linguloid or orbiculoid brachiopods and conodonts (Pepper *et al.*, 1954). The lag deposit at the base of the Sunbury Shale also contains some conodonts and a variety of phosphatic fish remains (teeth, scales, spines and broken dermal plates). The palynomorph assemblage within the Sunbury Shale is of low taxonomic diversity; therefore, the definitive assignment of the entire formation to a miospore zone has proven difficult. However, due to the complete lack of *Retispora lepidophyta* within the miospore assemblage, the Sunbury Shale has been assigned to the earliest Carboniferous VI Miospore Biozone (Coleman and Clayton, 1987; Heal, 2009) (Figure 2.2). The lowest recorded VI Miospore Biozone assemblage was obtained 15 - 20 cm above the base of the Sunbury Shale. Therefore, the boundary between the Devonian and Mississippian systems is either at, or very close to the base of the Sunbury Shale. Conodonts reported from the unit (*Siphonodella*) support this age, placing the Sunbury Shale in the early Carboniferous (De Witt, 1970; Eames, 1978; Hass, 1947; Sandberg *et al.*, 2002).

2.4 DEPOSITIONAL ENVIRONMENT

2.4.1 Ohio Shale

The presence of logs of land plants within the Ohio Shale most likely represents material washed into the epicontinental sea from the surrounding land masses. As such, the fossils present in the Ohio Shale appear to indicate a normal marine or brackish-water environment of deposition (Schwietering, 1979).

2.4.1.1 Huron Member

Based on geochemical analyses carried out by Perkins *et al.* (2008), Rimmer (2004) and Rimmer *et al.* (2004), the Huron Member was deposited under predominantly anoxic conditions, with intermittent dysoxic conditions. Investigation of these units has led to the interpretation of a transgressive-regressive sequence, where the lower and upper Huron Members document transgression and the middle Huron Member represents the regressive phase of the sequence (Ettensohn, 1992). The *Protosalvinia* Zone consists of regressive black shales with interbedded grey shales that represent sediment accumulation below the pycnocline in an oxic cratonic basin (Ettensohn *et al.*, 1988).

2.4.1.2 Three Lick Bed

Due to the fossil assemblage and the presence of burrows, a higher oxygen concentration is suggested for the greenish-grey shale beds of the Three Lick Bed (Provo *et al.*, 1978), in comparison to the underlying black shales of the Huron Members. A 'Tyson Plot' of amorphous organic matter, palynomorphs and phytoclasts ('woody' material) suggests that the grey shales were deposited in an oxic shelf environment, while the intervening black shales were deposited in a distal suboxic-anoxic basin setting (Clayton *et al.*, 2012). However, the presence of linguloid brachiopods within the grey shale beds suggests that oxygen concentrations still remained relatively low. It is suggested that the bottom waters coincided with the pynocline, leading to a dysaerobic environment. The three grey shale beds are considered to represent three brief periods of sea-level lowstand that coincided with major deltaic progradation from the north and east, whereas the intercalated two black shale beds are of deeper marine origin, similar to the depositional environment of the Huron Shale Member (Ettensohn *et al.*, 2009).

2.4.1.3 Cleveland Member

Due to the presence of finely disseminated organic matter, the absence of benthic fossils and the presence of pyrite and siderite nodules, a deepwater, anoxic, basin floor environment has been suggested for the Cleveland Member (Ettensohn and Barron, 1981) (Figure 2.6). For anoxic conditions to prevail, the marine basin may have been density stratified (warmer, less saline water sitting on top of colder more saline bottom waters) which may have cut off circulation between the oxygen rich surface waters and the oxygen-poor bottom waters, creating an anoxic benthic environment.

Rimmer (2004) used trace element ratios (Ni/Co, V/Cr, V/(V+Ni) and Mo concentration) and C-S-Fe plots to assess redox conditions in the Upper Devonian black shales from Kentucky. Perkins *et al.* (2008) also used trace element ratios (V/Mo, Cr/Mo) to assess redox conditions in the same stratigraphy. Their interpretations are shown in Figure 2.3. Different trace element ratios provided each study with slightly different results for the redox conditions expected at the time of deposition. However, in the data provided by Perkins *et al.* (2008), sampling resolution did not appear to be high enough within the Cleveland Member (6 samples) to make a distinct determination between the redox conditions present during the deposition of the upper and lower units.

Algeo (2004) analysed ratios of (Mo/Al)/TOC and (V/Al)/TOC and found a slight enrichment in V within the upper middle Cleveland Member, and a depletion in Mo throughout the upper Cleveland Member. The ratio of these two, TOC corrected, trace elements would then support lower oxic conditions within the lower Cleveland Member relative to the upper Cleveland

Member, as suggested by Perkins *et al.* (2008), although Algeo (2004) suggested that the depletion of Mo in the upper Cleveland may have resulted from the successive deposition of black shales, leading to a drawdown in the inventory of trace elements, such as Mo in the upper ocean. However, a constant nutrient inventory would be required to sustain the primary productivity that led to the deposition of organic-rich black shales. Algeo (2004) based his redox interpretations on the degree of pyritisation of total Fe (DOP_T), which recorded the majority of the shales as being anoxic. Taking all this data into account, it is likely that denitrification was active during the deposition of the majority of the Famennian black shales in Kentucky, although possibly under varying levels of intensity.

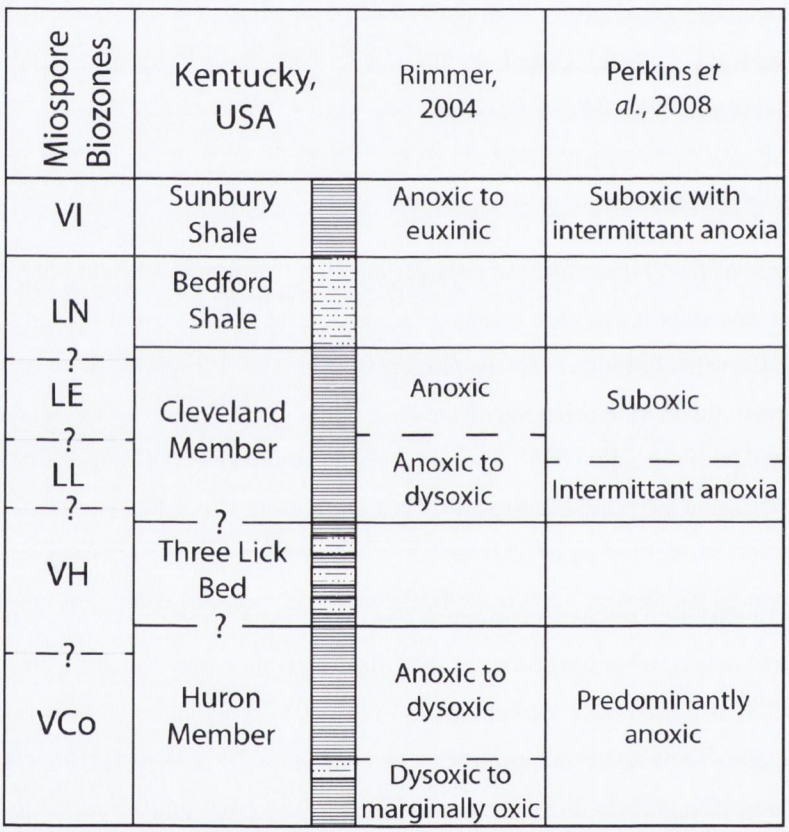

Figure 2.3. Summarised oxic conditions within the northeastern Kentucky shales, based on geochemical analyses carried out by Perkins *et al.* (2008) and Rimmer (2004), shown alongside the generalised stratigraphy and known Miospore Biozones.

The presence of the Robinson Dropstone (Figures 2.4 and 2.5) at the top of the Cleveland Member has led to the interpretation that alpine glaciation took place at this time on the adjacent Acadian highlands to the east. This is further evidenced by a temporally equivalent diamictite deposit found approximately 500 kilometres to the east in Maryland and Pennsylvania (Clayton *et al.*, 2010). As the base of the LN Miospore Biozone has been placed within the upper Cleveland Member (Heal, 2009), the upper Cleveland Member may be considered to be contemporaneous with global cooling and continental glaciation which took place in the high southern latitudes of Gondwana, as evidenced by glacial deposits located in South America and Africa (Caputo and Crowell, 1985; Crowell, 1999; Streel *et al.*, 2000; Streel *et al.*, 2012; Wicander *et al.*, 2011). However, transgression associated with the Hangenberg Black Shale in Germany may also coincide with the top of the Cleveland Member, as this marks the beginning of the LN Miospore Biozone. It remains to be established whether the upper Cleveland Member coincides with the onset of glaciation, or transgression. Additional palynological studies of the Cleveland Member may help to determine the depositional history of this unit further.

Figure 2.4. The granitic 'Robinson Dropstone' located near Morehead, northeastern Kentucky.

Figure 2.5. The Robinson Dropstone. The dropstone stratigraphically sits at the top of the Cleveland Member, and was once overlain by the black shales of the Cleveland Member that have since been eroded. The contact between the Cleveland Member and the dropstone can be seen in this image.

2.4.2 Bedford Shale

The olive green colour of the Bedford Shale, due to the presence of the clay minerals illite and chlorite, suggests that it was deposited in a dysaerobic environment, as there was enough oxygen in the water column to thoroughly oxidise the organic matter, but not enough oxygen to deposit iron oxides, such as hematite, as this would have imparted a red colour on the shales. This is further supported by the presence of a depauperate fauna typical of dysaerobic settings (Kammer, 1985; Pashin and Ettensohn, 1992b) and the presence of pyrite and siderite nodules, of which both are stable under reducing conditions (Garrels and Christ, 1965).

Wave ripples are present on some of the siltstone beds, indicating that the Bedford / Berea sequence may represent a series of storm dominated shelf deposits in the northeastern Appalachian basin, where the majority of the Bedford Shale was likely deposited at the distal margins of a mud-rich turbiditic slope (Pashin and Ettensohn, 1987) (Figure 2.7). However, recent interpretations of the ongoing Acadian orogeny have led to the possibility of alpine glaciation on the adjacent Acadian highlands to the east, which appear to be contemporaneous with global cooling and glaciation centred around the palaeo-South Pole. This has led to the interpretation that the Bedford Shale represents distal lowstand deposits related to alpine glaciation in the adjacent highlands (Brezinski *et al.*, 2010).

2.4.3 Sunbury Shale

The Sunbury Shale is thought to have been deposited under similar conditions to the Cleveland Member of the Ohio Shale due to their similar lithologies. However, the Sunbury Shale represents the deepest, most organic-rich and most widespread of the all the basinal black shale units studied herein (Ettensohn, 2008).

As previously discussed, conflicting views exist regarding the redox conditions that existed during the deposition of the sediments (Figure 2.3), where redox conditions for the Sunbury Shale range from suboxic to euxinic (Perkins *et al.*, 2008; Rimmer, 2004; Rimmer *et al.*, 2004). Rimmer (2004) plotted the concentration of the element molybdenum (Mo) against the Ni/Co ratio. This was used as a proxy for redox conditions as the ratio of Ni/Co has been used as an indicator of oxygen levels (Dypvik, 1984) and Mo becomes enriched in sulphate reducing environments (Dean *et al.*, 1997). The relationship between Ni/Co and Mo can therefore be used as a proxy for redox conditions as long as Mo has good correlation with the C_{org} content in the samples. This led to the conclusion that the Sunbury Shale was deposited under anoxic to euxinic conditions.

Perkins *et al.* (2008) used the V/Mo ratio to show that the Sunbury Shale was predominantly suboxic with intermittent anoxia through the middle of the formation. It was suggested that as vanadium (V) accumulates under both suboxic and anoxic conditions, and Mo accumulates predominantly under reducing anoxic conditions, the ratio of V/Mo may be a better proxy for anoxia than Mo plotted against Ni/Co . Rimmer (2004) used many other proxies, including C-S-Fe plots, V/Cr, and V/(V + Ni) and degree of pyritisation, to infer anoxia during the deposition of the Sunbury Shale. Taken together, these studies conclude that redox conditions were at least suboxic during the deposition of the Sunbury Shale, with intermittent periods of anoxia occurring within the unit.

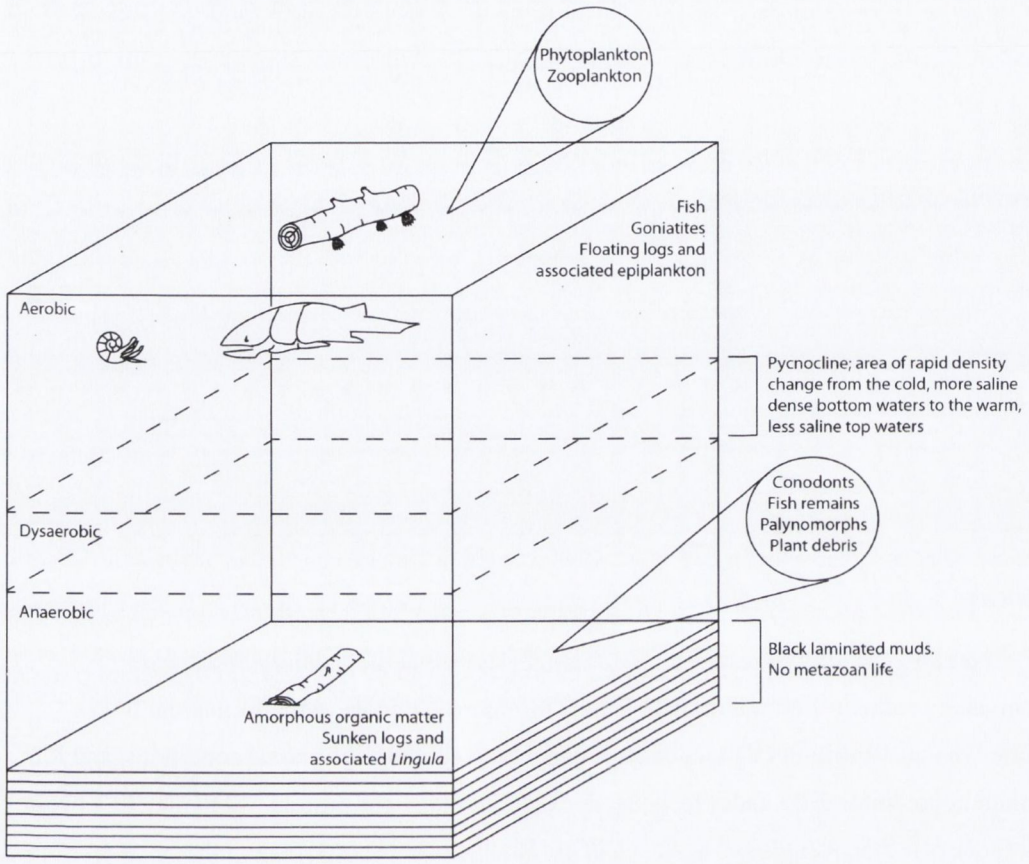

Figure 2.6. Interpreted depositional environment based on anoxic bottom water conditions during deposition of the majority of the black shales. Modified from Barron and Ettensohn (1981). Not drawn to scale.

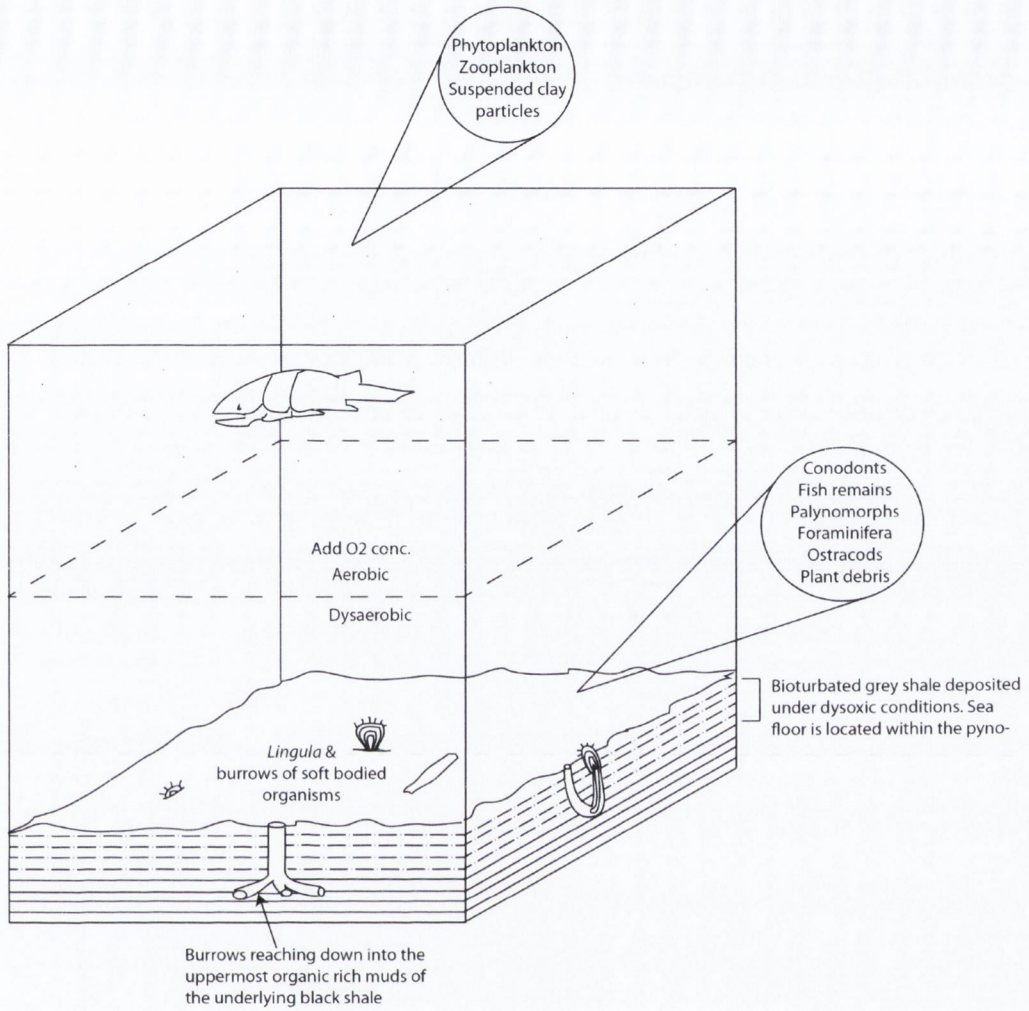

Figure 2.7. Interpreted depositional environment based on dysoxic bottom water conditions during the deposition of the majority of the grey shales. Modified from Barron and Ettensohn (1981). Not drawn to scale.

2.5 GLOBAL CORRELATION

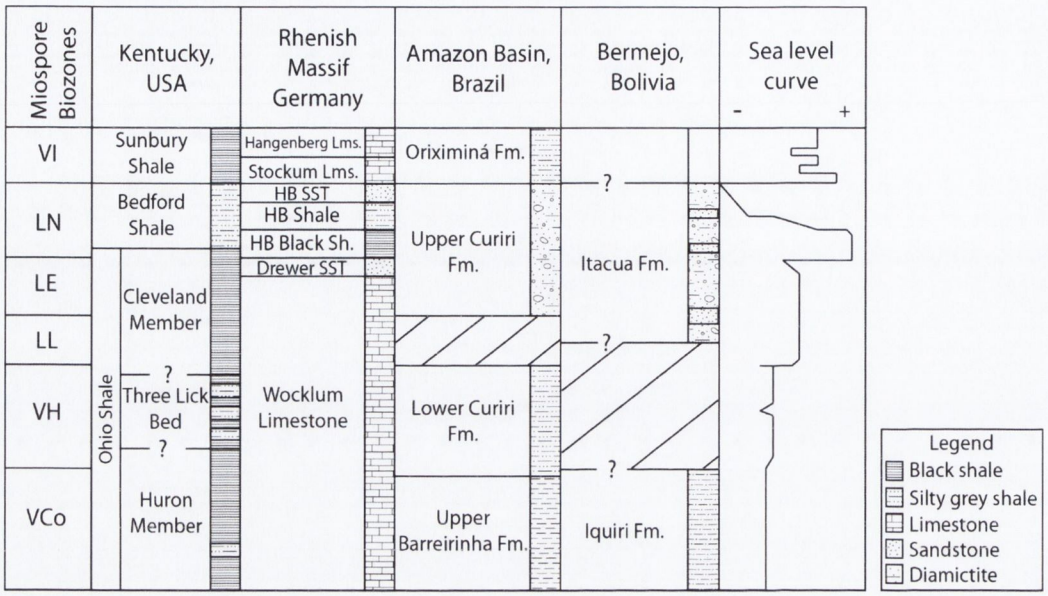

Figure 2.8. Global late Devonian stratigraphic correlations. Kentucky stratigraphy is based on Clayton *et al.*, (2012) and Coleman and Clayton, (1987). German stratigraphy is based on Kaiser *et al.* (2008) and Streel *et al.* (2012). Brazilian stratigraphy is based on Melo and Loboziak, (2003). Bolivian stratigraphy is based on Wicander *et al.* (2011). Sea level curve is based on Streel *et al.* (2012) and Johnson *et al.* (1985).

Kaiser *et al.* (2011) used the Late Devonian sequence stratigraphic successions of the Rhenish Massif in Germany (Figure 2.8) as a reference for event phases for the Hangenberg biotic crisis. This locality records a shallowing upwards sequence in the Wocklum Limestone, which culminates in a lowstand deposit, recorded by the Drewer Sandstone (Bless, 1993). This is followed by the deposition of the transgressive Hangenberg Black Shale (HBS), representing a phase of maximum flooding within the Middle *praesulcata* Conodont Zone (Becker, 1996) and the LN Miospore Biozone (Higgs and Streel, 1994). The globally recognised faunal extinction takes place at the base of the HBS (Caplan and Bustin, 1999). The beginning of regression is marked by the green-grey, silty Hangenberg Shale, followed by the maximum lowstand deposition of the Hangenberg Sandstone, within the upper Middle *praesulcata* Conodont Zone and the LN Miospore Biozone. Because these are regressive facies, they have been correlated with the Bedford Shale of Kentucky, which has also been assigned to the LN Miospore Biozone (Coleman and Clayton, 1987). This regression is thought to have led to the second phase of extinction within the Hangenberg biotic crisis, which led to a decline in conodonts, miospores and acritarchs towards the end of the Devonian (Becker, 1993; Riegel, 2008). The Hangenberg Sandstone is overlain by the Stockum Limestone, marking the initiation of transgression. However a slight sea level fall within the Stockum Limestone is recorded at the D/C boundary.

The overlying Hangenberg Limestone appears to record a return to normal marine conditions within the VI Miospore Biozone.

If this sequence of events is superimposed on to the stratigraphy in Kentucky, the majority of the HBS should correlate to the top of the Cleveland Member of the Ohio Shale, and possibly to the base of the Bedford Shale. This would imply that below the HBS-equivalent sediments at the top of the Cleveland Member, there exists a shallowing upwards sequence, most likely recorded within the remainder of the lower Cleveland Member. As mentioned above, the Bedford Shale would appear to be equivalent to the regressive Hangenberg Shale and Sandstone units. This suggests that the upper Bedford Shale records a globally recognised lowstand. The trangressive shales of the Sunbury Shale are most likely equivalent to the Stockum and Hangenberg limestones, where short sea level falls, corresponding to those in the Stockum Limestone, may have also have taken place at the base of the Sunbury Shale.

2.6 PALAEOCLIMATE

Globally recognisable lithology changes near the Devonian / Carboniferous boundary are thought to be due to eustatic sea-level changes (Becker, 1996; Bless, 1993), brought about by the waxing and waning of high latitude glaciers (Streel *et al.*, 2000). The deposition of diamictites in Brazil and Bolivia took place during the LE-LN miospore biozones (Díaz-Martínez *et al.*, 1999; Melo and Loboziak, 2003; Perez-Leyton, 1991; Streel *et al.*, 2012; Wicander *et al.*, 2011), and possibly also during the LL Miospore Biozone in Bolivia (Wicander *et al.*, 2011). Both the Bedford Shale and the top few centimetres of the upper Cleveland Member have been assigned to the LN Miospore Biozone (Coleman and Clayton, 1987; Heal, 2009). The glacigenic strata found in Maryland and Pennsylvania, USA, are contemporaneous with the Bedford Shale and the upper few centimetres of the Cleveland Member in Kentucky, where the granitic Robinson Dropstone was found (Brezinski *et al.*, 2009).

The development of glaciers in the low palaeo-latitudinal position of the rising Acadian Mountains (~25°S – 30°S) most likely took place after the initial development of higher latitude glaciers on Gondwana. The LE Miospore Biozone has not yet been located within the stratigraphy in Kentucky, however, if it does exist, it is likely to be found within the Cleveland Member of the Ohio Shale Shale, below the horizon that contains the Robinson Dropstone. Because glacial deposits have been located within the LE, and possibly the LL miospore biozones in South America, it may be possible that glaciers were developing on the adjacent Acadian Mountains at this time. The development of glaciers on the Acadian Mountains are likely to be, at least in part as a result of changing climatic conditions within the latest Famennian, although, it is also likely that alpine glaciers developed alongside the increasing altitude of the emerging Acadian

Mountains. However, to carry a dropstone, weighing approximately 3 tonnes, to the deep marine sediment of the Cleveland Member, it is likely that an iceberg calved off a glacier at or near sea-level, which would require more than localised altitude changes to account for the glacial activity in this region.

Dropstones and diamictites are more likely to be deposited during the melting phase of a glacier rather than during their initial growth and development. Therefore, this period may be diagnostic of a period of both glacial cooling and interglacial warming. Considering that the glacial period may have lasted up to 3 million years (Wicander *et al.*, 2011), it is likely that the climate fluctuated throughout this period. Ice age cycles within the Pleistocene often follow a 'sawtooth' shape, where the slow build up of ice is often followed by relatively abrupt melting during the interglacial periods (Lisiecki and Raymo, 2007). This may also be true of glaciations recorded during the Late Devonian.

Chapter 3

Materials and Methods

3.1 MATERIALS

Materials studied in order to carry out this research include bulk shale samples from Kentucky, extracted *Tasmanites* specimens, extracted *Protosalvinia* thalli from various localities within North America and Brazil, and extracted *Protosalvinia* spores. Samples of Tasmanite Oil Shale, containing large, easily extractible specimens of *Tasmanites* were obtained from Tasmania in order to perform preliminary chemical and thermal maturation tests. *Tasmanites* were chosen for this project because they are a widely occurring and long ranging genus (Proterozoic - Recent) found in marine settings. *Tasmanites* are relatively large when compared to other common palynomorphs, allowing for easier extraction from the rock matrix, whilst also requiring a smaller number of extracted specimens per sample for stable isotope analysis.

The chosen stratigraphic interval, covered in more detail in Chapter 2, coincides with recognised glaciation and deglaciation around the palaeo-south pole, in addition to coeval glacial deposits identified to the east of the Appalachian Basin, ensuring good stratigraphic coverage of known climate changes. The Upper Devonian – Lower Carboniferous shales, analysed within this thesis, are organised into two main lithologies, organic-poor grey shale and organic-rich black shale. The grey shale contains a higher proportion of spores and terrestrial material than the black shales, which are dominated by amorphous organic material (AOM) and marine fossils, such as prasinophycean algae (*Tasmanites*, *Leiosphaeridia*), acritarchs, fish teeth and scales.

3.1.1 Bulk samples

Bulk organic residues were prepared from the collected shale samples, as outlined in Section 3.3. The stable nitrogen isotope signature of the bulk organic residues was analysed as part of this project to provide a stratigraphic comparison to the extracted *Tasmanites* specimens. The bulk organic contents of these shales ranges from terrestrial plant material to marine fish remains, therefore the isotopic signature of the bulk organic residues is a mixture of various organic components, each carrying their own distinct $\delta^{15}N$ value. The organic-rich black shales (TOC 7-12 %, Perkins *et al.*, 2008) are overwhelmingly comprised of amorphous organic material (AOM), which likely contributes the majority of the $\delta^{15}N$ signal within the black shale units. The grey shale units contain very little, if any, AOM, and the overall organic carbon content typically remains below 0.5 % (Perkins *et al.*, 2008). The organic components found within the grey shale units are typically a mixture of terrestrial plant material, spores, prasinophytes, acritarchs and fish remains. It is therefore likely that the bulk $\delta^{15}N_{org}$ signal obtained from the grey shales is a mixture of these components.

3.1.2 *Tasmanites* spp.

Tasmanites is a thick walled, spherical palynomorph, belonging to the prasinophyte algae (Tappan, 1980). It is a widely occurring and stratigraphically long-ranging genus, ranging from Proterozoic – Recent (Wicander and Playford, 2008). Newton (1875) erected this genus, because of its abundance within the Tasmanian 'Tasmanite' and the Australian 'White Coal'. The modern, living equivalent of *Tasmanites,* is thought to be *Pachysphaera* (Boalch and Guy-Ohlson, 1992; Wall, 1962). The fossil specimen however, generally possess thicker walls. It has been suggested that *Tasmanites* had a two phase life cycle; a motile and non-motile phase (Guy-Ohlson, 1988). The fossil phycomata commonly found dispersed in sediments are representative of the non-motile, cyst forming phase. The pore structure, noted by Newton (1875) in his description of *Tasmanites*, appears to be dependent upon the developmental stage at the time of deposition and the state of preservation (Guy-Ohlson and Boalch, 1992). Many of the specimens analysed as part of this thesis did not contain obvious pores within the surface of the fossil, however they are all thought to belong to *Tasmanites* spp. (Figure 3.1).

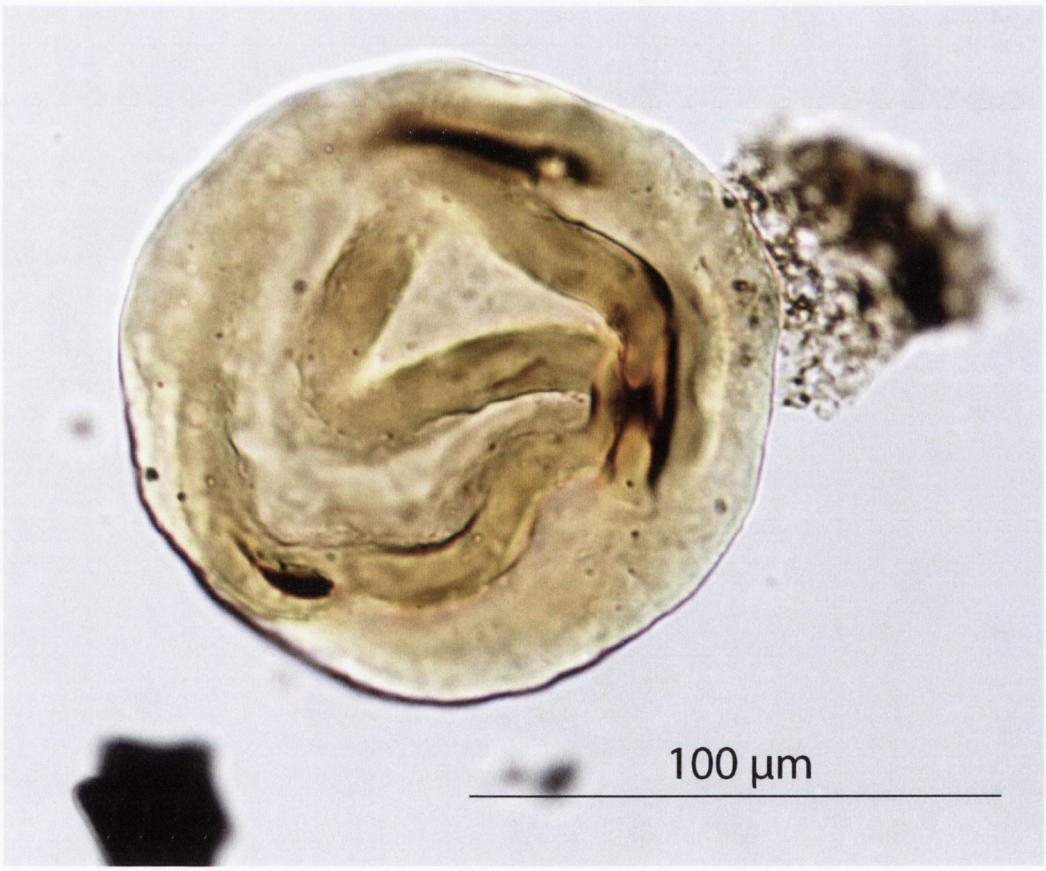

Figure 3.1. *Tasmanites* spp., extracted from the Cleveland Member of the Late Devonian stratigraphy in northeastern Kentucky.

Prauss and Riegel (1989) noted that the distribution of mass occurrences of prasinophyte algal fossils, such as *Tasmanites* and *Leiosphaeridia*, are associated with high palaeolatitudes and epicontinental, often near-shore environments. The correlation of prasinophyte mass occurrences to black shale formation was suggested to be due to density stratification, controlled by a thermocline or a halocline, rather than an area of upwelling. However, many of the shales studied as part of this thesis contain high numbers of *Tasmanites*, in conjunction with normal marine fossil phytoplankton assemblages, suggesting that upwelling may have facilitated in the development of the organic-rich black shales. The rocks studied herein were deposited in a low latitudinal, epicontinental setting, perhaps reflecting density stratification and brackish or marginal marine settings (Ettensohn, 2008; Mason *et al.*, 2012).

Revill *et al.* (1994) proposed that *Tasmanites* found in the Tasmanite Oil Shale occupied an environmental niche similar to modern sea-ice diatoms, forming algal blooms in an area supplied with meltwater from surrounding glaciers. Glacial deposits recognised on the eastern margin of the Appalachian Basin may help to explain the relatively low latitudinal setting in which these Late Devonian *Tasmanites* have been deposited. However, modern prasinophytes are also found in large quantities within the Mediterranean Sea, located approximately 35°N (Siokou-Frangou *et al.*, 2010), therefore the occurrence of large numbers of prasinophytes within the Late Devonian Appalachian Basin is not suggested to be anomalous.

Modern prasinophycean algae are light dependent, but have the ability to move vertically in the water column from 10 m in depth down to 100 m (Vigran *et al.*, 2008), possibly improving their ability to assimilate nutrients. Ackmann *et al.* (1970) suggested that modern prasinophyte blooms are related to the enrichment of the water column by nitrogen and phosphates. The availability and isotopic signature of nitrogen can vary according to climatic and palaeogeographic changes, such as those that occurred during the Late Devonian. It is therefore hoped that the analysis of the $\delta^{15}N$ signature of *Tasmanites*, in contrast to their associated bulk shale, may help to explain nutrient conditions and some of the known climatic changes which occurred during the deposition of the Upper Devonian organic-rich black shales within the Appalachian Basin.

Tasmanites were found in nearly all of the Upper Devonian – Lower Mississippian Kentucky shale samples analysed for this project. However, their abundance and size changes dramatically from sample to sample, most obviously observed in the grey shale horizons, where *Tasmanites* decrease in both abundance and size. For example, *Tasmanites* extracted from the Cleveland Member measure approximately 100 – 200 µm in diameter, and contain between 200 - 400 specimens per gram, whereas the overlying Bedford Shale contains <5 *Tasmanites* per gram, which measure approximately 80 - 100 µm in diameter. However, there are clear dilution effects

to be taken into account, such as the increase in clay minerals (mostly illite) in the grey shales, as opposed to the black shales which are dominated by AOM. Either way, for the purposes of extraction and analysis, both the grey and black shales each bear their own set of unique difficulties which must be overcome in order to perform stable nitrogen isotope analyses on the *Tasmanites* specimens contained in each lithology.

3.1.3 *Protosalvinia* spp.

Protosalvinia Dawson, 1884 is a small fossil plant of probable algal origin that occurs in abundance through a thin but widespread stratigraphic interval within the Upper Devonian (Famennian) black shale successions in the Appalachian, Illinois and Michigan basins of the USA (Over *et al.*, 2009). It has also been reported from the Michigan Basin in Canada (Russell, 1985) and the Amazon Basin of Brazil (Niklas *et al.*, 1976; Loboziak *et al.*, 1997).

The natural affinities of *Protosalvinia* remain uncertain. It has been assigned by some authors (e.g., Schopf and Schwietering, 1970; Niklas, 1976) to the order Fucales (brown algae) but has been considered by others (e.g., Niklas and Phillips, 1976; Gray and Boucot, 1977) to be transitional between algae and bryophytes. The biomolecular signature of *Protosalvinia* is neither distinctly marine, nor distinctly terrestrial (Mastalerz *et al.*, 1998).

Several species of *Protosalvinia* have been erected, but Niklas and Phillips (1976) convincingly demonstrated that of the three of the most commonly recorded, *P. ravenna*, and *P. furcata* were different ontogenetic stages of *P. arnoldii*. Significantly, all three forms produced identical spore tetrads in hypodermal conceptacles on the thalli (Niklas and Phillips, 1976). These authors also interpreted the tetrads as meiotic products of a sporangium, and noted the presence of sporopollenin. Taylor and Taylor (1987) noted that the durable nature of *Protosalvinia* spores compares closely with that of spores produced exclusively by modern land plants, but also pointed out that the spore wall architecture does not correspond to that of any known fossil or living spore. Taylor and Taylor (1987) also agreed with Niklas and Phillips (1976) that the presence of a distinct suture beneath the proximal trilete mark firmly establishes the meiotic nature of the tetrad.

Loboziak *et al.* (1997) noted the presence of a large (90 – 250 μm) *Retusotriletes* sp. in dispersed miospore assemblages from the same stratigraphic interval as *Protosalvinia* spp. in the Amazon basin. They described this taxon as "Thick-walled (6-10 μm), smooth retusoid miospores with winged curvaturae" and suggested that it may have been derived from *Protosalvinia*.

Samples of *Protosalvinia* were collected from two localities, both roadcuts, near Vanceburg and Morehead in eastern Kentucky, USA, in order to confirm the tentative assertion of Loboziak *et al.* (1997) concerning the nature of the spores produced by *Protosalvinia*, and to erect a new

species to accommodate these spores. It is anticipated that this will facilitate the recognition of the *Protosalvinia* Zone in some successions where the parent plant is absent.

Protosalvinia spp. (Figure 3.2) occur abundantly through the lowermost 3 m of the middle Huron Member of the Ohio Shale, constituting the '*Protosalvinia* Zone.' The only other macroplants recorded are indeterminate coalified stems. The *Protosalvinia* Zone consists of regressive black shales with interbedded grey shales that represent sediment accumulation below the pycnocline in an anoxic cratonic basin (Ettensohn *et al.*, 1988).

Figure 3.2. *Protosalvinia* thalli extracted from the Huron Member of the Upper Devonian units, along the I64E, northeastern Kentucky.

Recent conodont work by Over *et al.* (2009) correlated occurrences of *Protosalvinia* in the eastern United States from the Uppermost *marginifera* Zone, up to the Lower *expansa* Zone, or the GF Miospore Biozone, up to the VCo Miospore Biozone, respectively, within the Famennian stage of the Late Devonian. Further samples containing *Protosalvinia* spp. were obtained from six other localities in North America (Figure 3.3) and Brazil (Figure 3.4) in order to carry out a regional and latitudinal stable isotope study of the enigmatic macrofossil. It was hoped that this would provide a time restricted window into the isotopic information within and between the palaeo-basins of North America (Appalachian, Illinois, Michigan and Amazon palaeo-basins), and the possible isotopic change brought about through large palaeolatitudinal differences between North America (~25°S) and Brazil (~55°S).

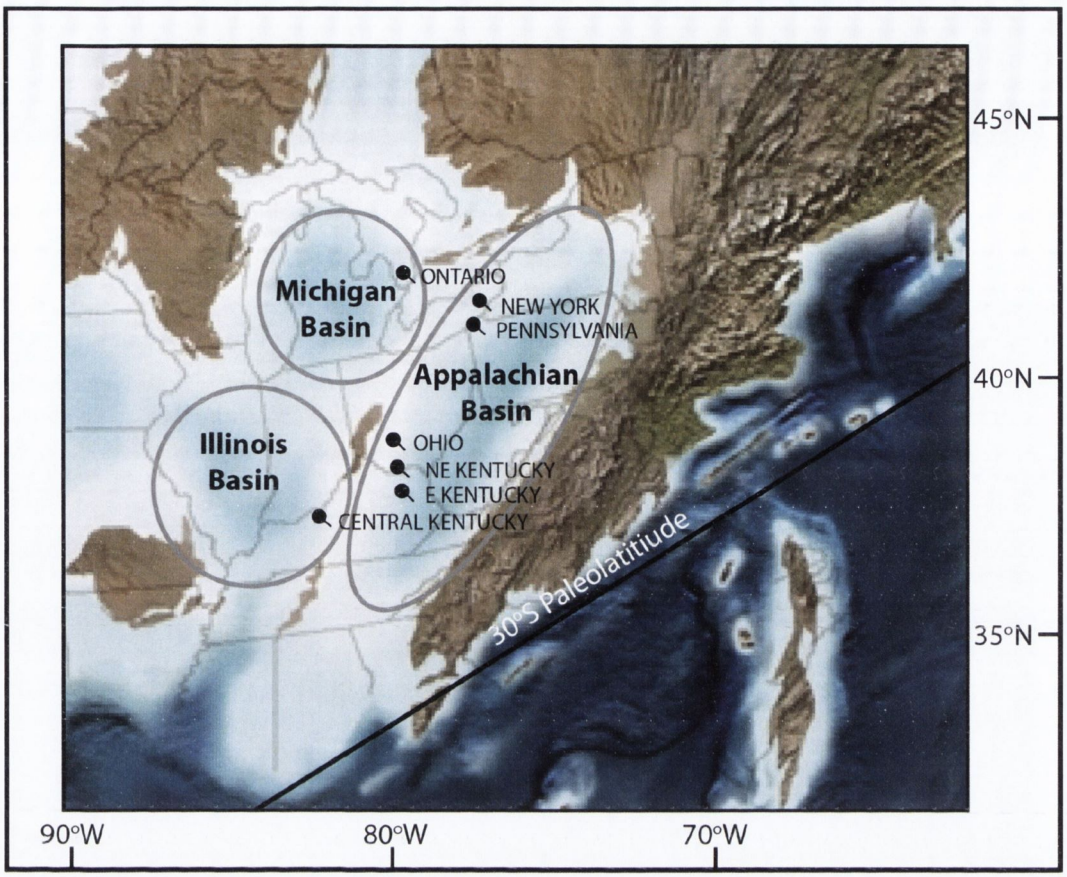

Figure 3.3. *Protosalvinia* sample localities relative to the palaeogeography of the North American Late Devonian basins (modified from Blakey, 2011).

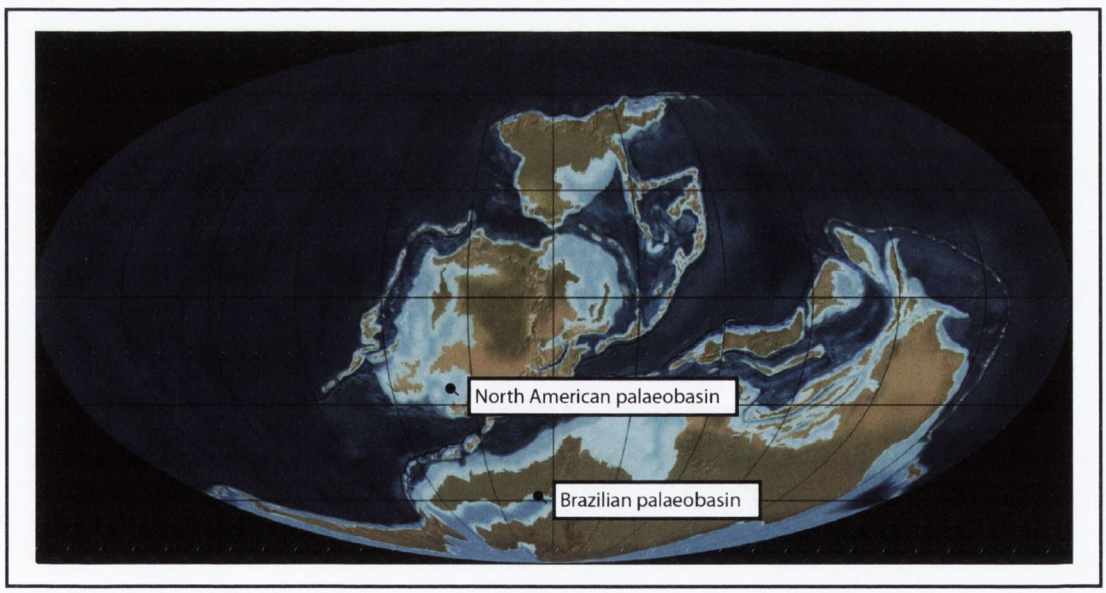

Figure 3.4. Late Devonian palaeogeography, showing the North American and Brazilian basins. (Modified from Blakey, 2011)

The *Protosalvinia* Zone in Brazil is associated with the lower Curiri Formation, which has been assigned to the VH Miospore Biozone (Melo and Loboziak, 2003), making the occurrence of *Protosalvinia* in the Brazilian strata slightly younger than the those found in the North American strata. Samples of *Tasmanites* were also extracted and analysed from four of North American sample localities (eastern and northeastern Kentucky, Ohio and Ontario) to provide further information on the stable isotope signature within and between the Appalachian and Michigan palaeo-basins.

3.2 SAMPLE LOCALITIES

The main samples for this research were obtained from roadcuts located in Lewis and Rowan counties, northeastern Kentucky, USA. The location and stratigraphic position of the samples investigated are shown in Figures 3.3, 3.5 and 3.6.

1. KY10E, N38°35.748', W83°20.566', 2 km east of Vanceburg
2. I64W, N38°10.810' W83°34.081', approximately 14 km west of Morehead
3. KY801N, N 38°9.128' W83°33.098', at the junction with KY1722
4. KY2520N, N38°08.378', W83°32.151', approximately 12km west of Morehead

Samples of *Protosalvinia* were obtained from seven localities in North America and one locality in Brazil:

5. Northeastern Kentucky, KY10E, 2 km east of Vanceburg (same as first locality)
6. Eastern Kentucky; I64E, Huron Member of the Ohio Shale
7. Central Kentucky; I65 and KY245, Clegg Creek Member of the New Albany Shale
8. New York; Twentymile Creek, South Ripley, Ellicot Shale
9. Pennsylvania; Twelvemile Creek, South of Northeast, Ellicot Shale,
10. Ohio; High Banks Metro Park, Columbus, Huron Member of the Ohio Shale
11. Ontario; Five samples covering two meters of stratigraphy were obtained from a core (OGS 82-1, Russell, 1985) taken from the Kettle Point Formation in Lambton County, Ontario.
12. Brazil; 200 m upstream from the ITACIMPASA pier (formerly CAIMA cement industry). S40°21'03 ", W56°12' 02". Amazonas Basin - Curiri Formation.

A sample of the Tasmanite Oil Shale was obtained from the Lower Permian Quamby Group located at Latrobe, Northern Tasmania, Australia. These shales contain large *Tasmanites* (> 500

μm) in abundance and are therefore ideal for the preliminary chemical and maturation tests carried out as part of this project.

13. Northern Tasmania, Australia; Latrobe, Lower Permian Quamby Group

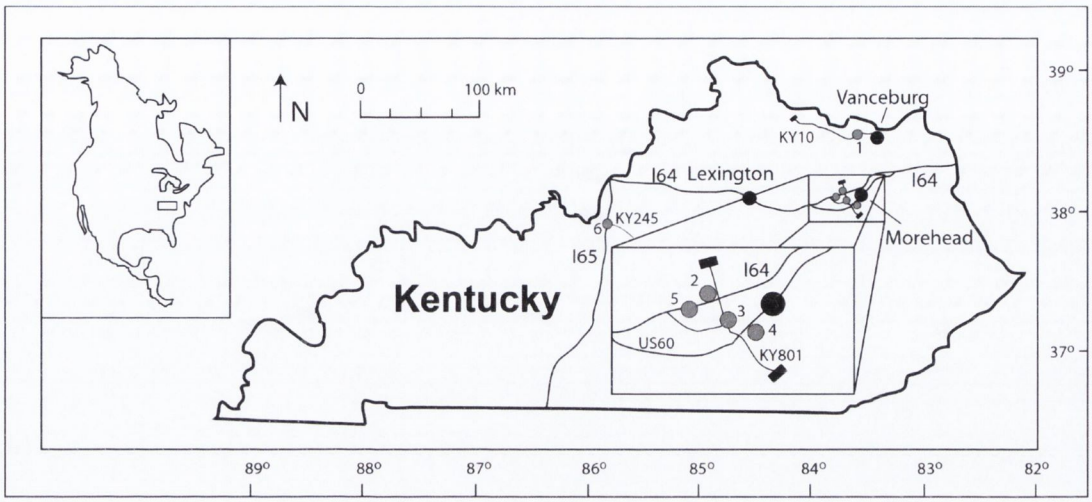

Figure 3.5. Outline of sampling localities in northeastern Kentucky.

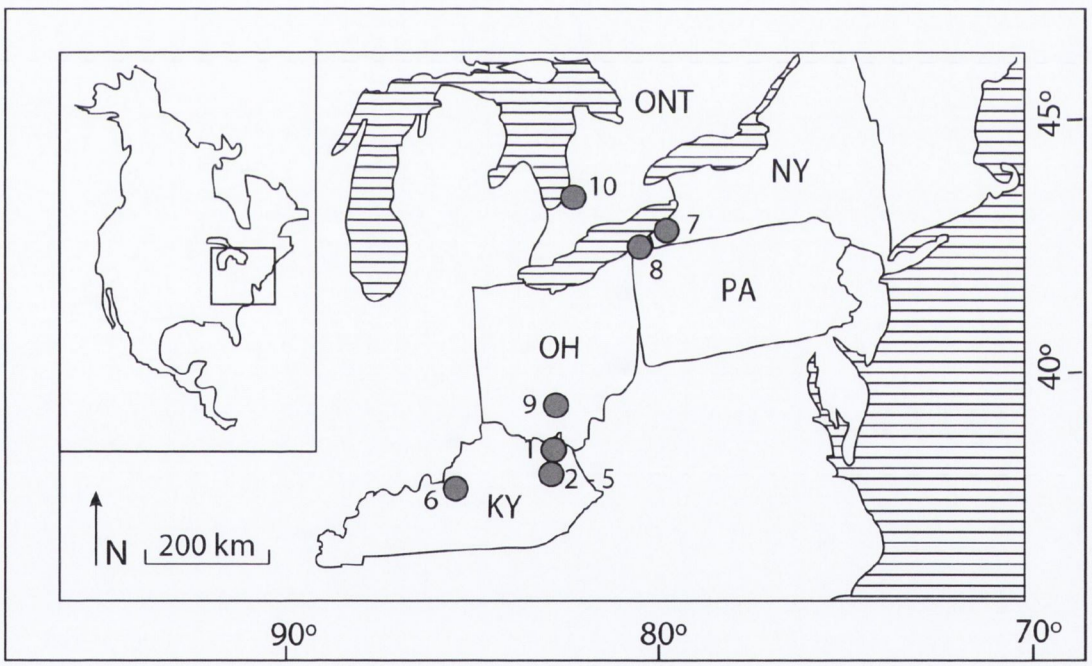

Figure 3.6. Outline of sample localities within North America.

3.2.1 Sampled sections

Stratigraphic sections analysed as part of this project (Figure 3.11) were located within northeastern Kentucky, USA (Figure 3.5). Samples were collected from roadcuts of known Late Devonian – Early Mississippian age. Each sampled section is detailed and figured below.

3.2.1.1 KY10E, N38°35.748', W83°20.566', 2 km east of Vanceburg

Thirty samples were collected and analysed from a roadcut along KY10E. These comprised 18 samples from the Huron Member, one sample from the Three Lick Bed and 11 samples from the Cleveland Member of the Ohio Shale (Figure 3.7). Samples were collected at approximately 2 m intervals through the section. The top of the section is thought to be close to the top of the Cleveland Member, and the base of the section is thought to be near the base of the Huron Member.

3.2.1.2 I64W, N38°10.810' W83°34.081', approximately 14 km west of Morehead

Nineteen samples were collected and analysed from a roadcut along I64W, at the Three Lick Bed type section (Figure 3.8). All samples are thought to be within the Three Lick Bed, with one sample collected from each of the three soft greenish - grey shale horizons. Samples were collected at intervals of between 0.3 – 1 m.

3.2.1.3 KY801N, N 38°9.128' W83°33.098', at the junction with KY1722

Twenty six samples were collected and analysed from a roadcut along KY801N, comprised of two samples from the Huron Member, one sample from the Three Lick Bed, six samples from the Cleveland Member, 13 samples from the Bedford Shale and four samples from the Sunbury Shale (Figure 3.9). Samples were collected at intervals of between 0.5 – 1 m. The Bedford Shale is represented by darker shales, similar in appearance to the black shales of the Ohio Shale, with a slightly varved appearance at approximately 4 m distance from the outcrop.

3.2.1.4 KY2520N, N38°08.378', W83°32.151', approximately 12km west of Morehead

Thrity six samples were collected and analysed from a roadcut along KY2520N, comprised of two samples from the Cleveland Member, 16 samples from the Bedford Shale and 18 samples from the Sunbury Shale (Figure 3.10). Samples were collected at intervals of approximately 0.25 m, although gaps in the analaysed section occur where *Tasmanites* were not abundant enough to run samples on the nano-EA IRMS.

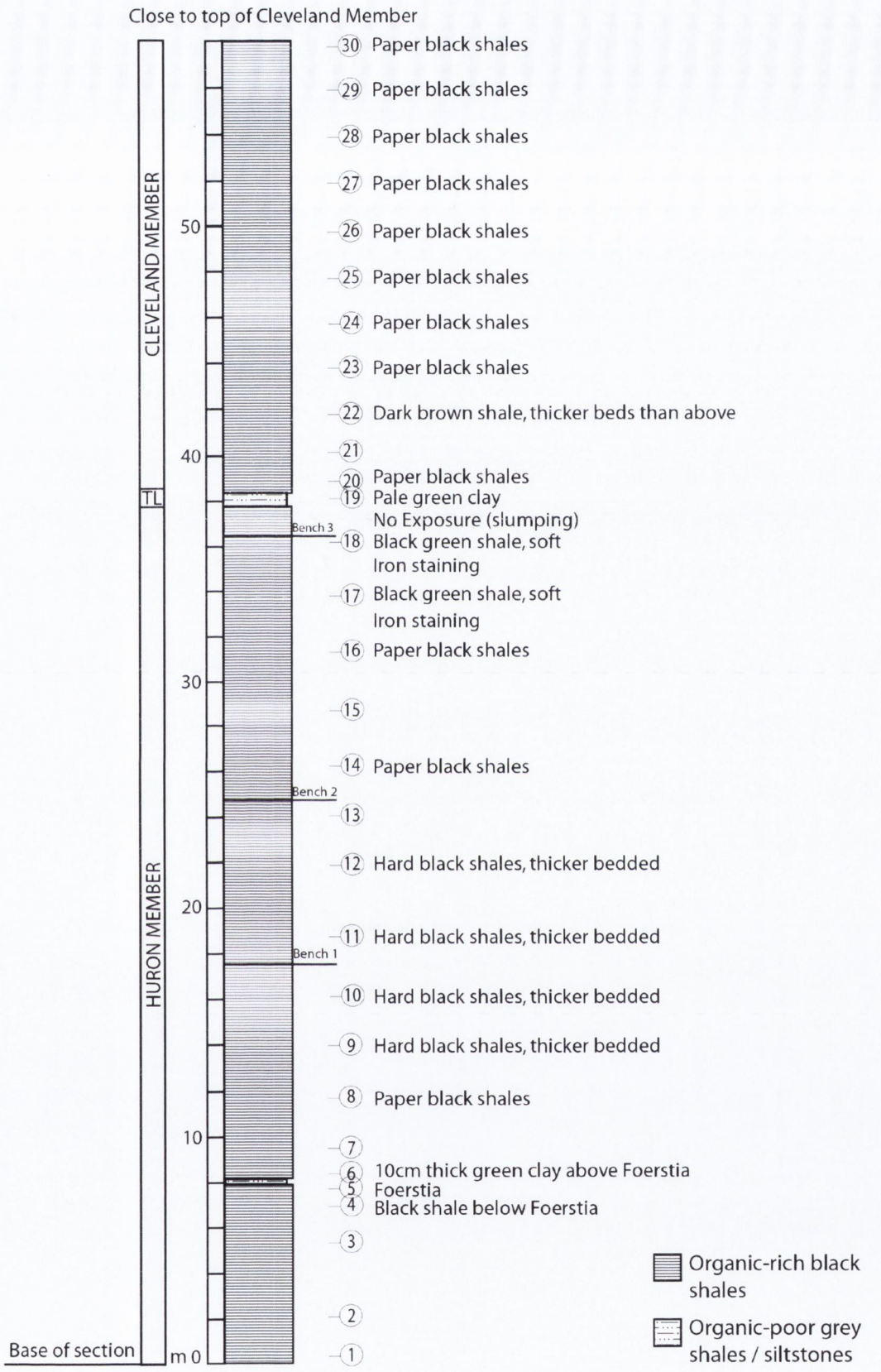

Figure 3.7. Collected samples at KY10E, near Vanceburg, Kentucky.

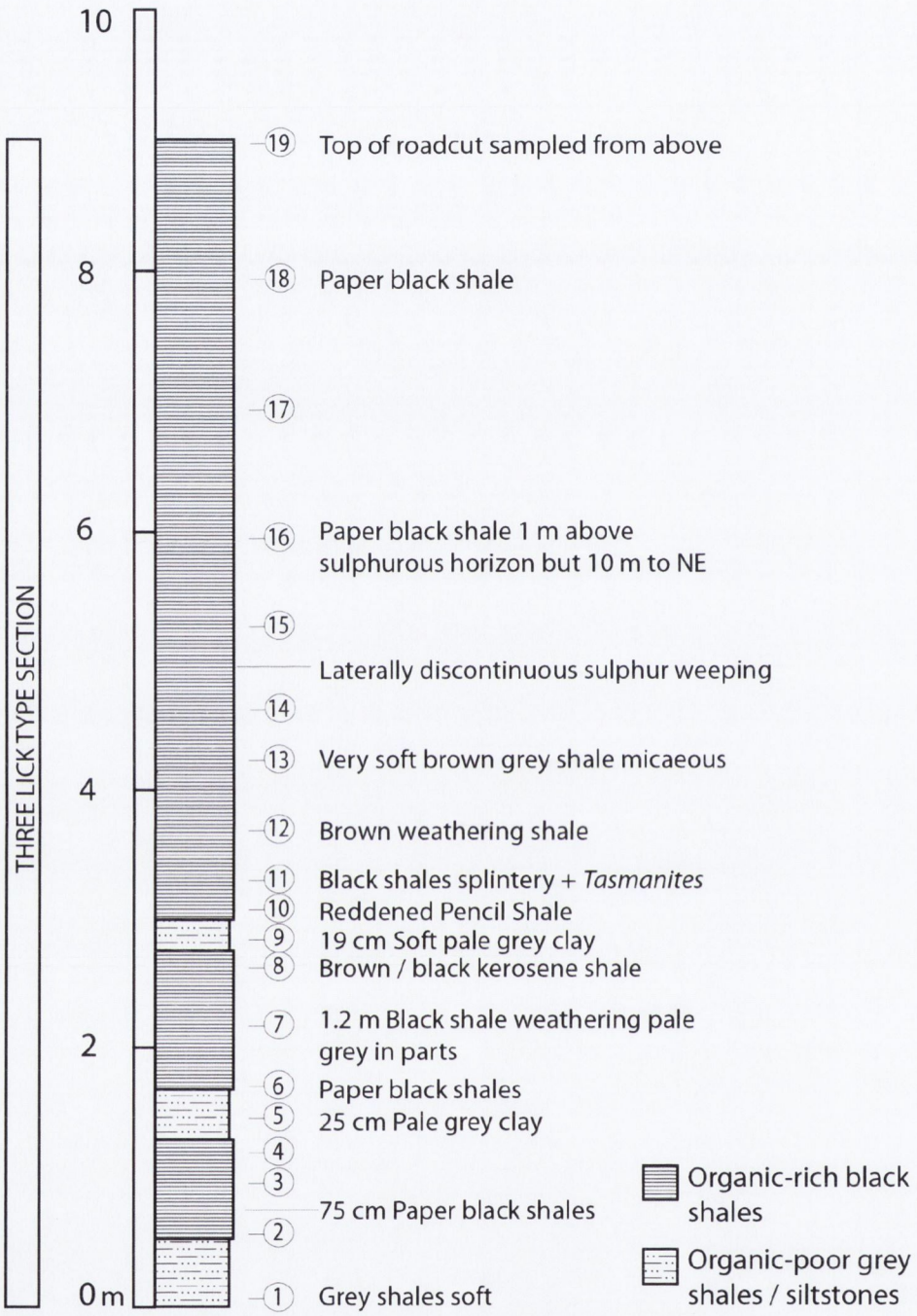

Figure 3.8. Collected samples at I64W, Three Lick Bed type section

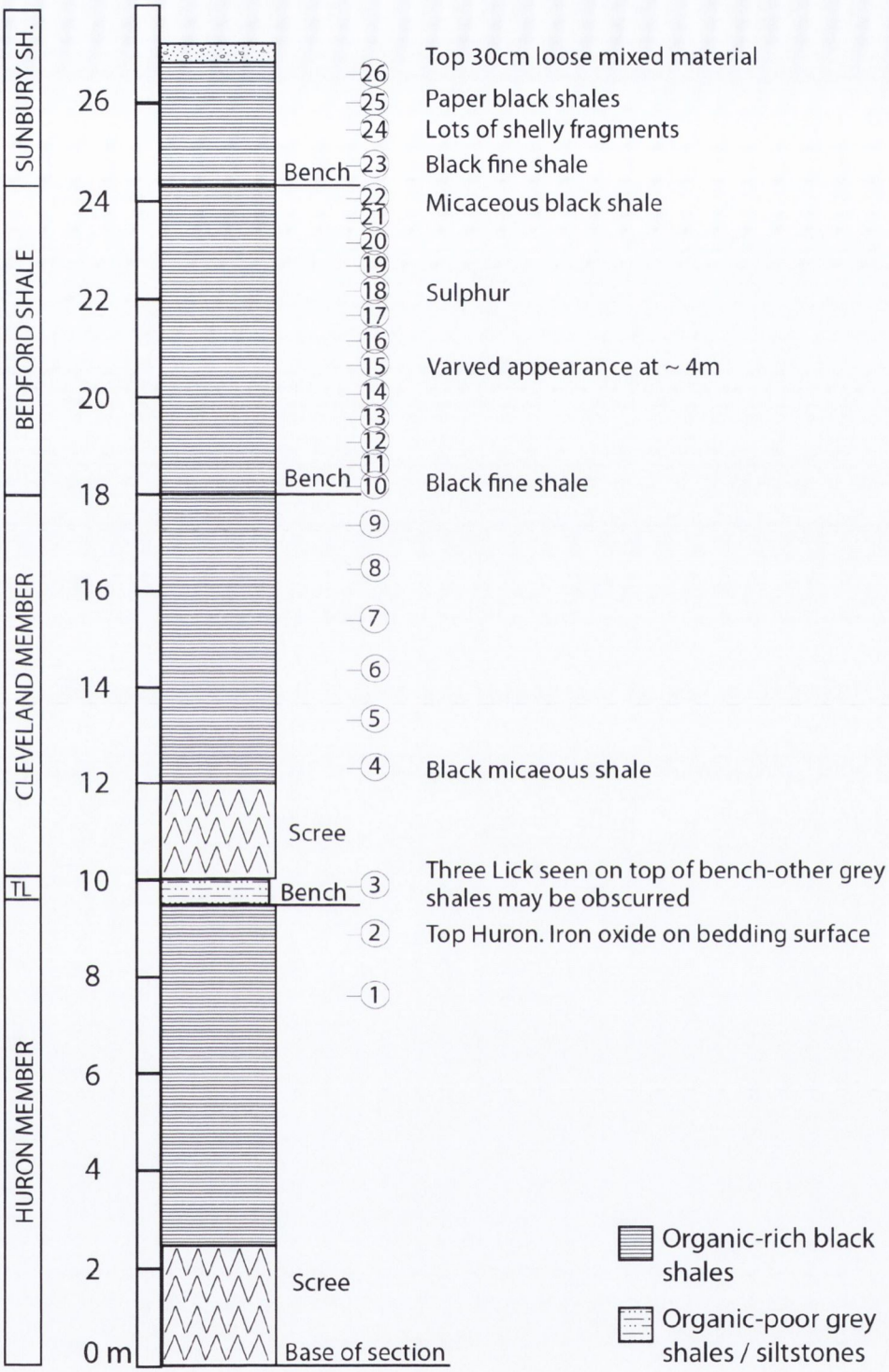

Figure 3.9. Collected and analysed samples from KY801N, near Morehead, Kentucky.

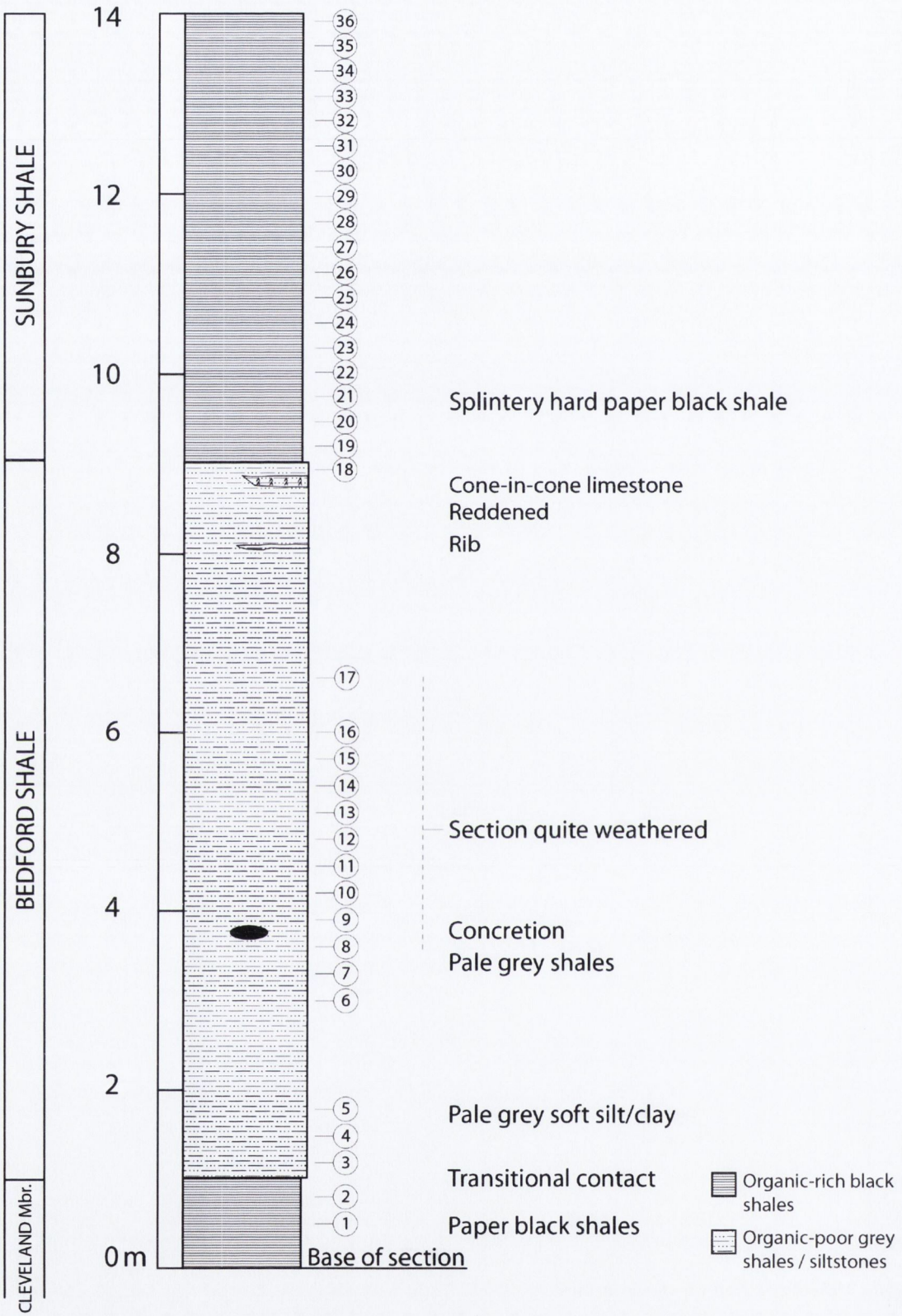

Figure 3.10. Collected and analysed samples from KY2520N, near Morehead, Kentucky.

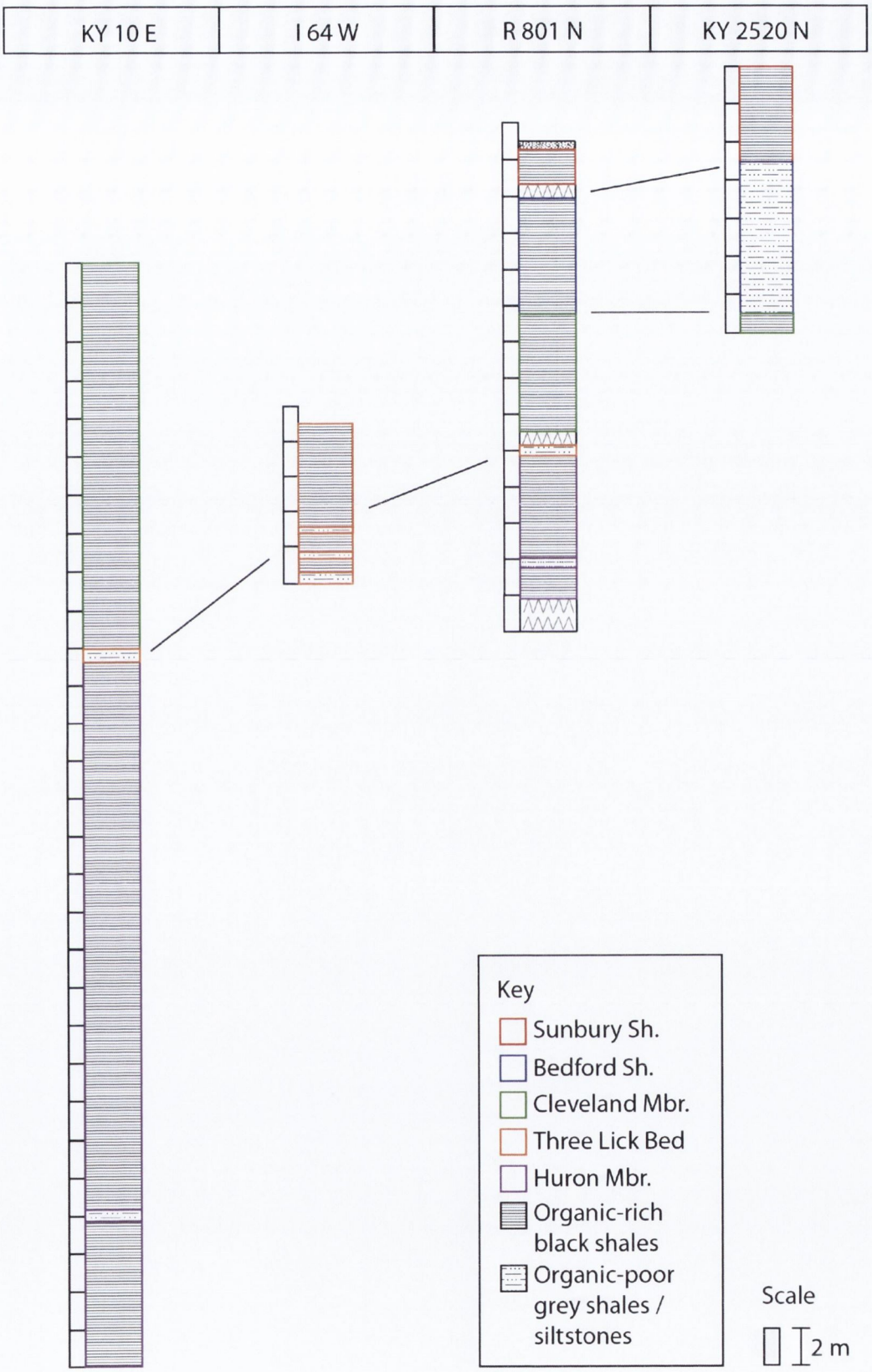

Figure 3.11. Stratigraphic correlation of sampled sections.

3.3 SAMPLE PREPARATION

3.3.1 Chemical treatment (Figure 3.12)

200 g of each sample was placed in 32 % hydrochloric acid to remove any carbonates. Samples were then decanted and placed into 40% hydrofluoric acid for the period of one week. Samples were then rinsed in a 20 µm sieve until neutral. Following acid digestion, 15-20 g of the organic residues were removed for palynological investigation and bulk organic isotopic analyses. Up to half of the organic residue from the *Protosalvinia* samples was put aside for the extraction of *Protosalvinia* thalli. The remaining organic residues were immersed in sodium hypochlorite (NaClO) at a temperature of 60°C for 12-72 hours with the NaClO being topped up every 24 hours. This process is commonly performed in clay mineralogical analysis in order to oxidise and remove organic matter (Lavkulich and Wiens, 1970). In this study, the process was used to remove excess AOM from the black shale samples. The samples used for analysis of the spores of *Protosalvinia* were immersed in NaClO for 12 hours only. This step was successful in exposing and releasing the enclosed tetrads of the *Protosalvinia* through the chemical break-down of the thalli. The *Protosalvinia* samples were then rinsed through a 20 µm sieve and oven dried at 40 °C.

The quantity of AOM in each sample dictated the duration of treatment with NaClO, as samples containing higher proportions of AOM required more time in NaClO. Once the majority of the AOM was removed, the samples were rinsed through a 20 µm sieve, then placed in a centrifuge for 5 minutes to remove any excess NaClO. Following this, a further procedure was carried out, typically performed as part of the clay mineralogy process to remove free iron oxides (Mehra and Jackson, 1960). One hundred fifty ml of 0.3 M sodium-citrate solution, 20ml of 1 M sodium-bicarbonate solution and 4 g of sodium-dithionite were added to each sample, then placed in an oven at 80°C for 15 minutes. Each sample was then washed through a 20 µm sieve and set aside to dry in an oven at 60°C.

3.3.2 Sample extraction

The processed and dried samples were then individually immersed in de-ionised water and placed into an ulstrasonic bath for a period of 15 minutes, following which each sample was divided into a range of size fractions using six sieves (300 µm, 200 µm, 125 µm, 75 µm, 45 µm, 20 µm), allowing easier separation of the various organic constituents. The samples were then set aside to dry in an oven overnight at 60°C. The samples containing *Protosalvinia* thalli were placed in an ultrasonic bath for a maximum period of one minute in order to maintain the structure of the thalli. Each size fraction was then individually placed onto gloss paper under a binocular microscope, where *Tasmanites* spp., *Protosalvinia* thalli and *Protosalvinia* tetrads were extracted

from the sample using a very fine paint brush wetted with de-ionised water to allow temporary adhesion. The separated samples were placed onto individually marked gloss paper holders. Up to 1,500 specimens of *Tasmanites* were picked per sample, depending upon the abundance and availability in each sample (Figure 3.13).

<table>
<tr><td colspan="5">PROCESSING METHODS</td></tr>
<tr><td colspan="5">Rock Samples</td></tr>
<tr><td>HCl</td><td>HCl</td><td>HCl</td><td>HCl</td><td>HCl</td></tr>
<tr><td>HF</td><td>HF</td><td>HF</td><td>HF</td><td>HF</td></tr>
<tr><td rowspan="11">Sieve 20 µm
↓</td><td>Sieve 20 µm</td><td>Sieve 20 µm</td><td>Sieve 20 µm</td><td>Sieve 20 µm</td></tr>
<tr><td>Ultrasonic bath 1 min</td><td>NaClO 12 hours</td><td>NaClO 24-72 hours</td><td>NaClO 24-72 hours</td></tr>
<tr><td>Sieve 20 µm</td><td>Sieve 20 µm</td><td>Sieve 20 µm</td><td>Sieve 20 µm</td></tr>
<tr><td rowspan="10">Dried at 40°C
↓</td><td>Centrifuge 5 mins</td><td>Centrifuge 5 mins</td><td>Centrifuge 5 mins</td></tr>
<tr><td>Ultrasonic bath 15 mins</td><td>$Na_2S_2O_4$, $C_6H_5Na_3O_7$, $NaHCO_3$</td><td>$Na_2S_2O_4$, $C_6H_5Na_3O_7$, $NaHCO_3$</td></tr>
<tr><td>Sieved 20 µm, 45 µm, 75 µm, 125 µm, 200 µm, 300 µm</td><td>Oven 80°C 15 mins</td><td>Oven 80°C 15 mins</td></tr>
<tr><td rowspan="8">Dried at 40°C
↓</td><td rowspan="8">Sieve 20 µm
↓</td><td>Sieve 20 µm</td></tr>
<tr><td>Ultrasonic bath 15 mins</td></tr>
<tr><td>Sieve 20 µm, 45 µm, 75 µm, 125 µm, 200 µm, 300 µm</td></tr>
<tr><td>Dried at 60°C
↓</td></tr>
<tr><td>Palynological slides pre-pared, inclusive of AOM</td><td>*Protosalvinia* thalli extracted</td><td>*Protosalvinia* tetrads / spores extracted</td><td>Palynological slides prepared, exclusive of AOM</td><td>*Tasmanites* extracted</td></tr>
</table>

Figure 3.12. Flow chart indicating the chemical processing undertaken for each set of samples.

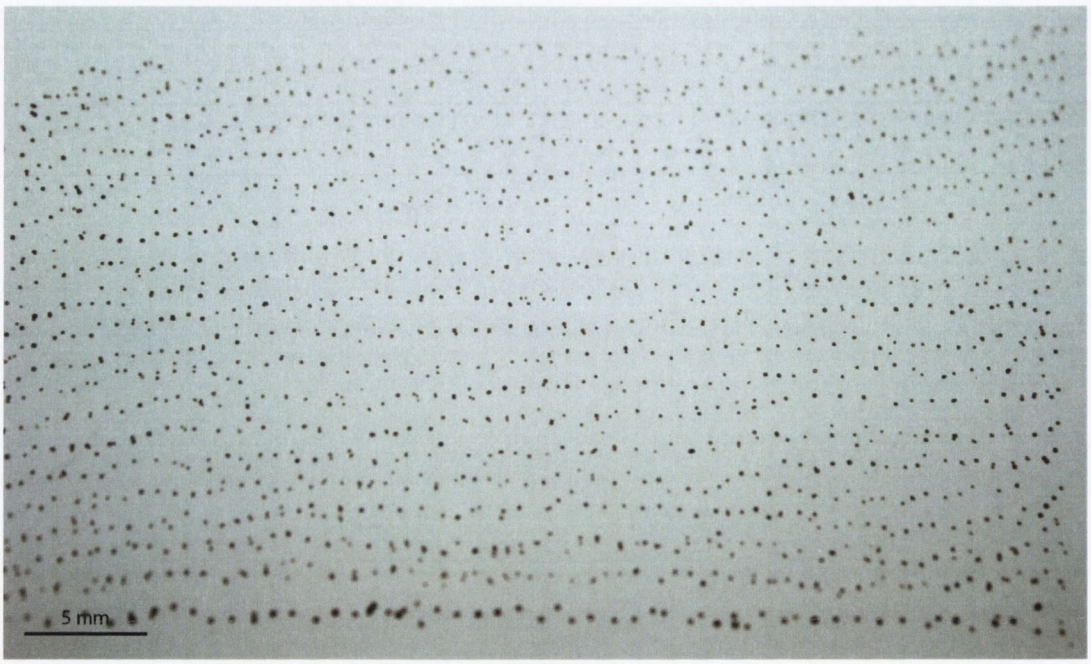

Figure 3.13. Extracted *Tasmanites* specimens (~ 1500) placed on gloss paper, following extraction from a single sample, using a fine paint brush under a binocular microscope.

3.4 SAMPLE ANALYSES: METHODS

3.4.1 Palynology

Both the post HF bulk organic residues and the post NaClO residue were mounted onto glass slides for palynological investigation. The palynological slides assisted in the identification of productive samples containing abundant and large *Tasmanites* specimens. The slides were also valuable for palynological age determination of the sections, and in establishing a new species of miospore, liberated from the *Protosalvinia* thalli.

3.4.2 Stable isotopes

The stable isotope ratios of bulk organic residues and *Protosalvinia* thalli were determined using a CE Instruments 1112 Elemental Analyser (EA) and Thermo Delta^{Plus} continuous flow – isotope ratio mass spectrometer (CF-IRMS). The oxidation tube was maintained at a temperature of 900 °C and the reduction tube was kept at a temperature of 650 °C. Nitrogen and carbon isotope ratios were measured against IAEA references NO-3, N-2 and a laboratory standard L-Alanine, and are expressed relative to atmospheric N_2 (Air) and the V-PDB (Vienna Pee Dee Belemnite), respectively. The stable isotope ratios are given in the conventional 'δ' notation and are expressed

in permil (‰). Two replicate samples were analysed for each of the bulk samples to measure the standard deviation within the samples, and to ensure consistency within the results.

Tasmanites contain 0.3- 0.5 % nitrogen and 30 % carbon by weight, giving them a C:N ratio of between 60:1 and 100:1. The *Tasmanites* in this study are between 75-200 μm in diameter and weigh approximately 0.5 μg. In order to attain on-scale peaks on a standard configuration of the EA - IRMS for N_2, between 5,000 and 8,000 specimens of *Tasmanites* would be required per sample for a single N_2 analysis. To reduce the required sample size, modified low-volume, transparent silica reaction tubes (Elemental Microanalysis P/N C1057) were used in the oxidation and reduction columns of the EA, in place of the standard tubes (C1069). The internal volume of the low volume tubes (LVTs) is 18 ml as opposed to the 70 ml of the standard tubes, giving increased N_2 and CO_2 peak sizes with a reduced helium carrier gas flow of 65 ml/min, compared with 85 ml/min used in the standard tubes. The net effect of using the low volume tubes is that sample sizes can be reduced by approximately 45 %, (enabling viable isotopic analysis on 2,500 – 4,000 specimens of *Tasmanites* per sample). As this study sets out to analyse the glacial – interglacial changes in $\delta^{15}N$, the number of samples required to make such a study feasible would cover the entire stratigraphic range, or up to 100 samples, plus replicates. The large number of specimens of *Tasmanites* required for such a task would be impractical without further modification to the set up of the EA – IRMS.

3.4.2.1 Nano-EA

The elemental analyser (EA) is most commonly used as a standalone piece of equipment for weight % N and C determination. The helium carrier gas is used at a high flow rate through the EA (~85 ml/min) but at a very low flow rate in the IRMS (~0.3 ml/min). The Finnegan Conflo III is the interface between the EA and IRMS, reducing the gas flow (8 ml/min) with a vent valve before the 'open split', a tube that allows the high vacuum of the IRMS to draw ~0.3 ml/min of the sample and carrier gas mixture into the IRMS.

The reduction in gas flow from 85 ml/min to 0.3 ml/min means that only 0.35% of the sample gas enters the IRMS and the rest is vented. This loss is compounded when samples such as *Tasmanites* contain small amounts of N (~0.3 - 0.5 %), and large amounts of C (~30 %), giving them an average C:N ratio of ~ 85:1. This leads to further difficulties when performing dual analyses, as separate samples must be prepared and analysed for the investigation of each parameter. However, when carrying out N analyses, the large C:N ratio can lead to the carry-over of excess carbon from the preceding sample, in the form of carbon monoxide, interfering with the subsequent sample N_2 peak. An ascarite trap was attached to the EA during nitrogen analyses, to prevent any CO_2 or CO from entering the IRMS and possibly interfering with the N_2 peaks.

Polissar *et al.* (2008) outlined a practical way to significantly reduce the sample size required to maintain linearity by placing a cryogenic trap between the EA and the IRMS, which they have termed a nano-EA. A similar system was built at Trinity College Dublin as part of this project (Figures 3.17 and 3.18). Within this modified set up of the standard EA-IRMS system, the sample is still converted to N_2 and CO_2 within the oxidation and reduction tubes of the EA. However, before the sample enters the GC column, it is trapped in a silica gel packed column by a liquid N (LN2) cold trap (-196 °C), while the excess He from the EA passes through the trap and is vented. The packed silica column is then heated by immersing it in a container of water at room temperature. This releases the concentrated sample into a 0.32 mm capillary GC column, where the separation of N_2 and CO_2 takes place at a flow rate of approximately 2 ml/min. The new GC column also produces sharper N_2 and CO_2 peaks than the standard GC column. This aspect of the nano-EA system further supplements the gains made in sample peak intensity, as a broad, rounded N_2 or CO_2 peak may fall short of linearity, requiring a larger sample size. The sample is then carried into the open split in the Conflo III. Approximately 15% of the sample gas is analysed with this system and the optimised flow rates.

The net effect of the modified system is that it yields significantly larger N_2 and CO_2 peaks (Figures 3.14 and 3.15). The decrease in sample size required for linearity is up to two orders of magnitude, making this piece of equipment extremely useful in analysing genus specific organic constituents. However, in addition to trapping and concentrating the N_2 within the sample, it also traps and concentrates the N_2 blank from both the He and O_2 gas lines. This leads to an experimentally deduced blank of approximately 1.5 V. The blank signal (1.5 V, -2.5 to -5.5 ‰) must be mathematically subtracted from the sample plus blank signal to yield the true $\delta^{15}N$ value of the sample.

The number of *Tasmanites* required per sample using the nano-EA-IRMS was between 60 and 120 specimens (dependent upon the average size of the *Tasmanites* in each sample). This quantity yielded a mass 28 peak intensity, excluding the blank, of approximately 3 V. This is a dramatic reduction in sample size (approximately 2,500 – 4,000 specimens before the addition of the nano-EA would yield a mass 28 peak intensity of just over 1 V), making the analysis of the stable isotope signature of *Tasmanites* a much more obtainable goal. *Tasmanites* were weighed into 5 x 3.5 mm tin cups (Figure 3.16). The smaller than standard sized tin cups were used instead of the larger cups in order to increase the longevity of the low volume oxidation tube. The smaller tin cups weigh approximately 10 mg, whereas the larger cups weigh approximately 30 mg, increasing the quantity of tin to be oxidised, and thereby reducing the sample capacity of the oxidation tube.

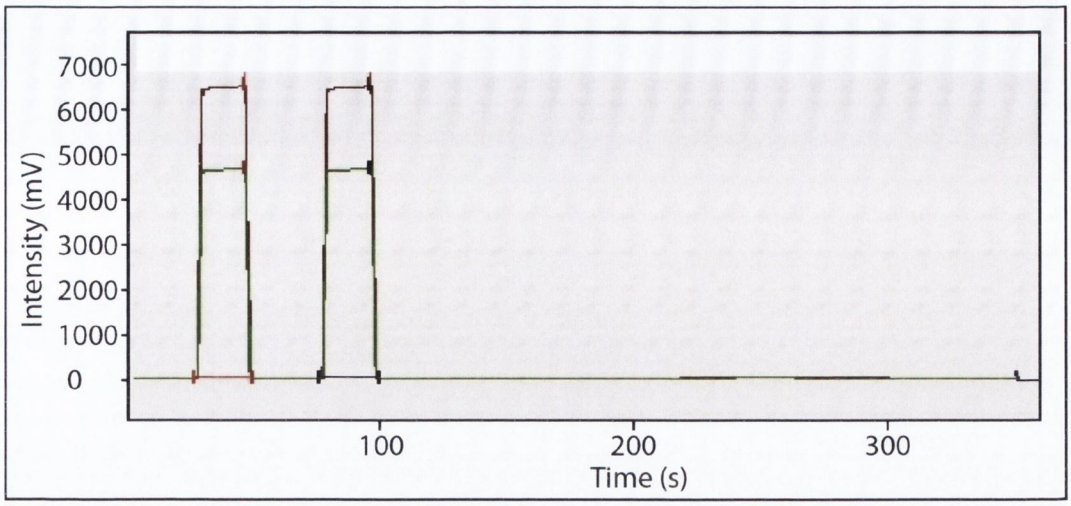

Figure 3.14. Output profile of a blank run (no sample) on a standard setup of the EA-IRMS. The minor amount of N contained within the He carrier gas is shown as a negligible peak between 200 and 300 s.

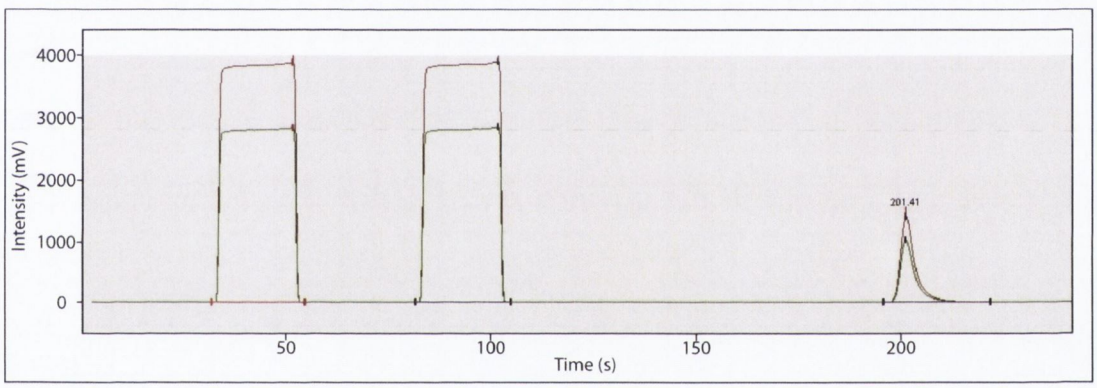

Figure 3.15. Output profile of a blank run (no sample) on the nano-EA-IRMS. The minor quantity of N contained within the He carrier gas is trapped within the nano-EA and fed into the IRMS, where a peak is recorded due to the significant reduction in He dilution brought about by driving off the excess He within the cryogenic trap.

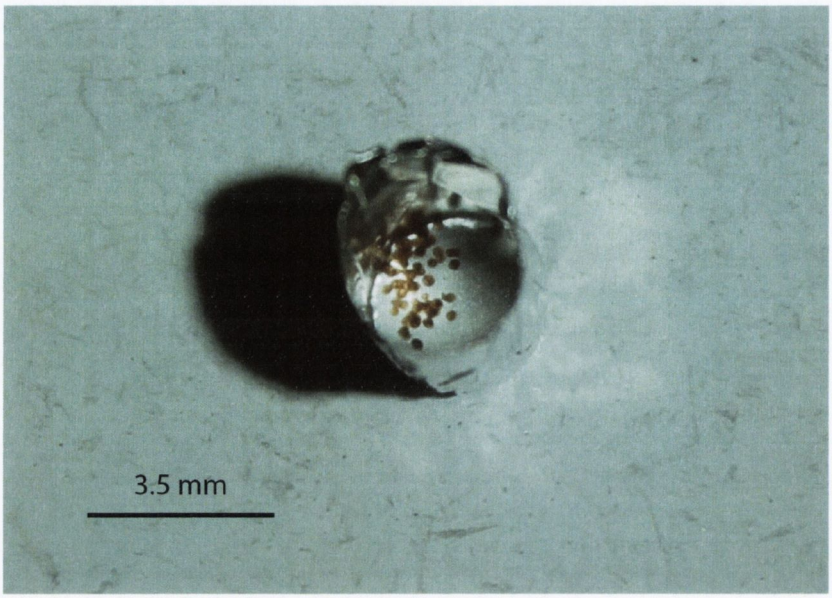

Figure 3.16. Extracted specimens of *Tasmanites* (~ 60 - 120) placed in a tin cup prior to analysis on the nano-EA-IRMS. This resulted in a significant reduction in *Tasmanites* specimens than that required on the general setup of the EA-IRMS (~ 2,500 – 4,000 specimens).

3.4.2.2 Blank reduction

The blank was relatively high (~4 V intensity) when the new nano-EA system was first installed and tested. This blank was reduced from 4 V down to 1.5 V by removing very slight leaks along the He and O_2 gas lines, which are acceptable in 'standard' high flow mode, and using IAEA standards to improve the trapping time required to drive off excess He, while trapping the full sample. The oxygen line continued to have leaks which were found to originate within the gas control module in the EA, located behind the electronic control board. As this problem did not resolve with new solenoid valves fitted to the oxygen line, a pneumatically driven oxygen loop was installed and the gas control module was bypassed. The loop carries an approximate volume of 2 mL of O_2 and the timings are controlled by the EA software.

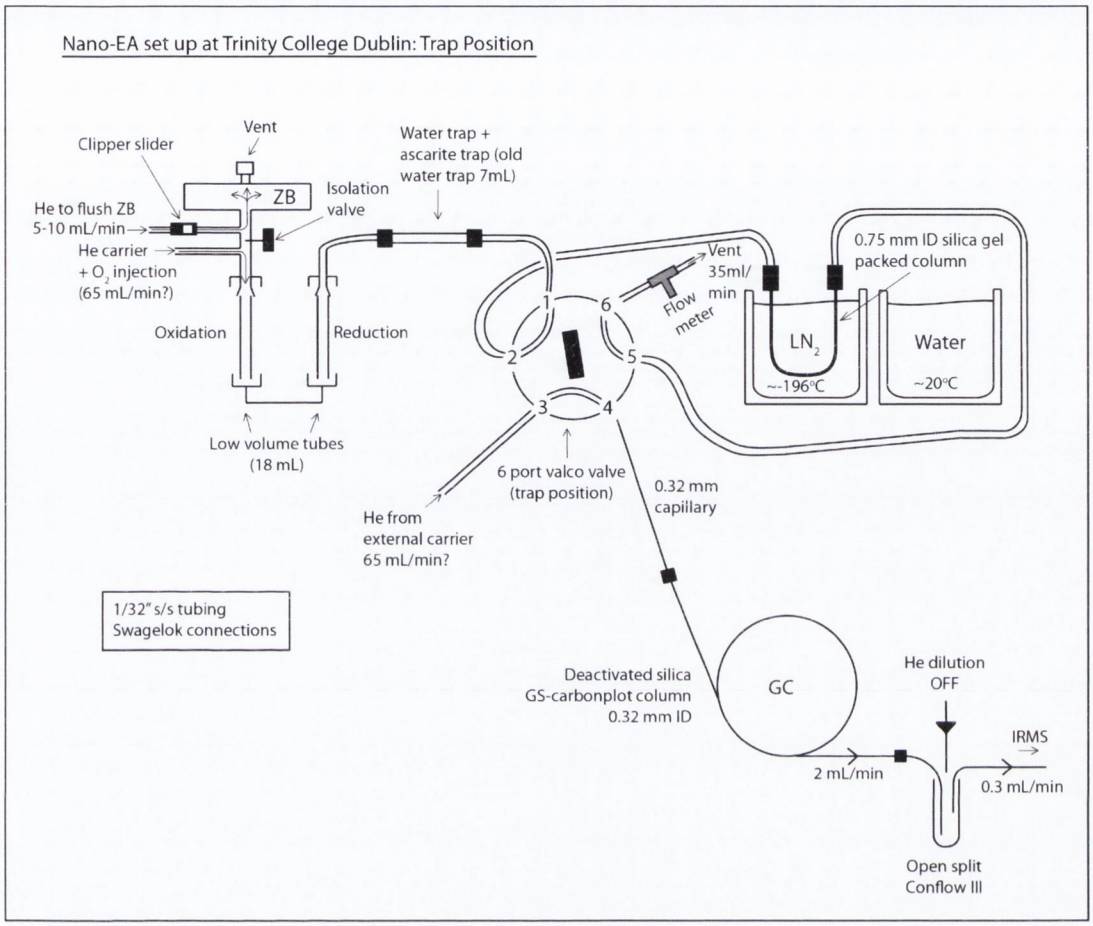

Figure 3.17. Schematic diagram of the nano-EA IRMS in trap position. The entire system mainly consists of the zero-blank autosampler, the oxidation and reduction tubes of the EA, a water and carbon trap, followed by the 6-port valco valve which controls the switch from vent to trap positions. The sample gas is trapped in the silica column when it is immersed in liquid N.

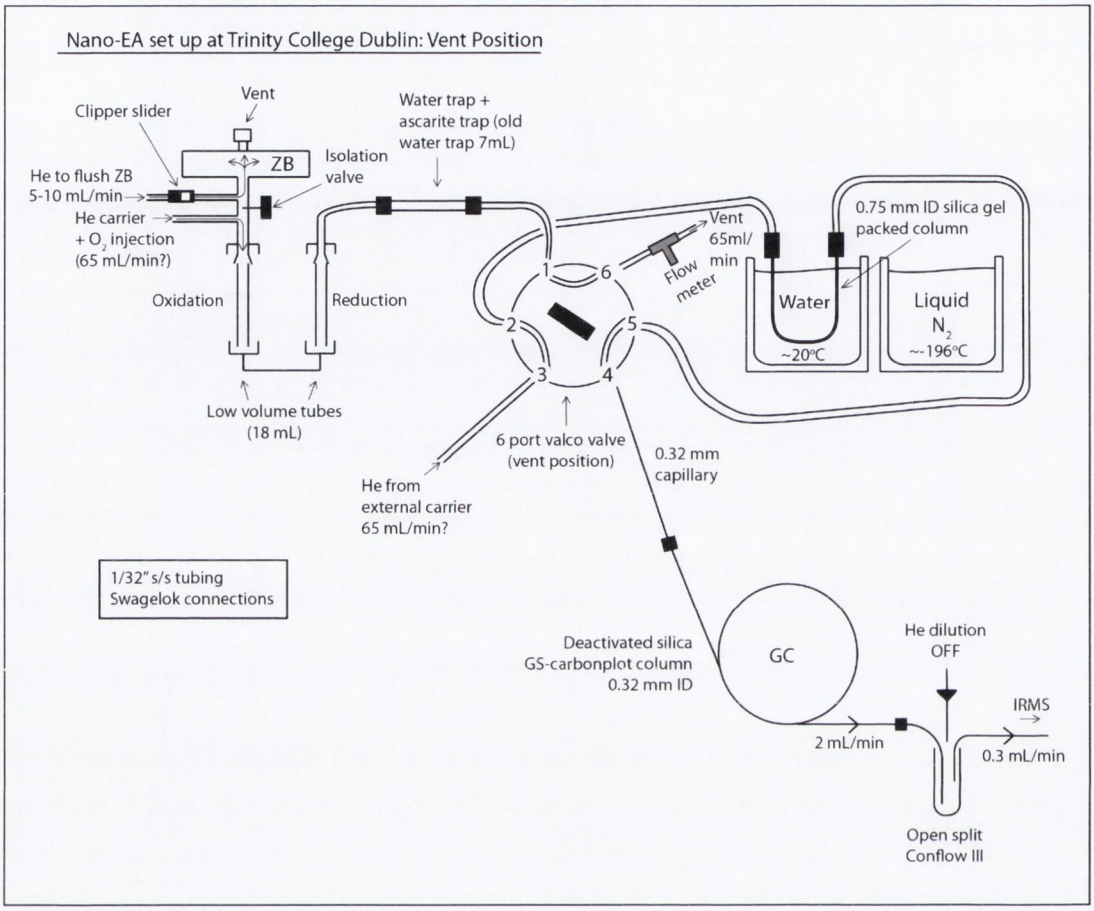

Figure 3.18. Schematic diagram of the nano-EA IRMS in vent position. Once the carrier gas (He) has been driven off in the trap position, the valco valve is switched to vent position and the sample is released from the silica column by immersing it in water at room temperature. The sample gas enters the GC column and then into the Conflo III, where the sniffer draws 0.3 ml / min of the sample gas into the IRMS.

3.4.2.3 Blank correction

Concentrated N_2 from the He and O_2 gas lines accumulates in the packed column while the column is immersed in LN2. This leads to a background N_2 blank of approximately 1.5 V. During sample analysis, mixing occurs between the background N_2 and the sample gas within the packed column. A blank correction must therefore be made following data collection. The blank contribution was measured either side of every sample, and the average of these measured blanks was taken as the blank component of each sample. Each individual sample therefore had its own set of blank measurements with which to make the appropriate blank correction calculations. Blank corrections were carried out as outlined in Polissar *et al.* (2008).

Using experimentally determined mean values for the N_2 peak area and the $\delta^{15}N$ signal for the blank contribution, the basic equation for correction is as follows:

$$\delta_c = \frac{A_m\delta_m - \bar{A}_b\bar{\delta}_b}{A_m - \bar{A}_b} \qquad [1]$$

where δ_c is the blank corrected $\delta^{15}N$ signal for the sample, A_m is the measured N_2 peak area of the sample mixed with the blank, δ_m is the measured $\delta^{15}N$ signal of the sample mixed with the blank, $\bar{A}_b$ is the average measured N_2 peak area of the blank contribution and $\bar{\delta}_b$ is the average measured $\delta^{15}N$ signal of the of the blank contribution.

Uncertainty (σ) in the blank corrected sample (δ_c) is a combination of analytical uncertainty (σ_a) in the IRMS measurement (±0.08‰) and variability in the $\delta^{15}N$ signal and the peak area of the blank (the quantity of N_2 within the blank). By removing the blank contribution from each measurement in eq 1 and subtracting the analytical uncertainty, eq 1 becomes:

$$\sigma_{\delta c}^2 = \left(\frac{\delta_m}{A_m - \bar{A}_b} + \frac{\delta_b - \delta_c}{A_m} + \frac{\bar{A}_b\bar{\delta}_b - A_m\delta_m}{(A_m - \bar{A}_b)^2}\right)^2 \sigma_{A_b}^2 + \left(\frac{A_b}{A_m - \bar{A}_b}\right)^2 \sigma_{\delta b}^2 - \left(\frac{A_m}{A_m - \bar{A}_b}\right)^2 \sigma_a^2$$

[2]

This equation is based on the rule for combined standard uncertainties; the square root of the sum of the squares.

3.4.3 Preliminary testing

Laboratory heating and a range of chemical treatments were carried out on the alga *Tasmanites*, to ascertain what effect the procedures would have on their carbon and nitrogen isotope composition. While various research has been completed in relation to acid treatment, thermal maturation and weathering of kerogen or whole rock samples, little work has been carried out on the effects of these three processes on a single type of palynomorph. The material used for this investigation was obtained from the Lower Permian Quamby Group at Latrobe, Northern Tasmania, Australia, often referred to as the Tasmanite Oil Shale. These shales contain large *Tasmanites* (> 500 μm) in abundance, which reduces the need to extract large quantities of *Tasmanites* in order to attain linearity on the general set up of the EA-IRMS. A peak palaeotemperature of 60 °C was calculated from a vitrinite reflectance value of 0.55 % R_r, obtained from adjacent rocks of the same group, using the method of Barker and Goldstein (1990).

This investigation was carried out on the EA-IRMS before the nano-EA was built. The sample was therefore chosen due to the abundance of large *Tasmanites* and their ease of extraction from the rock matrix, a friable mix of quartz, illite, chlorite and jarosite, without the use of chemical treatments. Crushing the shale by hand with a mortar and pestle to ~1-2 mm particles was followed by ultra-sonic disaggregation in de-ionized water for 15 minutes, yielding clean *Tasmanites* specimens with minimal residual matrix attached to the phycomata. Samples were oven dried at 40 °C immediately after disaggregation. For each sample, replicates of either 50 or 200 clean phycomata were placed in 8x6 mm tin capsules using a fine paint brush and a binocular microscope, for carbon and nitrogen analyses, respectively.

3.4.3.1 Control sample

Part of the sample was used as a control sample, to which the isotopic ratio of all of the treated *Tasmanites* samples could be compared. The control *Tasmanites* specimens were extracted from the rock matrix using the method described above.

3.4.3.2 Experimental thermal maturation

The sample was crushed to <2 mm. Nine 3 g sub-samples were wrapped in aluminium foil and placed in a ceramic tube in a Lenton tube furnace. The samples were heated for 100 days in an inert atmosphere (argon) to temperatures of 75 °C ±3 °C, 85 °C ±3 °C, 95 °C ±3 °C, 105 °C ±3 °C, 115 °C ±3 °C, 125 °C ±3 °C, 140 °C ±3 °C, 155 °C ±2 °C and 170 °C ±2 °C. Following cooling, the samples were placed into an ultrasonic bath in de-ionised water, dried, and then

picked for analysis. Samples of heated *Tasmanites* were also picked and mounted onto glass slides to assess their Palynomorph Darkness Index (Goodhue and Clayton, 2010) (Figure 3.19).

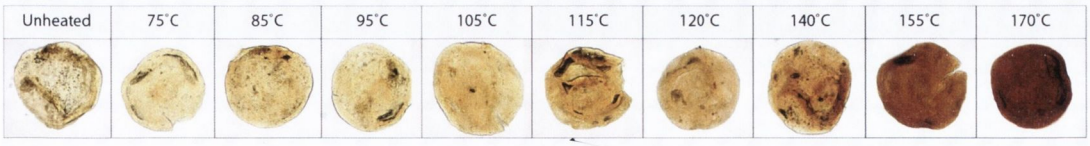

Figure 3.19. Laboratory heated specimens of *Tasmanites*. Samples were heated in an inert atmosphere (argon) in a Lenton tube furnace for 100 days to imitate natural thermal maturation. Specimens were extracted from the Tasmanite Oil Shale following experimental thermal maturation.

3.4.3.3 Chemical treatment

Six chemical treatments routinely used in palynological preparation; CH_3COOH, HCOOH, HNO_3, HCl, cold HF and hot HF, and a treatment method used as part of the preparation for soil and clay mineral analysis; NaClO, $Na_2S_2O_4$, $C_6H_5Na_3O_7$ and $NaHCO_3$, were chosen for this investigation. The sample was crushed to <2 mm. Seven 2 g sub-samples were exposed to one of the above listed chemical treatments for 8 hours, with the exception of the clay mineralogy treatment. This treatment included exposing the 2 g sub-sample to NaClO for 24 hours. Following this, the sample was washed with distilled water and placed in a centrifuge to remove excess NaClO. The sample was then placed in a water bath 80 °C and exposed to $Na_2S_2O_4$, $C_6H_5Na_3O_7$ and $NaHCO_3$ for 15 mins. After each treatment, all samples were washed with distilled water until neutral, dried, and picked for analysis.

3.4.3.4 Oxidation with hydrogen peroxide

2 g of crushed sample (<2 mm particles) was exposed to hydrogen peroxide (H_2O_2) for a total of five hours, after which, the sample was washed with distilled water, and then picked for analysis. The purpose of this treatment is to simulate weathering of outcrop material.

3.4.3.5 Analysis

Nitrogen and carbon isotope ratios were measured against a laboratory standard L-Alanine and are expressed relative to atmospheric N_2 (Air) and the V-PDB (Vienna Pee Dee Belemnite), respectively. Samples were run on a generalised set up of the EA-IRMS, using modified low volume oxidation and reduction tubes in order to reduce the sample size. *Tasmanites* contain approximately 0.35 % nitrogen and 30 % carbon by weight, giving them a C:N ratio of 85:1. The *Tasmanites* used in this experiment measure between 200-600 µm in diameter. Approximately 200 specimens of *Tasmanites* per sample were required to obtain an on-scale N_2 peak, but only 50 *Tasmanites* per sample were needed for a reliable CO_2 peak. An ascarite trap was attached to the

EA while the nitrogen samples were being processed, preventing the CO_2 from entering the IRMS and interfering with N_2 peaks.

The low concentration of nitrogen in *Tasmanites* yields low-intensity N_2 peaks, despite the large number of phycomata analysed per sample. Linearity in the IRMS, for $\delta^{15}N$ with N_2 peak intensity, was established before the samples were run. A range of sample weights of L-Alanine were run and their $\delta^{15}N$ values plotted. For N_2, a 'base of linearity' value was identified as approximately 400 mV and all *Tasmanites* data presented here are from N_2 peaks above this value (Figure 3.20). Bahlmann *et al.* (2010) found an inverse correlation between total nitrogen content and measurement precision, where samples containing 0.35 % N should have a standard deviation of approximately 0.2 ‰. Replicate analysis of L-Alanine standards in this study yielded a 1SD precision of 0.16 ‰ for $\delta^{15}N$ and 0.05 ‰ for $\delta^{13}C$.

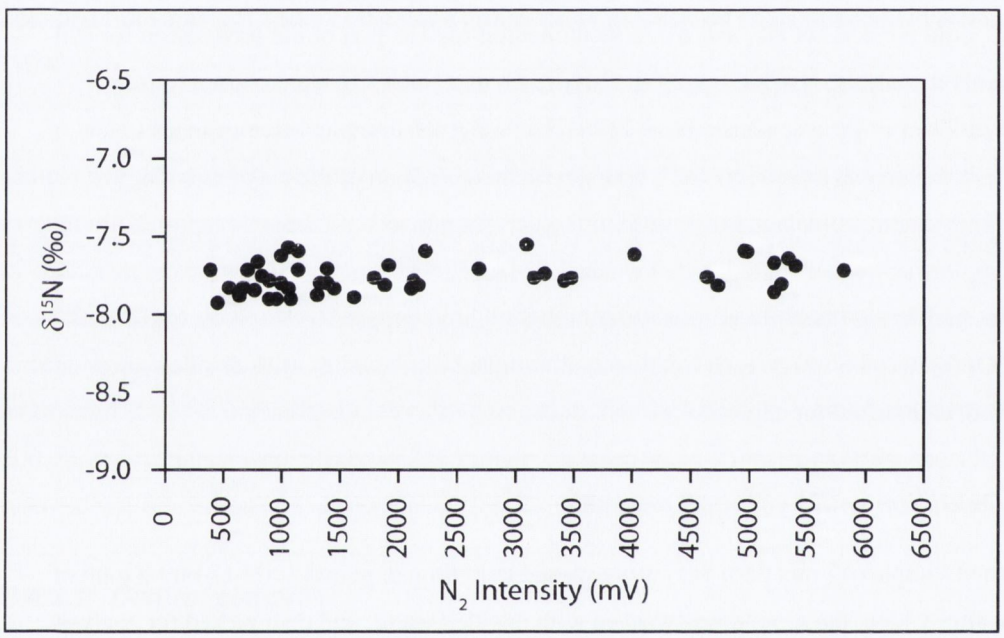

Figure 3.20. Linearity plot of a range of sample weights of a laboratory standard L-Alanine, recording varying ranges of peak N_2 intensities against the $\delta^{15}N$ signal recorded on a standard setup of the EA-IRMS. The smallest possible N_2 peak, at which linearity was maintained, was approximately 400 mV.

3.4.4 Trace Elements

This research was made possible due to recent advances in laser ablation inductively coupled plasma mass spectrometry. The investigation into trace element ratios within palynomorphs such as *Tasmanites* is purely explorative and is merely intended to support the main body of research within this thesis.

Following the chemical preparation method, as outlined above, to extract *Tasmanites* from their bulk material, a range of trace element ratios within the extracted *Tasmanites* were analysed using laser ablation inductively coupled plasma mass spectrometry (LA-ICP-MS) at Trinity College Dublin (Photon Machines Analyte Excite Excimer UV laser coupled to a Thermo Scientific iCAP Q, model s, Quadrupole ICP mass spectrometer).

Three specimens of extracted *Tasmanites,* ranging in diameter from 80 to 200 µm, were picked from each sample and placed onto double sided scotch tape, which had been previously attached to glass slides (Figure 3.21). The walls of the algal tests are composed of a complex "lipoid" substance that resists chemical breakdown (Tappan, 1980) and can sometimes contain small quantities of diagenetic pyrite and silica (Schieber, 1996), some of which will have been removed during processing. The trace element data presented in Chapter 4 are composed of a composite of *Tasmanites* extracted from various sample localilties, including KY10E (Huron Member), I64W (Three Lick Bed), KY801N (the majority of the Cleveland Member) and KY2520N (the top of the Cleveland Member, the Bedford Shale and the Sunbury Shale).

Two sets of NIST 612 glass standard and two sets of 'blanks', the double sided scotch tape, were analysed following every 20 specimens to ensure stability of analysis. Sixteen elements were analysed; vanadium (V), chromium (Cr), manganese (Mn), iron (Fe), cobalt (Co) nickel (Ni), copper (Cu), zinc (Zn), strontium (Sr), molybdenum (Mo), cadmium (Cd), tin (Sn), barium (Ba), cesium (Ce), thorium (Th), and uranium (U). The circular spot size varied from 85-150 µm, depending on the diameter of the specimen being analysed. Laser fluence was at 2.35 J/cm^2, and 30 shots of the laser with an output and frequency of 20 % and 2 Hz, respectively, were completed on each specimen.

The output profile (Figure 3.22) was analysed using the Iolite software. The outer walls of the *Tasmanites* record higher concentrations of trace elements, possibly due to contamination from the rock matrix or processing methods. The trace element data was therefore targeted to analyse the trace element concentration recorded within the *Tasmanites* specimens rather than the outer walls.

As the analysed specimens are the phycomata of pelagic green algae, rather than bulk sediment, the study hopes to achieve a better understanding of the upper ocean during the Late Devonian. The trace elements found in the algae are also elements that managed to survive sedimentation, and this should also reveal information about oxic conditions at the bottom of the water column. However, this means that nutrient conditions within the photic zone, inferred from the trace element ratios, may have been altered due to secondary processes, following degradation either within the water column or following sedimentation. This study is experimental and was

carried out in order to support the main body of research within this thesis. Further analyses would be required before distinct conclusions could be drawn from the results.

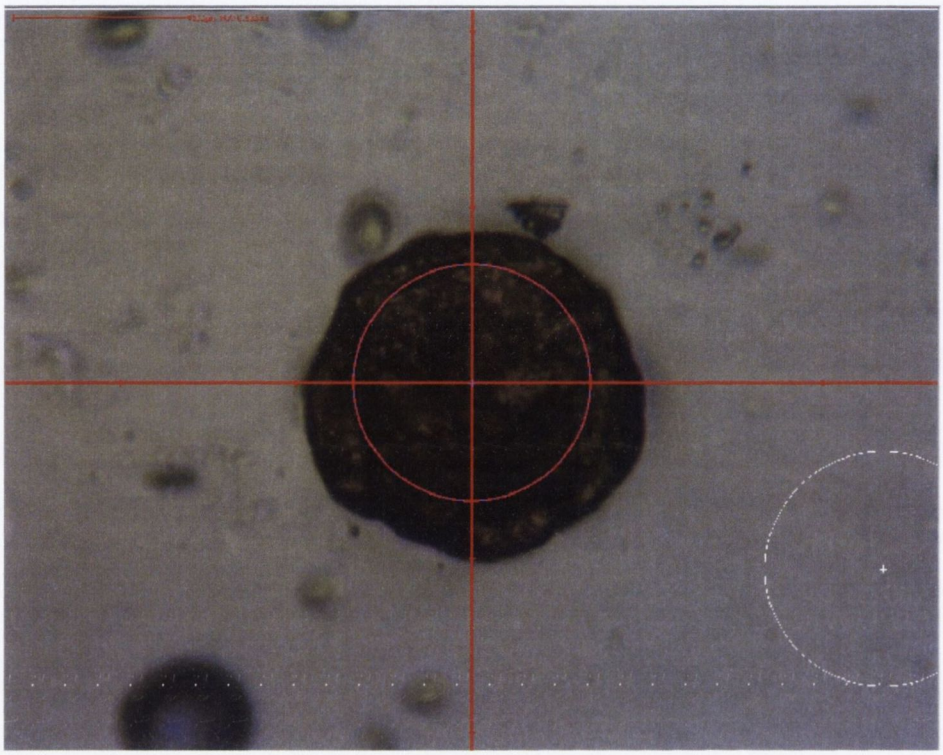

Figure 3.21. Screengrab of a *Tasmanites* specimen as it is being aligned to the laser (LA-ICP-MS), before ablation took place.

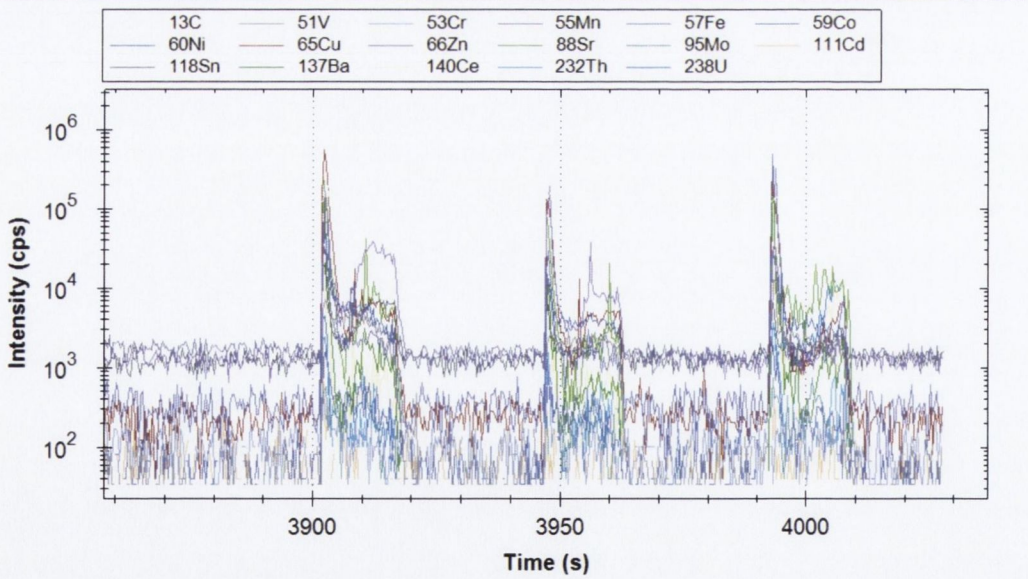

Figure 3.22. Output profile of three *Tasmanites* specimens during trace element analysis on the LA-ICP-MS. The initial peaks are suggested to be contamination on the outer surface of the specimens. This was disgarded during analysis with the Iolite software.

Chapter 4

Results

4.1 PRELIMINARY TESTING

Average isotopic values of 12.62 ‰ ($\delta^{15}N$) and -10.34 ‰ ($\delta^{13}C$) were determined for the control sample of *Tasmanites* extracted from the Tasmanite Oil Shale. This value varied slightly with certain chemical treatments, however, experimental heating did not cause any significant isotopic change in the $\delta^{15}N$ and $\delta^{13}C$ of the *Tasmanites*. The standard deviation of the control sample was quite substantial (0.76 ‰ $\delta^{15}N$, 0.39 ‰ $\delta^{13}C$), possibly due to the lack of any chemical treatment in the extraction process. This may be the result of the inclusion of minor quantities of rock matrix on the extracted *Tasmanites*. Every effort was made to extract *Tasmanites* free from contamination by the rock matrix, but as the stock of 'clean' *Tasmanites* was depleted through selection for analysis, specimens containing rock matrix impurities may have been analysed, leading to higher standard deviations between sample analyses. The isotopic ratio obtained for the picked rock matrix was much more negative than the extracted *Tasmanites*, with an average $\delta^{15}N$ value of -0.64 ‰ (0.29 wt% nitrogen) and an average $\delta^{13}C$ value of -14.37 ‰ (8.04 wt% carbon). Recorded standard deviations are also quite high for many of the other investigated samples. This is possibly due to a depletion in the stock of 'clean' specimens over time, as outlined above, and possibly due to the nature of the rock matrix, where there may be difficulty in fully removing all contaminants from the outer surface of the *Tasmanites* using each investigated treatment method in isolation.

4.1.1 Experimental thermal maturation

The results of experimental maturation are shown in Figures 4.1, 4.2 and 4.3. Experimental thermal maturation, carried out in an inert atmosphere over 100 days, does not appear to cause any significant variation in the $\delta^{15}N$ and $\delta^{13}C$ values in the palynomorph, *Tasmanites*. Minor positive trends were observed in both $\delta^{15}N$ and $\delta^{13}C$ towards the higher temperature range (125 °C – 170 °C), but because these values are generally located within error of the control sample, they are not deemed to be of any significance for the purposes of this research. Further testing at higher temperatures may yield greater isotopic variation, but is beyond the scope of this research. Following the construction of the nano-EA, the samples were analysed again, the results of which are shown in Figure 4.2. The discrepancy is most likely due to the reduced stock of 'clean' *Tasmanites* within each sample, and as the nano-EA analyses a much smaller proportion of these specimens (6-10 specimens, compared to 200 specimens), the likelihood of error is somewhat greater than the samples run on the general set up of the EA – IRMS.

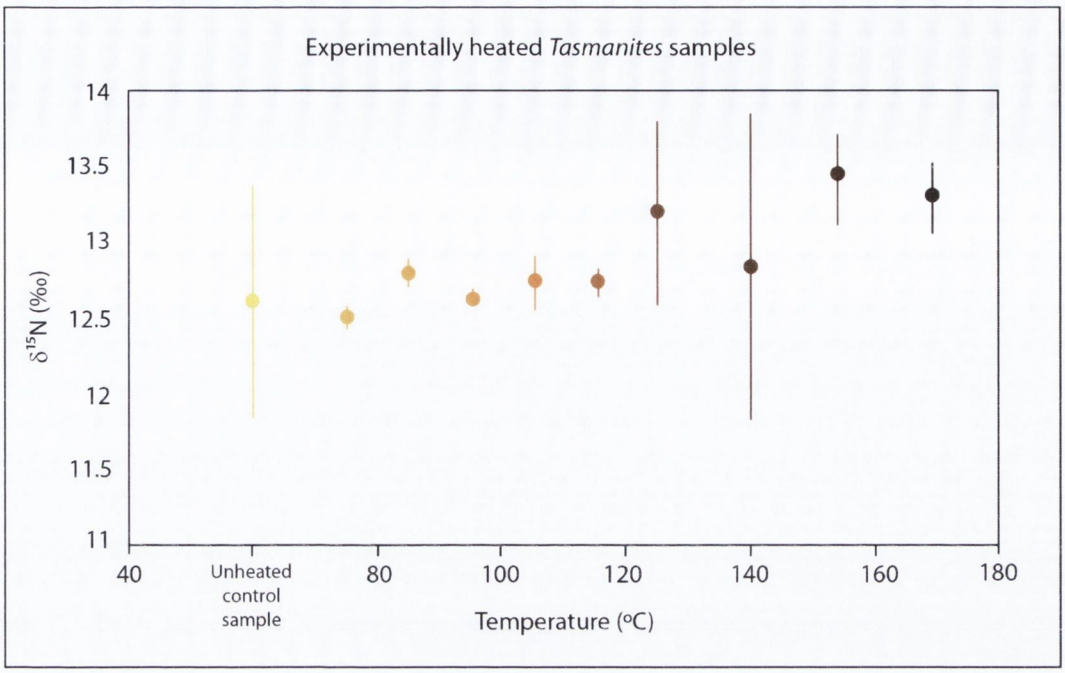

Figure 4.1. $\delta^{15}N$ of *Tasmanites* versus temperature, following experimental laboratory heating in an inert atmosphere for 100 days. Range of 60 °C (unheated control sample) - 170 °C. Error bars ± 1SD.

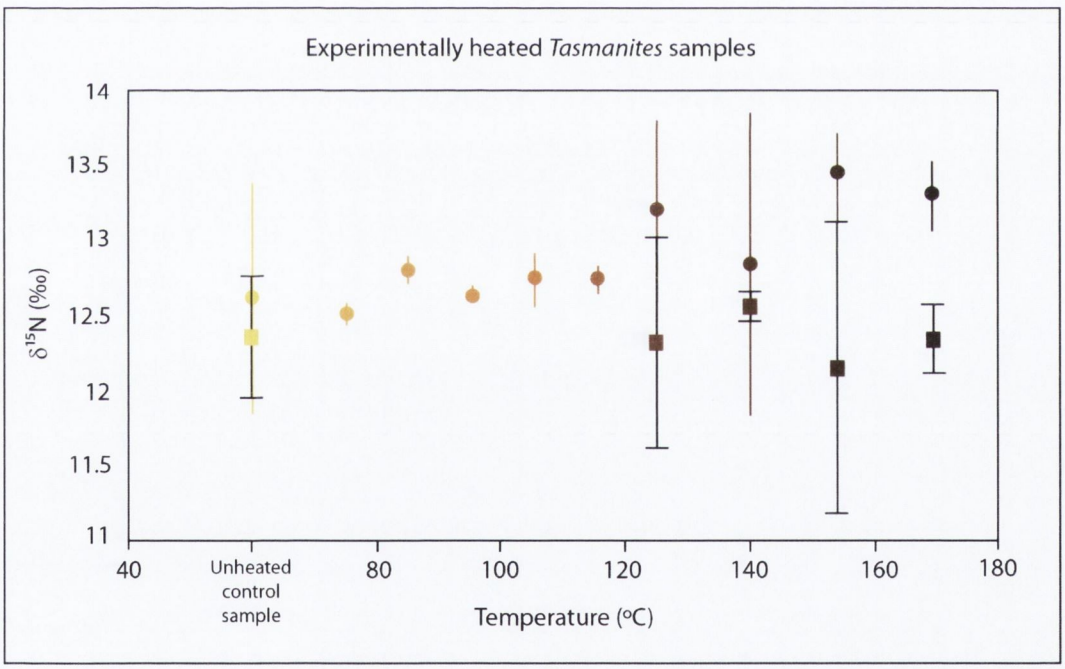

Figure 4.2. $\delta^{15}N$ of *Tasmanites* versus temperature for general set up of EA-IRMS and nano-EA-IRMS. Range of 60 °C (unheated control sample) - 170 °C. Error bars ± 1SD. Data points collected on the EA-IRMS are shown as closed circles and data points from the nano-EA-IRMS are shown as closed squares.

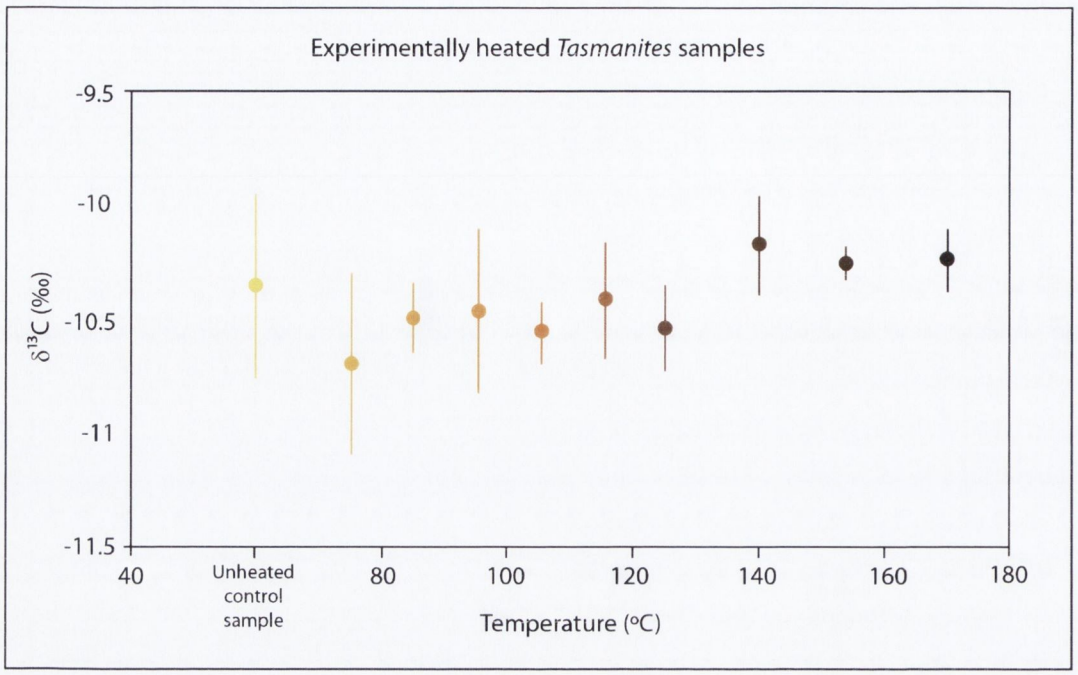

Figure 4.3. $\delta^{13}C$ of *Tasmanites* versus temperature, following experimental laboratory heating in an inert atmosphere for 100 days. Range of 60°C (unheated control sample) – 170°C. Error bars ± 1SD.

4.1.2 Chemical treatment

Processing *Tasmanites* with a range of chemical treatments had varying effects on their isotopic signature (Figure 4.4). With the exception of HCOOH, CH_3COOH and HNO_3, all other chemical treatments investigated caused little to no isotopic variation in either $\delta^{15}N$ or $\delta^{13}C$. Treating the sample with HCOOH for 8 hours led to a less positive (lighter) $\delta^{15}N$ value in the *Tasmanites* specimens of just over 1‰, however, it led to almost no change in the $\delta^{13}C$ value relative to the control sample. Exposure to CH_3COOH for 8 hours led to a significantly less positive (lighter) $\delta^{15}N$ value (> - 2.5 ‰), but again caused little to no change in the $\delta^{13}C$ value (+ 0.2 ‰). Unsurprisingly, a highly negative $\delta^{15}N$ value of -21.6 ‰, and an increased weight percentage of nitrogen (2.83 %) was recorded for the sample exposed to HNO_3, almost certainly due to contamination by HNO_3. The same process led to a slight, but not significantly, lighter (more negative) $\delta^{13}C$ of approximately - 0.5 ‰, relative to the control sample. The clay mineralogy treatment, which includes immersion in NaClO for 24 hours at 60 °C, and subsequent short term exposure (15 minutes) to $Na_2S_2O_4$, $C_6H_5Na_3O_7$ and $NaHCO_3$, caused very little change in the $\delta^{15}N$ value of the *Tasmanites*. This treatment, however led to a slightly heavier (less negative) $\delta^{13}C$ value of approximately + 0.55 ‰, relative to the control sample.

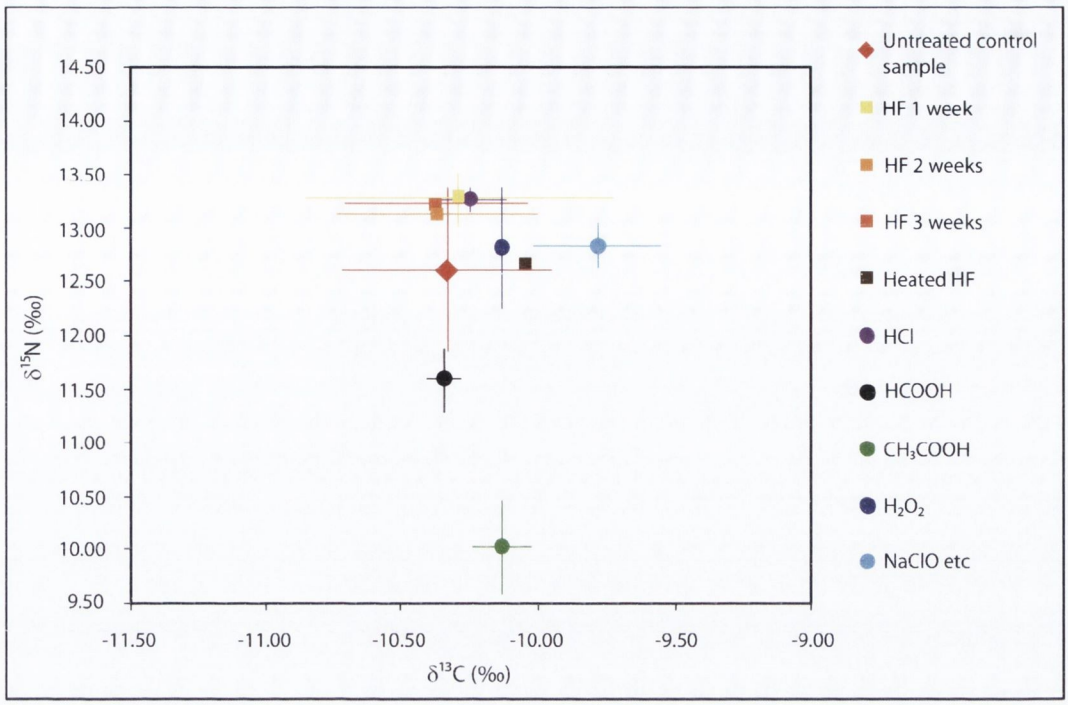

Figure 4.4. Plot of $\delta^{13}C$ versus $\delta^{15}N$ of *Tasmanites*, each subjected to a range of chemical treatments, shown as the legend in the chart area. Nitric acid is shown in Figure 4.5. Error bars ± 1SD.

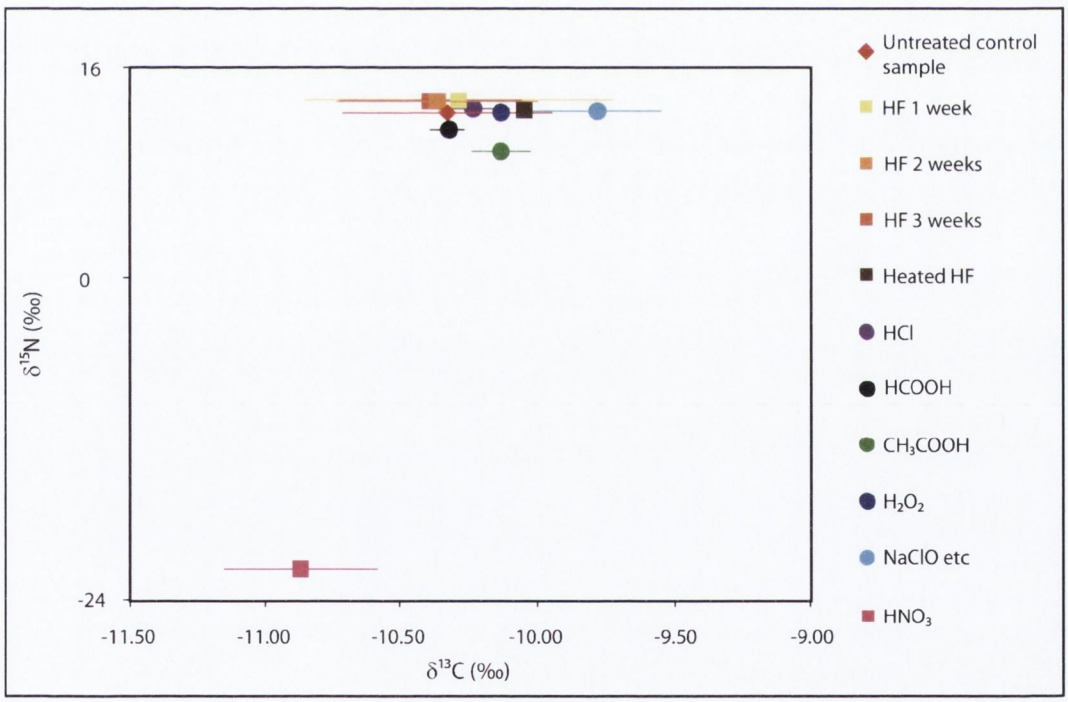

Figure 4.5. Plot of $\delta^{13}C$ versus $\delta^{15}N$ of *Tasmanites* subjected to a range of chemical treatments, inclusive of nitric acid. Error bars ± 1SD.

4.1.3 Oxidation

Exposure to H_2O_2 for a period of five hours, in order to experimentally induce the conditions of natural weathering, caused little to no isotopic change in either the $\delta^{15}N$ or $\delta^{13}C$ of the *Tasmanites* specimens (Figure 4.4 and Figure 4.5).

4.2 PALYNOLOGY

Palynological slides were prepared for each section and analysed as part of this project. As the samples contain mostly AOM, assessing their approximate stratigraphic position often proved difficult as palynomorphs were frequently obscured and engulfed by the large quantities of AOM contained within the black shales (Figure 4.6). Additional palynological slides were prepared following the clay mineralogy treatment method (Figure 4.7), which included the immersion of the sample in NaClO at 60 °C for 24 hours. The resulting sample contained significantly reduced levels of AOM, permitting easier identification of palynomorphs, which were then present in much higher concentrations than before the treatment due to the removal of excess AOM. However, this process may have inadvertently led to the removal or dissolution of some of the more fragile palynomorphs or parts of palynomorphs, such as the cingulum or zona, the outer exine or the spines (Figure 4.8). This can make identification of key palynomorphs very difficult as their defining features may be absent following this treatment method. The loss of such features may generate difficulties when trying to assess the stratigraphic palynology of a section. Further work is required to investigate this in greater detail, but if the treatment is shown to have a negligible impact, it offers great potential for future palynology of black shales.

The palynological slides were used to assess the general abundance and relative size of the *Tasmanites* contained within each unit and section of collected samples. The high quantity of AOM often obscured the accurate measurement of the abundance of *Tasmanites* following HF treatment alone, therefore further slides were prepared to re-assess the abundance of *Tasmanites* within the black shale units following the clay mineralogy treatment method.

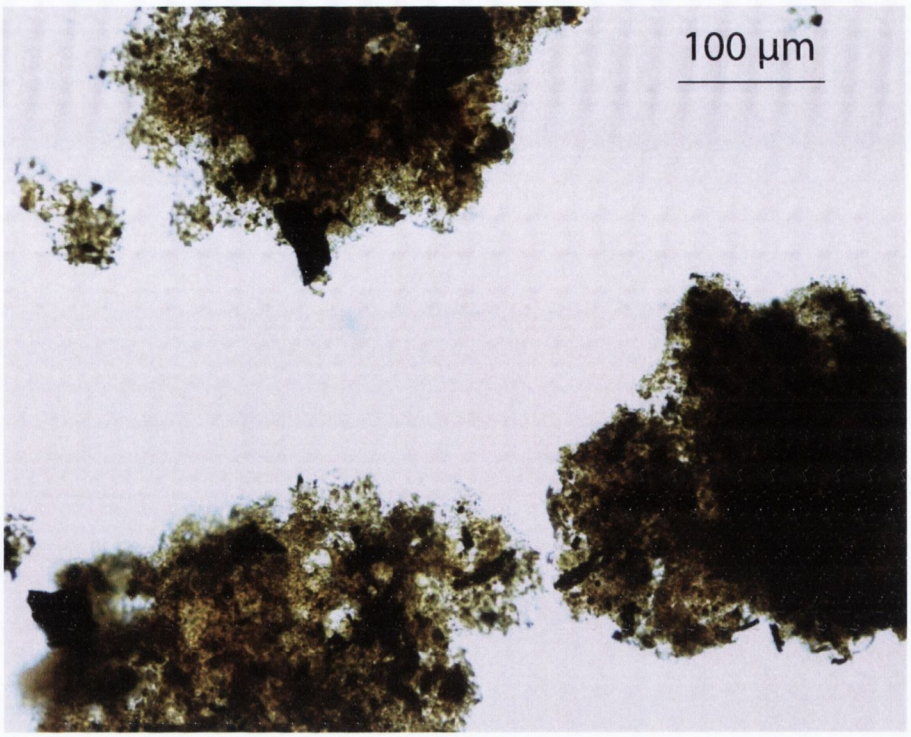

Figure 4.6. Photomicrograph of a black shale sampled from the Cleveland Member (KY10E) and processed using standard palynological techniques (HF) alone (not bleached).

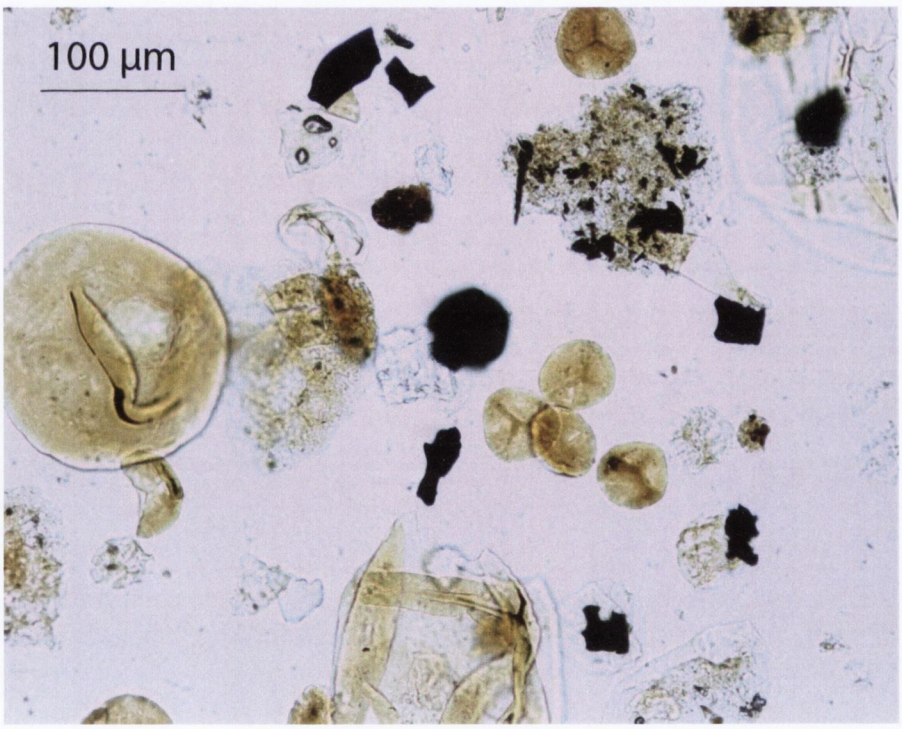

Figure 4.7. Photomicrograph of the same Cleveland Member sample as Figure 4.6, processed using standard palynological techniques, followed by immersion in NaClO at 60°C for 24 hours.

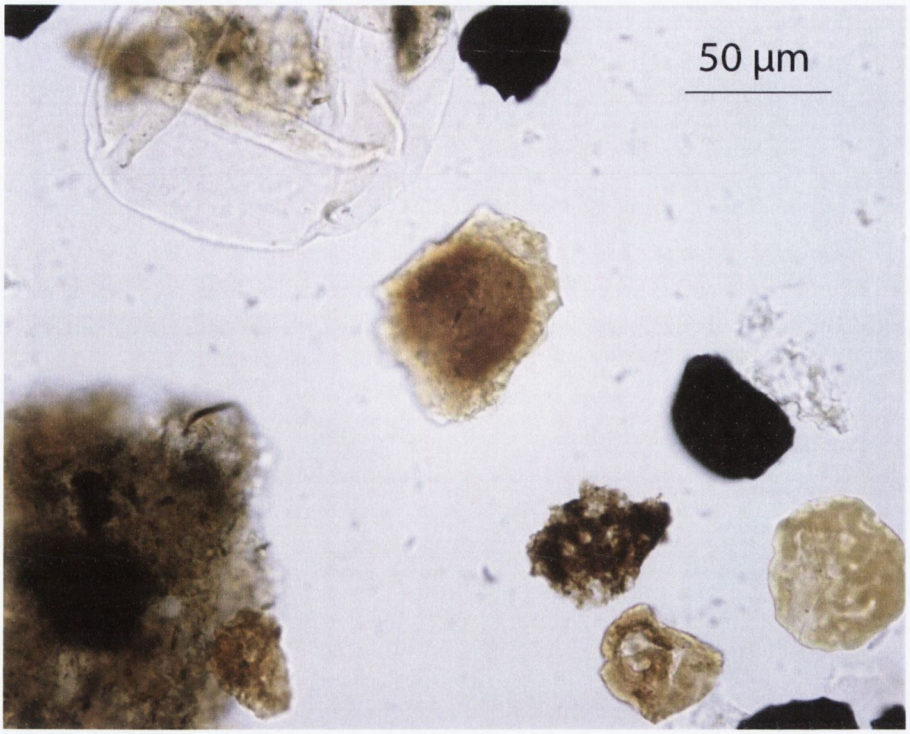

Figure 4.8. Degradation of zona possibly brought about by exposure to NaClO.

4.2.1 *Protosalvinia* spp.

A new species of spore, *Retusotriletes loboziakii* Rooney, Clayton and Goodhue 2013, was erected from the enigmatic Late Devonian fossil, *Protosalvinia.* The post-HF residue contained isolated *Protosalvinia* thalli and dispersed palynomorphs. The NaClO treatment disaggregated many of the *Protosalvinia* thalli, freeing tetrads identical to the dispersed tetrads from the HF preparations. No individual spores were extracted from the *in situ* tetrads, but their morphology is identical to the naturally dispersed spores in the post-HF residues.

4.2.1.1 Systematic palaeontology

Anteturma SPORITES H. Potonié 1893

Turma TRILETES (Reinsch) Dettmann 1963

Suprasubturma ACAMERATITRILETES Neves and Owens 1966

Subturma AZONOTRILETES (Luber) Dettmann 1963

Infraturma LAEVIGATI (Bennie & Kidston) R. Potonié 1956

Genus *Retusotriletes* Naumova 1953 emend. Streel 1964

Type species. *Retusotriletes simplex* Naumova 1953

Retusotriletes loboziakii Rooney, Clayton and Goodhue 2013

Plate 1, figures 1-5, 7

Synonymy.

Retusotriletes sp. Loboziak *et al.*, 1997, plate 1, fig. 1.

Holotype. Plate 1, figure 1.

Type locality. Roadcut on Kentucky Route 10 East, near Vanceburg, Kentucky, U.S.A. (N38°9.87', W83°35.528).

Diagnosis. Trilete acamerate miospore with circular amb. Suturae distinct, extending 75%–80% of spore radius, straight to slightly sinuous, bordered by narrow ridges. Suturae terminate in curvaturae perfectae, clearly defined by prominent curvatural ridges. Exospore laevigate to scabrate, very thick except for relatively thin contact areas.

Dimensions.

Overall diameter of 18 specimens from sample 1: 168 (189) 207 µm.
Overall diameter of 22 specimens from sample 1b: 171 (191) 209 µm.
The mean distal exospore thickness is 9 µm.

Remarks. Lateral and oblique compressions of this species are common. Dispersed tetrads are also frequently observed; these lack any form of enclosing membrane. *Retusotriletes loboziakii* Rooney, Clayton and Goodhue 2013 is distinguished from other species of *Retusotriletes* by its large overall size, thick exospore, circular amb and curvaturae perfectae. *Retusotriletes distinctus* Richardson 1964 is similar in size to *Retusotriletes loboziakii* Rooney, Clayton and Goodhue 2013, but has longer suturae and darker triangular areas within the contact areas. *Retusotriletes avonensis* Playford 1964 is smaller than *Retusotriletes loboziakii* Rooney, Clayton and Goodhue 2013. (i.e. 62 to 104 µm). The exospore of the former is thickened around the equator and its curvaturae are not clearly defined interradially. The spores in the dissociated tetrad illustrated by Chaloner and Orbell (1971, fig. 1E) are clearly *Retusotriletes loboziakii* Rooney, Clayton and Goodhue 2013.

Derivation of name. The species is named for the late Stanislas Loboziak who published extensively on Famennian spores and who, together with Jose Henrique Gonçalves Melo, Luiz P. Quadros and Maurice Streel, noted that the parent plant of dispersed, large specimens of *Retusotriletes* sp. in Brazil may be *Protosalvinia* sp.

4.2.1.2 Stratigraphical palynology

The post-HF organic residues are dominated by AOM, therefore the post-NaClO residues were analysed for the purposes of stratigraphical palynology. The post-NaClO residues are dominated by *Leiosphaeridia* spp. and *Tasmanites* spp., and also including well-preserved miospores. In addition to *Retusotriletes loboziakii* Rooney, Clayton and Goodhue 2013, *Hystricosporites* sp., *Retusotriletes incohatus* Sullivan 1964, *Rugospora phillipsii* Clendenning, Eames and Wood 1980 and *Rugospora radiata* (Jushko) Byvscheva 1985 are also present. *Vallatisporites hystricosus* (Winslow) Byvscheva 1985 was not recorded, although it is present stratigraphically higher in the Ohio Shale in eastern Kentucky.

The presence of *Rugospora radiata* and the absence of *Vallatisporites hystricosus* indicates that samples collected from I64E and KY10E, Kentucky, are both referable to the VCo Miospore Biozone *sensu* Maziane *et al.* (1999). According to Streel (2009), the base of the VCo Biozone is no older than the Upper *trachytera* Conodont Biozone and its top, defined by the base of the VH Biozone, is no younger than the Middle *expansa* Conodont Biozone. Therefore, the miospore-based age for the *Protosalvinia* Zone in eastern Kentucky is consistent with the conodont biostratigraphy of Over *et al.* (2009).

On the basis of the dispersed miospore assemblages observed, the presence of *Rugospora radiata* and the absence of *Vallatisporites hystricosus*, the *Protosalvinia* Zone in eastern Kentucky is slightly older (the VCo Miospore Biozone) than it is in the Amazon Basin of Brazil (the VH Miospore Biozone). This contention requires further testing as only two miospore assemblages were investigated in the former area and neither is diverse.

Plate 4.1. All images are x500. Selected photomicrographs (Nomarski Interference Contrast) of *Retusotriletes loboziakii* Rooney, Clayton and Goodhue 2013 and *Protosalvininia* sp. The specimens are housed in the Geological Museum, Trinity College Dublin (TCD), Dublin 2, Ireland; the individual specimen numbers are prefixed 'TCD'.

1. *Retusotriletes loboziakii* TCD.60360, sample 1b. Holotype.
2. *Retusotriletes loboziakii* TCD.60361, sample 1b.
3. *Retusotriletes loboziakii* TCD.60362, sample 1. The pseudo-ornamentation is produced by adhering fragments of amorphous organic matter (AOM).
4. *Retusotriletes loboziakii* TCD.60363, sample 1b. Fragmented tetrads; three spores with curvaturae perfectae clearly visible.
5. *Retusotriletes loboziakii* TCD.60364, sample 1b. Intact tetrad.
6. *Protosalvininia* sp. TCD.60365, sample 1b. Thallus with a conceptacle containing a single tetrad.
7. *Retusotriletes loboziakii* TCD.60366, sample 1b. Fragmentary tetrad; lateral (top) and oblique (bottom) compressions.

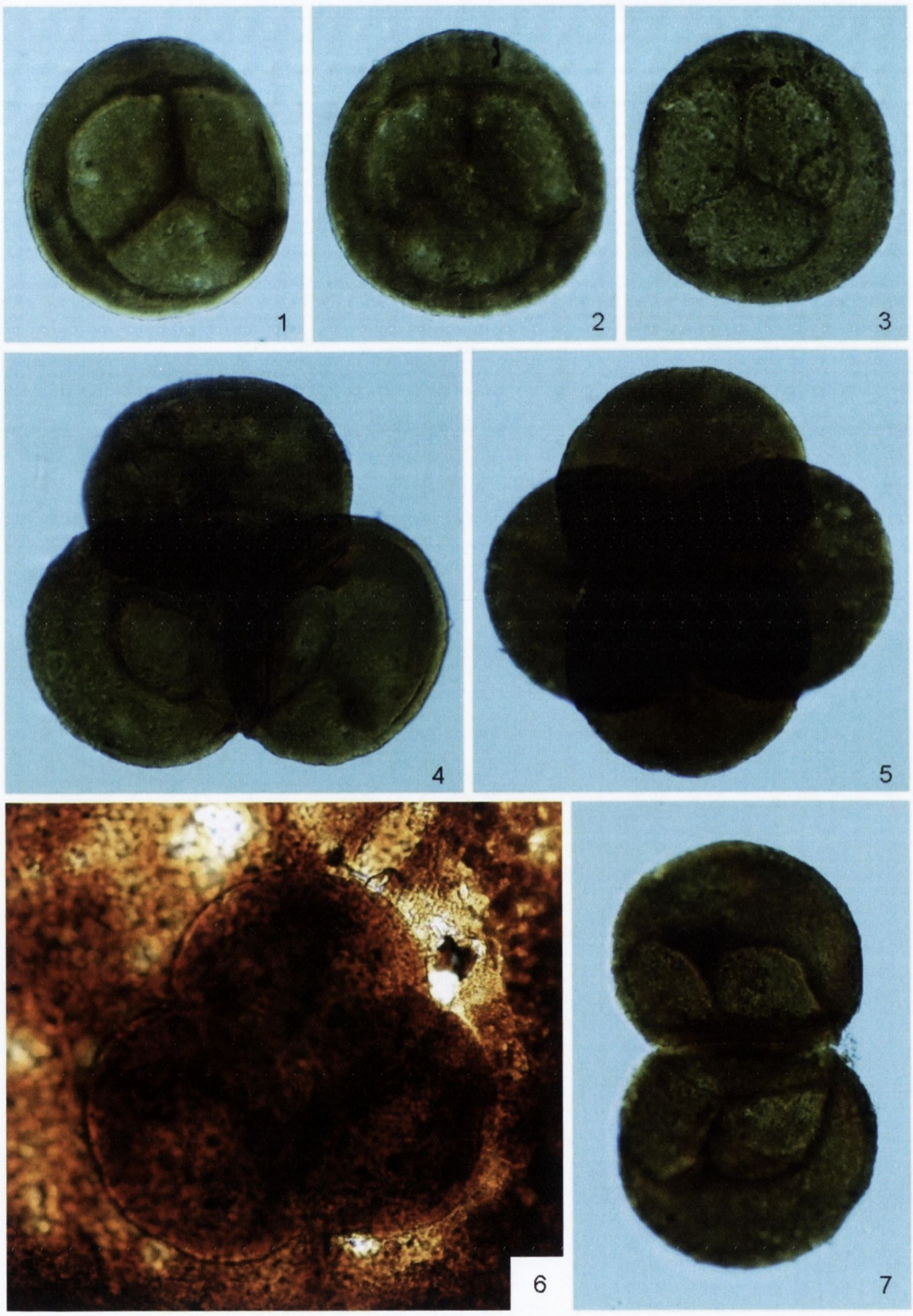
1
2
3
4
5
6
7

4.3 STABLE ISOTOPES

4.3.1 The *Protosalvinia* Zone

The isotopic results for the *Protosalvinia* samples are shown in Table 4.1and illustrated in Figures 4.9 and 4.10. Results are based on the average of two replicate analyses, with the exception of the *Protosalvinia* thalli from northeastern Kentucky, where not enough sample was available for a replicate analysis. The $\delta^{15}N$ signature of the enigmatic fossil remains relatively similar throughout the Appalachian, Michigan and Illinois basins. There is some slight variation (0.2 – 1.74 ‰), however, possibly brought about through degradation of the thalli. The thalli proved more difficult to analyse for the two samples with more positive (heavier) isotopic signatures, located in northeastern and central Kentucky (1.70 ‰ and 1.74 ‰, respectively). The material used for these two analyses were visually degraded, leading to the tentative assumption that degraded material may record a heaver $\delta^{15}N$ signal than the non-degraded material.

The *Protosalvinia* thalli extracted from the sample obtained from Brazil recorded a $\delta^{15}N$ value of 5.46 ‰ (± 0.2 ‰), much more positive (heavier) than any of the values recorded for North America. Tetrads of spores were also extracted and analysed from the sample obtained from northeastern Kentucky. The tetrads recorded a $\delta^{15}N$ value of 3.18 ‰ (± 0.2 ‰), which is more positive (heavier) than all of the $\delta^{15}N$ values recorded for the *Protosalvinia* thalli within North America.

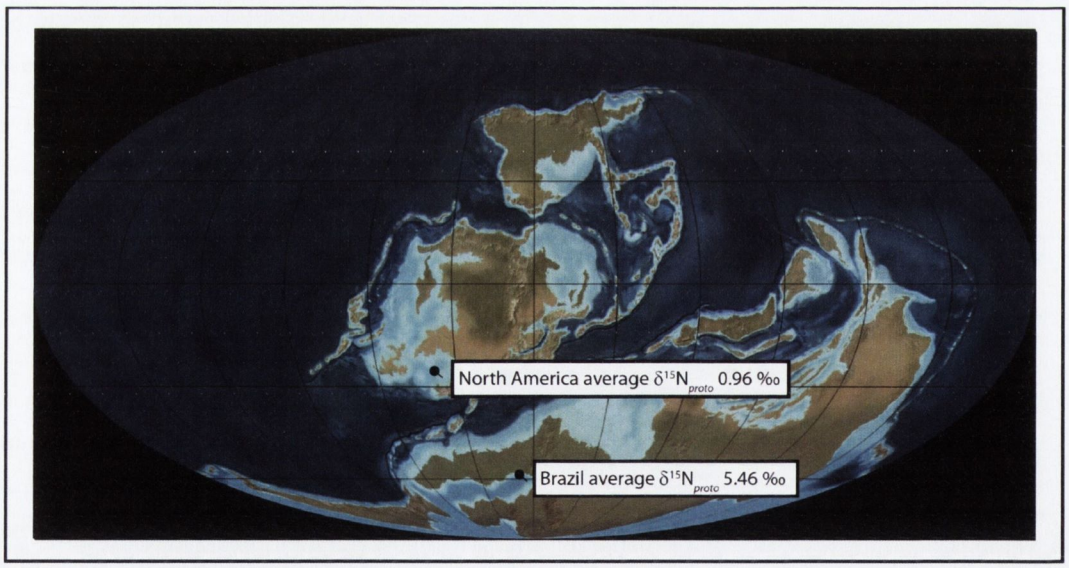

Figure 4.9. *Protosalvinia* $\delta^{15}N$ results, averaged from North America and Brazil, shown against Late Devonian palaeogeography (modified from Blakey, 2011).

Tasmanites samples were also extracted from four of the North American samples, listed in Table 4.1Table 4.1and shown in Figures 4.10 and 4.11. The $\delta^{15}N$ offset between the *Protosalvinia* thalli and *Tasmanites* is similar for three out of four of the samples, whereas the *Tasmanites* record a $\delta^{15}N$ value between 1.9 – 2.64 ‰ more positive (heavier) than the *Protosalvinia* thalli. The fourth sample, extracted from northeastern Kentucky, had a significantly smaller offset of 0.63 ‰. However, this *Protosalvinia* sample did not have a replicate due to the lack of material and it is possible that the *Protosalvinia* thalli were degraded, leading to a heavier $\delta^{15}N$ value, and a smaller offset between the *Protosalvinia* thalli and the *Tasmanites* specimens.

The tetrads of spores were extracted from this sample because of the high number of specimens available in comparison to other samples. This may be an indicator of degraded thalli, where many of the tetrads have been released into the sediment following degradation of the thalli. Another possibility is that the heavier isotopic signature may simply be a result of higher quantities of tetrads analysed with the *Protosalvinia* thalli, thereby mixing the lighter $\delta^{15}N$ signal of the thalli and the heavier $\delta^{15}N$ signal of the spores to record an isotopic signature intermediate between the two.

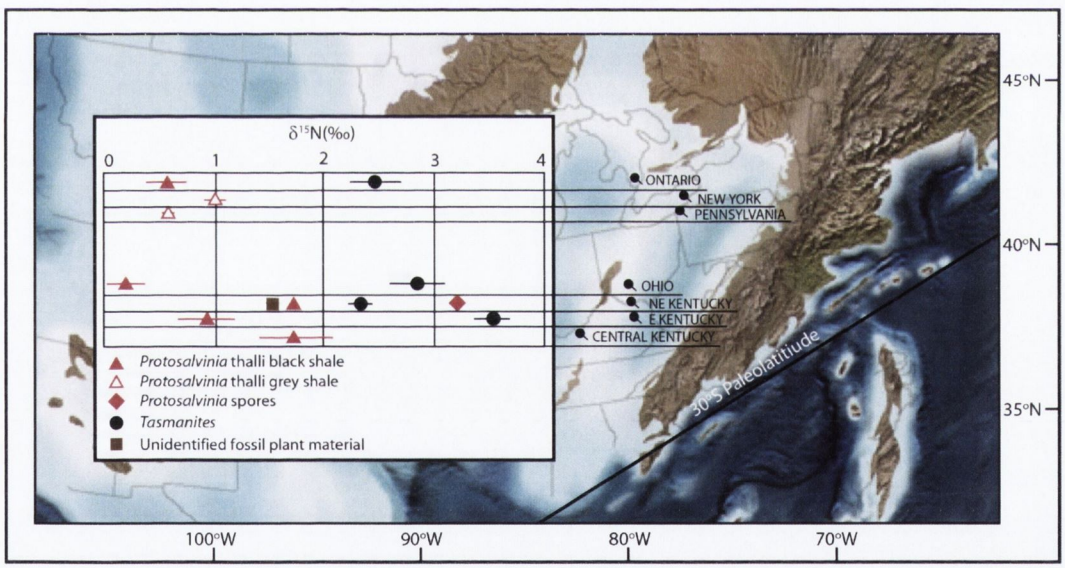

Figure 4.10. $\delta^{15}N$ results from *Protosalvinia* thalli, *Protosalvinia* spores and *Tasmanites* within the Appalachain, Illinois and Michigan basins in North America. Late Devonian palaeogeography is modified from Blakey (2011).

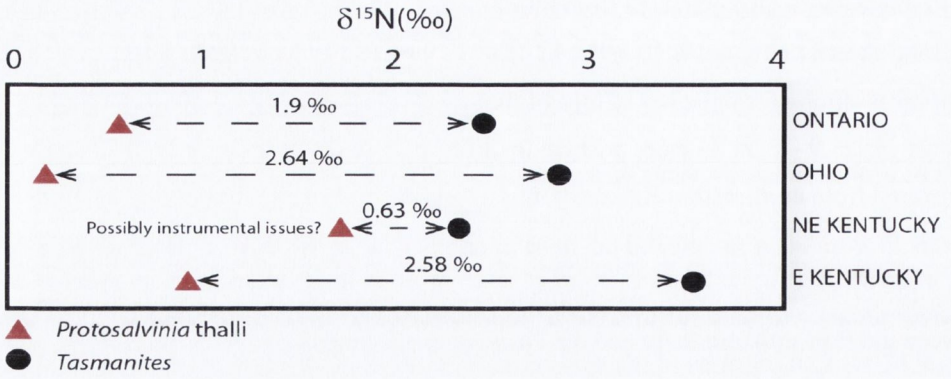

Figure 4.11. $\delta^{15}N$ offset recorded between *Tasmanites* samples and *Protosalvinia* thalli extracted from the same samples within North America.

SAMPLE	SAMPLE LOCALITIES	$\delta^{15}N$ (‰)	BASIN
Protosalvinia thalli	Ontario_140.75m	0.66	Michigan
Protosalvinia thalli	Ontario_141.39m	0.65	Michigan
Protosalvinia thalli	Ontario_141.8m	0.49	Michigan
Protosalvinia thalli	Ontario_142.32m	0.56	Michigan
Protosalvinia thalli	Ontario_142.71m	0.47	Michigan
Protosalvinia thalli	New York	1.01	Appalachian
Protosalvinia thalli	Pennsylvania	0.58	Appalachian
Protosalvinia thalli	Ohio	0.20	Appalachian
Protosalvinia thalli	Northeastern Kentucky	1.70	Appalachian
Protosalvinia thalli	Eastern Kentucky	0.93	Appalachian
Protosalvinia thalli	Central Kentucky	1.74	Illinois
Protosalvinia thalli	Brazil	5.46	Amazon
Protosalvinia tetrads	Northeastern Kentucky	3.18	Appalachian
Tasmanites	Ontario_140.75m	2.47	Michigan
Tasmanites	Ohio	2.84	Appalachian
Tasmanites	Northeastern Kentucky	2.33	Appalachian
Tasmanites	Eastern Kentucky	3.51	Appalachian

Table 4.1. $\delta^{15}N$ results of *Protosalvinia* thalli, *Protosalvinia* spores (tetrads) and *Tasmanites* obtained from each locality.

4.3.2 Bulk organic residues

All bulk organic residues were analysed on a standard configuration of the EA-IRMS at the TCD Geochemistry Unit. Results are based on two replicate analyses wherever possible. Several samples from the Bedford Shale at KY2520N are based on a single measurement due to difficulties

encountered with the samples and the instrumentation. Full suites of data are provided in Figures 4.19, 4.21, 4.23 and 4.25, for reference. $\delta^{15}N_{bulk}$ is used from here on to denote the $\delta^{15}N$ value of the bulk organic residues, following treatment with HCl and HF.

4.3.2.1 KY801N section

The $\delta^{15}N_{bulk}$ results for KY801N are shown in Figure 4.12. The sampled section at KY801N, near Morehead, covers in brief, the key segments of the Upper Devonian stratigraphy analysed as part of this project. This section will be used to compare and contrast with the composite section, assembled from the data collected from the other three sample localities. The bulk organic residues of the samples collected at KY801N record $\delta^{15}N_{bulk}$ values that range from + 0.95 ‰ up to + 4.6 ‰ (average 2.5 ‰). The only grey shale sample within the section, stratigraphically recognised as the Three Lick Bed, records a heavier $\delta^{15}N_{bulk}$ (4.3 ‰) than the black shales located on either side of this horizon (2.2 ‰ and 1.9 ‰). If this grey shale sample is excluded from the chemostratigraphic curve for KY801N, the remaining black shales record a general increasingly positive (heavier) $\delta^{15}N_{bulk}$ from the Huron Member (1.4 ‰) to the middle of the Cleveland Member (2.8 ‰). The upper portion of Cleveland Member records a slightly less positive (lighter) $\delta^{15}N$ value (0.95 ‰). This slight decrease is followed by an increasingly positive trend in $\delta^{15}N_{bulk}$ that begins at the very top of the Cleveland Member and is recorded throughout the Bedford and Sunbury shale formations. The top of the Bedford Shale records a slight deviation towards a less positive (lighter) $\delta^{15}N_{bulk}$ before continuing its increasingly positive (heavier) $\delta^{15}N_{bulk}$ trend through the base of the Sunbury Shale.

4.3.2.2 KY10E section

The $\delta^{15}N_{bulk}$ results for KY10E are shown in Figure 4.13. The KY10E section comprises the Huron Member, the Three Lick Bed and the majority of the Cleveland Member of the Ohio Shale. The bulk organic residues collected from KY10E, record an increasingly positive trend in $\delta^{15}N_{bulk}$ from the bottom to the top of the section. The $\delta^{15}N_{bulk}$ values range from -1 ‰ to +3.2 ‰ (average 0.6 ‰).

Two grey shale horizons are visible in the section, the lowermost of these grey shales is located just above the *Protosalvinia* Zone, within the middle Huron Member. The second grey shale horizon is located in the middle of the section and corresponds to the Three Lick Bed, which is concentrated at this outcrop locality into one grey shale horizon.

The $\delta^{15}N_{bulk}$ values recorded for the two grey shale outcrops are 1.7 ‰ and 2 ‰, respectively, recording more positive (heavier) values than their immediate surrounding bulk organic black shale residues (0 ‰ and 0.4 ‰, respectively). The $\delta^{15}N_{bulk}$ values recorded for the

black shales within the Huron Member range from - 1 ‰ to + 0.5 ‰ (average - 0.1 ‰), with more negative values located towards the bottom of the Huron Member, and becoming more positive towards the top.

The bulk organic residues of the Cleveland Member range from 0.1 ‰ to 3.2 ‰ (average 1.5 ‰), becoming increasingly positive towards the top of the section. The bulk organic black shale residues located at the top of the section, or stratigraphically, within the upper Cleveland Member, record more positive (heavier) $\delta^{15}N_{bulk}$ values than both of the bulk grey shale units located further down the stratigraphy, reaching $\delta^{15}N_{bulk}$ values of between 2.5 ‰ and 3.2 ‰.

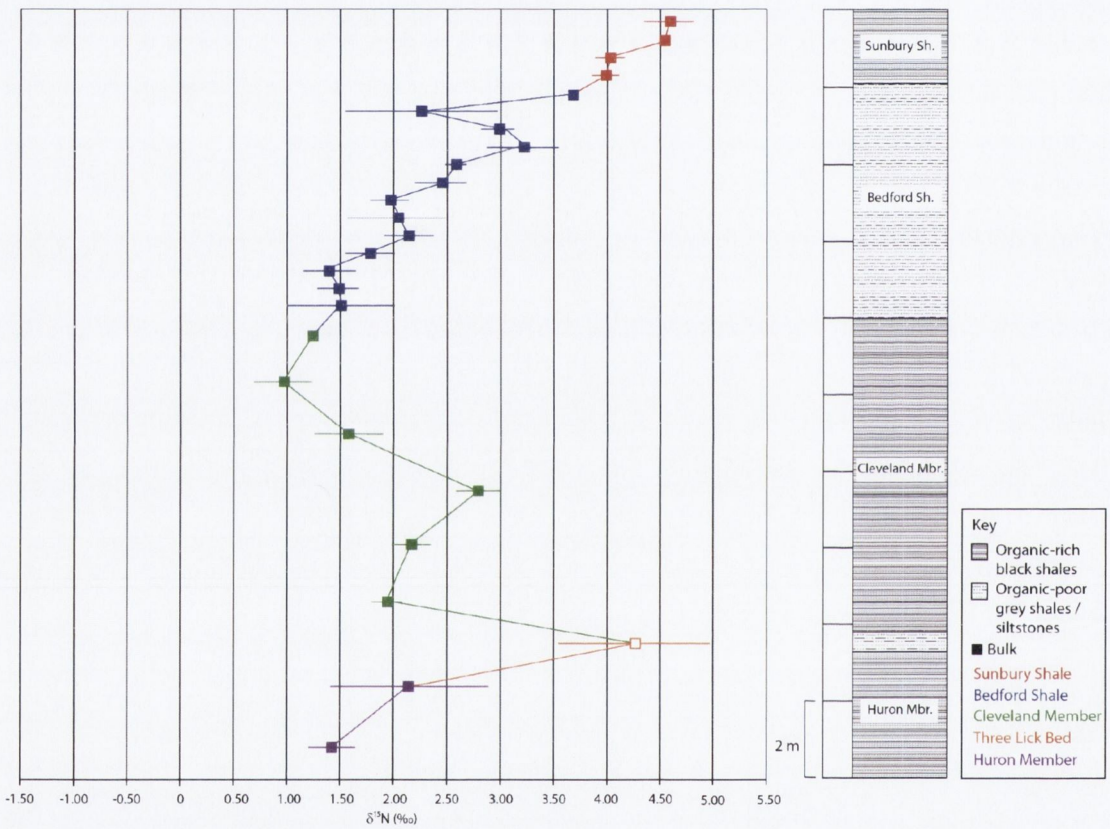

Figure 4.12. $\delta^{15}N_{bulk}$ results for KY801N. Closed squares represent bulk black shale samples, open squares represent bulk grey shale samples. Error bars ± 1SD

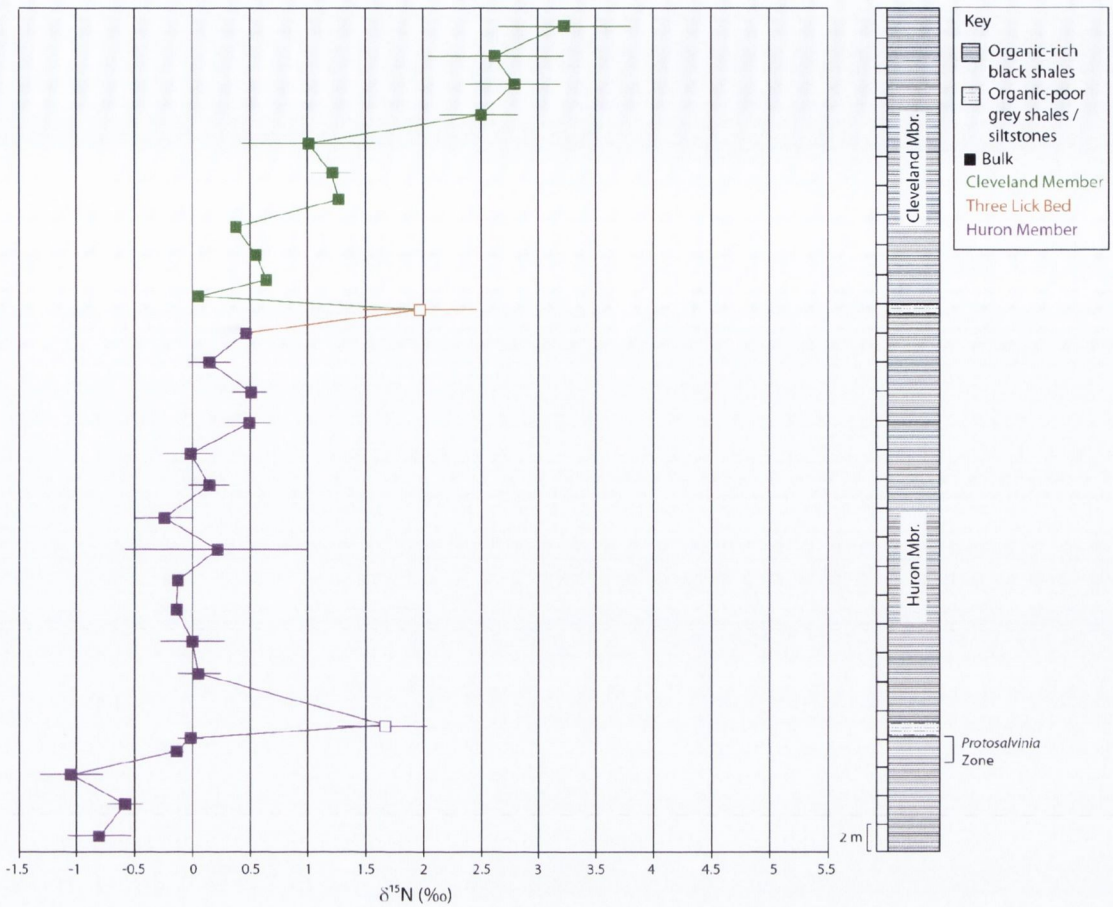

Figure 4.13. $\delta^{15}N_{bulk}$ results for KY10E. Closed squares represent bulk black shale samples, open squares represent bulk grey shale samples. Error bars ± 1SD

4.3.2.3 I64W, Three Lick Bed type section

The $\delta^{15}N_{bulk}$ results for I64W are shown in Figure 4.14. The bulk organic residues from the Three Lick Type Section record a very slight positive trend in $\delta^{15}N_{bulk}$ values from the bottom to the top of the section, punctuated by abrupt increases in $\delta^{15}N$ for each of the three grey shale horizons that characterise the Three Lick Bed. The $\delta^{15}N_{bulk}$ values range from 0.9 ‰ to 3.1 ‰ (average 1.8 ‰). The three grey shale beds record $\delta^{15}N$ values, from the lowermost bed to uppermost bed, of 2.1 ‰, 2.6 ‰ and 2.4 ‰, respectively. The intervening black shales record an average $\delta^{15}N_{bulk}$ of 0.9 ‰. Above the final grey shale horizon, the average $\delta^{15}N_{bulk}$ value of the black shale is approximately 1.8 ‰, with two abrupt increases in $\delta^{15}N_{bulk}$ of 3.1 ‰ and 3 ‰, punctuating the observed background $\delta^{15}N_{bulk}$ signal near the middle of the section and at the very top of the section, respectively.

4.3.2.4 KY2520N section

The $\delta^{15}N_{bulk}$ results for KY2520N are shown in Figure 4.15. The bulk organic residues collected from KY2520N, record $\delta^{15}N_{bulk}$ values that range from - 0.6 ‰ to + 5.4 ‰ (average 2.3 ‰). This section contains the uppermost Cleveland Member, the entire Bedford Shale, and the majority of the Sunbury Shale. The sample obtained from the Cleveland Member recorded a $\delta^{15}N_{bulk}$ value of 3.6‰.

The Bedford Shale consists of a basal black shale sample ($\delta^{15}N_{bulk}$ 4.3 ‰) followed by grey shale deposited throughout the rest of the formation at this outcrop locality. The $\delta^{15}N_{bulk}$ values for the Bedford Shale range from 2.8 ‰ to 5.4 ‰ (average 3.4 ‰) and the $\delta^{15}N_{bulk}$ signal stays relatively constant throughout the grey shale (2.8 ‰ to 3.6 ‰). This signal is, however, interrupted within the upper third of the Bedford Shale by a steady increase in $\delta^{15}N_{bulk}$ up to 5.4 ‰. The $\delta^{15}N_{bulk}$ value falls again to 2.8 ‰ at the top of the Bedford Shale.

A conspicuous change to black shales directly above the Bedford Shale demarcates the boundary between the Bedford and Sunbury shales. The Sunbury Shale consists of black shale through to the top of the sampled section. The $\delta^{15}N_{bulk}$ values for the Sunbury Shale range from - 0.7 ‰ to + 3.7 ‰ (average 1.5 ‰). Two oscillations in the $\delta^{15}N_{bulk}$ signal are clearly evident within the Sunbury Shale at this outcrop locality. The samples can be packaged together to create average values covering the two oscillations. The first five samples record an average $\delta^{15}N_{bulk}$ value of 1.2 ‰. This drops to an average of -0.5 ‰ for the subsequent three samples, before increasing to 3.3 ‰ within the following four samples. This value then falls again to 0.4 ‰ within the subsequent two samples, before increasing to 2.5 ‰ within the uppermost two samples of this section. Sampling resolution was highest within the KY2520N section, possibly covering a sufficient range of samples to register such oscillations within the chemostratigraphic curve.

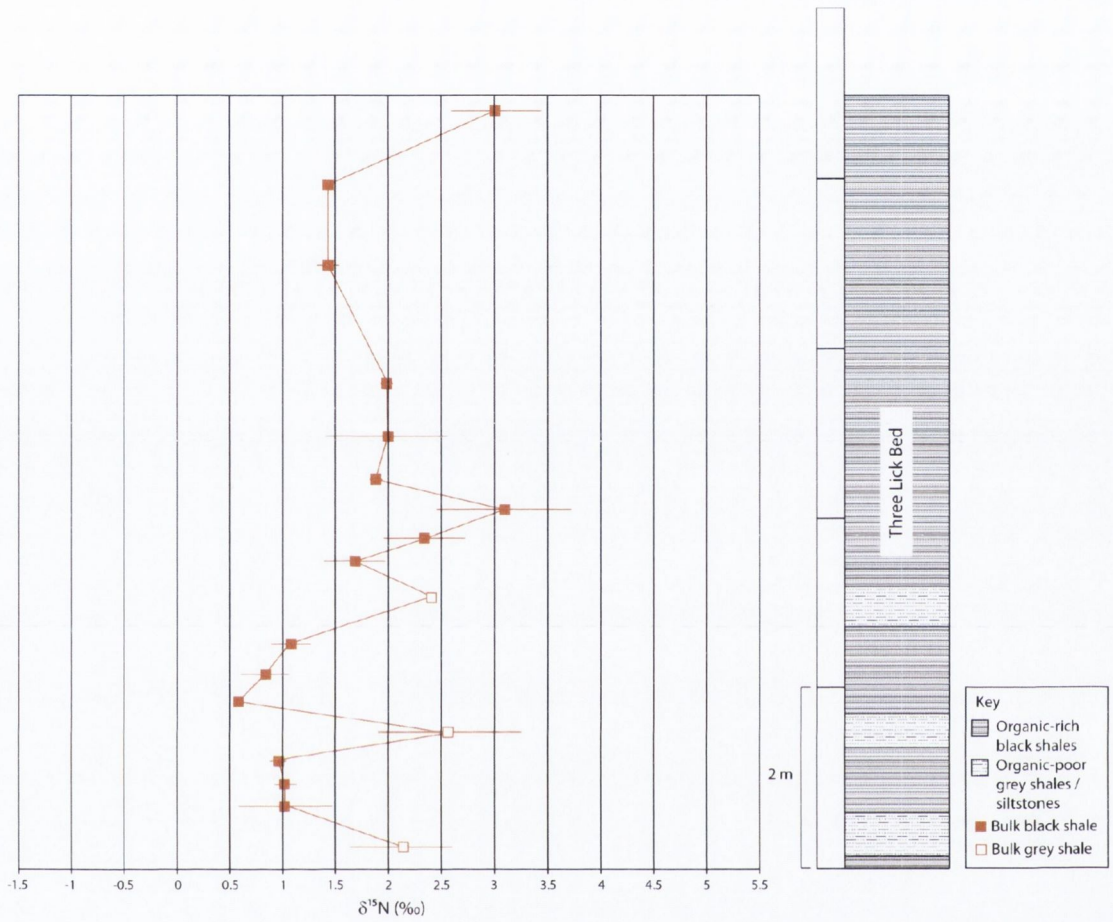

Figure 4.14. $\delta^{15}N_{bulk}$ results for I64W. Closed squares represent bulk black shale samples, open squares represent bulk grey shale samples. Error bars ± 1SD

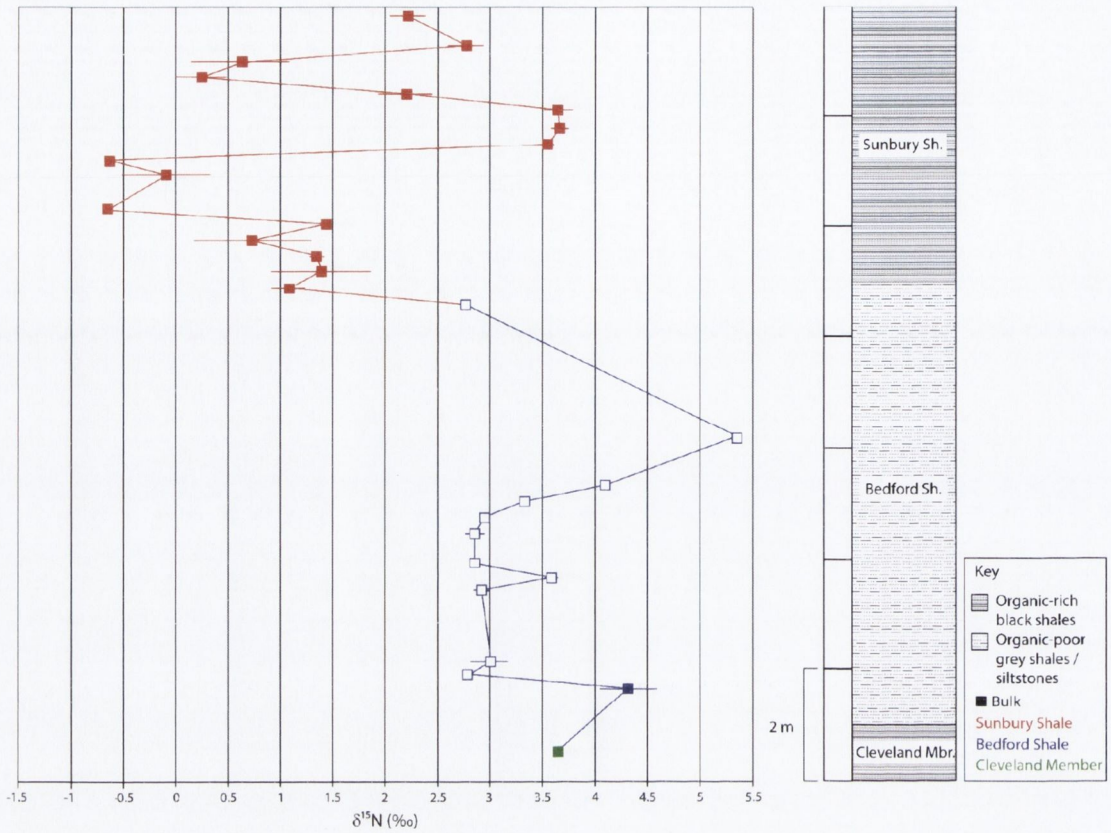

Figure 4.15. $\delta^{15}N_{bulk}$ results for KY2520N. Closed squares represent bulk black shale samples, open squares represent bulk grey shale samples. Error bars ± 1SD.

4.3.2.5 Composite section

The $\delta^{15}N_{bulk}$ results for the bulk organic residues are shown in Figure 4.16. Because this is a composite section, there may be baseline isotopic discrepancies between each of the sample localities, dependent upon conditions at each locality at the time of deposition. Three different sample localities, KY10E, I64W and KY2520N have been combined into one composite section, based on their approximate location within the stratigraphy. The Huron Member and most of the Cleveland Member are from the KY10E section, the Three Lick Bed is from the Three Lick Type Section along the I64W, and the very top of the Cleveland Member, the Bedford and Sunbury shales are all from the KY2520N section.

The $\delta^{15}N_{bulk}$ values of the black shales range from - 1 ‰ (lower Huron Member) to + 4.3 ‰ (lowermost Bedford Shale). Each black shale section records a general trend towards more positive $\delta^{15}N_{bulk}$ values, with slight offsets in their baseline isotopic signatures, possibly due to differing sample localities. The two black shale samples (topmost Cleveland Member and lowermost Bedford Shale) from the base of the KY2520N section have $\delta^{15}N_{bulk}$ values consistent with those found towards the top of the Cleveland Member from the KY10E section. However,

these $\delta^{15}N_{bulk}$ values are more positive (heavier) than those found in the Sunbury Shale, which is positioned at the top of the KY2520N section. The average trendline recorded by $\delta^{15}N_{bulk}$ appears to have shifted back towards less positive (lighter) values at the base of the Sunbury Shale, with a similar slope to the trendline recorded by the Ohio Shale of increasingly positive (heavier) $\delta^{15}N_{bulk}$ values towards the top of the section. Two obvious isotopic oscillations appear to be superimposed over this less positive average $\delta^{15}N_{bulk}$ trendline for the Sunbury Shale, with $\delta^{15}N_{bulk}$ values varying from those similar to the Huron Member (- 0.7 ‰ to + 0.7 ‰), to those recorded within the upper Cleveland Member (2.2 ‰ to 3.7 ‰).

The apparent lack of similar oscillations within the Cleveland and Huron members of the Ohio Shale may be an artefact of their lower sampling resolution compared with the higher sampling resolution within the Sunbury Shale. The sampling resolution at KY2520N may have been high enough to cover a sufficient range of samples to register such oscillations within the chemostratigraphic curve. It is possible that sampling resolution was not high enough within previous sections to catalogue possible isotopic oscillations that may exist in the underlying black shale sections, such as the Cleveland and Huron members of the Ohio Shale.

The nitrogen isotope composition of the majority of the black shale samples remains between - 1‰ and + 1.5 ‰ through most of the section. However, values above +1.5 ‰ are observed at various locations throughout the stratigraphy. These increases in $\delta^{15}N_{bulk}$ occur in the black shales located above the three grey shale horizons of the Three Lick Bed, within the top half of the Cleveland Member, the lowermost sample within the Bedford Shale, and within the two oscillations recorded in the Sunbury Shale.

The grey shales record a more positive (heavier) baseline $\delta^{15}N_{bulk}$ than the black shales, and overall record a similar trend towards more positive values throughout the section. The $\delta^{15}N_{bulk}$ values of the grey shales range from + 1.6 ‰ (above the *Protosalvinia* Zone) up to + 5.4 ‰ (middle Bedford Shale). A gradual enrichment in ^{15}N is recorded through the composite section (from + 1.6 ‰ up to + 3 ‰), up to the middle portion of the Bedford Shale, where an abrupt increase in $\delta^{15}N_{bulk}$ is recorded (from 3 ‰ up to 5.4 ‰) over a relatively short section of sampled material. This abrupt increase in $\delta^{15}N_{bulk}$ is followed by a decrease to 2.8 ‰, similar to average values recorded in the lower third of the Bedford Shale.

Overall, there is a gradual trend towards more positive (heavier) $\delta^{15}N_{bulk}$ values from the base of the Huron Member to the top of the Bedford Shale, punctuated by abrupt increases in the $\delta^{15}N_{bulk}$ signal. The $\delta^{15}N_{bulk}$ values begin to fall at the top of the Bedford Shale and into the base of the Sunbury Shale, where the $\delta^{15}N_{bulk}$ values begin to oscillate between less and more positive values, around a less positive (lighter) average $\delta^{15}N_{bulk}$ trendline than the underlying units.

4.3.2.6 Comparison of composite section and KY801N

A gradual trend of increasingly positive $\delta^{15}N_{bulk}$ values, from the bottom to the top of the stratigraphy, is evident in both sections (Figure 4.17). The two sections appear to record opposite isotopic trends within the upper part of the Cleveland Member. Whereas the KY10E section records increasingly positive (heavier) $\delta^{15}N_{bulk}$ values towards the top of the Cleveland Member, the section at KY801N seems to record a less positive (lighter) trend over the equivalent stratigraphy. The top of the KY801N section is thought to be quite close to the top of the Cleveland Member; however, it may be located further down in the Cleveland Member than previously thought, or perhaps this apparent anomaly may be due to low sampling resolution, where isotopic excursions exist within each section, but only parts of the curves are observed due to the lack of detailed sampling.

Both sections record a gradual increase in $\delta^{15}N_{bulk}$ values within the Bedford Shale, followed by a decrease towards the top of the formation. However, the uppermost sample within the Bedford Shale at KY801N records a positive shift in the $\delta^{15}N_{bulk}$ value that is not mirrored in the composite section. As the Bedford Shale at KY801N consists of black shales rather than grey shales, it is possible that the uppermost sample was wrongly assigned to the Bedford Shale, and may belong at the base of the Sunbury Shale. Further work is required to investigate this claim.

The lack of $\delta^{15}N_{bulk}$ oscillations within the Sunbury Shale at KY801N, similar to those observed in the composite section (KY2520N), may be due to low sampling resolution, where the isotopic deviations and shifts in $\delta^{15}N_{bulk}$ are not documented due to the fact that only four Sunbury Shale samples were collected and analysed from KY801N. It may also be that these findings are locality specific, and therefore do not exist at KY801N.

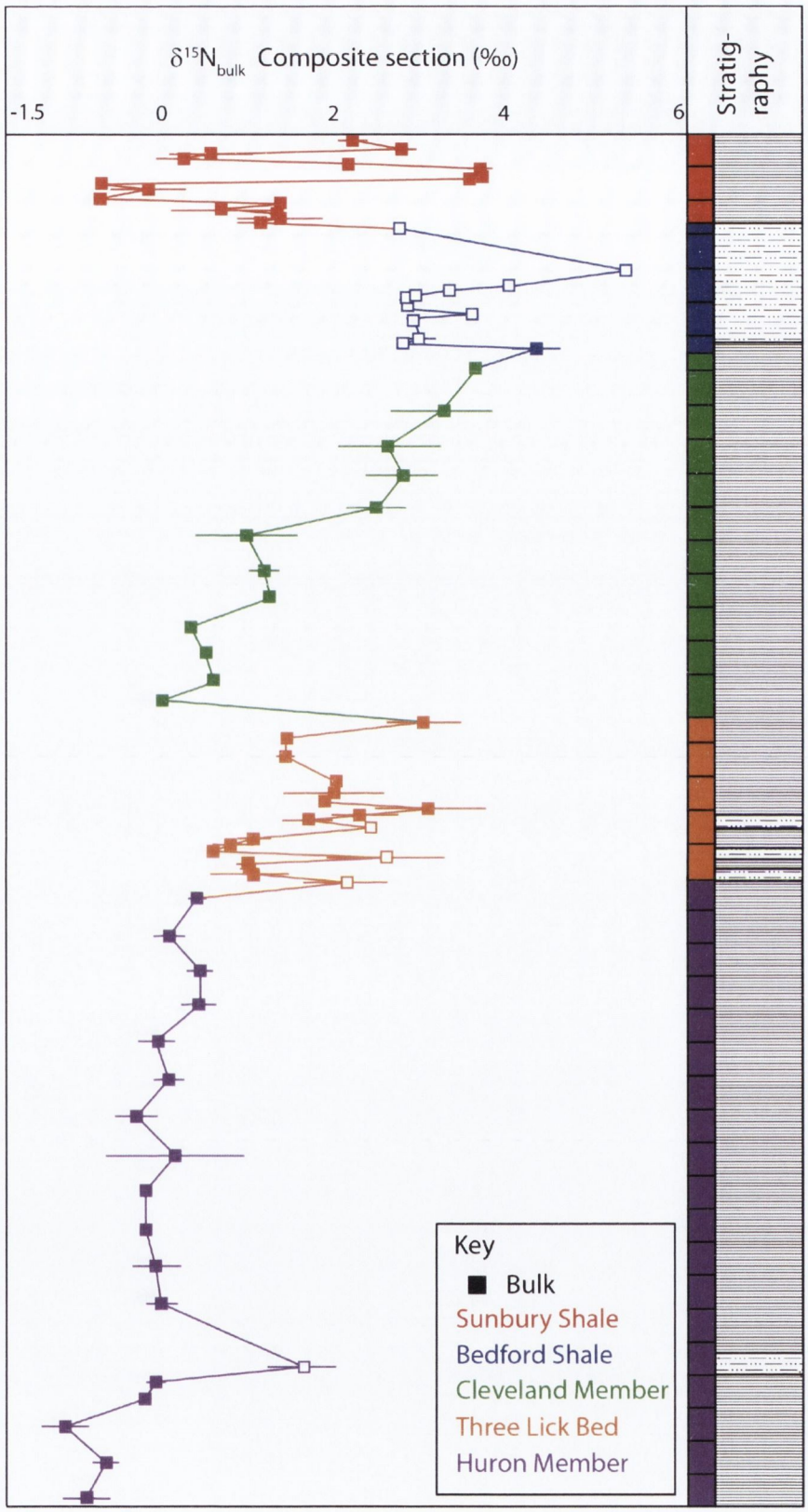

Figure 4.16. Composite section containing $\delta^{15}N_{bulk}$ results of KY10E, I64W and KY2520N. Closed squares represent bulk black shale samples, open squares represent bulk grey shale samples. Error bars ± 1SD

Figure 4.17. Comparison of $\delta^{15}N_{bulk}$ results from the composite section (solid line) and the KY801N section (dashed line).

4.3.3 *Tasmanites* spp.

Extracted samples of *Tasmanites* were analysed on the nano-EA-IRMS system. Three replicate samples were analysed wherever possible, but some samples did not contain enough *Tasmanites* specimens for three separate analyses. A small number of replicate data points (five) have been removed due to possible contamination, where the inclusion of organic debris, similar in appearance to *Tasmanites,* with a slightly more reddish hue, may have led to erroneous results. These data points are easily distinguishable by their very positive (heavy) $\delta^{15}N$ values when compared with the replicate samples, possibly indicating that the unknown organic debris may have originated from a much higher trophic level. This only occurred in samples where there were very few *Tasmanites* available for analysis, and is therefore not a factor for the overwhelming majority of the samples.

All of the recorded data points are included in Figures 4.19, 4.21, 4.23 and 4.25, for reference. $\delta^{15}N_{Tas}$ will be used from here on to denote the $\delta^{15}N$ value recorded from extracted samples of *Tasmanites*.

4.3.3.1 KY801N section

The $\delta^{15}N_{Tas}$ results for KY801N are shown in Figure 4.18. The $\delta^{15}N$ values of the *Tasmanites* extracted from the KY801N section range from + 2.3 ‰ to + 4.2 ‰ (average + 3.5 ‰). The $\delta^{15}N_{Tas}$ values remain relatively steady throughout the section, with the greatest variation on either side of the average isotopic signal (3.5 ‰) recorded within the Cleveland Member (2.3 ‰ to 4.2 ‰). This is followed by a stabilisation of the $\delta^{15}N_{Tas}$ signal through the majority of the Bedford Shale. The $\delta^{15}N_{Tas}$ values record a slight increase toward more positive (heavier) values at the top of the Bedford Shale and the base of the Sunbury Shale, which is followed by a brief decline to a less positive (lighter) $\delta^{15}N_{Tas}$ before returning to slightly heavier $\delta^{15}N_{Tas}$ values at the top of the Sunbury Shale. The *Tasmanites* sample extracted from the condensed Three Lick Bed horizon at this locality records $\delta^{15}N_{Tas}$ values very similar to the *Tasmanites* extracted from the black shales either side of this grey shale sample (~3.5 ‰).

4.3.3.2 KY10E section

The $\delta^{15}N_{Tas}$ results for KY10E are shown in Figure 4.20. The $\delta^{15}N$ values of the *Tasmanites* extracted from the KY10E section range from + 2.3 ‰ to + 5.4 ‰ (average + 4 ‰). This section consists of the Huron and Cleveland Members of the Ohio Shale. The $\delta^{15}N_{Tas}$ values increase steadily from the base of the Huron Member to the top of the Cleveland Member, with variation greater than 1 ‰ on either side of this trendline recorded throughout the section.

The sample obtained from the Three Lick Bed at this locality did not contain enough *Tasmanites* to run on the nano-EA-IRMS and is therefore absent from the data. The *Tasmanites* sample extracted from the grey shale horizon, located directly above the *Protosalvinia* Zone within this section, records very little change in the $\delta^{15}N_{Tas}$ value compared against the two samples located directly below, within the *Protosalvinia* Zone (~2.6 ‰). However, the sample located approximately 3 m above the grey shale horizon recorded a $\delta^{15}N_{Tas}$ value of 3.9 ‰, which is approximately 1.3 ‰ heavier than the *Tasmanites* extracted from the grey shale. The $\delta^{15}N_{Tas}$ value fluctuates (> 2 ‰) throughout the rest of section.

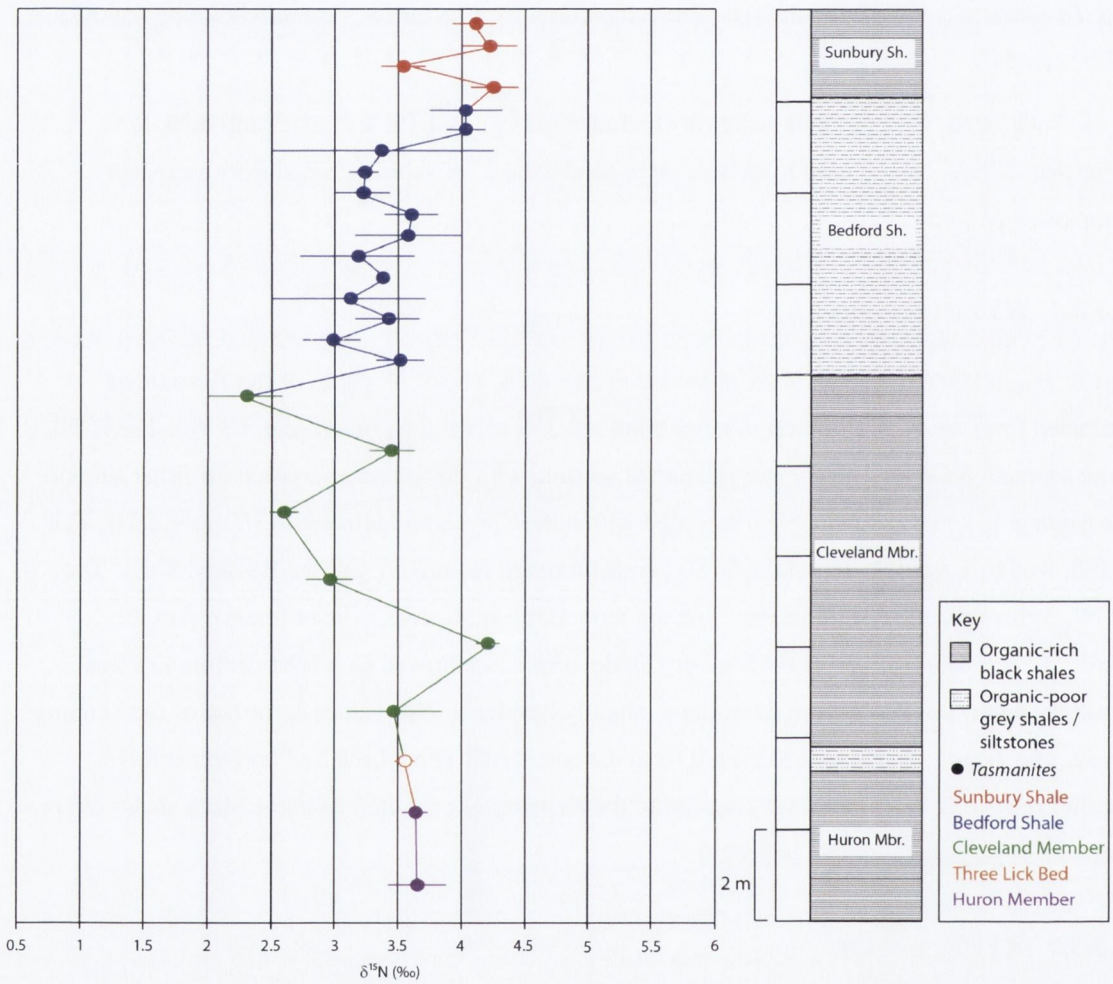

Figure 4.18. $\delta^{15}N_{Tas}$ results for KY801N. Closed circles represent bulk black shale samples, open circles represent bulk grey shale samples. Error bars ± 1SD.

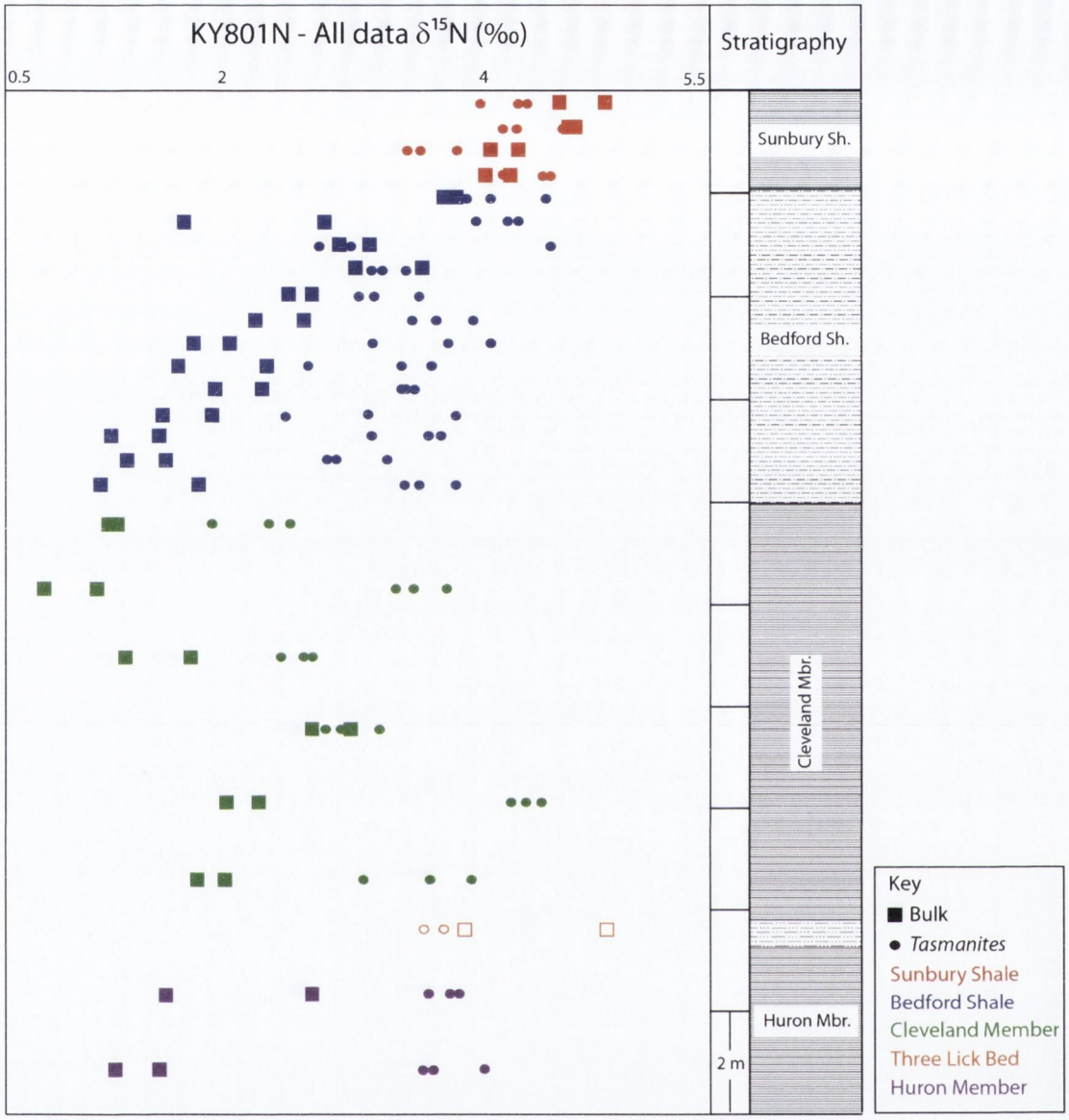

Figure 4.19. $\delta^{15}N_{Tas}$ and $\delta^{15}N_{bulk}$ results for KY801N. Closed circles or sqaures represent black shales, open circles or squares represent grey shales. All data points obtained for KY801N are included.

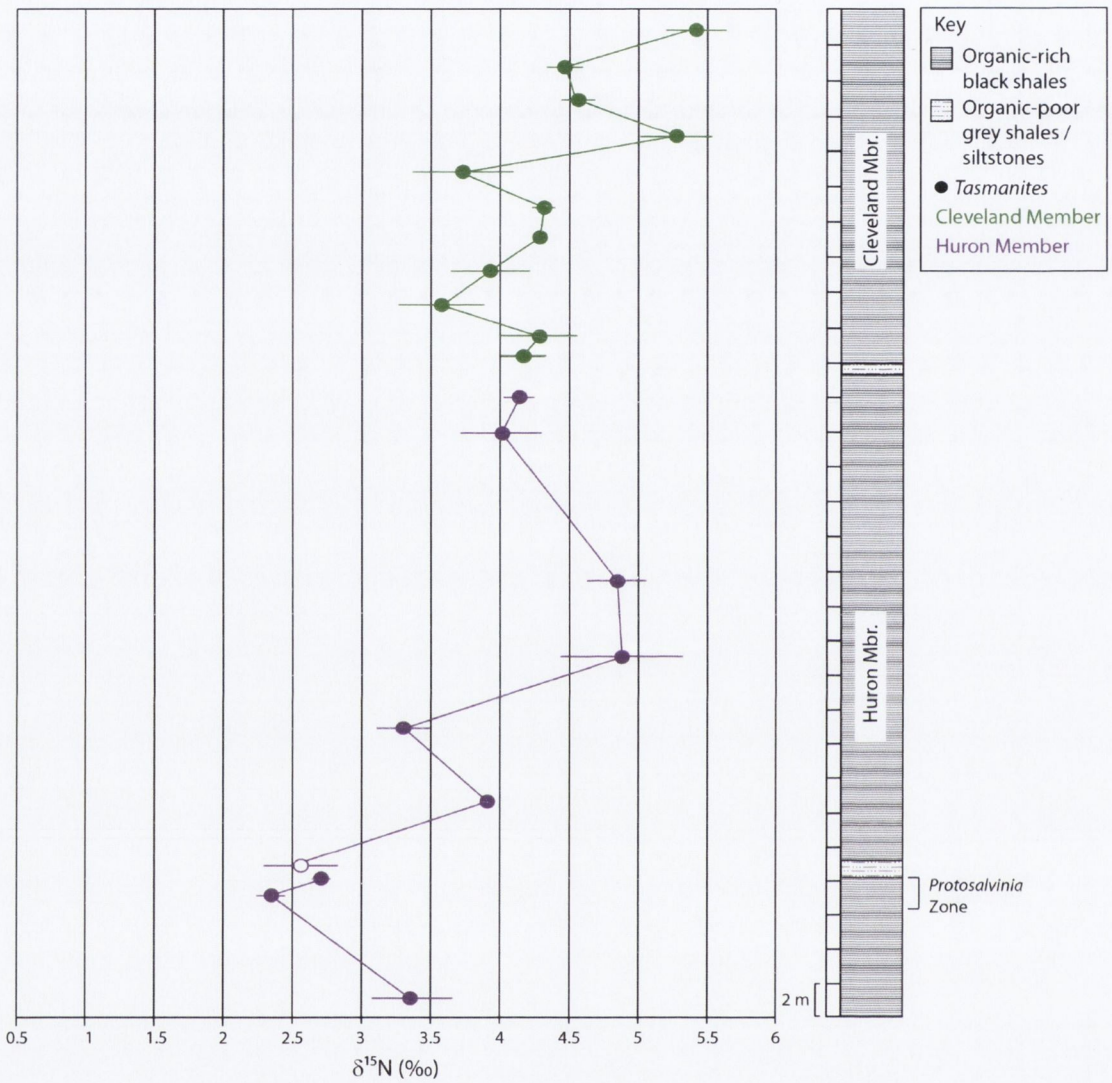

Figure 4.20. $\delta^{15}N_{Tas}$ results for KY10E. Closed circles represent bulk black shale samples, open circles represent bulk grey shale samples. Error bars ± 1SD.

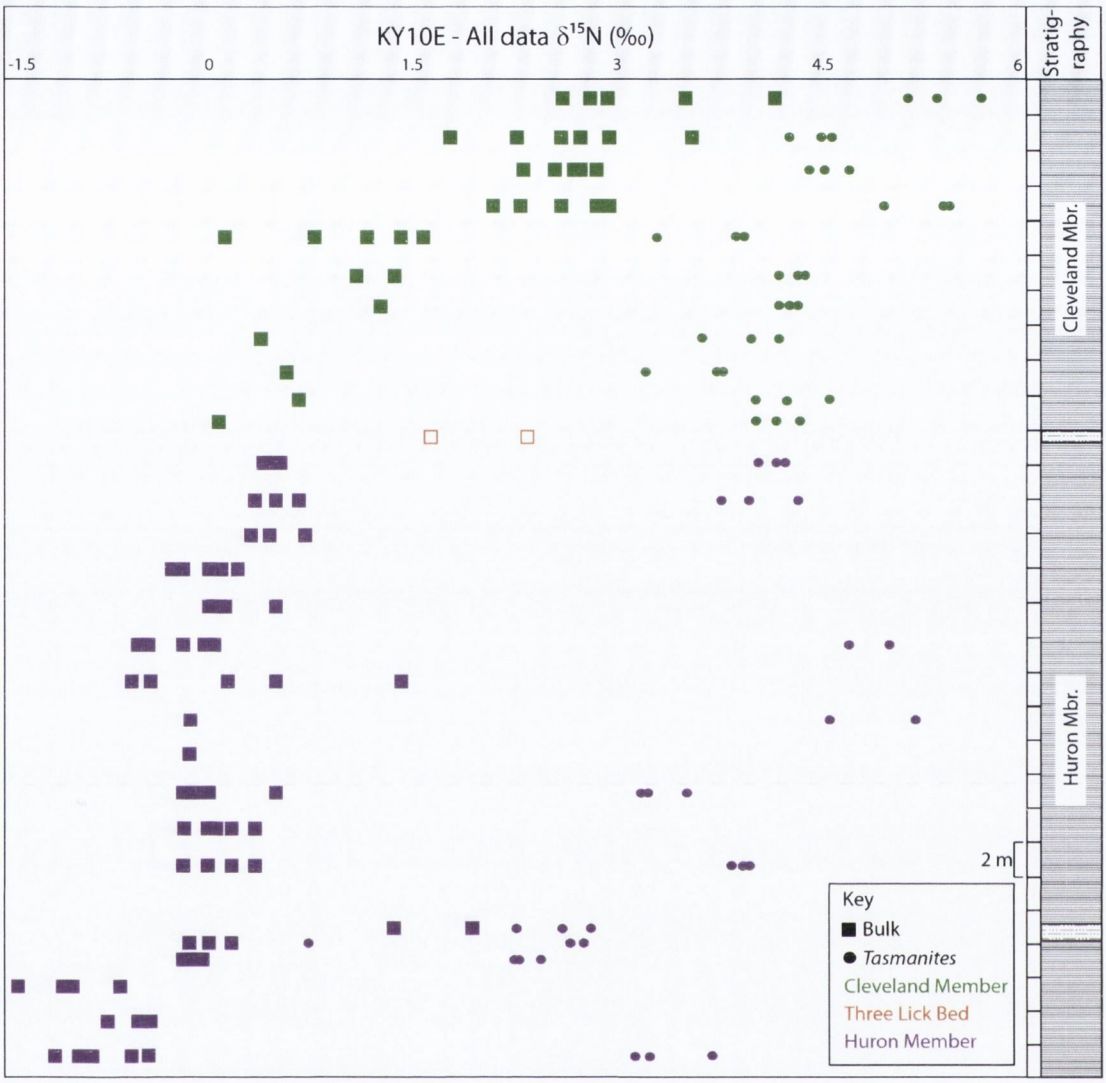

Figure 4.21. $\delta^{15}N_{Tas}$ and $\delta^{15}N_{bulk}$ results for KY10E. Closed circles or squares represent black shales, open circles or squares represent grey shales. All data points obtained for KY10E are included.

4.3.3.3 I64W, Three Lick Bed type section

The $\delta^{15}N_{Tas}$ results for I64W are shown in Figure 4.22. The $\delta^{15}N$ values of the *Tasmanites* extracted from the Three Lick Type Section range from + 0.8 ‰ to + 3.7 ‰ (average + 3 ‰). The *Tasmanites* extracted from the three grey shale beds within this section record less positive (lighter) $\delta^{15}N_{Tas}$ values than the *Tasmanites* extracted from the black shales. However, the number of *Tasmanites* extracted from the upper and lower grey shale horizons was significantly smaller than the number of *Tasmanites* analysed for the rest of the section, due to the lack of sufficient numbers of *Tasmanites* found within the grey shale horizons. This may have introduced greater error within the blank correction, leading to under corrected results. This can occur when the amount of N

within the He carrier gas significantly exceeds the amount of N within the sample, leading to underestimation of the isotopic signature of the sample due to its low concentration of N.

A sufficient number of *Tasmanites* were extracted from the middle grey shale horizon to perform a reliable blank correction; however, none of the grey shales contained enough *Tasmanites* to carry out replicate analyses to verify their results. Therefore, the *Tasmanites* data obtained from the grey shale samples in this section should be interpreted with caution. The middle grey shale sample also recorded the least amount of variation from the *Tasmanites* extracted from the black shales, possibly indicating that the other two grey shale samples should have less extreme isotopic variation than is observed within the data. Overall, a minor gradual positive trend (~ + 0.5 ‰) is observed from the bottom to the top of the section, with slight variation in the $\delta^{15}N_{Tas}$ values within the black shales.

4.3.3.4 KY2520N section

The $\delta^{15}N_{Tas}$ results for KY2520N are shown in Figure 4.24. The $\delta^{15}N$ values of the *Tasmanites* extracted from the KY2520N section range from + 1.5 ‰ to + 4.6 ‰ (average + 2.8 ‰). This section contains the uppermost Cleveland Member, the entire Bedford Shale, and the majority of the Sunbury Shale. The *Tasmanites* extracted from the uppermost Cleveland Member recorded $\delta^{15}N_{Tas}$ values of 4.2 ‰ and 3.6 ‰. The *Tasmanites* extracted from the black shale sample located towards the base of the Bedford Shale records a $\delta^{15}N_{Tas}$ value of 4.6 ‰. The $\delta^{15}N_{Tas}$ rapidly decreases to less positive (lighter) values throughout the grey shales that document the remainder of the Bedford Shale (1.5 ‰ to 2.9 ‰). Two slight isotopic oscillations021s (> 1 ‰) are observed within the middle of the Bedford Shale. However, much of this is located within error of the replicate analyses. Sampling resolution is lower in the upper third of the Bedford Shale due to the lack of sufficient numbers of *Tasmanites* within the samples.

The $\delta^{15}N_{Tas}$ values within the Sunbury Shale range from + 1.5 ‰ to + 4.3 ‰ (average + 3 ‰). Two clear isotopic oscillations are observed within the data, which covers the majority of the Sunbury Shale. The detection of unambiguous isotopic curves within this section may have been due to increased sampling resolution. In previous sections, sampling resolution may have been too low to trace isotopic curves which may or may not exist in the underlying Ohio Shale.

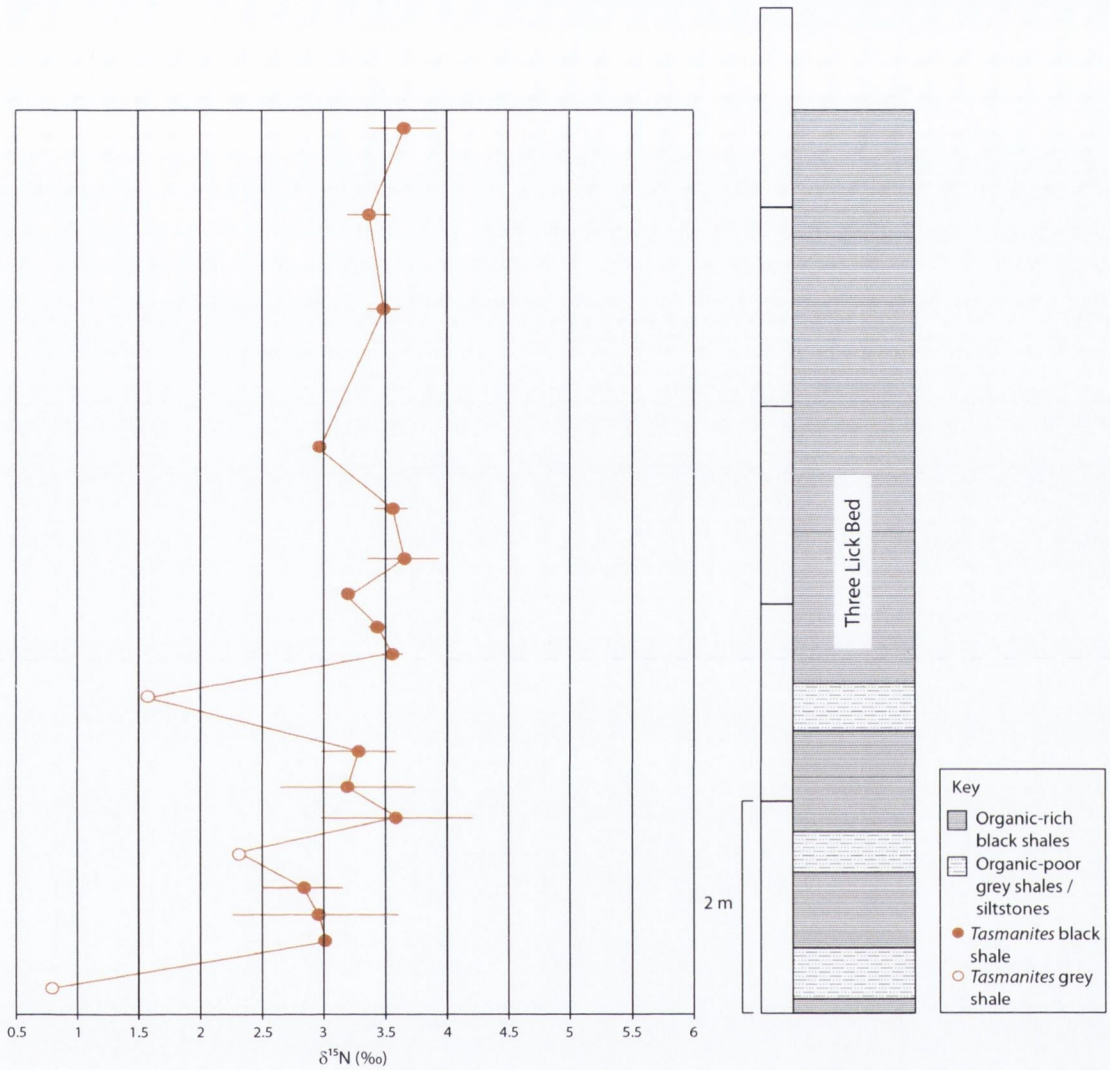

Figure 4.22. $\delta^{15}N_{Tas}$ results for I64W. Closed circles represent bulk black shale samples, open circles represent bulk grey shale samples. Error bars ± 1SD.

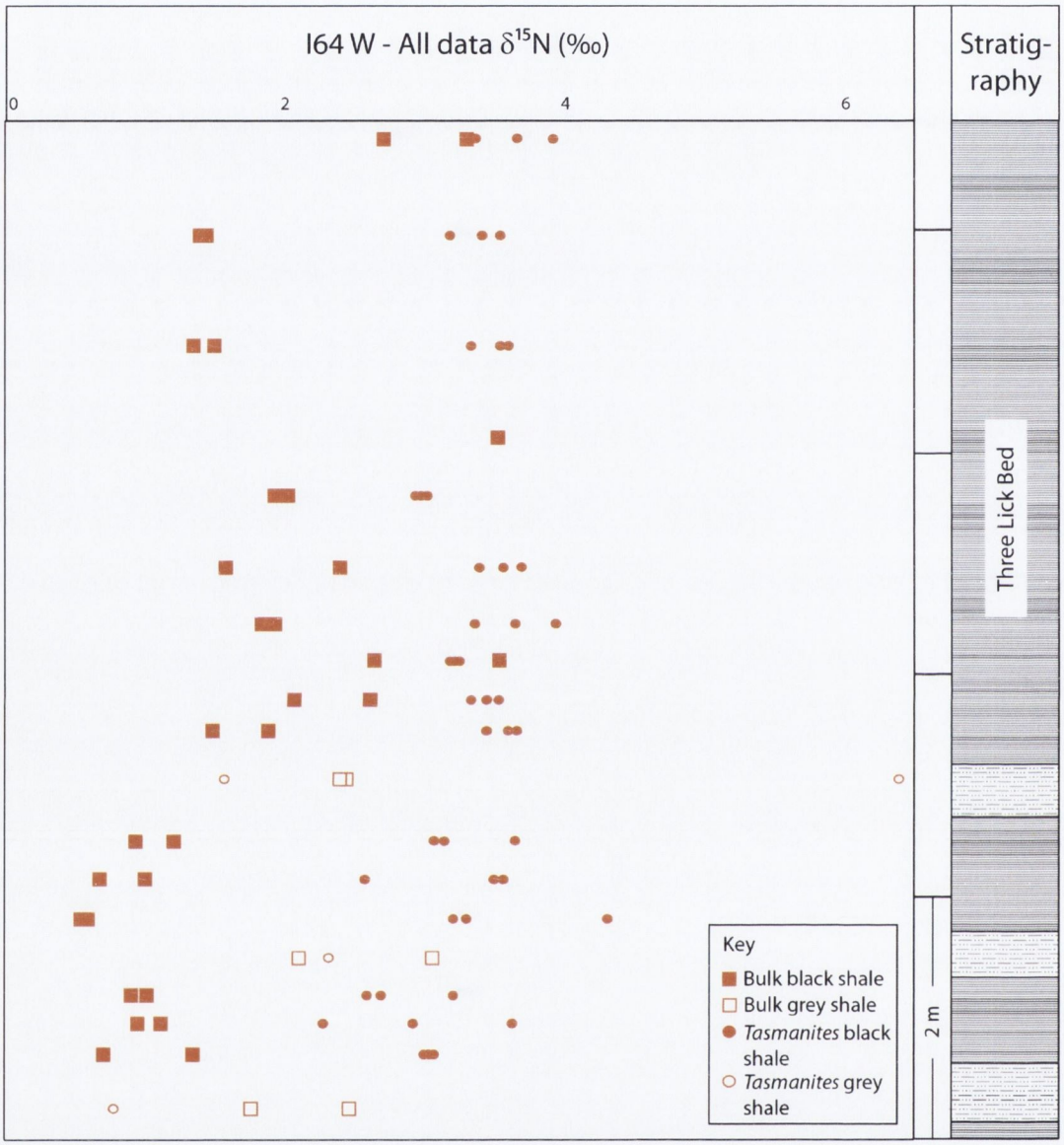

Figure 4.23. $\delta^{15}N_{Tas}$ and $\delta^{15}N_{bulk}$ results for I64W. Closed circles or squares represent black shales, open circles or squares represent grey shales. All data points obtained for I64W are included. One outlier from the top grey shale horizon (*Tasmanites* specimen) was discarded from the dataset due to possible contamination.

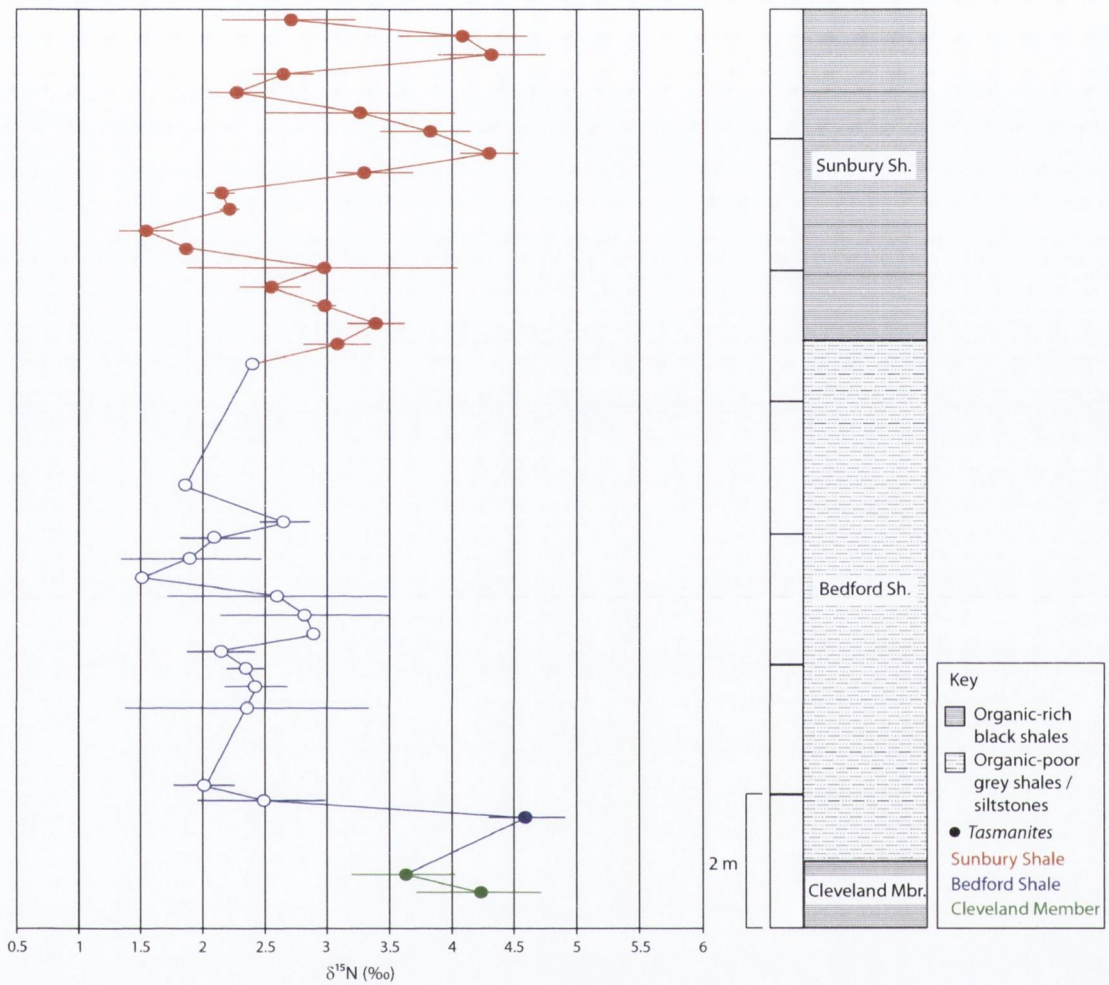

Figure 4.24. $\delta^{15}N_{Tas}$ results for KY2520N. Closed circles represent bulk black shale samples, open circles represent bulk grey shale samples. Error bars ± 1SD.

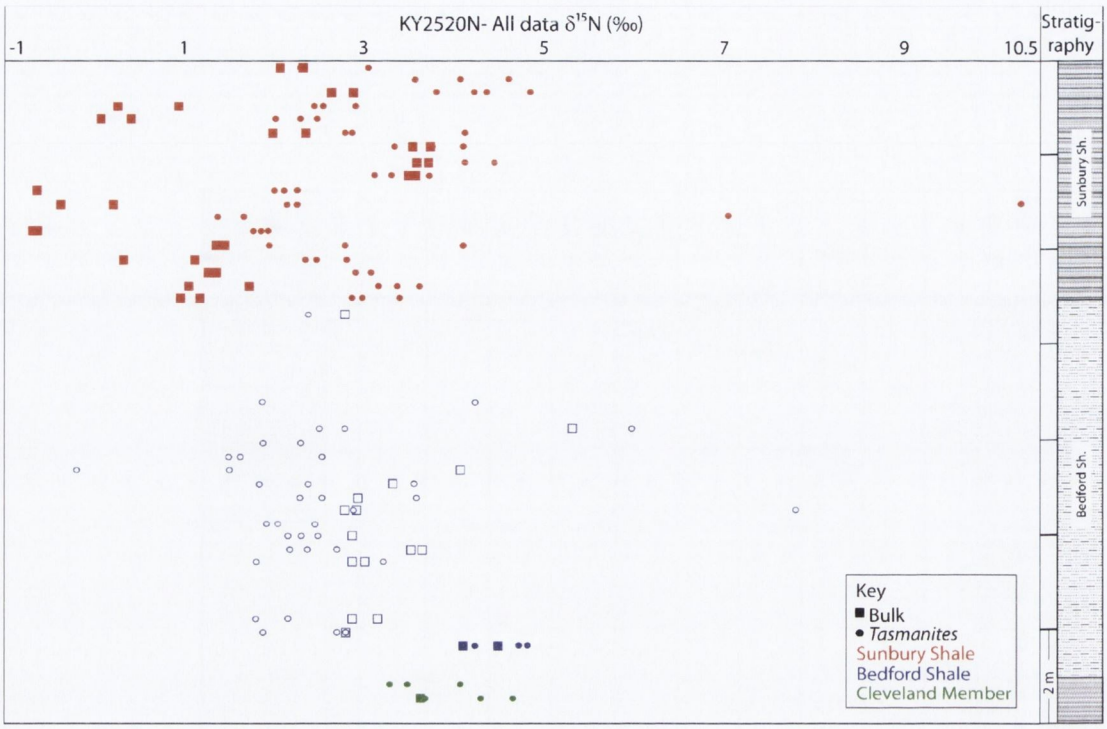

Figure 4.25. $\delta^{15}N_{Tas}$ and $\delta^{15}N_{bulk}$ results for KY2520N. Closed circles or squares represent black shales, open circles or squares represent grey shales. All data points obtained for KY2520N are included. Some of the outliers, seen here, were discarded from the dataset due to possible contamination. The grey panels have been added to distinguish between the bulk and *Tasmanites* datasets.

4.3.3.5 Composite section

The $\delta^{15}N_{Tas}$ data for the composite section are shown in Figure 4.26. The $\delta^{15}N$ values for extracted *Tasmanites* range from 0.8 ‰ to 2.9 ‰ within the grey shales, and 1.5 ‰ to 5.4 ‰ within the black shales. The *Tasmanites* extracted from the grey shales appear to have slightly or less positive (lighter) $\delta^{15}N_{Tas}$ values than those extracted from the black shales, however, as discussed above, the $\delta^{15}N_{Tas}$ for the three grey shale units of the Three Lick Bed should be interpreted with caution. If these values are removed, the *Tasmanites* extracted from the grey shale samples do not necessarily record less positive (lighter) $\delta^{15}N_{Tas}$ values than the *Tasmanites* extracted from the black shale units. There is, however a notable decrease in $\delta^{15}N_{Tas}$ (4.6 ‰ to 2.5 ‰) recorded at the base of the Bedford Shale as the lithology changes from black to grey shale. This adjustment in the $\delta^{15}N_{Tas}$ signal may or may not be due, in part, to the lithologic change.

Increasingly positive $\delta^{15}N_{Tas}$ values are recorded from the older *Tasmanites* at the bottom of the Huron Member, to the younger *Tasmanites* at the top of the Huron Member. This is followed by a slight decrease in $\delta^{15}N_{Tas}$ within the Three Lick Bed, which begins another increasingly positive $\delta^{15}N_{Tas}$ trend up to the base of the Bedford Shale. An abrupt decrease in $\delta^{15}N_{Tas}$ values near

the base of the Bedford Shale defines the beginning of another, less positive (lighter) $\delta^{15}N_{Tas}$ trendline, that gradually becomes more positive towards the top of the section, similar to the trendlines recorded within the Ohio Shale. Within the Cleveland and Huron Members of the Ohio Shale, isotopic variation may be absent or not as apparent as the isotopic variation recorded in the Sunbury Shale, possibly due to reduced sampling resolution.

4.3.3.6 Comparison of composite section and KY801N

As illustrated in Figure 4.27, the *Tasmanites* extracted from the Huron Member, and the base of the Cleveland Member of KY801N, record very similar values to those extracted from the top of the Huron Member, and the base of the Cleveland Member in the composite section. The range of isotopic variation within rest of the Cleveland Member appears to be quite similar in both sections; however, the general trend of isotopic variation appears to be in opposite directions, where the $\delta^{15}N_{Tas}$ values show a general positive trend in the composite section, and a general less positive trend in the KY801N section. As mentioned previously, this may be due to low sampling resolution within the Cleveland Member, where abrupt isotopic changes may exist, similar to those recorded in the Sunbury Shale, but only parts of these curves may be observed where sampling resolution is low. This could lead to the observation of opposing trends like those seen in the two sections. It may also be due to differing basin parameters at each sample locality, as will be discussed in the following chapter.

The Bedford Shale sampled at KY801N consists of black shales throughout the formation, whereas the composite section contains grey shales through all but the base of the Bedford Shale. The *Tasmanites* extracted near the base of the Bedford Shale at KY801N do not record the same abrupt decrease in $\delta^{15}N_{Tas}$ that was recorded in the composite section, suggesting that the change in lithology within the composite section is an important factor to consider when interpreting these results. Even though the sampling resolution appears to be quite similar at this point in the stratigraphy, the range of isotopic variation appears to be lower in the KY801N section than in the composite section.

Only four samples were analysed from the Sunbury Shale at KY801N, but the slight isotopic variation appears to be very similar to the base of the Sunbury Shale in the composite section. However, no conclusions should be drawn when comparing such a low number of samples.

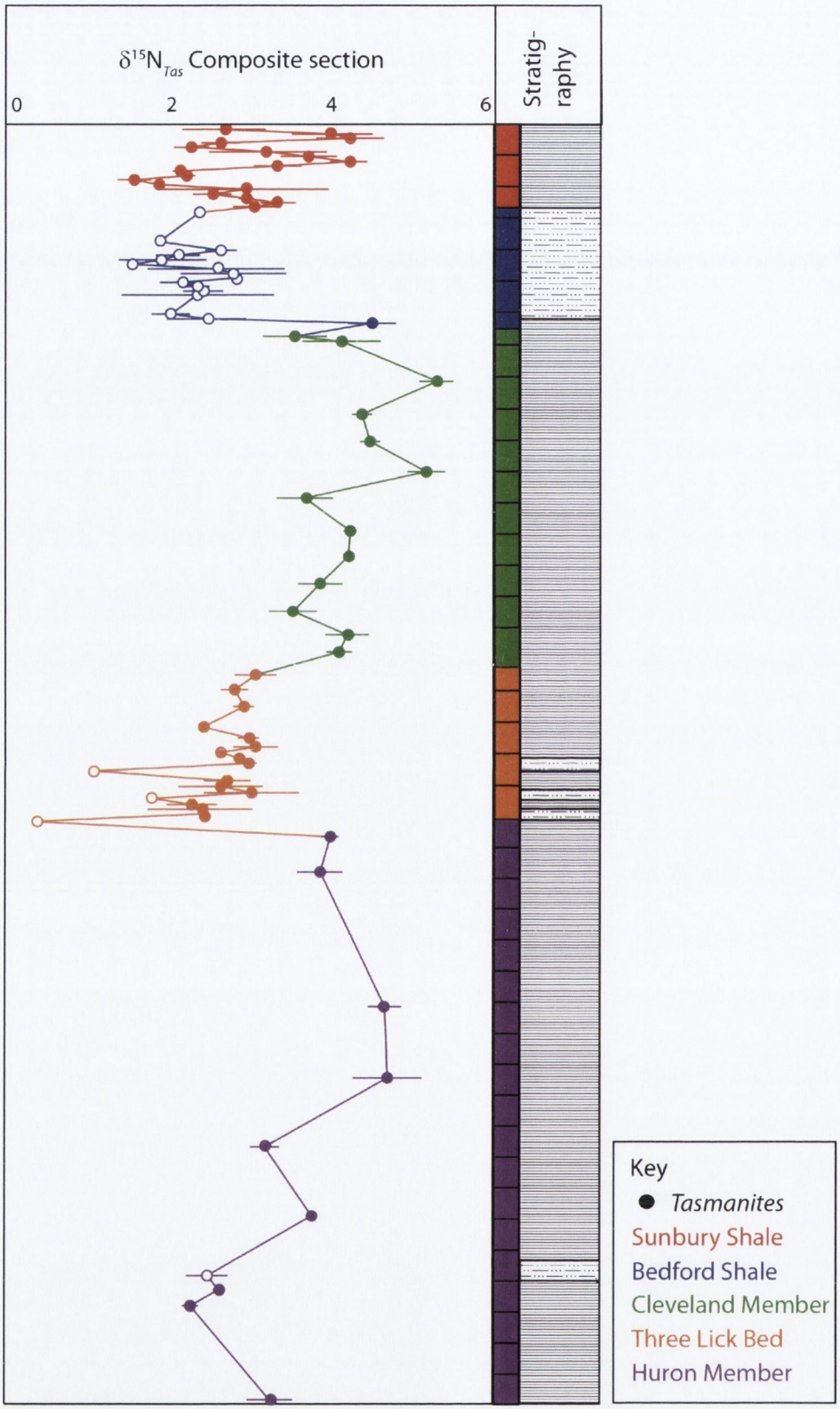

Figure 4.26. Composite section containing $\delta^{15}N_{Tas}$ results of KY10E, I64W and KY2520N. Closed squares represent bulk black shale samples, open squares represent bulk grey shale samples. Error bars ± 1SD.

Figure 4.27. Comparison of $\delta^{15}N_{Tas}$ results from the composite section (solid line) and the KY801N section (dashed line).

4.3.4 Comparison of $\delta^{15}N_{bulk}$ and $\delta^{15}N_{Tas}$

4.3.4.1 Composite section

The $\delta^{15}N_{Tas}$ data generally show good correlation with the $\delta^{15}N_{bulk}$ data throughout the composite section (Figure 4.28). There appears to be a noticeable offset between the less positive (lighter) bulk organic residues and the more positive (heavier) *Tasmanites* at the bottom of the section and diminishing towards the top of the section. At certain points within the stratigraphy the bulk organic residues record similar, or sometimes heavier, $\delta^{15}N_{bulk}$ values than the *Tasmanites*. This occurs within most of the grey shales and within some of the black shale samples collected along I64W and KY2520N. These samples include two black shale samples located above the grey shale units of the Three Lick Bed, the uppermost sample at the top of the Cleveland Member, sampled from KY2520N, the lowermost sample within the Bedford Shale, and the samples recording the abrupt positive isotopic deviations within the Sunbury Shale. A slightly different trend, however, is noted between the *Tasmanites* data and the bulk organic residues within samples collected along KY10E. Excluding the grey shale horizon located above the *Protosalvinia* Zone, the $\delta^{15}N_{Tas}$ data from this section mirror the increases in $\delta^{15}N_{bulk}$, where a consistent offset of between 2 and 5 ‰ is maintained between the two datasets. This offset becomes less apparent towards the top of the KY10E section (within the Cleveland Member), where the $\delta^{15}N_{bulk}$ values record similar values to the $\delta^{15}N_{Tas}$ data.

The bulk organic grey shale residues generally record a more positive (heavier) $\delta^{15}N_{bulk}$ signature than the bulk organic black shale residues. However, *Tasmanites* samples extracted from grey shales occasionally recorded a less positive (lighter) $\delta^{15}N_{Tas}$ signature than those extracted from black shales, but often recorded no change at all from the $\delta^{15}N_{Tas}$ of the black shales.

4.3.4.2 KY801N

As illustrated in Figure 4.29, both the bulk organic residues and *Tasmanites* datasets appear to become less positive in the Cleveland Member, before becoming more positive through the Bedford Shale and into the Sunbury Shale. The majority of the $\delta^{15}N_{bulk}$ samples record values 1 to 2 ‰ less positive (lighter) than the $\delta^{15}N_{Tas}$ samples. However, at various locations within the KY801N section, the $\delta^{15}N_{bulk}$ increase to values that are similar to, or heavier than, $\delta^{15}N_{Tas}$. This occurs within the grey shale horizon of the Three Lick Bed, within the middle of the Cleveland Member, towards the top of the Bedford Shale, and throughout the Sunbury Shale.

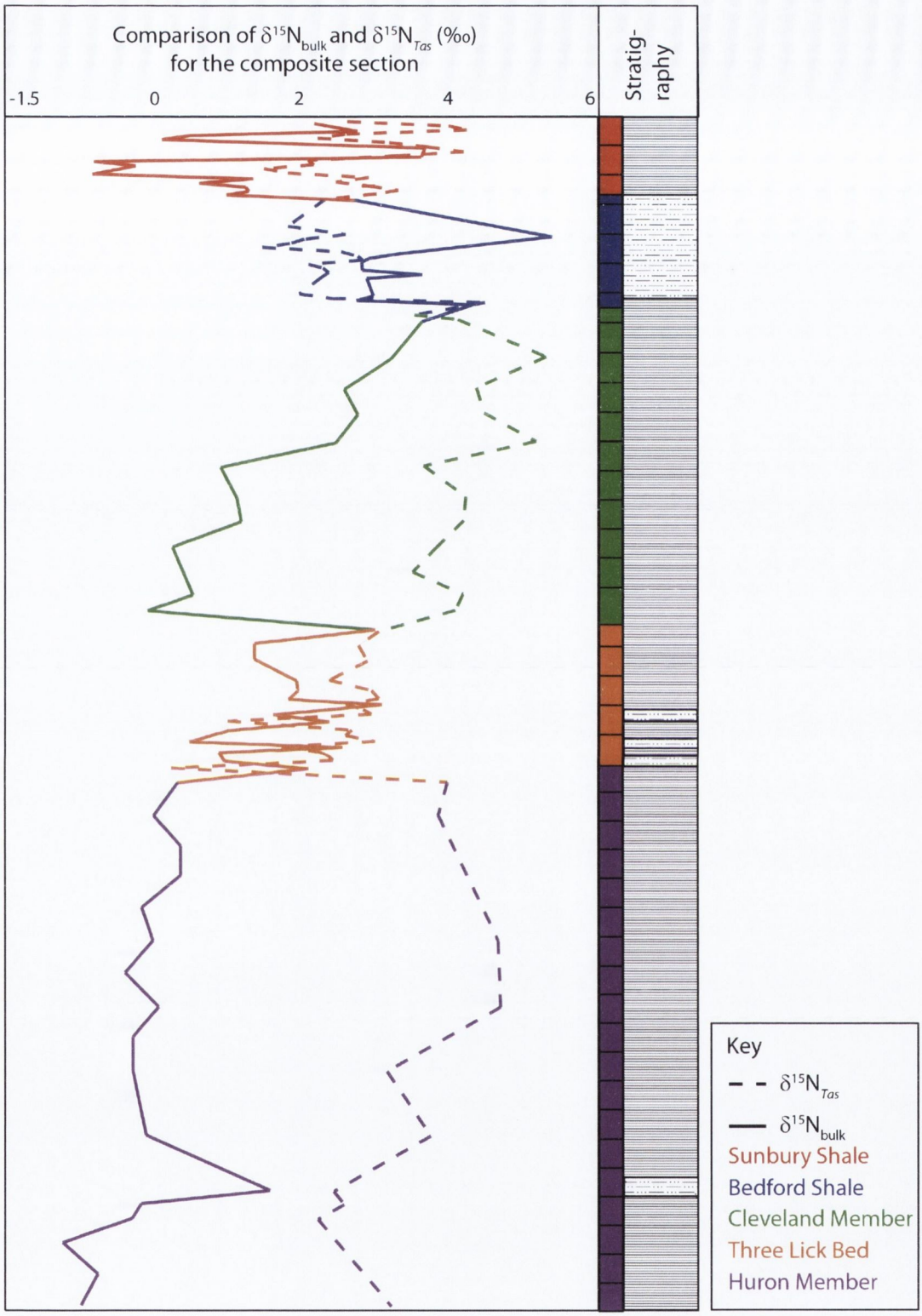

Figure 4.28. Comparison of $\delta^{15}N_{Tas}$ (dashed line) and $\delta^{15}N_{bulk}$ (solid line) results for the composite section.

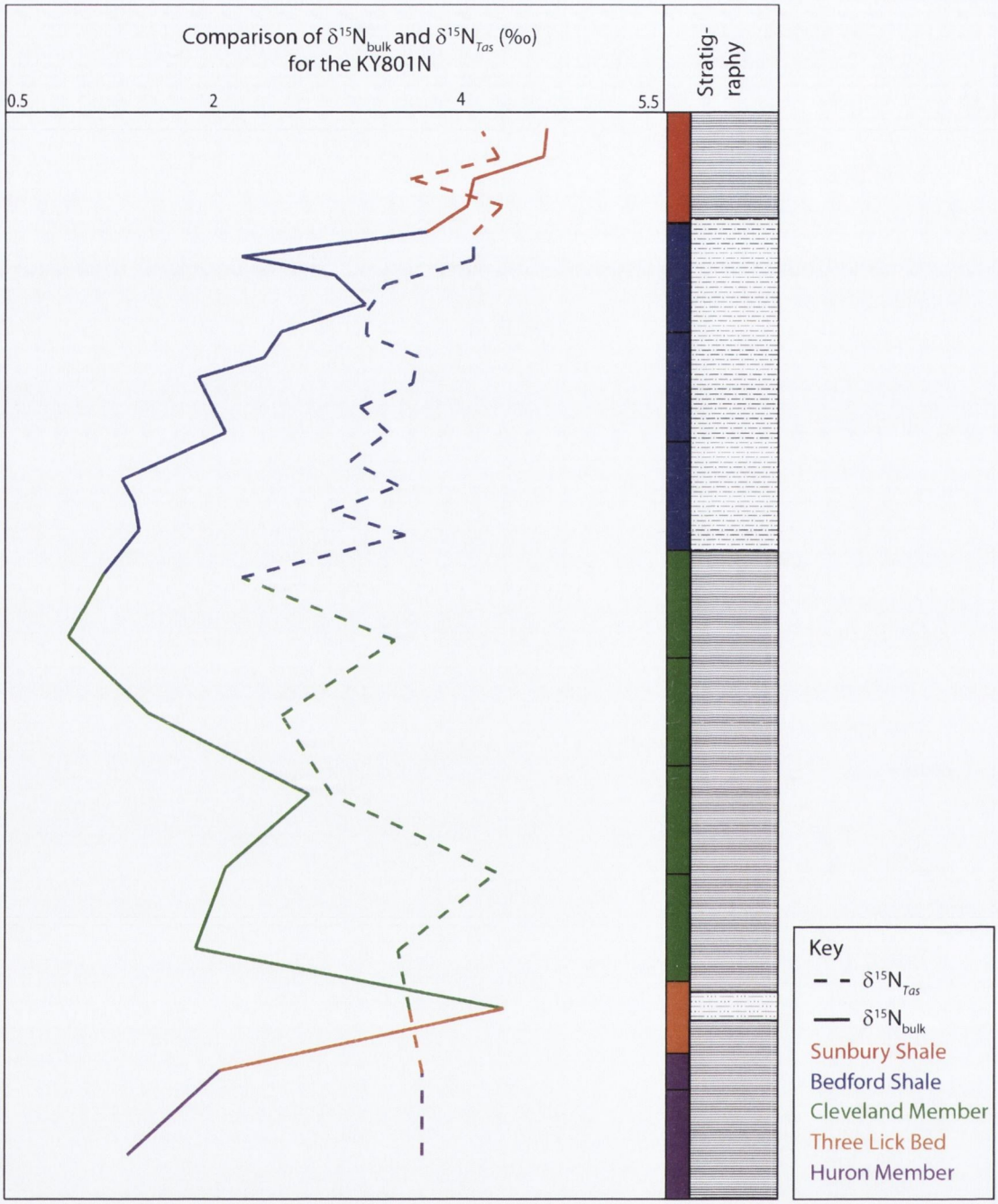

Figure 4.29. Comparison of $\delta^{15}N_{Tas}$ (dashed line) and $\delta^{15}N_{bulk}$ (solid line) for KY801N.

4.4 TRACE ELEMENTS

Because a range of spot sizes were used throughout the analyses, only the ratios, rather than the quantities, of the various elements will be presented. Ratios have been chosen based on their relevance to nutrient and oxic conditions. Uranium, Th, and Cu were used as markers of possible contamination on the outer surface of *Tasmanites*, where residual contaminant organic material may have still been attached to the specimens, or possible contamination arising from the treatment methods used to extract *Tasmanites* from the rock matrix. Many elements were disregarded either due to the low concentrations recorded within the *Tasmanites*, or the lack of published data available to aid in the interpretation of the results.

Other studies have utilised cadmium as a proxy for nutrient conditions (Bruland and Lohan, 2006) however, its concentration in the *Tasmanites* specimens was too low to be a reliable indicator of change. As discussed in Chapter 1, V, Mo and Ni concentrations have been shown to increase within bulk sediments under anoxic conditions (Perkins *et al.* 2008; Rimmer, 2004). Ratios of V/Cr_{Tas}, V/Mo_{Tas}, $V/(V+Ni)_{Tas}$ and Ni/Co_{Tas} are presented in Figures 4.30 and 4.31 to aid in the interpretation of oxic conditions, where increases in V/Cr, V/(V+Ni) and Ni/Co, and a decreasing V/Mo ratio in bulk sediments have been suggested to equate to increased anoxia (Perkins *et al.*, 2008; Rimmer, 2004; Tribovillard *et al.*, 2006). Varying concentrations of Fe, Ni, Zn and Co are proposed as possible indications of changing nutrient conditions. Higher Fe concentrations are expected when *Tasmanites* were utilising a higher proportion of nitrate, and higher Ni concentrations and lower Fe concentrations are expected when *Tasmanites* are utilising urea or ammonium as their main N source (Price and Morel, 1991; Raven *et al.*, 1992). Where nutrient conditions are low, in open waters, Co is capable of replacing Zn (Whitfield, 2001), therefore, a higher concentration of Co is expected under low nutrient conditions. Ratios of Fe/Ni_{Tas} and Zn/Co_{Tas} are also presented in Figures 4.32 and 4.33 to aid in the interpretation of changing pelagic nutrient conditions within the Late Devonian Appalachian Basin.

Each of the oxic indicating ratios (V/Cr_{Tas}, V/Mo_{Tas}, $V/(V+Ni)_{Tas}$, Ni/Co_{Tas}) show a small degree of variation through the Huron Member, followed by increased variation recorded in the Three Lick Bed. An overall increase in each of the ratios is recorded in the lower Cleveland Member, followed by a general decrease in the upper Cleveland Member, and an increase at the very top of the Cleveland Member recorded in the 2 samples from the base of KY2520N section. This is followed by a further decrease in each of the ratios in the Bedford Shale, and increased variation within the Sunbury Shale. The Ni/Co_{Tas} ratio records similar changes to the other oxic indicating ratios, but makes no real distinction between the upper and lower Cleveland Members.

The ratios presented as indicators of nutrient conditions, Fe/Ni_{Tas} and Zn/Co_{Tas}, each record several increases within the middle Huron Member, the Cleveland Member and the Sunbury Shale, possibly indicating increased nutrient conditions during these times.

The Ba/Zn_{Tas} ratio is presented in Figures 4.32 and 4.33, recording increases within the grey shales of the Bedford Shale and the grey shale horizon located above the *Protosalvinia* Zone within the Huron Member. The Ba/Zn_{Tas} ratio did not record increases within the grey shale horizons of the Three Lick Bed.

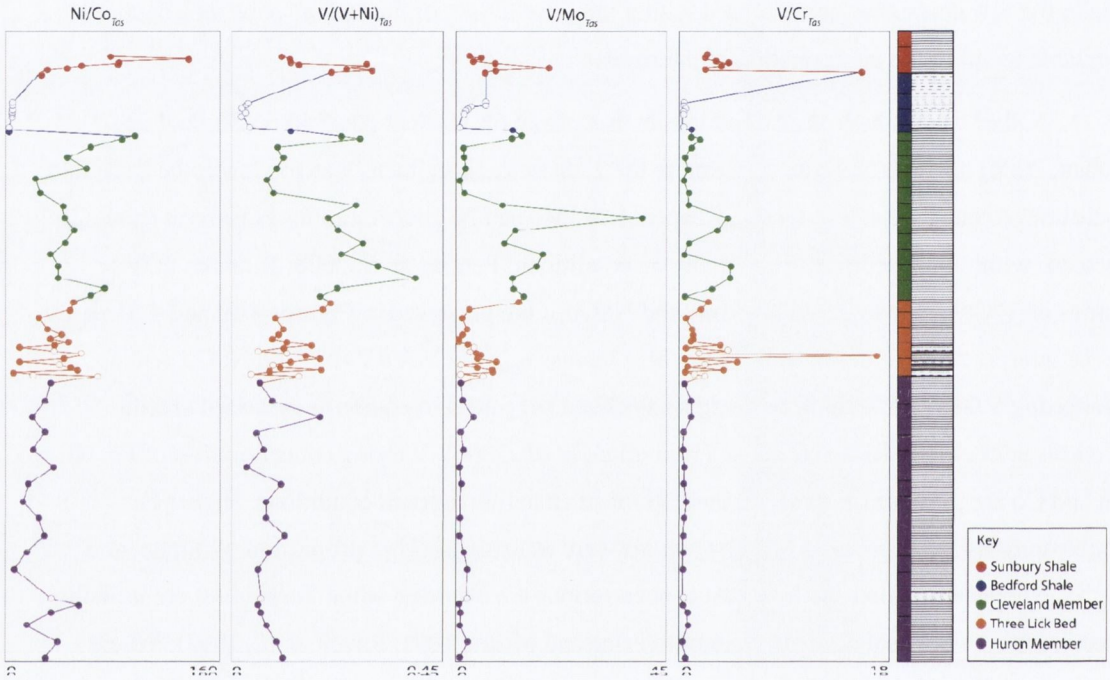

Figure 4.30. Trace element ratios obtained from specimens of *Tasmanites*, which were extracted from Upper Devonian Kentucky shales. Ratios shown may tentatively be related to oxic conditions.

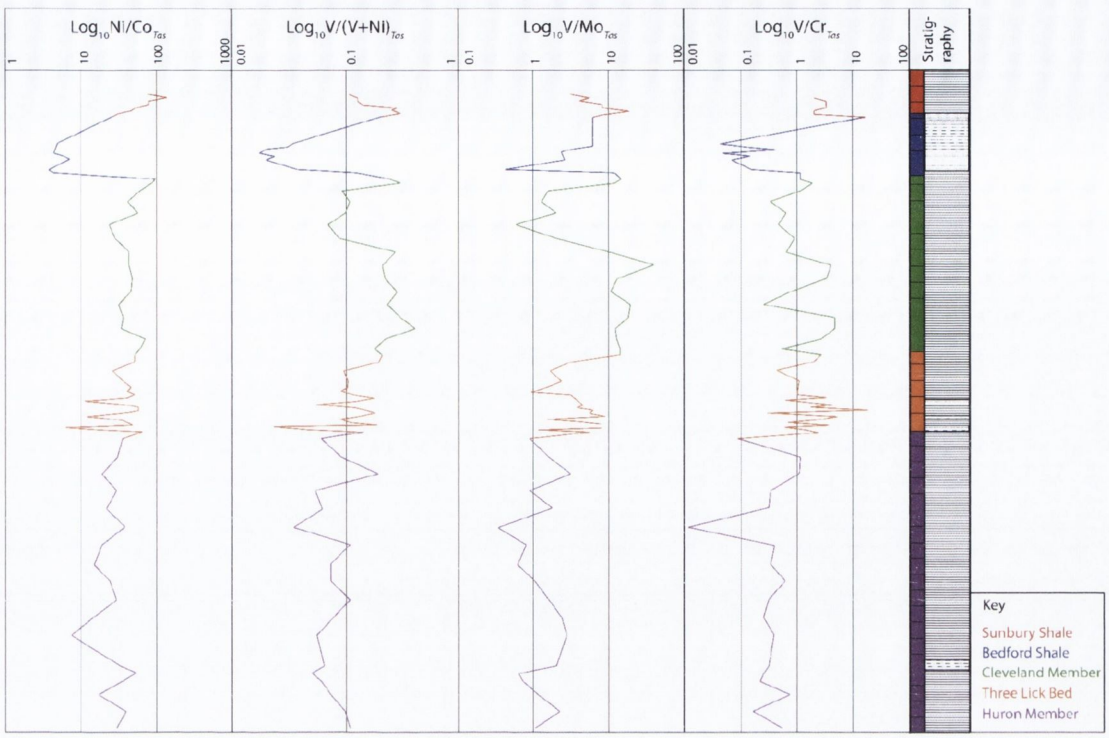

Figure 4.31. Logarithm of trace element ratios, Ni/Co, V/(V+Ni), V/Mo and V/Cr, of specimens of *Tasmanites*, as possible proxies for oxic conditions.

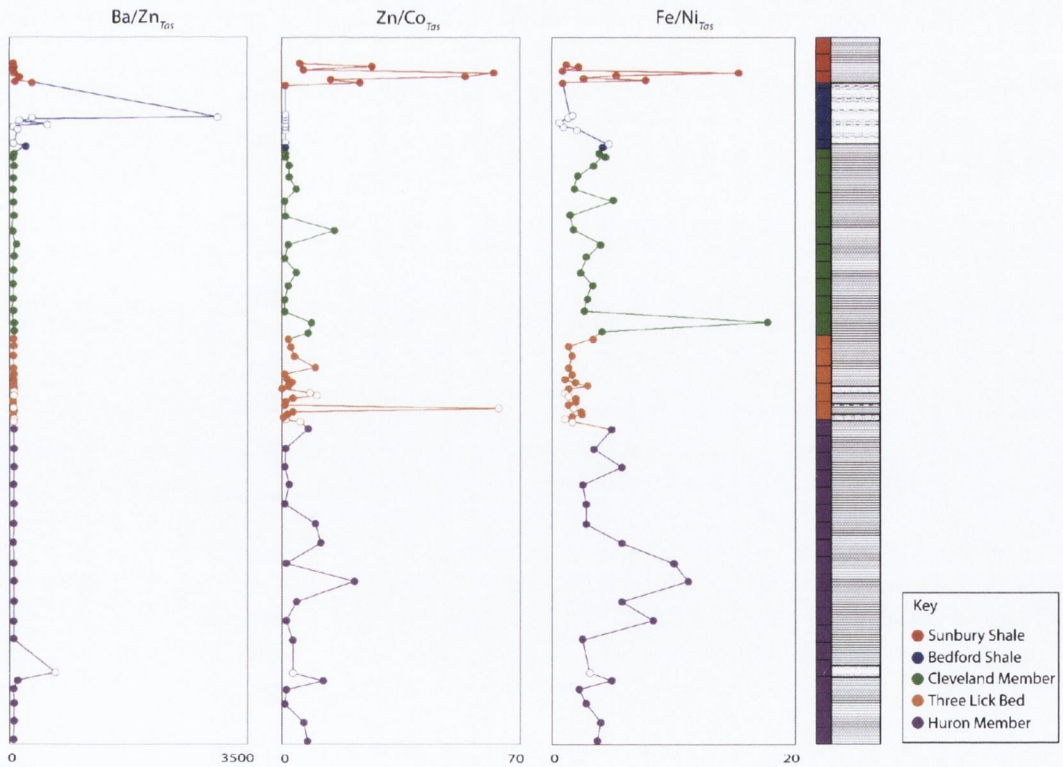

Figure 4.32. Trace element ratios obtained from specimens of *Tasmanites*, which were extracted from Upper Devonian Kentucky shales. Ratios shown may tentatively be related to nutrient conditions (Zn/Co, Fe/Ni) and degradation (Ba/Zn).

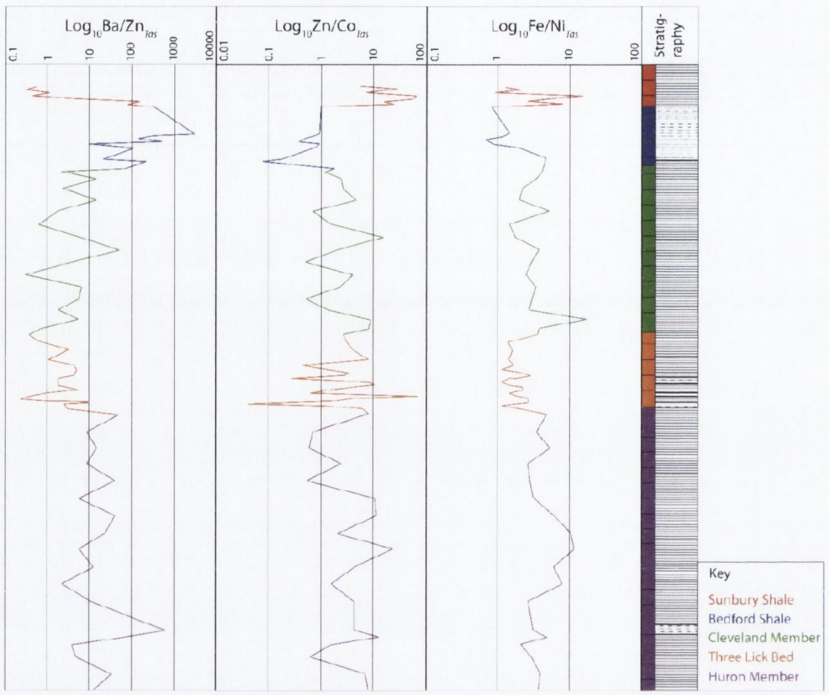

Figure 4.33. Logarithm of trace element ratios, Ba/Zn, Zn/Co and Fe/Ni, of specimens of *Tasmanites*, as possible proxies for degradation (Ba/Zn) and nutrient conditions (Zn/Co, Fe/Ni).

Chapter 5

Discussion

5.1 PRELIMINARY TESTING

In the majority of nitrogen and carbon isotope studies, a certain level of small, and presumably insignificant, isotopic deviation is disregarded within the interpretations due to the precision limitations of the instruments and the heterogeneous nature of some of the standards. As a consequence, most isotopic excursions are recorded greater than 1 ‰. It was hypothesised that thermal maturation and chemical treatment may alter the original isotopic signal, possibly obscuring or exagerating isotopic changes. Therefore isotopic change that took place during preliminary testing was deemed to be significant if it was close to, or greater than 1 ‰.

5.1.1 Experimental thermal maturation

Previous studies have suggested that low-grade metamorphism does not significantly alter the $\delta^{15}N$ signal (Ader *et al.*, 2006; Boudou *et al.*, 2008), although Jia (2006) found increasing $\delta^{15}N$ values with increasing levels of metamorphism, and Schimmelmann *et al.* (2009) observed fluctuating $\delta^{15}N$ values in kerogen within the aureole of a dike. Samples of *Tasmanites* analysed as part of this research recorded $\delta^{13}C$ and $\delta^{15}N$ values within error of the control sample. Therefore, it is suggested that low level thermal maturation does not significantly affect nitrogen and carbon isotope results of palynomorphs. However, there does seem to be slight ^{13}C and ^{15}N enrichment as the temperature is increased, most likely due to the lighter ^{12}C and ^{14}N being preferentially driven off due to higher mobility. This may become more significant when dealing with higher rank samples. Because this study was based on experimental thermal maturation carried out under laboratory conditions, it is possible that naturally matured samples may yield different results. However, validation was outside the scope of this research because I did not have access to a range of naturally matured samples containing large enough *Tasmanites* in abundance to extract and run on a general setup of the EA-IRMS and, in any case, the samples used were of low and uniform maturation.

5.1.2 Chemical treatment

Under most circumstances, the inorganic matrix must first be broken down in order to extract palynomorphs from a rock sample.Chemical treatments were chosen for this study based on their standard palynological use, and their ability to effectively remove unwanted material. Three of the chosen treatments (HCOOH, CH_3COOH and HNO_3) produced significant changes to the $\delta^{15}N$ values of the *Tasmanites*, whereas two treatments (HNO_3 and the clay mineralogy treatment) caused slight variation in the $\delta^{13}C$ value of the *Tasmanites*. The HCOOH, CH_3COOH and HNO_3 treatments are not required for the extraction of palynomorphs from rock samples, and therefore can be avoided when preparing samples for stable isotope analysis. However, the clay mineralogy

treatment method was necessary to remove excess AOM from organic-rich black shales. Due to the slightly heavier $\delta^{13}C$ value recorded in the *Tasmanites* specimens (+ 0.55 ‰) following this treatment method, it is important for future analyses of $\delta^{13}C$ in palynomorphs to take this slight corruption of signal into consideration. It was also noted that this treatment method possibly led to the removal or dissolution of some of the fragile palynomorphs, or outer components of palynomorphs. This may have a greater impact when analysing the stable isotope signature of the thin walled and fragile palynomorphs. However, the length of exposure to NaClO in particular may be reduced depending on the quantity of AOM in the sample, and the quantity of sample being processed.

5.1.3 Oxidation

Five hour exposures to H_2O_2 in order to replicate the conditions of natural weathering led to no discernable change to the stable isotope signature of the *Tasmanites*. However, this study was carried out under laboratory conditions that may not adequately represent natural weathering conditions. The Lower Permian sample from which the *Tasmanites* were extracted, may also have been exposed to weathering prior to experimentation and analysis. However, it appears from the exposure to H_2O_2, that oxidation does not have any immediate impact on the stable isotope signature of *Tasmanites*.

5.2 PALYNOLOGY

As outlined previously, immersing a sample in NaClO at 60 °C for 24 hours appeared to cause dissolution or removal of some palynomorphs, or some of the outer exine or walls of the palynomorphs, though no quantitative analysis was attempted. This degradation may be due to the time period that the sample was exposed to NaClO. This method to remove AOM could possibly be enhanced and improved with further testing using shorter periods of exposure time and smaller sample sizes.

Large sample sizes were processed for this project to extract as many *Tasmanites* as possible per sample. The nano-EA had not been constructed, nor tested for linearity, while chemical processing and the extraction of specimens took place, therefore the quantity of specimens required per sample was estimated, so that processing and extraction could continue without the nano-EA in place. Therefore, the use of smaller sample sizes in the future may reduce the quantity of AOM requiring removal from the sample, thereby reducing the exposure time necessary to produce a clean sample. If this treatment method can be refined such that no significant damage is caused to the palynomorphs, it offers great potential for the palynological investigation of black shales, which are often obscured by high quantities of AOM.

5.3 STABLE ISOTOPES

The composite section and the KY801N section record isotopic change throughout the sections in both the bulk samples and the *Tasmanites* samples. Sampling resolution within the Cleveland Member of both sections appears to be inadequate to fully interpret this stratigraphic interval. However, increased sampling resolution within the Sunbury Shale of the composite section led to the recognition of significant, well-defined isotopic oscillations in both the bulk and *Tasmanites* samples. It is possible that similar isotopic variation also exists within the Cleveland and Huron Members of the Ohio Shale. However, sampling resolution should be increased in future isotopic studies of this formation to investigate this trend further.

5.3.1 Possible interpretations

Following the analysis of the nitrogen isotope data, a range of possible interpretations of the recorded changes are presented and discussed throughout this section.

5.3.1.1 Thermal maturation

As mentioned in Chapter 2, the thermal history of the sampled area is limitedwhich was the reason for choosing this area. The peak palaeotemperature recorded for the succession is 80 °C and no intrusive activity is known to have taken place near any of the sampled localities. Even so, thermal maturation studies were carried out on the *Tasmanites* specimens to investigate the effect of thermal maturation on their stable isotope signature. As illustrated in Section 4.1.1, experimentally induced low level thermal maturation did not have any significant effect on either the $\delta^{15}N$ or the $\delta^{13}C$ values of the *Tasmanites*. Therefore, thermal maturation is not thought to account for the isotopic changes recorded through the succession in either the bulk or the *Tasmanites* samples.

5.3.1.2 Chemical treatment

As discussed in Section 4.1.2, the chemical treatments carried out to extract *Tasmanites* specimens from the bulk samples appear to have had very little impact on the isotopic signature of the *Tasmanites*. It is therefore unlikely that the isotopic changes recorded within the chemostratigraphic curve presented for *Tasmanites* was caused by chemical treatments carried out prior to the analyses. However, studies were not carried out to assess the impact of these chemicals on the bulk samples.

Studies have shown that the inorganic N fraction contained within clay minerals in sediments can be relatively significant (Carman *et al.*, 1996; Freudenthal *et al.*, 2001; Kienast *et al.*, 2005; Schubert and Calvert, 2001). The analysis of total sample N will therefore include this

inorganic N fraction if it is present within the sample, leading to isotopic results which are a mixture of the organic and inorganic N fraction. Treatment with HCl and HF removed these inorganic components, while preserving the organic residue of the bulk samples. The EA-IRMS also has an upper limit on sample size, as complete oxidation of large samples becomes difficult. Consequently, in order to reduce sample weights, bulk samples were treated with HF and HCl to remove the inorganic fraction prior to analysis. This process reduced the sample weight required per analysis while maintaining linearity within the IRMS.

Kennedy *et al.* (2005) carried out an investigation into the effects of HCl on the nitrogen isotope signature of bulk marine sediments and found that treatment with HCl led to a small and relatively indistinguishable change in the $\delta^{15}N$ value of the bulk marine sediment. Schmidt and Gleixner (2005) carried out tests on the effects of HF treatment on soils and shales. Their study showed that these shale containing less organic C (~ 0.5 %) recorded no discernable change in $\delta^{15}N$ relative to the untreated sample. However their study also revealed that the shale containing a higher concentration of organic C (~ 5 %) recorded a less positive (lighter) $\delta^{15}N$ value, by approximately 3 ‰ following treatment with HF. It was suggested that this change may have been due to the removal of microbially altered biomass following HF treatment. However, this explanation was offered for soil and compost samples rather than the shale samples, for which an explanation for the differences between the two samples was not given. The study was also carried out on just two shale samples, and therefore is not conclusive. As mentioned above, studies have shown that the inorganic N fraction can be quite significant within marine sediments (Carman *et al.*, 1996; Freudenthal *et al.*, 2001; Kienast *et al.*, 2005). This inorganic N is often bound to, or adsorbed by clay minerals, mainly illite (Schubert and Calvert, 2001), which is removed during HF treatment. This will most likely lead to a change in the $\delta^{15}N$ signal of the bulk sediment, but not necessarily the $\delta^{15}N$ of the bulk organic fraction of the sample.

The isotopic changes recorded in the bulk sediment are thought not to be due to treatment methods. However, it is possible that the chemostratigraphic curve is slightly offset due to HF treatment. The black shales analysed for this project all contain similar concentrations of organic C. Therefore, any possible alteration of the original $\delta^{15}N$ signal brought about by treatment with HF should be reflected in all of these samples equally, as all samples were treated by identical procedures. This is further reinforced by the similar isotopic changes recorded in both the bulk material and the *Tasmanites* specimens through the section. The HF treatment was not found to cause any significant change in the $\delta^{15}N$ signal of the *Tasmanites* specimens, therefore isotopic changes reflected in both the $\delta^{15}N_{bulk}$ and the $\delta^{15}N_{Tas}$ are more likely explained by original environmental isotopic variation, rather than chemical treatments. These synchronised $\delta^{15}N_{bulk}$ and

the $\delta^{15}N_{Tas}$ changes are observed throughout the sections, further verifying the fidelity of the bulk isotopic signal.

As mentioned previously, the offset brought about by chemical treatment is likely to cause the $\delta^{15}N_{bulk}$ to become lighter (Schmidt and Gleixner, 2005). As bulk marine sediment is mostly composed of phytoplanktonic organisms, the $\delta^{15}N_{bulk}$ signal should mainly be composed of diazotrophic bacteria and non-diazotrophic phytoplankton (*Tasmanites*). Following the mixing of these groups within the bulk sediment, the average $\delta^{15}N$ value should be similar to, or less positive than the $\delta^{15}N$ value for non-diazotrophic phytoplankton (*Tasmanites*), because terrestrial components and higher trophic level organisms would constitute a relatively small amount of the overall bulk organic matter, and therefore would not contribute as much to the $\delta^{15}N_{bulk}$ value as phytoplanktonic and diazotrophic organisms. A $\delta^{15}N_{bulk}$ offset brought about by chemical treatment of the shales studied in this thesis is therefore unlikely, because the $\delta^{15}N_{bulk}$ is, at times, a similar value to $\delta^{15}N_{Tas}$, which record the isotopic signal of non-diazotrophic primary producers. If the recorded $\delta^{15}N_{bulk}$ values were offset due to treatment with HF, the original value of the shales would, at times, be heavier, by approximately 3 ‰ (Schmidt and Gleixner, 2005), than the value recorded for *Tasmanites* and other primary producers, which comprise the majority of the organic material within the shales. Chemical treatment is therefore not considered a reliable explanation for the isotopic changes recorded within the stratigraphy.

5.3.1.3 Weathering

Most of the sampling was carried out on outcrops located along roadcuts, where the samples would have been exposed to a certain degree of weathering, although every effort was made to avoid sections that looked overly weathered. *Tasmanites* specimens were exposed to H_2O_2 simulate weathering on their $\delta^{15}N$ value. As outlined in Chapter 4, exposure to H_2O_2 for five hours caused little to no isotopic fractionation within the *Tasmanites* specimens, therefore weathering is unlikely to be responsible for isotopic changes recorded in the *Tasmanites* chemostratigraphic curve.

Organic-rich black shales typically have low permeability and porosity and this will reduce their tendency to weather. However, Leythaeuser (1973) and Clayton and Swetland (1978) noted that weathering can lead to a significant reduction in the organic C content of shale samples. All samples collected for the construction of the chemostratigraphic curve were collected from outcrops, rather than boreholes, and therefore have all been exposed to a similar degree of weathering. The chemostratigraphic curve for the bulk material also records similar changes to the *Tasmanites* data, which suggests that the bulk sediments record an original isotopic signal that has not been significantly affected by weathering. Therefore, weathering is not thought to be a reasonable explanation for the isotopic change observed within this dataset.

5.3.1.4 Diagenesis

The majority of studies report an increase in the $\delta^{15}N$ of sedimentary organic matter following diagenetic alteration, although some studies have also reported a decrease in the $\delta^{15}N$ of sedimentary organic matter under anaerobic conditions (Libes and Deuser, 1988; Altabet *et al.*, 1991; Altabet *et al.*, 1999; Lehmann *et al.*, 2002; Möbius *et al.*, 2011). Exact mechanisms for diagenetic alteration remain unknown, though kinetic isotope fractionation during protein hydrolysis (Gaye-Haake *et al.*, 2005; Möbius *et al.*, 2010) and deamination (Macko and Estep, 1984) during the degradation of organic matter have been proposed as the likely reasons for observed ^{15}N enrichments.

The main controlling factor in organic matter degradation is oxygen exposure time (Möbius *et al.*, 2011). Many of the bulk grey shale samples record higher ^{15}N concentrations in comparison to their surrounding bulk black shale samples. The majority of the mud precursors of the grey shale horizons are thought to be deposited under suboxic conditions, rather than oxic conditions. Therefore, the extent of possible diagenetic alteration is unknown. However, this is a consideration that should be taken into account when interpreting the chemostratigraphic curve.

Robinson *et al.* (2012) compiled as much existing data as possible to interpret the extent of diagenetic alteration on the $\delta^{15}N$ values of bulk sedimentary marine samples. They observed that where sediment accumulates slowly, the offset between the $\delta^{15}N$ recorded in the sinking flux of organic matter and the bulk sediment accumulating on the sea floor is often greater than in areas that experience high accumulation rates, such as continental margin settings. Within continental margin settings, there appears to be a negligible difference between the sinking flux $\delta^{15}N$ and bulk sea floor $\delta^{15}N$. They concluded that $\delta^{15}N_{bulk}$ records predominantly reflect changes in the $\delta^{15}N$ of the sinking flux exported to the sediment, rather than differences in diagenetic alteration. As such, the majority of isotopic changes presented in this thesis are not thought to be reflective of diagenetic alteration.

As mentioned in Chapter 1, extracted sedimentary N fractions (diatom frustules, foraminifera and chlorophyll degradation products) have been used as a means to avoid diagenetic alteration that may cause changes in the $\delta^{15}N$ signal recorded in the bulk sample. The extracted *Tasmanites* are anticipated to provide an equivalent extracted sedimentary N fraction resistant to diagenetic alteration. If the *Tasmanites* specimens have indeed resisted diagenetic alteration, the close correspondence between isotopic changes recorded in the *Tasmanites* and bulk chemostratigraphic curves would suggest a lack of diagenetic alteration in the bulk samples.

5.3.1.5 Variation in organic composition

This research was carried out to investigate climate changes that occurred during the Late Devonian Hangenberg Event. The research included the analysis of the nitrogen isotope signal of bulk shales from Kentucky, as well as the extracted palynomorph, *Tasmanites*. The comparison of the two isotopic signals was hypothesised as a method capable of distinguishing between an isotopic change brought about by variation in the organic composition of the shales, and an externally driven change, such as climate change. As explained in Chapter 1, the $\delta^{15}N$ value of organisms records their relative trophic position within the food web, and therefore changes within the bulk organic composition can lead to recorded changes in the $\delta^{15}N_{bulk}$ signal. The isotopic changes recorded through the chemostratigraphic curve presented for *Tasmanites* are unlikely to be due to variation in organic composition, because the samples consisted of handpicked genus specific specimens.

The $\delta^{15}N$ value for primary producers, such as *Tasmanites*, is reflective of baseline nitrogen uptake, which can be influenced by rates of denitrification, nitrogen fixation, and relative nutrient utilisation (Altabet and Francois, 1994). Rates of denitrification may not change the overall organic composition of the bulk sediment, but may leave its signature in primary producers consuming the heavier nitrate upwelled from denitrification zones. However, this does not constitute a change in organic content. Increased nitrogen fixation, on the other hand, can lead to an increase in cyanobacterial input to the bulk sediment, leading to variations in the organic content of the bulk samples. If nitrate supply in the upper ocean is low, the growth of cyanobacteria can also lead to a change in the $\delta^{15}N$ signal of primary producers, such as *Tasmanites*, as they can become a vital source of N within a N-limited eco-system.

It is possible that the AOM within many of the black shale samples has a predominantly cyanobacterial source owing to the extremely light $\delta^{15}N_{bulk}$ values (> 1 ‰) recorded within some of the black shales throughout the sections studied (Rau *et al.*, 1987; Kuypers *et al.*, 2004; Arnaboldi and Meyers, 2006; Emeis and Weissert, 2009; Melchin *et al.*, 2013). This is due to the ability of cyanobacteria to fix their own N directly from atmospheric N_2. $\delta^{15}N$ values of between - 3‰ and 1‰ are expected for organic matter from extant marine N_2-fixing cyanobacteria (Carpenter *et al.*, 1997; Minagawa and Wada, 1986) (Figure 5.1). Nitrogen-fixing bacteria (such as cyanobacteria) can outcompete other phytoplankton under N-limited, or low N:P, conditions, but at a high energy cost. The most suitable conditions for cyanobacterial blooms arises as a result of high denitrification (Somes *et al.*, 2010). Denitrification occurs in areas where there are suboxic conditions, often near the base of the pycnocline. As deep waters are upwelled to the surface, heterotrophic bacteria (denitrifying bacteria) can use nitrate (NO_3^-) as an electron acceptor,

effectively removing it from the marine system in its usable form and returning it to the atmosphere as either N_2 or N_2O (Codispoti and Richards, 1976).

Denitrification can lead to the upwelled water recording an N:P ratio significantly lower than that of the Redfield ratio (16:1). Under these low N, high P conditions, N-fixers, such as cyanobacteria use the excess P to form cyanobacterial blooms, which will be recorded as a relatively less positive (light) $\delta^{15}N_{bulk}$ signal in the sediments accumulating below this region. However, if the N:P ratio in the upper ocean approximates the Redfield ratio, due to the high energy cost of fixing atmospheric N and the lack of excess P, cyanobacteria lose their competitive advantage to other phytoplankton (Melchin *et al.*, 2013). This will be recorded in the bulk sediment as a more positive (heavier) $\delta^{15}N_{bulk}$ signal, indicating a reduction in cyanobacterial biomass contributing to the bulk sediment. It is likely that cyanobacteria has contributed to the organic content of at least some of the black shale samples analysed as part of this thesis. Possible samples include those within the Huron Member and the lower Cleveland Member of the Ohio Shale, and the less positive (lighter) $\delta^{15}N_{bulk}$ samples from the Three Lick Bed and the Sunbury Shale.

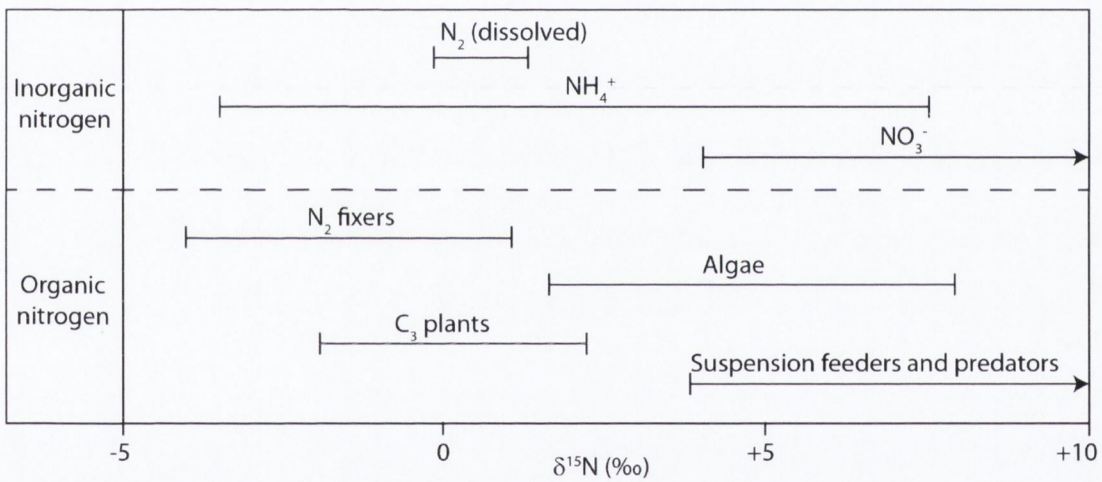

Figure 5.1. Typical $\delta^{15}N$ values expected for various inorganic and organic nitrogen present in the marine environment. Modified from Rau *et al.* (1987) and Arnaboldi and Meyer (2006).

Several of the black shales within the Three Lick Bed, the upper Cleveland Member and the Sunbury Shale record more positive (heavier) $\delta^{15}N_{bulk}$ values than are expected for N-fixing bacteria (> +1 ‰). This change may be partially due to a reduction in cyanobacteria as the N:P ratio in the photic zone increases. This reduction in cyanobacteria could be responsible for the heavier $\delta^{15}N_{bulk}$ signal recorded in the stratigraphy, where the $\delta^{15}N_{bulk}$ begins to resemble the $\delta^{15}N$ signal recorded by non-N fixing primary producers ($\delta^{15}N_{Tas}$), suggesting a greater addition of non-N fixing phytoplankton to the AOM and the overall bulk sediment. It is also possible that the heavier signal could be due to increases in the proportion of terrestrial and animal debris within the bulk samples (Figure 5.1). However, the proportion of marine to terrestrial material (based on

vitrinite, inertinite and liptinite) increases through the Huron Member and remains relatively stable throughout the Cleveland Member (Rimmer *et al.*, 2004), out of synchronisation with the changes recorded in $\delta^{15}N_{bulk}$. The proportion of AOM also remains relatively high within all of the black shale samples in comparison to other components, and therefore the dilution effect caused by increases in terrestrial and animal debris is not considered to be a robust explanation for the recorded change in $\delta^{15}N_{bulk}$.

Within the Three Lick Bed, following deposition of the mud precursors of the grey shale horizons, increases recorded in the $\delta^{15}N_{bulk}$ signal are not reflected in the $\delta^{15}N_{Tas}$ signal (Figure 5.2), suggesting that the changes observed in the bulk material may be due to variation in organic content, such as reduced cyanobacterial input, rather than a change in the overall $\delta^{15}NO_3^-$. Where there is a lack of AOM in the grey shale samples, the $\delta^{15}N_{bulk}$ signal is consistently more positive (heavier) than the $\delta^{15}N_{Tas}$ signal, and often heavier than the $\delta^{15}N_{bulk}$ signal of the surrounding black shales (with the exception of the base of the Bedford Shale). This may be due to variation in organic content between the two lithologies, where the black shale consists mainly of AOM, acritarchs, prasinophytes, fish remains and terrestrial debris, the grey shale contains little to no AOM, a lower proportion of acritarchs, prasinophytes and fish remains, and higher proportions of terrestrial debris. It is probable that the lack of AOM in the grey shale horizons, is responsible for much of the change observed in the $\delta^{15}N_{bulk}$ between the two lithologies. The upper Cleveland Member and the black shale at the base of the Bedford Shale record $\delta^{15}N_{bulk}$ values that do not correspond to high levels of cyanobacterial input. The subsequent grey shales of the Bedford Shale record a decrease in the $\delta^{15}N_{bulk}$ signal, and a contemporaneous decrease in $\delta^{15}N_{Tas}$. This is the opposite trend observed within the grey shales of the Three Lick Bed and the Huron Member, where increases in $\delta^{15}N_{bulk}$ are coeval with observed decreases in $\delta^{15}N_{Tas}$. The majority of the *Tasmanites* samples extracted from the grey shale horizons in the Bedford Shale record similar changes in $\delta^{15}N$ to the bulk samples, implying that the change in the $\delta^{15}N_{bulk}$ signal between the two lithologies cannot be entirely explained by variation in organic composition.

In summary, the variation in $\delta^{15}N$ within the bulk samples may be partially due to variation in the organic composition. However, it cannot account for all of the variation as similar isotopic changes are recorded within the genus-specific *Tasmanites* samples. The variation observed in the $\delta^{15}N$ curves show a close correspondence between the bulk samples and the *Tasmanites* samples, with an offset between the two chemostratigraphic curves of between 0 ‰ and 4.5 ‰ through the section. The *Tasmanites* samples generally record more positive (heavier) $\delta^{15}N_{Tas}$ values than the bulk black shale samples, and less positive (lighter) $\delta^{15}N_{Tas}$ values than the bulk grey shale samples. Variation in organic content within the bulk samples, such as cyanobacterial input, rather than being a hindrance to isotopic studies, can often aid in the interpretation of palaeoenvironmental conditions, as will be discussed in the following section.

Figure 5.2. Isotopic changes possibly brought about by variation in the organic content of the bulk samples. The grey panels refer changes in either $\delta^{15}N_{bulk}$ or $\delta^{15}N_{Tas}$, outlined in the legend. The yellow panels refer to suggested changes in cyanobacterial input based on $\delta^{15}N_{bulk}$ values.

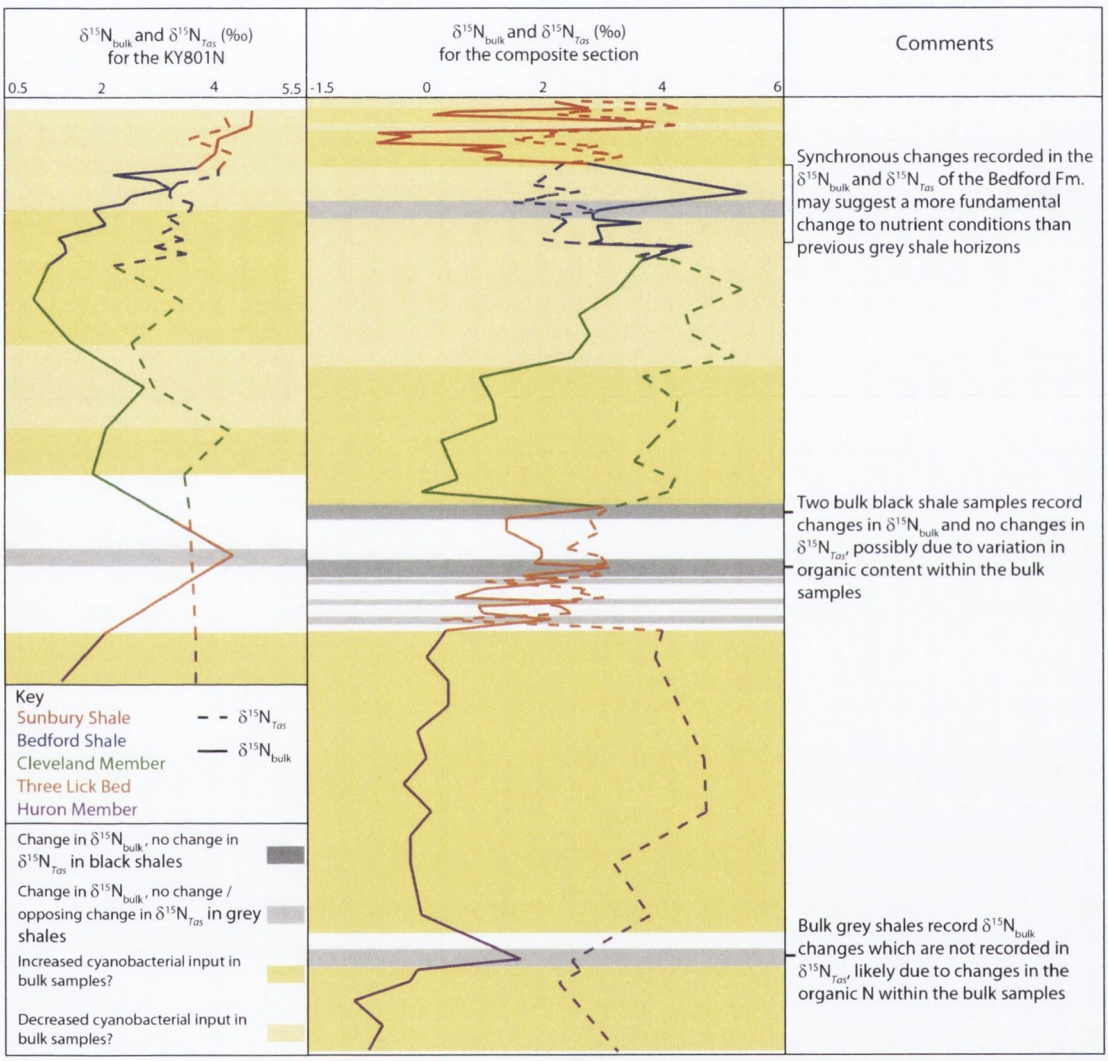

5.3.1.6 Climate and eustatic sea level change

As discussed in previous chapters, glacial deposits have been recorded in Upper Devonian sediments from South America, Africa and North America (Brezinski *et al.*, 2008, 2009, 2010). The deposition of these glacial sediments coincides with the deposition of some of the shales collected from Kentucky and analysed as part of this thesis. Because the shales are contemporaneous with known glacial / interglacial events, it is likely that some of the isotopic variation observed through the stratigraphy may be related to this Late Devonian climate change. The nitrogen cycle, and the isotopic indicators produced by it, can be quite complex, leaving diverse tracers in different areas of the ocean. Attempting to prove that a multifaceted system, such as the climate, caused the observed isotopic changes is difficult, as parameters vary throughout the ocean, and the effects of climate change may be quite distinct, depending on the palaeogeography of the locality in question. Comparisons to modern glacial / interglacial cycles, and consideration of some key parameters associated with nitrogen isotope changes and climate disturbances are therefore critical. The following sections briefly discusses selected modern $\delta^{15}N$ records and some regional parameters which may have an influence on the $\delta^{15}N$ signal within sedimentary records. Subsequently, an attempt will be made to reconcile the isotopic changes recorded within the Kentucky sections with Late Devonian climate changes and sea level changes.

5.3.1.6.1 Modern glacial / interglacial $\delta^{15}N$ record

Modern marine downcore $\delta^{15}N_{bulk}$ values record Quaternary glacial / interglacial changes. It has been observed that during glacial periods, denitrification and N-fixation are significantly reduced (Altabet *et al.*, 1995; Haug *et al.*, 1998; Deutsch *et al.*, 2004; Galbraith *et al.*, 2004), such that $\delta^{15}N_{bulk}$ values in areas of either intense denitrification or high rates of N-fixation, appear to return to $\delta^{15}N_{bulk}$ values similar to that recorded for average marine nitrate (~ 5 ‰). During interglacial periods, denitrification and N-fixation increase in intensity, recording opposing $\delta^{15}N_{bulk}$ signals in different areas of the ocean, which results in significant spatial variation in $\delta^{15}N_{bulk}$.

Regions dominated by denitrification, such as the Arabian Sea, record lighter $\delta^{15}N_{bulk}$ values during glacial periods, and regions dominated by high rates of nitrogen fixation, such as the Cariaco Basin, record heavier $\delta^{15}N_{bulk}$ values during glacial periods (Figure 5.3). Nitrogen-fixation often occurs as a response to high rates of denitrification, and therefore can lag behind increased rates of denitrification. This leads to an initial deglacial increase in $\delta^{15}N_{bulk}$, often followed by either a slight or significant decrease in $\delta^{15}N_{bulk}$, depending on the area of the ocean being studied (Figure 5.4). The marine system therefore appears to self regulate the long term nitrogen budget of the ocean, regardless of climate conditions, by increasing N-fixation during times of high denitrification, and reducing N-fixation when denitrification rates drop (Meckler *et al.*, 2011). These variations are recorded as distinct N isotope changes in different areas of the ocean.

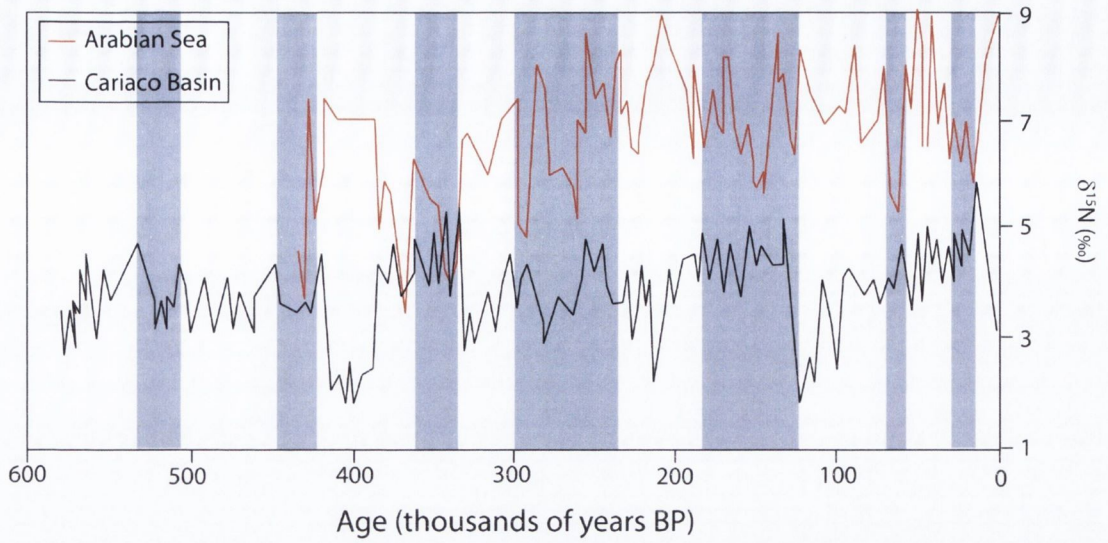

Figure 5.3. Outline of bulk downcore sedimentary $\delta^{15}N$ changes in the Arabian Sea and the Cariaco Basin, compiled and modified from Altabet *et al.* (1995) and Haug *et al.* (1998). Blue lines represent glacial periods. Opposing $\delta^{15}N$ trends are recorded at each locality due to differences in the dominant processes at each site. Denitrification rates decrease in the Arabian Sea and N-fixation rates decrease in the Cariaco Basin during these glacial intervals, produing $\delta^{15}N$ values similar to the modern average marine $\delta^{15}NO_3^-$.

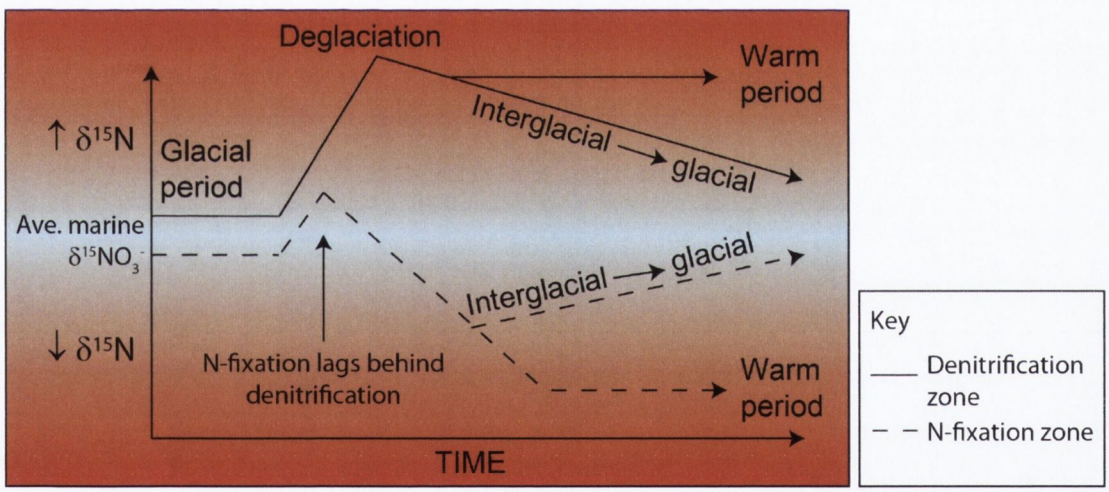

Figure 5.4. Generalised changes in $\delta^{15}N$ suggested to occur within denitrification zones and N-fixation zones over a glacial to interglacial transition. The $\delta^{15}N$ of bulk sediments are thought to resemble the average marine $\delta^{15}NO_3^-$ during glacial periods. This is followed by an intial deglacial increase in $\delta^{15}N$ in both regions due to higher rates of denitrification. The N-fixation zone then records an interglacial decrease in $\delta^{15}N$, as N-fixation rates increase and become dominant. The denitrification zone records a slightly lighter interglacial $\delta^{15}N$ value following the intial deglacial $\delta^{15}N$ maximum. This is due to increases in sedimentary denitrification and N-fixation, however, the region is still dominated by water column denitrification.

However, many localities will record very little change in $\delta^{15}N_{bulk}$ between glacial and interglacial periods, such as those recorded in the Caribbean Sea (~ 4 – 5 ‰) and the Gulf of Mexico (~ 2 – 4 ‰) (Ren *et al.*, 2009; Meckler *et al.*, 2011). Based on modern glacial / interglacial sediments, interglacial periods record the most extreme and spatially distinct $\delta^{15}N_{bulk}$ values, and glacial periods commonly record a return to $\delta^{15}N_{bulk}$ values similar to the average marine $\delta^{15}NO_3^-$ value (5 – 6 ‰) (Figures 5.3 and 5.4).

Local and regional processes are therefore important factors when considering climate change as the reason for recorded isotopic variation, because modern analogues suggest opposing $\delta^{15}N_{bulk}$ trends brought about by denitrification and N-fixation, fluctuating around an average marine $\delta^{15}NO_3^-$. The average marine $\delta^{15}NO_3^-$ is not known for the Late Devonian, however, as mentioned in Chapter 1, the atmosphere most likely contained similar levels of N_2 as today (Hart, 1978). Due to the ability of the marine system to regulate its own nitrogen budget, it can be assumed that $\delta^{15}NO_3^-$ was similar to the modern average (~ 5 ‰), however, the real value may have been higher or lower than this value.

5.3.1.6.2 Oxic conditions

Oxic conditions are important when analysing nitrogen isotope records, as denitrification is constrained to areas containing low levels of oxygen within the upper kilometre of the ocean (Sigman *et al.*, 2009). As noted in Chapter 1, oxic conditions are suggested to be the ultimate control on the $\delta^{15}N$ value recorded in ocean sediments due to its influence on denitrification rates. The shales studied within this thesis record varying oxic conditions, and differing opinions exist as to the exact levels of anoxia present during the deposition of many of the shales (Figure 5.5) (Rimmer, 2004; Rimmer *et al.*, 2004; Perkins *et al.*, 2008). It is likely that denitrification played at least a partial role in the Late Devonian Appalachian Basin, as oxic conditions are generally recorded as being quite low throughout the sections studied.

Modern water column denitrification zones are limited in their extent, located mainly in the Eastern Tropical North and South Pacific, and the Arabian Sea. These areas are characteristic of heavy $\delta^{15}NO_3^-$ (8 – 15 ‰) due to the fractionation effect brought about by denitrifying bacteria (Galbraith *et al.*, 2013). This heavy nitrate is consumed by phytoplankton and deposited on the seafloor. The spread of anoxic bottom waters and suboxic subsurface waters can expand and intensify denitrification zones. However, if denitrification rates are intense enough, it can lead to the utilisation of nearly all the fixed nitrate within upwelled waters. Surface waters will then maintain a very low N:P ratio, leading to the growth of N-fixing cyanobacteria. $\delta^{15}N$ values of between - 3‰ and 1‰ are expected for organic matter from extant marine N_2-fixing cyanobacteria

(Minagawa and Wada, 1986; Carpenter *et al.*, 1997), therefore an increase in the growth of cyanobacteria will produce a lighter $\delta^{15}N_{bulk}$ within the surface ocean and the sedimentary record (Melchin *et al.*, 2013). Consequently, intense denitrification rates, brought about by expanding suboxic conditions may not always generate a heavier $\delta^{15}N_{bulk}$ signal in the sedimentary record, if most of the upwelled nitrate is denitrified, a lighter $\delta^{15}N_{bulk}$ signal will be brought about by increased N-fixation in the surface waters. These two processes appear to be the main drivers of change recorded in the nitrogen isotope signal of marine sediments. As these processes are ultimately initiated by the increase and expansion of suboxic zones, varying oxic conditions have been suggested to regulate the intensity of both denitrification and N-fixation (Haug *et al.*, 1998; Galbraith *et al.*, 2004; Galbraith *et al.*, 2013). This obviously raises the question of what drives low oxygen conditions in the water column.

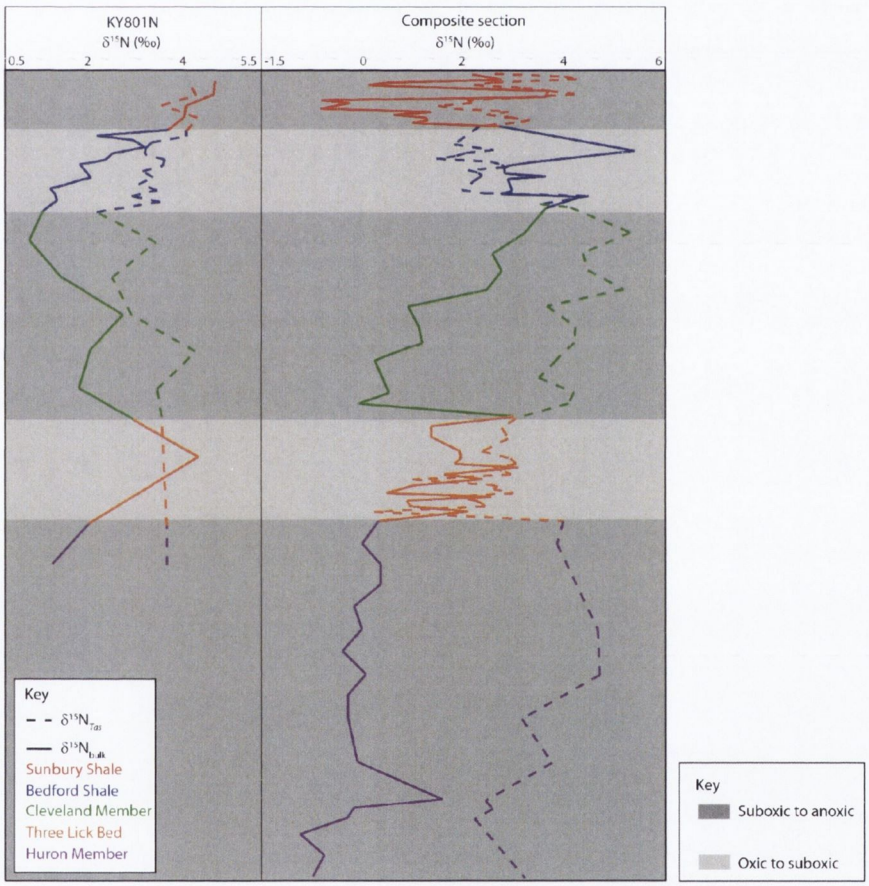

Figure 5.5. Generalised changes in oxic conditions, as suggested by Perkins *et al.* (2008), Rimmer (2004) and Rimmer *et al.* (2004).

Oceanic Anoxic Events (OAEs) have occurred at various times throughout the Phanerozoic, and have been attributed to a combination of processes, including sea-level change and increases in global temperatures (Hallam and Cohen, 1989; Landing, 2011), changes in ecosystem structure (Butterfield, 2009, 2011), nutrient cycling (Caplan and Bustin, 1999, Saltzman,

2005), large igneous provinces (Kidder and Worsley, 2010) and palaeogeographic distribution (Meyer and Kump, 2008). Butterfield (2009, 2011) discusses the differences between the largely anoxic Proterozoic oceans and the generally oxic oceans of the Phanerozoic and concludes that the main difference between them is the increase in the size of Phanerozoic phytoplankton (2-200 μm) compared with the dominant cyanobacteria (0.2-2μm) of the Proterozoic. It was suggested that this was brought about by the 'clearing' of the upper ocean by planktic metazoans (zooplankton). Prior to this, the oceans would have sustained a cycle of turbid upper oceans, which hinders the growth of larger, light dependent phytoplankton. A turbid ocean, dominated by smaller phytoplankton, with slow sinking rates, can lead to ocean stratification and anoxia (Figure 5.6).

Biomarker evidence of increased export of cyanobacteria during oceanic anoxic events during the Proterozoic and Phanerozoic would appear to corroborate this hypothesis. However, cyanobacterial blooms are most likely brought about due to the upwelling of nitrate-poor, phosphate-rich waters, which are the result of increased denitrification. The increase in water column suboxia, which promotes the expansion and intensification of denitrification, would have had to occur prior to the increase in cyanobacteria. It is possible that this change in ecosystem dynamics led to a sustained feedback mechanism on oceanic anoxia, although it is unlikely to be the sole cause or initiator of reduced oceanic oxygen conditions in the Late Devonian Appalachian Basin.

Meyer and Kump (2008) analysed a range of possible causes of widespread oceanic anoxia and came to the conclusion that the ultimate constraints on the redox state of the world's oceans were climate and palaeogeography. A warm climate coupled with basins capable of trapping nutrients were suggested to promote anoxia, and therefore the release of phosphate from anoxic settings. This may have fuelled cyanobacterial blooms, possibly enhancing anoxia even further.

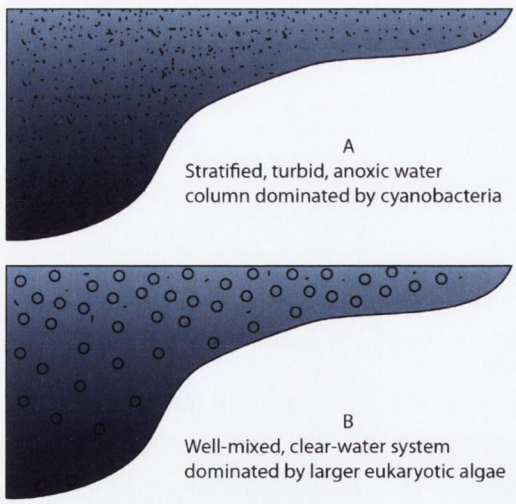

Figure 5.6. (A) Schematic of the cyanobacteria-dominated Proterozoic ocean and (B) the eukaryotic phytoplankton-dominated Phanerozoic ocean. Modified from Butterfield (2009).

5.3.1.6.3 Palaeogeographic considerations

Meyer and Kump (2008) noted the importance of palaeogeographic settings in the development of oceanic anoxia. They suggested that continental configurations which enhance nutrient trapping are suited to the development of oceanic anoxia, as this increases productivity and O_2 demand, which leads to increased denitrification, a low N:P ratio in surface waters, and the growth of cyanobacteria, which further increases oxygen demand, intensifying anoxia. The Cariaco Basin, located approximately 10°N, is a modern, deep, anoxic basin, which developed as a consequence of a structural depression on the northern shelf of Venezuela (Haug *et al.*, 1998, 2001). The basin is connected to the open ocean via shallow sills, restricting deep water ventilation. During interglacial periods, such as the Holocene, the basin receives nutrient fluxes through upwelled waters from the Caribbean Sea (Lin *et al.*, 1997). This leads to high productivity and O_2 demand, driving water column anoxia and increased denitrification. Denitrification will lead to a reduced N:P ratio in surface waters, increasing the extent of N_2 fixation, further enhancing anoxia (Figures 5.8 and 5.11). The recorded $\delta^{15}N_{bulk}$ value of interglacial sediments is therefore relatively low (2 – 3 ‰), as N-fixation lowers the average $\delta^{15}N$ of the sedimentary nitrogen (Haug *et al.*, 1998). During glacial periods it is hypothesised that nutrient fluxes, via upwelled water from the Caribbean Sea, are significantly reduced due to lowered glacial stage sea levels, causing the basin to become largely isolated from the open sea (Lin *et al.*, 1997). This reduces productivity and the consequent anoxia, leading to reduced denitrification, and an increase in the surface N:P ratio, close to the Redfield ratio (16:1) (Figures 5.8 and 5.10). This increase in the N:P ratio should reduce the rate of N-fixation within the basin, as cyanobacteria would be unable to compete with other phytoplankton for the available phosphorus. The reduction in N-fixation is recorded in the glacial sediments of the Cariaco Basin as an increase in sedimentary $\delta^{15}N$ (~ 5‰).

The opposite trend is observed within the denitrification zones of the Eastern Tropical North and South Pacific, and the Arabian Sea (Figures 5.9, 5.12 and 5.13). Sediment cores from these areas record less positive (lighter) relative $\delta^{15}N$ values during glacial periods, and more positive (heavier) relative $\delta^{15}N$ values during interglacial periods (Altabet *et al.*, 1995; Ganeshram *et al.*, 2002; Kienast *et al.*, 2002). This is explained by an increase in denitrification during interglacial periods. The higher than average marine $\delta^{15}NO_3^-$ values recorded at these localities (8 - 15 ‰) reflects the influence of denitrification on subsurface waters which are upwelled to the surface. Excess P can then be exported to the open ocean due to the unrestricted nature of these localities. This exported excess P then leads to the development of cyanobacterial blooms elsewhere in the ocean.

The extremely low $\delta^{15}N_{bulk}$ values recorded in some of the Kentucky sections suggest that N-fixation was the dominant process within at least parts of the Appalachian Basin at the time of

deposition. Taking the Cariaco Basin as a possible modern analogue to the Appalachian Basin, increases in the $\delta^{15}N_{bulk}$ can tentatively be assigned to glacial periods, or perhaps simply to lower sea level. However, the Cariaco Basin records increasing TOC during interglacial periods, and reduced TOC during glacial periods (Haug *et al.*, 1998). Algeo (2004) recorded increasing TOC concentrations (Figure 5.15) within the upper Cleveland Member, coinciding with increasing $\delta^{15}N_{bulk}$ within the composite section. This correlation is the opposite to what is found in the Cariaco Basin, and therefore cannot be viewed as a fully compatible modern analogue to the Appalachian Basin.

The Appalachian Basin is a foreland basin, measuring approximately 2,050 km long, by 530 km wide, at its broadest point, with an area of approximately 536,000 km^2 (Colton, 1970). The Cariaco Basin on the other hand is only approximately 4,000 km^2 (Escalona *et al.*, 2011). Due to the sheer size of the Appalachian Basin, and its connection to other nearby basins, such as the Michigan, Illinois and Black Warrier basins, it is likely that the Appalachian Basin continued to have a strong connection with the open ocean during periods of lowered sea level, whereas, the Cariaco Basin appears to have been quite restricted during glacial periods (Lin *et al.*, 1997). This may help to explain differences observed in the $\delta^{15}N$:TOC profiles between the two basins. The Appalachian Basin is further complicated by the fact that the Acadian orogen was ongoing at the time of deposition, therefore the depth of the basin is likely to have changed in accordance with tectonic activity occurring along the eastern margin of North America (Ettensohn, 2008).

The Appalachian Basin does not seem to compare well with modern coastal denitrification zones, as the $\delta^{15}N$ signal recorded within the Late Devonian Appalachian Basin appears to be dominated by N-fixation rather than denitrification. Because little is known about the average marine $\delta^{15}NO_3^-$ value of the Late Devonian, it is difficult to conclusively rule out the possibility that denitrification may have been the dominant feature of the Appalachian Basin. It is likely that denitrification took place within the basin, possibly to such an extent that the majority of the upwelled nitrate was converted to N_2 or N_2O by denitrifying bacteria, resulting in an extremely low N:P ratio in surface waters, thus leading to cyanobacterial blooms. It is also possible that the sample localities (Figure 5.7) are located in areas 'proximal' to and 'downstream' from active denitrification zones, where the export of excess P is restricted by basin parameters and therefore cannot be exported to the open ocean, leading to cyanobacterial blooms within the basin itself.

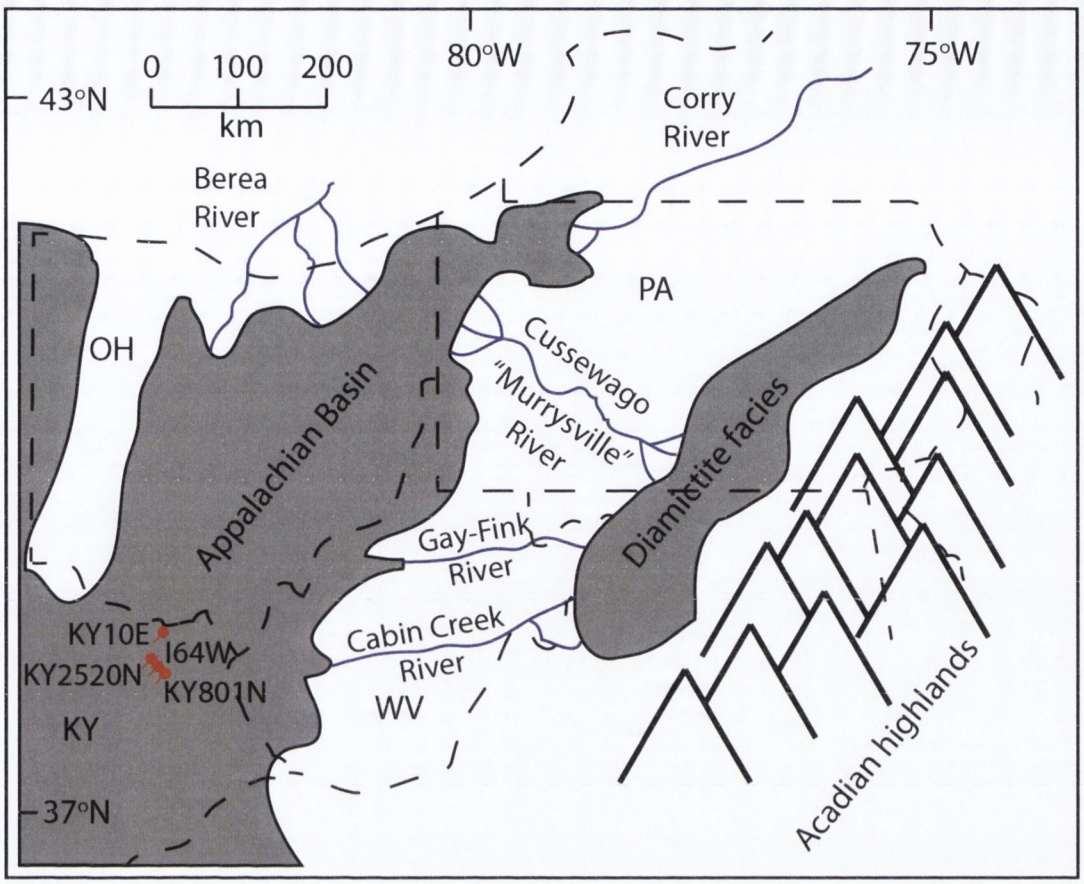

Figure 5.7. Hypothesised glaciation within the Appalachian Basin during the deposition of the Bedford Shale. The sample localities are shown as red pin markers.

One key piece of evidence may lie in the $\delta^{15}N$ signal recorded by *Protosalvinia* thalli and *Tasmanites*, extracted from samples deposited in various localities within the Appalachian, Michigan and Illinois basins. These specimens do not record the large change in $\delta^{15}N$ that would be expected between N-fixation and denitrification zones (> 4 ‰). The semi-restricted nature of the basins may have led to the near complete utilisation of nitrate within the denitrification zone, producing a low N:P ratio, while a continuous connection to the open ocean may have provided fresh sources of nitrate for the growth of phytoplankton on surface waters throughout the basin. This could have led to the offset in $\delta^{15}N$ recorded between the bulk samples and those of extracted *Tasmanites*, thus restricting the impact of denitrification. Denitrification may have been exacerbated by increased anoxia brought about by the possible leaching of salts from Silurian evaporite deposits, as described below.

The modern Gulf of Mexico is surrounded by salt domes at depth, which contributes to a hypersaline brine in the lowermost 200 m of the basin (Sackett *et al.*, 1979). Meckler *et al.* (2008)

suggested that this brine has led to density stratification and anoxic bottom waters, which in turn preserves the organic matter in the sediments within the Gulf of Mexico. It may be possible that salts leached out of Silurian evaporite deposits into the Michigan and Appalachian basins in the Late Devonian, which may have led to increased anoxia and high levels of preservation of organic matter.

The $\delta^{15}N$ signal, recorded by forams in the Gulf of Mexico, reveal a glacial to interglacial decrease in $\delta^{15}N$, most likely reflecting an interglacial increase in N-fixation (Meckler *et al.*, 2011). Similar changes may be evident within the Upper Devonian sediments of the Appalachian Basin, where lower $\delta^{15}N$ values may correspond to interglacial periods and higher recorded $\delta^{15}N$ values may correspond to glacial periods.

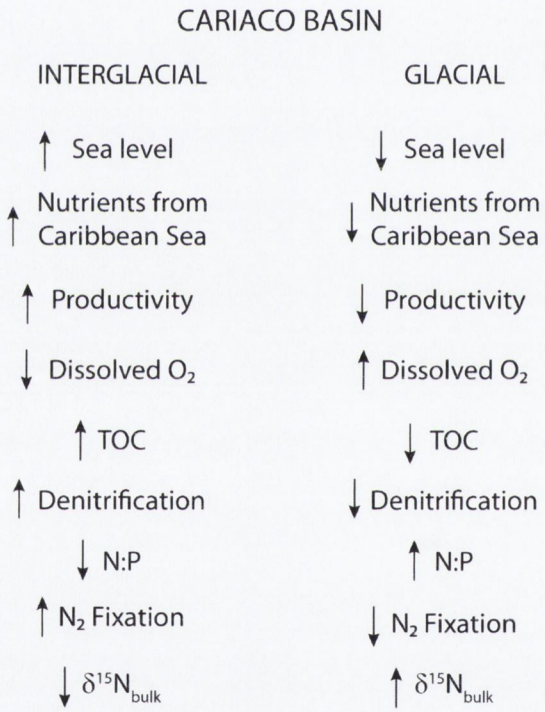

Figure 5.8. Flow chart outlining the likely processes that led to the recorded changes in $\delta^{15}N$ within the Cariaco Basin over glacial / interglacial cycles.

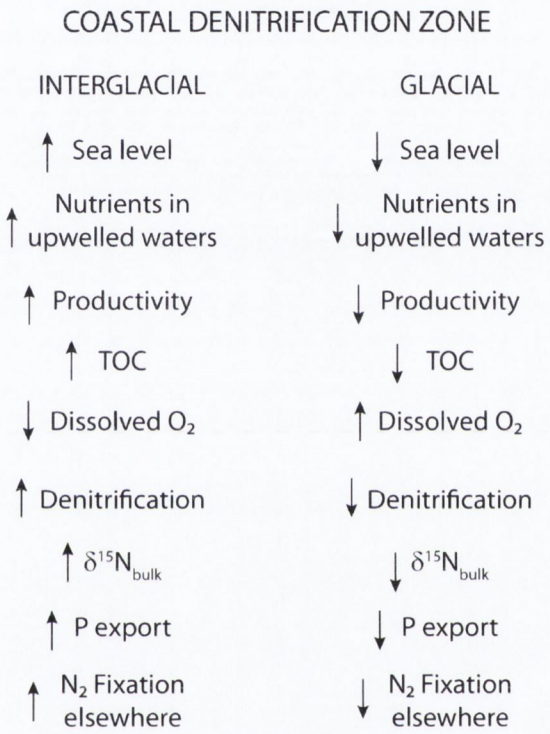

Figure 5.9. Flow chart outlining the likely processes that led to recorded changes in $\delta^{15}N$ within coastal denitrification zones over glacial / interglacial cycles.

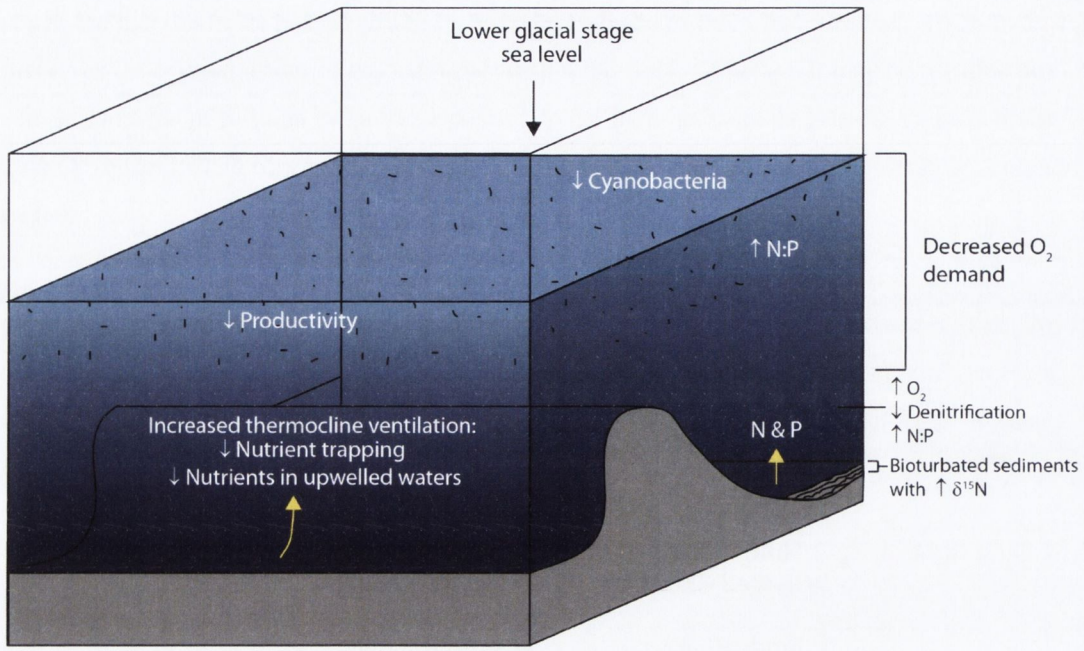

Figure 5.10. A box model outlining the conditions in a low-latitude, restricted marine basin during a glacial period. Based on likely glacial stage processes within the Cariaco Basin.

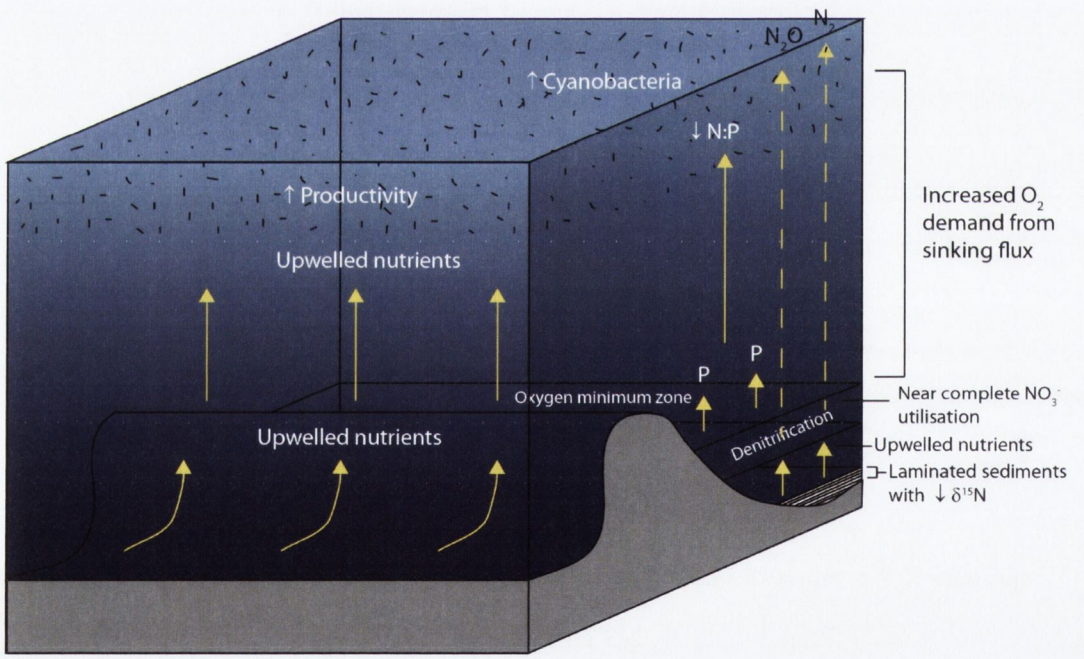

Figure 5.11. A box model outlining the conditions within a low-latitude, restricted marine basin during an interglacial period. Based on modern processes within the Cariaco Basin.

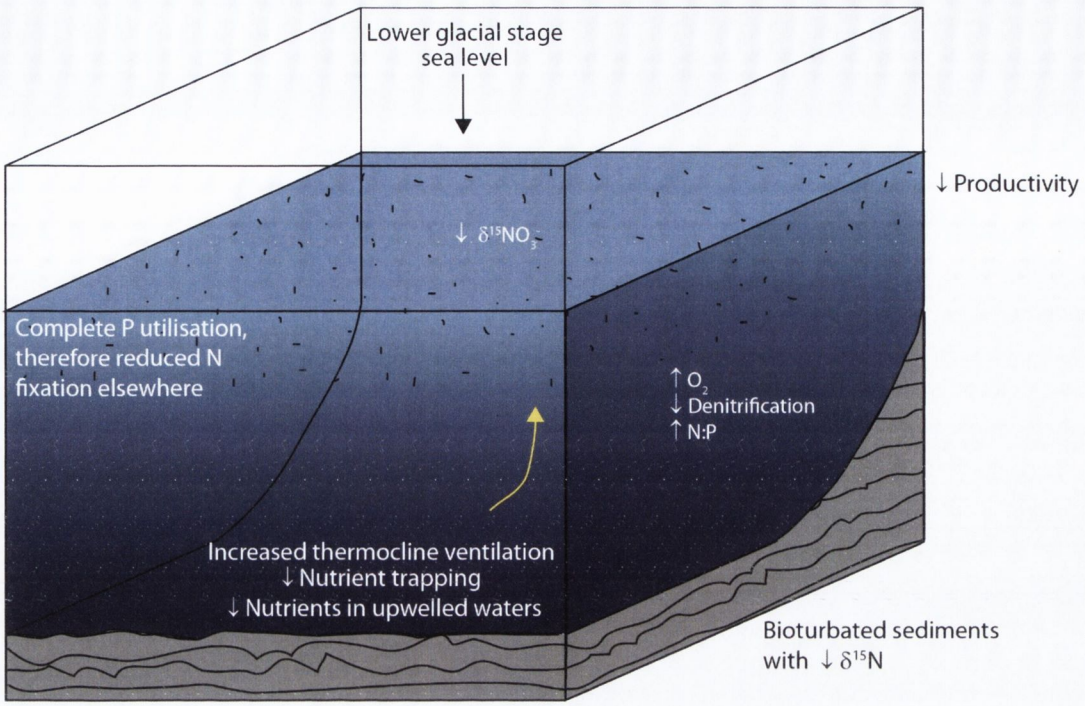

Figure 5.12. A box model outlining the conditions within a low-latitude, unrestricted, coastal marine basin during a glacial period. Based on modern processes within coastal denitrification zones.

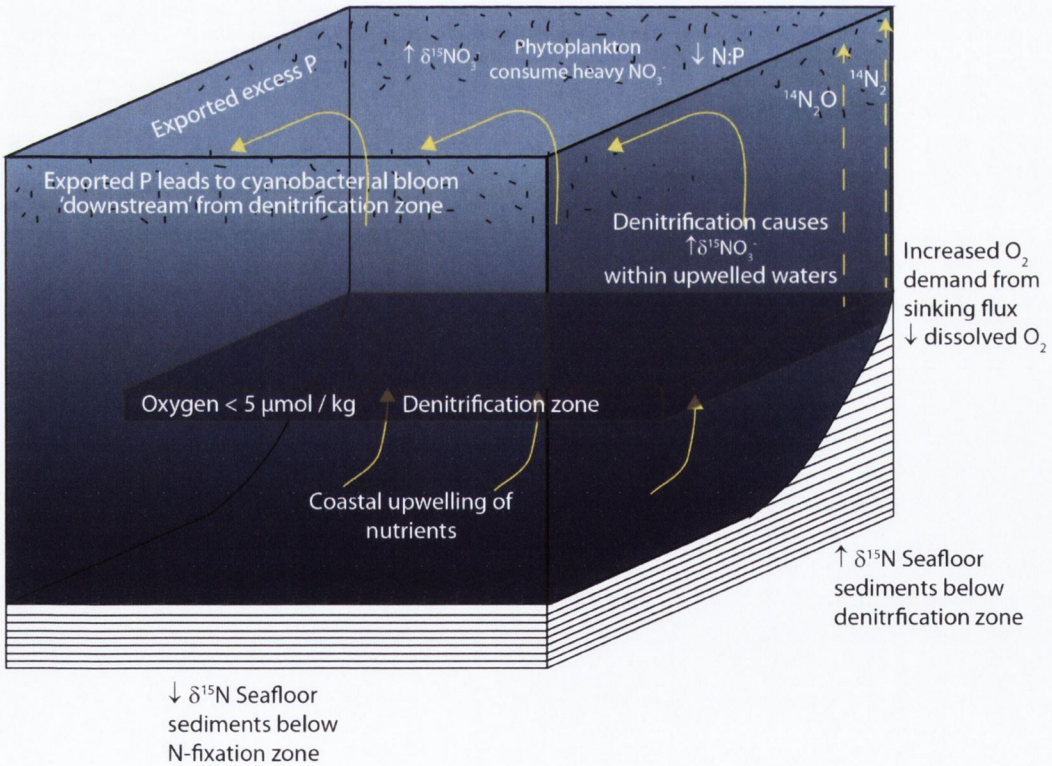

Figure 5.13. A box model outlining the conditions within a low-latitude, unrestricted, coastal marine basin during an interglacial period. Based on modern processes within coastal denitrification zones.

In summary, it is likely that the palaeogeography of the Appalachian Basin was somewhere between a restricted, N-fixation dominated basin (such as the Cariaco Basin) and an unrestricted, denitrification dominated coastal upwelling zone (such as the Arabian Sea). Box models were created to explain the various key processes in the range of basins. The Late Devonian Appalachian Basin was most likely a semi-restricted basin, with a continuous connection to the open-ocean and active denitrification and N-fixation processes occurring within the basin. If N-fixation was a dominant feature of the basin, the $\delta^{15}N_{bulk}$ and possibly the $\delta^{15}N_{Tas}$ could be expected to increase during glacial periods due to an overall reduction in N-fixation.

5.3.1.6.4 Regional climate

The Late Devonian Appalachian Basin was located within the subtropical trade wind belt, which may have encouraged coastal upwelling of nutrient rich waters (Liu *et al.*, 2010). Suboxia within subsurface waters may have led to reduced N:P ratios within these upwelled waters, stimulating the growth of N-fixing cyanobacteria (Figures 5.11 and 5.13). Based on the presence of palaeo-vertisols, the influx of siliclastic material, and the scarcity of calcareous material, Cecil *et al.*, (1998) noted that the climate of the Appalachian Basin was likely humid, with a distinct dry season. Seasonal rainfall may have led to influxes of nutrients from terrestrial sources, adding to the overall nutrient budget of the basin. However, due to the efficient biological removal of nutrients in estuaries, it is unlikely that terrestrial runoff accounts for large increases in the nutrient budget (Jickells, 1998), although the influx of fresh water may have enhanced stratification.

Increased monsoonal rains during the late Pleistocene appear to have led to the development of Eastern Mediterranean organic-rich sapropels through increased river discharge (Calvert *et al.*, 1992; Sachs and Repeta, 1999). It was suggested that this led to increased stratification within the water column, nutrient depleted surface waters, cyanobacterial blooms and lighter $\delta^{15}N$ values recorded during sapropel events (Sachs and Repeta, 1999). The heaviest $\delta^{15}N$ values recorded within the Eastern Mediterranean sediments appear to be confined to glacial stages (Calvert *et al.*, 1992).

It is possible that the change from arid conditions in the Early Devonian to humid conditions in the Late Devonian, along with the uplifting of the Acadian highlands, led to significant changes in river discharge and potential stratification within the Appalachian Basin, possibly contributing to the development of black shales (Cecil *et al.*, 1998). These regional climatic changes may have also have led to lighter $\delta^{15}N$ values recorded in the sediments as a consequence of terrestrial runoff and stratification. If regional climatic changes within the Appalachian Basin are similar to those of the Eastern Mediterranean, it may be possible that globally recognised glaciation may have had a similar impact on the isotopic signature of the Appalachian Basin, where $\delta^{15}N$ values may have become heavier during glacial periods. This

would correspond to the heavier $\delta^{15}N_{bulk}$ values recorded within the Cleveland Member and the Sunbury Shale.

In summary, changing regional climate patterns within the Late Devonian – Early Mississippian Appalachian Basin may have led to stratification brought about by increased terrestrial runoff, coastal upwelling due to the basins position within the subtropical tradewind belt, and consequently, a low N:P ratio in surface waters. A low N:P ratio within a semi-restricted basin may lead to an increase in the growth of cyanobacteria within the basin itself, rather than the export of excess P outside of the basin, producing a lighter $\delta^{15}N_{bulk}$ and possibly a lighter $\delta^{15}N_{Tas}$ signal, depending on the extent of N depletion in the surface waters. Globally induced glacial stages may be marked by heavier $\delta^{15}N$ values, such as those recorded within the Cleveland Member and the Sunbury Shale, although evidence for glaciation during the deposition of the Sunbury Shale has not been identified.

5.3.1.6.5 Indications of climate change in the Appalachian Basin

Taking these parameters into account, this section is intended to present possible interpretations of the nitrogen isotope signature recorded in Upper Devonian black shales from the Appalachian Basin (Figure 5.18).

The heavier $\delta^{15}N_{bulk}$ results from the Huron Member and the lower Cleveland Member of the KY801N section, in comparison to the composite section might be due to local variations in nutrient availability, N-fixation and upwelling within the basin. It is likely that the Huron Member and the lower Cleveland Member of the composite section (KY10E) record slightly higher rates of nitrogen fixation than the KY801N section, but generally, the $\delta^{15}N$ trends remain comparable until the middle of the Cleveland Member. The opposing $\delta^{15}N_{bulk}$ trends within the upper Cleveland Member most likely record changing N_{org} contributions and nutrient dynamics at each locality. Kienast *et al.* (2005) observed a difference of up to 2 ‰ in two sediment cores, less than 10 km apart, in the South China Sea during the last glacial maximum. The explanation provided for this offset was that each locality may have had a different origin of inorganic and organic nitrogen sources during the last glacial period, as a result of lowered sealevel.

The two sections in Kentucky are located approximately 60 km apart. The opposing $\delta^{15}N_{bulk}$ trends possibly record variations in organic nitrogen contributions and nutrients during a glacial period, coeval with continental glaciation recorded in South America. *Tasmanites* data appear to confirm this hypothesis as they record a similar trend, suggesting that the difference in $\delta^{15}N_{bulk}$ is not just a change in the type of organic matter, but a change in the nutrient dynamics at each locality. It would appear that N-fixation became more dominant within the upper Cleveland

Member at KY801N, and less dominant at KY10E during the hypothesised glacial period. Possible explanations include changes in upwelling locations, oxic conditions, and denitrification rates.

If we compare the analysed sections from Kentucky to those of the Rhenish Massif (Figure 5.14); the Drewer Sandstone records a eustatic regressive event in LE Miospore Biozone time, possibly brought about by polar glaciation, followed by the deposition of the precursor sediment of the Hangenberg Black Shale (HBS), recording a eustatic transgressive event during LE and LN Miospore Biozone times (Streel *et al.*, 2012). Both of these events possibly coincide with the deposition of the upper Cleveland Member of the Ohio Shale. As previously noted, during glacial periods, modern records appear to document a return to $\delta^{15}NO_3^-$ values similar to that of average marine nitrate. If it is assumed that the Late Devonian average marine nitrate was similar to modern marine nitrate (~ 5 ‰), then a recorded decrease away from this value in the $\delta^{15}N_{bulk}$ within the upper Cleveland Member of the KY801N section serves to question the hypothesis of a glacial period at this time. The increasing TOC values recorded in the upper Cleveland Member (Figure 5.15) indicate increased productivity within the basin, when productivity and preservation levels may have been higher due to increased anoxia. Rather than coinciding with the deposition of both the Drewer Sandstone and the HBS, the upper Cleveland Member may be coeval with the deposition of just the trangressive HBS (Figure 5.15). However, as previously stated, sampling resolution through the Cleveland Member may not have been sufficient to record possible glacial / interglacial events. Further work on this unit is required in order to eliminate some of the speculation for the observed changes in $\delta^{15}N$.

The main phase of regression and glaciation, recorded in the Rhenish Massif stratigraphy by the Hangenberg Shale and Sandstone, coincides with the deposition of the Bedford Shale (LN Miospore Biozone). The carbon isotope excursion associated with the Hangenberg event is also recorded within the upper LN Miospore Biozone. A general increase in $\delta^{15}N_{bulk}$ is recorded through the Bedford Shale of both sections, possibly coinciding with the Hangenberg C isotope excursion. The $\delta^{15}N_{Tas}$ from KY801N records slight, but mostly insignificant, changes, whereas the $\delta^{15}N_{Tas}$ from the composite section records slightly more variation within the mid-Bedford Shale. Neither section, however, records severe isotopic changes in $\delta^{15}N_{Tas}$ coinciding with the Hangenberg C isotope excursion.

A basal lag deposit separates the Devonian Bedford Shale and the Mississippian Sunbury Shale, defining a regional unconformity (Ettensohn, 1994). The Sunbury Shale has been assigned to the VI Miospore Biozone. The variation recorded in both $\delta^{15}N_{bulk}$ and the $\delta^{15}N_{Tas}$ within the Sunbury Shale (composite curve) suggests that very specific and abrupt changes took place during the deposition of this sequence. Ettensohn and Pashin (1997) proposed that the Sunbury Shale was deposited during the fourth tectophase of the Acadian orogen. It is possible that increased tectonic

activity within the Acadian orogen led to changes in oxic conditions within the Appalachian Basin. Eustatic sealevel changes are also recorded during the deposition of the Stockum Limestone of the Rhenish Massif. However, evidence of glacial activity has not been identified from the VI Miospore Biozone.

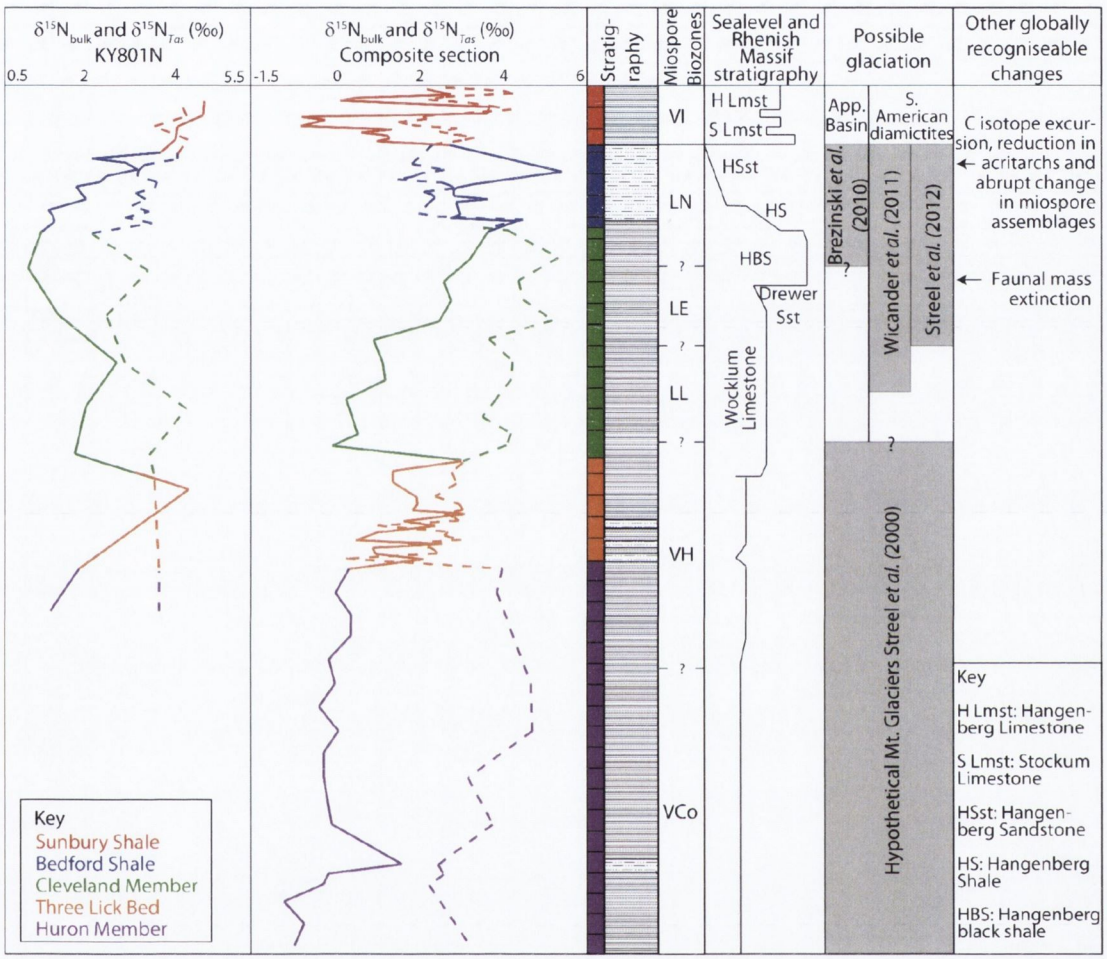

Figure 5.14. Correlation of known Late Devonian glaciation events (Brezinski *et al.*, 2010; Streel *et al.*, 2000; Streel *et al.*, 2012; Wicander *et al.*, 2011), extinction events (Myrow *et al.*, 2011), sealevel changes and Rhenish Massif stratigraphy (Streel *et al.*, 2012), to the isotopic curves obtained as part of this research.

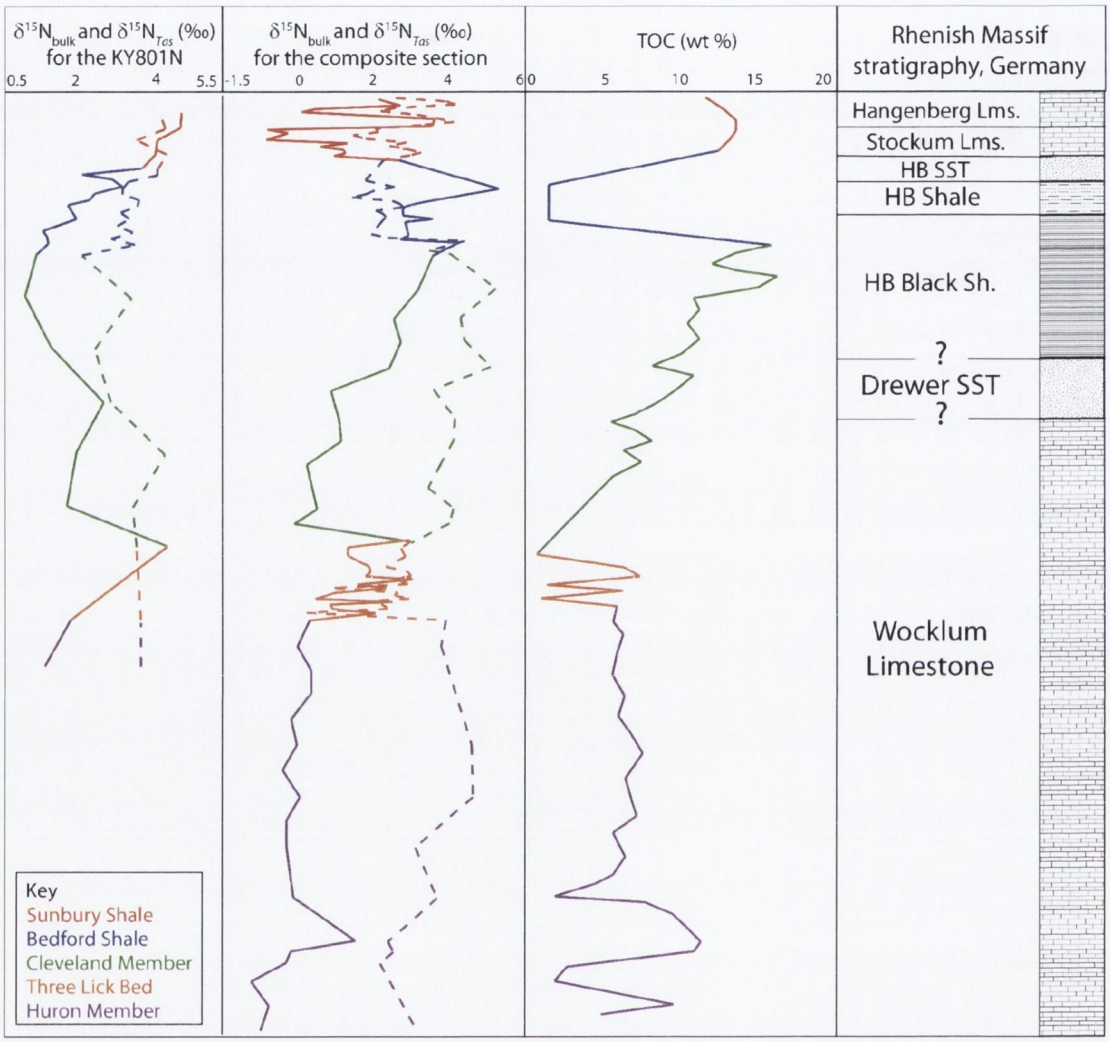

Figure 5.15. Isotopic changes observed within this thesis alongside TOC changes recorded by Algeo (2004). The Rhenish Massif stratigraphy is placed at positions of suggested approximate correlation. This is based on miospores, increasing TOC and opposing variation in bulk $\delta^{15}N$ values recorded in the Upper Cleveland Member., possibly coinciding with the transgressive HBS of the Rhenish Massif.

The $\delta^{15}N_{bulk}$ and the $\delta^{15}N_{Tas}$ may record the phases of active loading in the adjacent Acadian highlands and relaxation of tectonic activity during the deposition of the Sunbury Shale (Figures 5.16 and 5.17). In this case, it would be expected that increased loading would produce anoxic benthic waters as the basin is dragged below the pycnocline, and times of tectonic quiescence would result in relaxation of the basin, where benthic waters may become slightly less anoxic than during times of active loading. This may result in the abrupt changes recorded in the nitrogen isotope data, where changes in oxic conditions would have led to changes in the levels of N-fixation and denitrification. Lower levels of oxygen within subsurface waters, possibly brought about by increased tectonic loading, may lead to an increase in the intensity of denitrification. This would result in a reduction in the N:P ratio of upwelled waters, leading to an increase in N-fixation rates, and the production of organic matter with a lighter $\delta^{15}N_{bulk}$ signal, similar to the changes in the Cariaco Basin brought about by sealevel changes caused by glacial and interglacial periods. However, the initial increase in tectonic loading may also reduce the supply of freshwater and clastic material from previously established drainage networks (Ettensohn, 2008), thus leading to a reduction in freshwater supply and clastic material to the Appalachian Basin. The reduction in freshwater may diminish the extent of ocean stratification, increasing subsurface oxic conditions within the basin, thereby reducing the intensity of denitrification. This scenario could lead to a heavier $\delta^{15}N_{bulk}$ signal, contrary to the previous hypothesis, although, a reduction in clastic supply may have the opposite effect. Either way, basinal changes may have contributed to fluctuating oxic conditions within the basin, and thus may have had a significant impact on the $\delta^{15}N_{bulk}$ signal, and possibly the $\delta^{15}N_{Tas}$ signal. However, the time interval covering the deposition of the Sunbury Shale may be too short for these isotopic changes to be the result of tectonic activity.

In summary, the opposing $\delta^{15}N_{bulk}$ trends recorded within the upper Cleveland Member of the two sections may signify deposition during the eustatic transgression marked by the Hangenberg Black Shale within the Rhenish Massif, or possible changes in N_{org} contributions during a glacial period. Inreased sampling resolution may help to resolve this stratigraphic interval in greater detail. The Bedford Shale corresponds to a period of glaciation marked by the regressive Hangenberg Shale and Hangenberg Sandstone of the Rhenish Massif. Slight $\delta^{15}N$ changes within the Bedford Shale may correspond to the C isotope excursion that has been recorded towards the top of the LN Miospore Biozone at other localities. The isotopic variation recorded in the Sunbury Shale may be due to a combination of undocumented glacial events, eustatic sealevel changes within the VI Miospore Biozone and the onset of the fourth tectophase of the Acadian orogeny, possibly leading to changes in oxic conditions within the Appalachian foreland basin, and thus changes in $\delta^{15}N$ values. The isotopic variation recorded within the Sunbury Shale is certainly intriguing and should be examined in further detail, as it may provide additional information on

local and regional changes, and increase our understanding of the possible impact of basin development on sedimentary nitrogen isotope records.

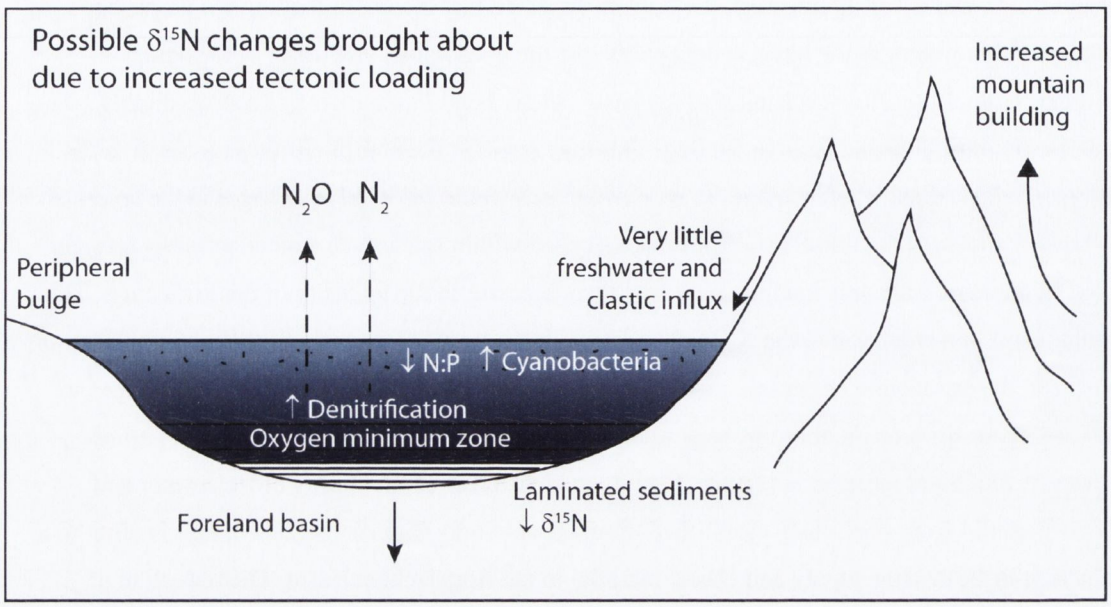

Figure 5.16. Possible $\delta^{15}N$ changes to sedimentary black shales in the Early Mississippian Appalachian Basin due to increased tectonic loading during the deposition of the Sunbury Shale.

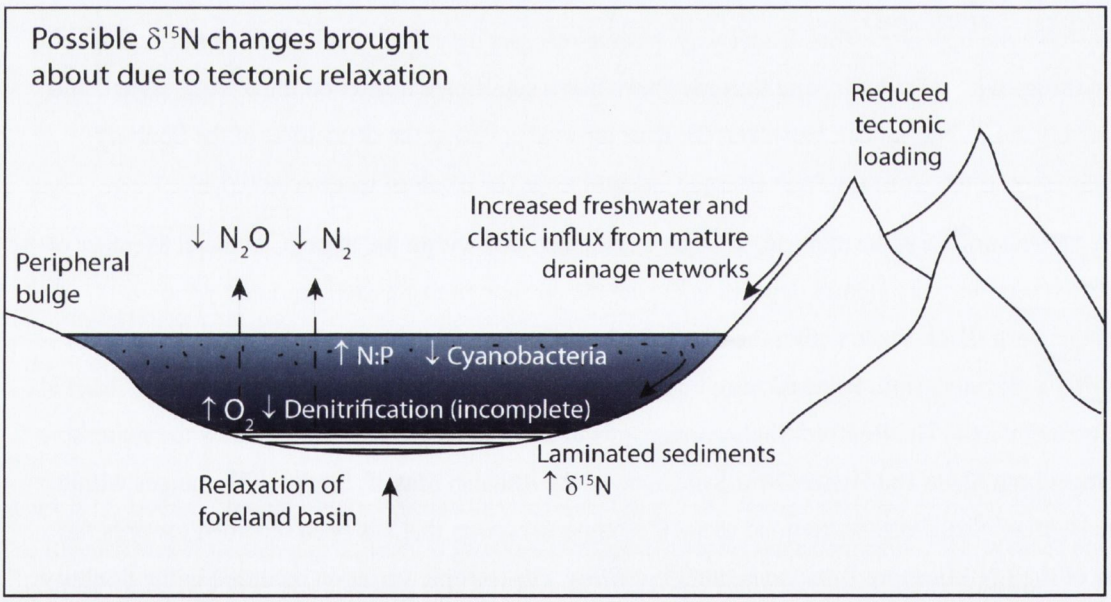

Figure 5.17. Possible $\delta^{15}N$ changes to sedimentary black shales in the Early Mississippian Appalachian Basin due to reduced tectonic loading during the deposition of the Sunbury Shale.

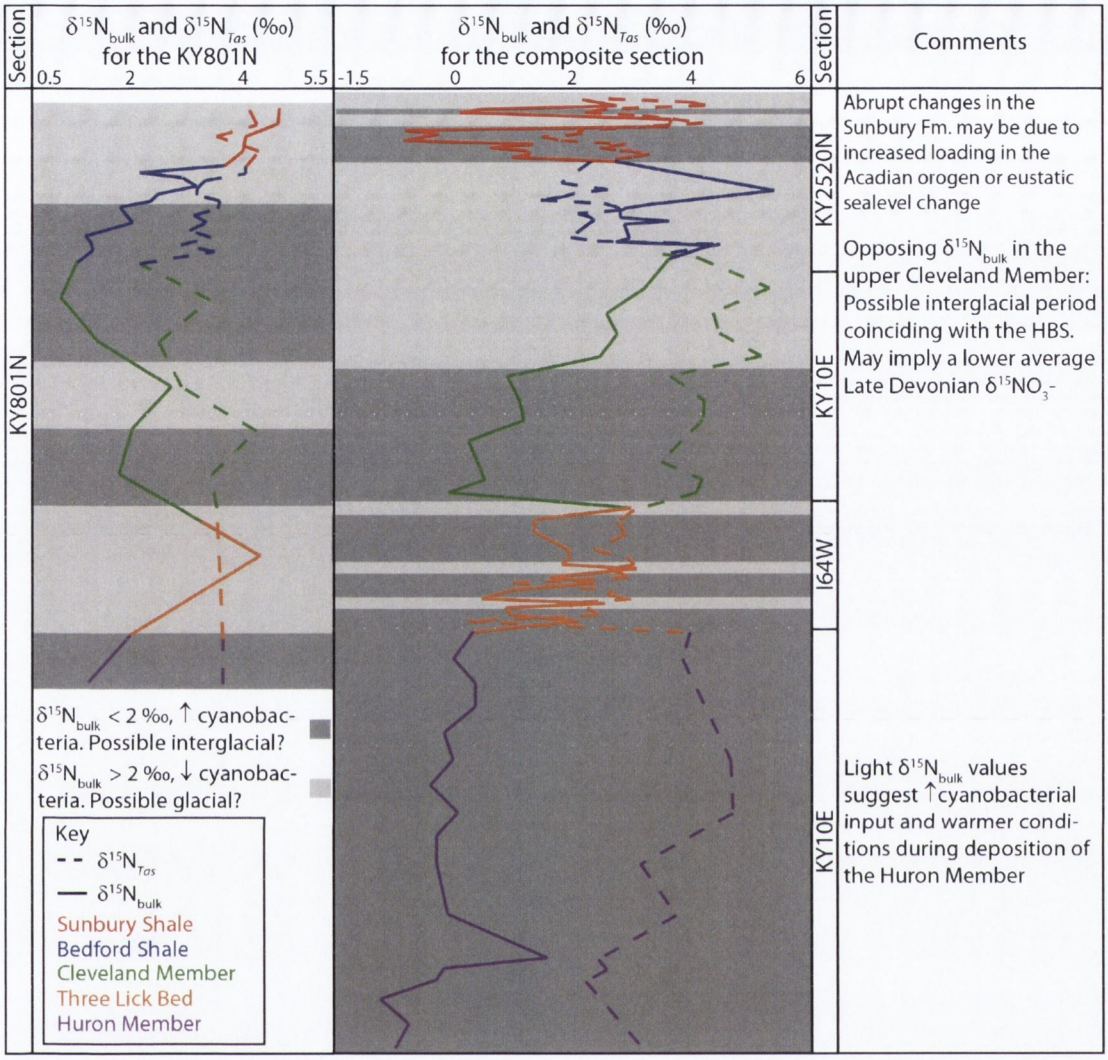

Figure 5.18. Possible glacial (lighter grey) and interglacial periods (dark grey), interpreted from increases and decreases in $\delta^{15}N_{bulk}$ values. $\delta^{15}N_{bulk}$ values above 2 ‰ are categorised as a reduction in cyanobacterial input and an increase in oxic conditions, thus may represent cooler, possibly glacial, periods. $\delta^{15}N_{bulk}$ values below 2 ‰ are categorised as an increase in cyanobacterial input and a decrease in oxic conditions, thus may represent interglacial periods. These isotopic changes are based on similar changes observed in the Cariaco Basin and Eastern Mediterranean sapropels. The Cleveland Member opposing trends within the Cleveland Member may suggest an interglacial period coinciding with the deposition of the Hangenberg Black Shale, or possibly variation in N_{org} input during a glacial period, as observed at the beginning of Section 5.3.1.6.5. The isotopic changes within the Sunbury Shale may correlate to increased loading in the Acadian orogen or eustatic sealevel changes rather than glacial / interglacial periods.

5.3.2 *Tasmanites* vs bulk material

The $\delta^{15}N$ of phytoplankton, such as *Tasmanites,* should be associated with the combined $\delta^{15}N$ of new N supplied to the euphotic zone from N-fixation and nitrate from upwelled waters (Karl *et al.*, 1997). The isotope effect brought about by the preferential uptake of lighter $\delta^{15}NO_3^-$ by phytoplankton is assumed to be of little significance within the Late Devonian Appalachian Basin, considering its low palaeolatitudinal position, where nitrate is often fully consumed. Large influxes of excess nutrients may have taken place due to increased terrestrial biomass and increased weathering, however, at low latitudes this will lead to increases in productivity within the water column, likely negating any short term relative isotope effect.

Throughout the majority of the sections studied, similarities are recorded between the $\delta^{15}N$ trends of both the bulk material and extracted specimens of *Tasmanites* (Figure 5.19). Meckler *et al.* (2011) and Ren *et al.* (2009) carried out analyses of the nitrogen isotope signature of different species of planktic formanifera from the Holocene back to the Last Glacial Maximum. The samples were collected from the low latitudinal regions of the Caribbean Sea and the Gulf of Mexico. Planktic foraminifera obtain N mostly from particulate organic matter (POM), and it was suggested that this should be similar to or correlated with the combined $\delta^{15}N$ of new N supplied to the euphotic zone, including nitrate from upwelled waters, and N-fixation. They found that the forams recorded higher $\delta^{15}N$ values during the Last Glacial Maximum (~ 5 – 6 ‰) than during the Holocene (~ 2 – 3.5 ‰) due to higher rates of N-fixation, contributing to the euphotic zone nitrogen budget during the Holocene. However, the $\delta^{15}N_{bulk}$ within these studies recorded only minor changes from the glacial to interglacial transition (a decrease of up to 1 ‰). Both studies observed an increase in terrigenous material and clay bound inorganic N in the glacial sediments, possibly contributing to the lack of isotopic change recorded between the glacial and interglacial bulk sediments.

The Upper Devonian Kentucky shales record larger variation in the bulk nitrogen isotope signal than that recorded for *Tasmanites*. This may be due to greater fluctuation in the extent and intensity of N-fixation and denitrification within the Appalachian Basin, or possibly due to the analysis of the bulk organic N fraction, rather than total N, where clay-bound inorganic N is removed from the $\delta^{15}N_{bulk}$ signal, leading to the observation of more extreme changes in $\delta^{15}N_{bulk}$. The observed difference between modern and Late Devonian trends may also be due to biological differences between *Tasmanites* and planktic foraminifera, or possibly a fundamental difference in the supply of nitrate available to both. The Holocene supply of nitrate to planktic foraminifera appears to be heavily influenced by cyanobacterial input, perhaps due to the direct uptake of N from POM sources, whereas *Tasmanites* are likely to consume a mixture of N from POM sources

and nitrate within the euphotic zone, possibly recording the average change in $\delta^{15}NO_3^-$ available to primary producers.

For some of the sections, the *Tasmanites* specimens record $\delta^{15}N$ values similar to the bulk organic material (~3 - 5 ‰). This occurs twice within the Three Lick Bed (composite section), where the $\delta^{15}N_{bulk}$ of two black shale samples increases to values similar to those of *Tasmanites*. As mentioned in Section 5.3.1.5, this may be reflective of changes in organic matter within the bulk sediment. The increases recorded in $\delta^{15}N_{bulk}$ within the upper Cleveland Member are similarly recorded in the $\delta^{15}N_{Tas}$ (composite section), possibly reflecting a more fundamental change in the availability of nutrients at this locality (KY10E). There is a possibility that these $\delta^{15}N$ increases are recording deglaciation within the Appalachian Basin, where both $\delta^{15}N_{bulk}$ and $\delta^{15}N_{Tas}$ may record increases in water column denitrification often observed at the onset of deglaciation (Figure 5.19).

Within the Cleveland Member of the KY801N section, the changes recorded in $\delta^{15}N_{bulk}$ and $\delta^{15}N_{Tas}$ are often opposing, where the $\delta^{15}N_{bulk}$ increases are matched by similar decreases in $\delta^{15}N_{Tas}$. It may be possible that the average marine $\delta^{15}NO_3^-$ was lower in the Late Devonian than it is today, and that these changes recorded at KY801N coincide with glacial periods, where decreased denitrification is recorded as a decrease in $\delta^{15}N_{Tas}$ and a decrease in N-fixation is recorded as a concomitant increase in $\delta^{15}N_{bulk}$.

The differences in the two trends are interesting and possibly suggest significant differences in nutrient dynamics within the Appalachian Basin between the two localities. Such dramatic changes are most likely influenced by environmental change occurring within the Late Devonian. However, it is difficult to hypothesise whether or not these specific isotopic changes are due to glacial / interglacial cycles. Increased sampling resolution and further palynological work to assess the stratigraphic position of the Cleveland Member may resolve some of the questions raised within this research.

The Bedford Shale is thought to have been deposited during a glacial period, and therefore should reflect a return to $\delta^{15}N$ values similar to the average marine $\delta^{15}NO_3^-$. The $\delta^{15}N_{Tas}$ and $\delta^{15}N_{bulk}$ values recorded through the Bedford Shale is suggestive of an overall lower Late Devonian $\delta^{15}NO_3^-$ (2 – 3.5 ‰) than the modern average $\delta^{15}NO_3^-$ (5 – 6 ‰). The slight variation recorded in $\delta^{15}N_{Tas}$ through the Bedford Shale may be due to the waxing and waning of polar glaciers as well as alpine glaciers on the adjacent Acadian highlands.

The Sunbury Shale records synchronous isotopic changes in both $\delta^{15}N_{Tas}$ and $\delta^{15}N_{bulk}$ values. As previously mentioned, glaciation is not known from this period of deposition, however, the variation may be due to the structural growth of the Acadian highlands leading to basinal changes, or a previously unknown glacial event. If basinal changes led to the recorded isotopic variation, this could have an impact on the future study of sedimentary N isotope records, as local

and regional palaeogeography could play quite a significant role in the possible causes of variation within the $\delta^{15}N$ record. Whether brought about by eustatic sea level change or regional changes due to Acadian uplift, nutrient dynamics were substantially altered at various times during the deposition of the Sunbury Shale. Further investigation of regionally distinct sections of similar age may help to constrain whether or not the isotopic variation was due to regional or global processes.

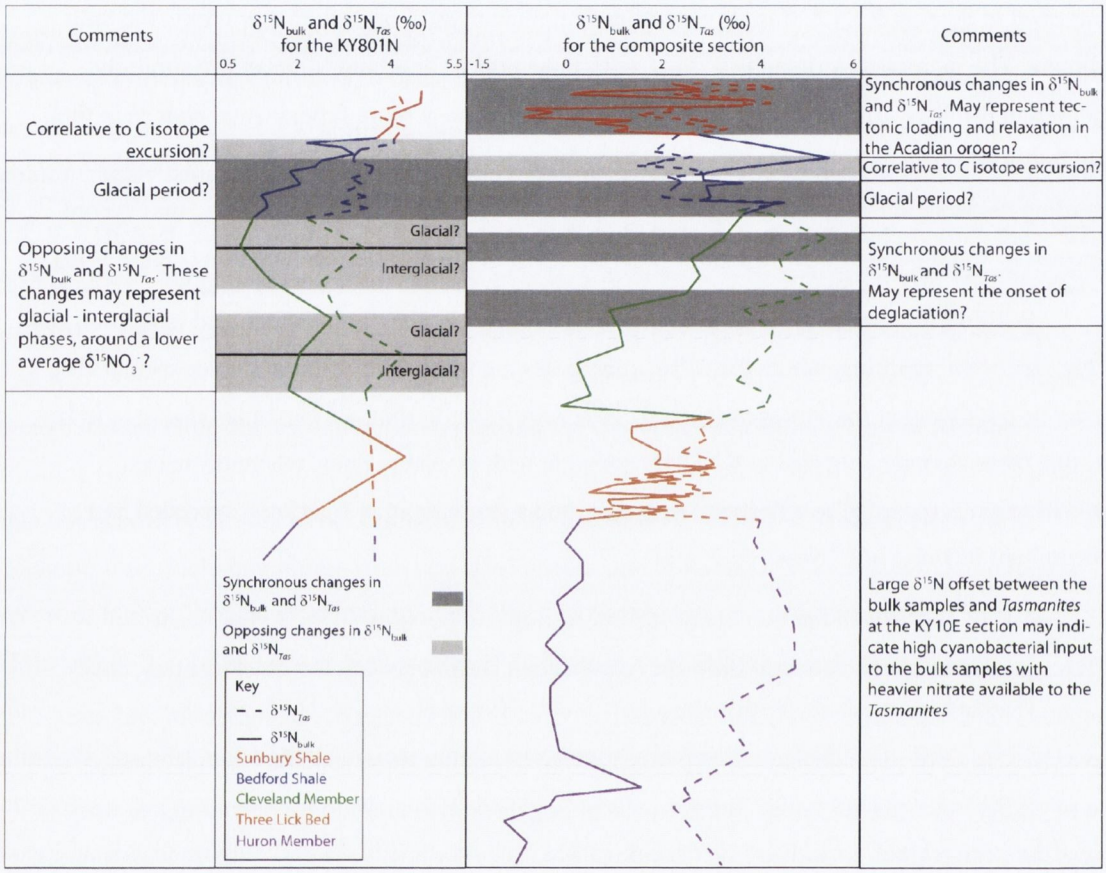

Figure 5.19. Possible interpretations of changes in $\delta^{15}N_{Tas}$ in comparison to changes in $\delta^{15}N_{bulk}$.

5.3.3 Protosalvinia spp.

Analytical results from the *Protosalvinia* samples show surprising similarity in the $\delta^{15}N_{Proto}$ values throughout North America. Slight variation is recorded, but this may be due to diagenetic alteration. As the stratigraphic occurrence of *Protosalvinia* is constrained to a relatively short interval, it was hoped that it may provide an insight into the isotopic variation within and between basins during the deposition of the Huron Member. A slight increase in $\delta^{15}N_{Proto}$ recorded at the KY10E section may indicate either diagenetic alteration or a change in nutrient conditions at this locality. A change in nutrient conditions at this locality may help to explain some of the $\delta^{15}N_{Tas}$ and $\delta^{15}N_{bulk}$ differences observed between the composite section and KY801N.

An interesting aspect of the results is that the $\delta^{15}N_{Proto}$ values recorded for the *Protosalvinia* thalli are generally quite light in comparison to the *Tasmanites* samples and the *Protosalvinia* spores, perhaps due to fundamental differences in the biochemical pathways for the uptake of N between *Tasmanites* and *Protosalvinia*. *Protosalvinia* thalli may have consumed POM composed mostly of cyanobacterial decay, whereas *Tasmanites* may have consumed a larger proportion of upwelled nitrate. This may be a consequence of differences in their relative positions within the euphotic zone (Meckler *et al.*, 2011). The heavier $\delta^{15}N_{Tas}$ is suggestive of a lower position within the euphotic zone, utilising upwelled nitrate, whereas *Protosalvinia* likely inhabited surface waters, where a larger proportion of lighter nitrogen is available due to cyanobacterial decay (Figure 5.20). The spores produced by the *Protosalvinia* thalli may have a heavier $\delta^{15}N$ signal due to trophic differences, where the spores take up nutrients the thalli before they are released, possibly leading to an isotopic enrichment of up to 3 ‰. The *Protosalvinia* thalli obtained from Brazil have a much heavier $\delta^{15}N_{Proto}$ value than those recorded from the North American samples, possibly due to latitudinal differences, where N-fixation is dramatically reduced within higher latitudes, and therefore does not contribute significantly to the $\delta^{15}N_{Proto}$ at the Brazilian locality. Ren *et al.* (2009) found a similar trend in modern planktic foraminifera, where low latitude-dwelling forams (outside of denitrification dominated zones) record lighter $\delta^{15}N$ values (2 – 4 ‰) than those that are found in higher latitudes (7 – 9 ‰).

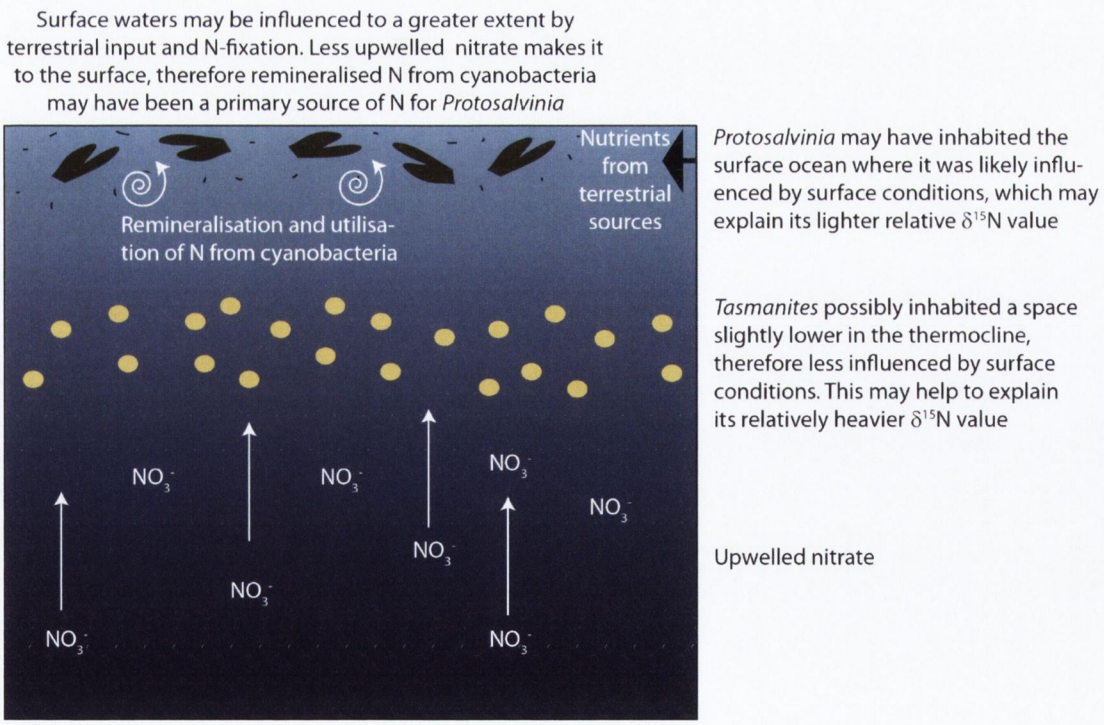

Figure 5.20. *Tasmanites* and *Protosalvinia* inhabiting different areas of the thermocline, a possible explanation for the observed differences in the $\delta^{15}N_{Proto}$ and $\delta^{15}N_{Tas}$ values.

5.4 TRACE ELEMENTS

As mentioned previously, the trace element work is experimental, and therefore any interpretations based on trace element data undertaken in this thesis are purely speculative. Assuming similar conclusions can be drawn from the trace element ratios of *Tasmanites* as bulk material, the V/Cr_{Tas} and $V/(V+Ni)_{Tas}$ ratios indicate increased anoxia in the lower Cleveland Member, and reduced anoxia in the upper Cleveland Member, with anoxia increasing within the two uppermost Cleveland Member samples (KY2520N section) (Figure 5.22). The ratios also indicate increasing oxic conditions throughout the deposition of the Bedford Shale, and increased anoxia during the deposition of the Sunbury Shale. Within the Three Lick Bed, oxic conditions are thought to have increased during the deposition of the three grey shale units. However, the ratios do not show clear evidence of increased oxic conditions, although a certain degree of variation exists throughout the deposition of the Three Lick Bed.

As Mo accumulates predominantly under anoxic conditions, and V accumulates under both suboxic and anoxic conditions (Perkins *et al.*, 2008), the V/Mo_{Tas} ratio should display an opposing trend to V/Cr_{Tas} and $V/(V+Ni)_{Tas}$. However, the recorded ratios to the contrary are quite similar (Figure 5.22). This may be due to the fact that these analyses were not carried out on sediments, and therefore do not reflect 'accumulation' of Mo under anoxic conditions, but rather, the *Tasmanites* values reflect a mixture of surface ocean conditions and bottom water conditions. Low oxygen bottom water conditions may lead to the preferential preservation of certain trace elements, such as V and Ni, within the phycomata of *Tasmanites*.

Similar ratios are examined, for comparative purposes, based on the published data of bulk Upper Devonian samples from Kentucky (Algeo, 2004; Rimmer, 2004; Perkins et al., 2008) (Figures 5.21, 5.23 and 5.24). Although *Tasmanites* ratios illustrate slight similarities to the bulk oxic indicating trace element profiles (Figure 5.21). However, no definite conclusions could be drawn from the comparison of the *Tasmanites* ratio and bulk ratios. If the *Tasmanites* data is analysed in isolation, it appears that the ratios within the Cleveland Member illustrate a clear difference between the upper and lower Cleveland members, possibly indicating a change in redox conditions associated with the increased preservation of V and Ni in the tetrapyrrole structures of *Tasmanites* under reducing conditions, as mentioned above. This hypothesis would indicate lower benthic oxygen conditions in the lower Cleveland Member and increased oxygen conditions in the upper Cleveland Member, similar to observations made by Perkins *et al.* (2008). However, the opposite has been reported in other published research (Rimmer, 2004; Rimmer *et al.*, 2004).

The *Tasmanites* data appear to record a slight increase in Mo_{Tas}, and a concomitant decrease in V_{Tas} through the upper Cleveland Member. Algeo (2004) observed the opposite, i.e., a decrease in the Mo_{bulk} to TOC concentration and an increase in the V_{bulk} to TOC concentration over

the same stratigraphic interval (Figure 5.23). The opposing trends for *Tasmanites* and bulk sediment may be caused by a change in the organic content within the amorphous organic matter (AOM) of the black shales, or possibly due to certain elements being retained, and others being released from phytoplankton under differing benthic conditions. Certain trace elements, such as Fe, Mo and Co are required for the process of nitrogen fixation to take place (Algeo, 2004; Morel *et al.*, 2006). The amorphous organic component of black shales can contain large proportions of cyanobacterial input (Kuypers *et al.*, 2004), and an increase recorded in the Fe, Mo and Co concentrations within bulk black shales may indicate increased cyanobacterial input, amongst other explanations.

The proliferation of nitrogen fixers, such as cyanobacteria, indicates areas of low N:P ratios. A decrease in Mo_{bulk} (Fe and Co concentrations were not available from existing studies) and a coincident increase in Mo_{Tas} within the upper Cleveland Member could be an indicator of the reduced growth of cyanobacteria, freeing up the Mo for other forms of phytoplankton. However, a reduction in cyanobacteria would imply higher nitrate conditions within the upper Cleveland Member, which is not necessarily mirrored by nutrient proxies, as outlined below. The recorded changes in Mo within the upper Cleveland Member also coincide with an increase in the $\delta^{15}N_{bulk}$ from the KY10E section, also indicating a decrease in the input of N-fixing bacteria within the upper Cleveland Member. However, the $\delta^{15}N_{bulk}$ results from the KY801N section record the opposite trend. Algeo (2004) also reports an increase in the Mo_{bulk} content within the Sunbury Shale, possibly indicating a return to N-fixing bacterial input to the organic sediment. This coincides with abrupt changes recorded in the $\delta^{15}N_{bulk}$ signal, indicating variability in the extent and intensity of N-fixation during the deposition of the Sunbury Shale. This variation within the Sunbury Shale is reflected within many of the trace element ratios of both bulk sediments and *Tasmanites*.

Similar to V, Ni is contained within tetrapyrrole structures preferentially preserved under reducing conditions. The Ni/Co ratio has also been utilised as an indicator of sedimentary redox conditions (Jones and Manning, 1994). However, Ni concentration has also been found to increase when phytoplankton is grown on urea rather than nitrate (Price and Morel, 1991), suggesting that the Ni concentration in *Tasmanites* may also be associated with nutrient conditions. Consequently, the variation observed in the Ni_{Tas} concentrations is most likely a combination of benthic redox conditions and pelagic nutrient conditions. Therefore, care must be taken when interpreting Ni_{Tas} ratios.

Phytoplankton grown on nitrate require more Fe and less Ni than phytoplankton grown on urea (Price and Morel, 1991; Raven *et al.*, 1992), and Co can substitute for Zn when concentrations are low (Whitfield, 2001), which can occur under oligotrophic conditions. Increases in these ratios

(Fe/Ni_{Tas} and Zn/Co_{Tas}) within the *Tasmanites* should therefore indicate increased nutrient conditions, and decreases should indicate reduced nutrient conditions (Figure 5.24). This suggests relatively poor nutrient conditions existed through the majority of the stratigraphy, with several increases in nutrient availability observed within the middle Huron Member, the Cleveland Member and the Sunbury Shale. This could be as a result of increased upwelling of nutrient rich waters during times of intensified trade winds, or perhaps an increase in the delivery of nutrients to the Appalachian Basin by terrestrial sources.

Trade winds are thought to be stronger during glacial periods (Parkin, 1974), when upwelled waters carry relatively less nutrients, due to increased oxic conditions throughout the water column, leading to less trapping of nutrients in deep water. Thus, glacial periods may correspond to reduced nutrient conditions in upwelling regions. However, denitrification is also likely to be lower during glacial periods, delivering water with a higher N:P ratio to the surface. The presence of Ni is not just determined by nutrient conditions, but also by oxic conditions, as discussed above. Within the Bedford Shale, the Fe/Ni_{Tas} ratio decreases, possibly indicating that *Tasmanites* were growing on greater quantities of urea, as the increase in oxic conditions should have led to a decrease in Ni. However, the concentration remains stable through the Bedford Shale. *Tasmanites* may have been growing on greater quantities of urea as a result of decreased nutrient conditions during this documented glacial period (Brezinski *et al.*, 2008, 2009, 2010).

The Zn/Co_{bulk} profile suggests low Zn and high Co conditions throughout the stratigraphy, with the exception of a minor increase in the ratio within the Cleveland Member and larger increases throughout the Sunbury Shale (Figure 5.24). The Cd/Co_{bulk} profile follows a very similar trend, where Zn and Cd appear to record coeval increases within the Cleveland Member and throughout the Sunbury Shale, possibly related to increased nutrient availability, as these elements have also been used as proxies for nitrate and phosphate (Bruland and Lohan, 2006).

These ratios compare well with the increases observed in the Fe/Ni_{Tas} and Zn/Co_{Tas} ratios, where increases, which indicate higher nutrient conditions, are recorded in the Cleveland Member and the Sunbury Shale. However, the increase recorded in the Fe/Ni_{Tas} and Zn/Co_{Tas} ratios in the middle Huron Member is not observed in the Zn/Co_{bulk} and Cd/Co_{bulk} ratios. $Cobalt_{Tas}$ also appears to be strongly associated with grey shale deposition, but remaining high into each subsequent black shale horizon. This may be due to the distribution of Co in sediments being strongly tied to the abundance of clastic material (Tribovillard *et al.*, 2006), such as that found within the grey shale horizons.

Increases in the Ba/Zn_{Tas} ratio are associated with *Tasmanites* deposited in the grey shale horizon located above the *Protosalvinia* Zone, the grey shales within the Bedford Shale, and the black shale sample at the base of the Sunbury Shale. As mentioned in Chapter 1, Ba forms barite

during the decay of organic matter, and is therefore used as a palaeoproductivity indicator. However, under these circumstances, an increase in Ba could be an indicator of degradation within the phycomata of *Tasmanites,* where increases may equate to increased degradation. This would tentatively suggest an increase in the degradation of *Tasmanites* under the presumed suboxic conditions that prevailed during grey shale deposition, although no such increase in Ba was observed for the grey shale horizons of the There Lick Bed. Barium, as an indicator of degradation within palynomorphs, is very speculative and requires further investigation before it could be considered as a sufficient proxy.

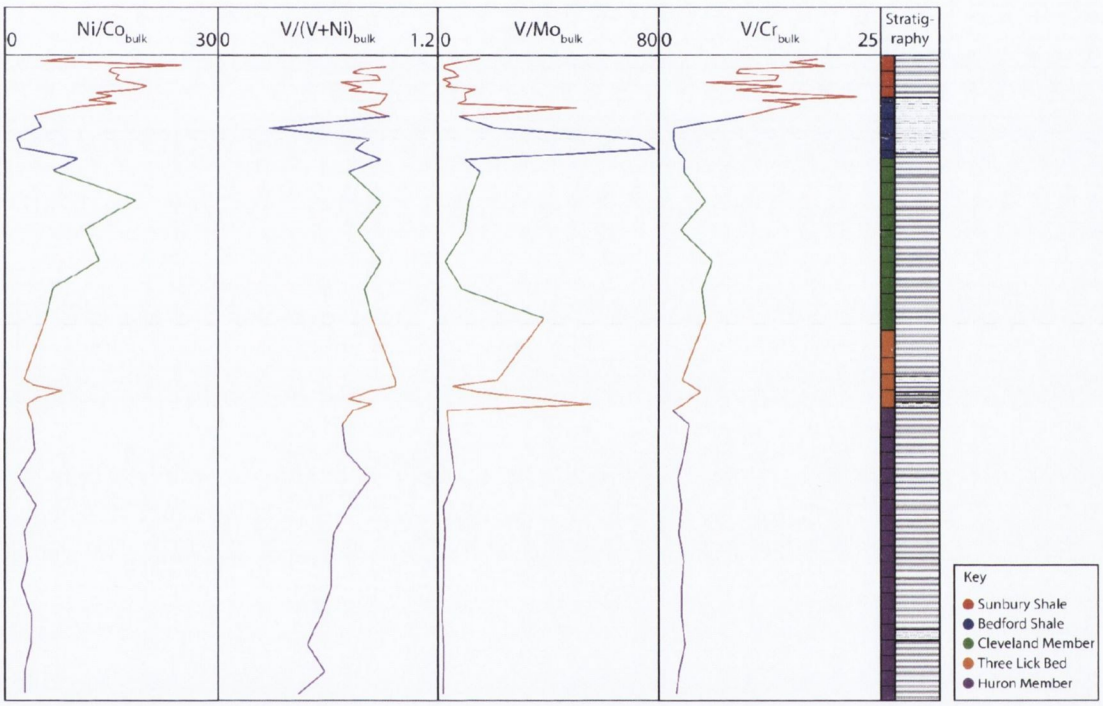

Figure 5.21. Oxic indicating bulk trace element ratios for the Upper Devonian – Lower Mississippian strata in Kentucky (modified from Perkin *et al.*, 2008).

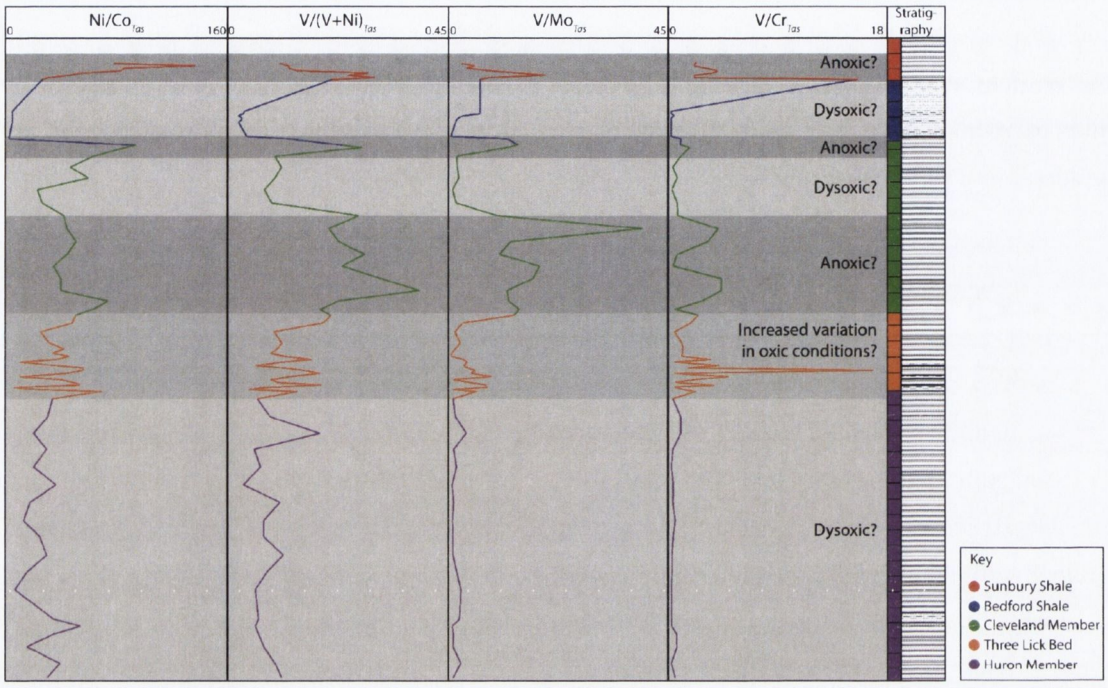

Figure 5.22. Possible oxic indicating trace element ratios obtained from specimens of *Tasmanites*. Light grey panels indicate decreasing ratios, possibly indicating dysoxic to oxic conditions. Darker grey panels refer to increasing ratios and possibly indicate anoxic conditions.

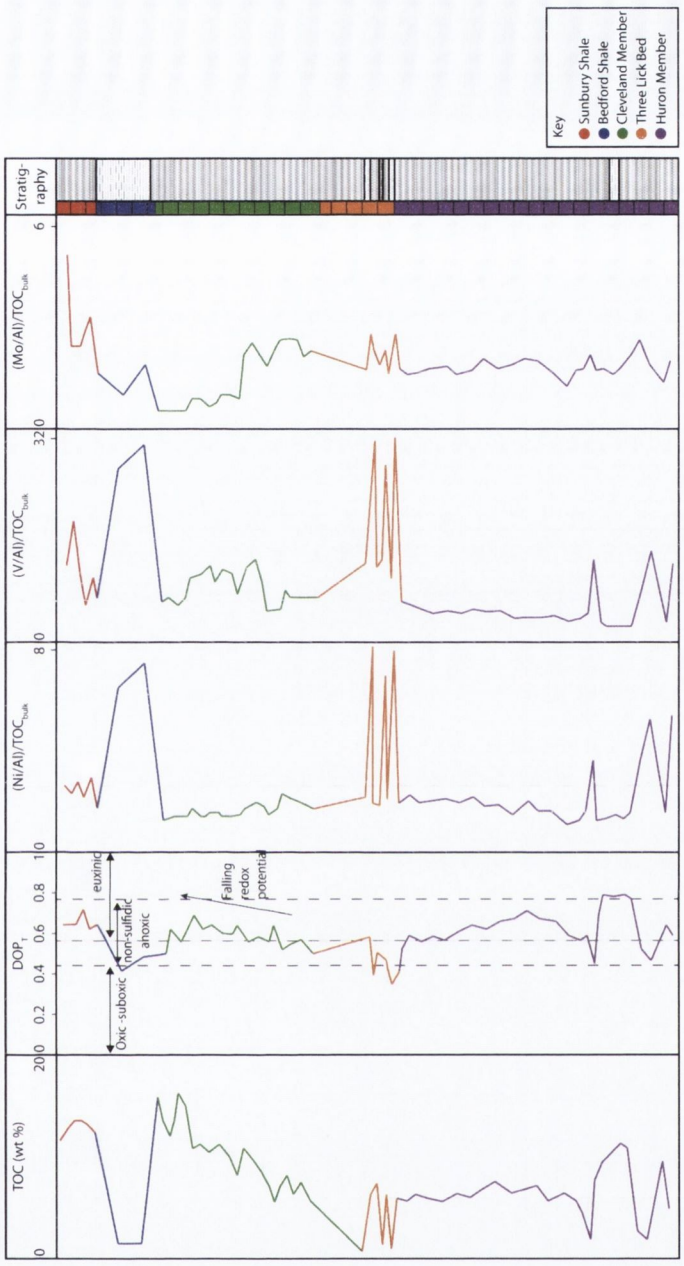

Figure 5.23. Total organic carbon (TOC), degree of pyritisation (DOP) and bulk trace element ratios for the Upper Devonian – Lower Mississippian strata in Kentucky. Modified from Algeo (2004).

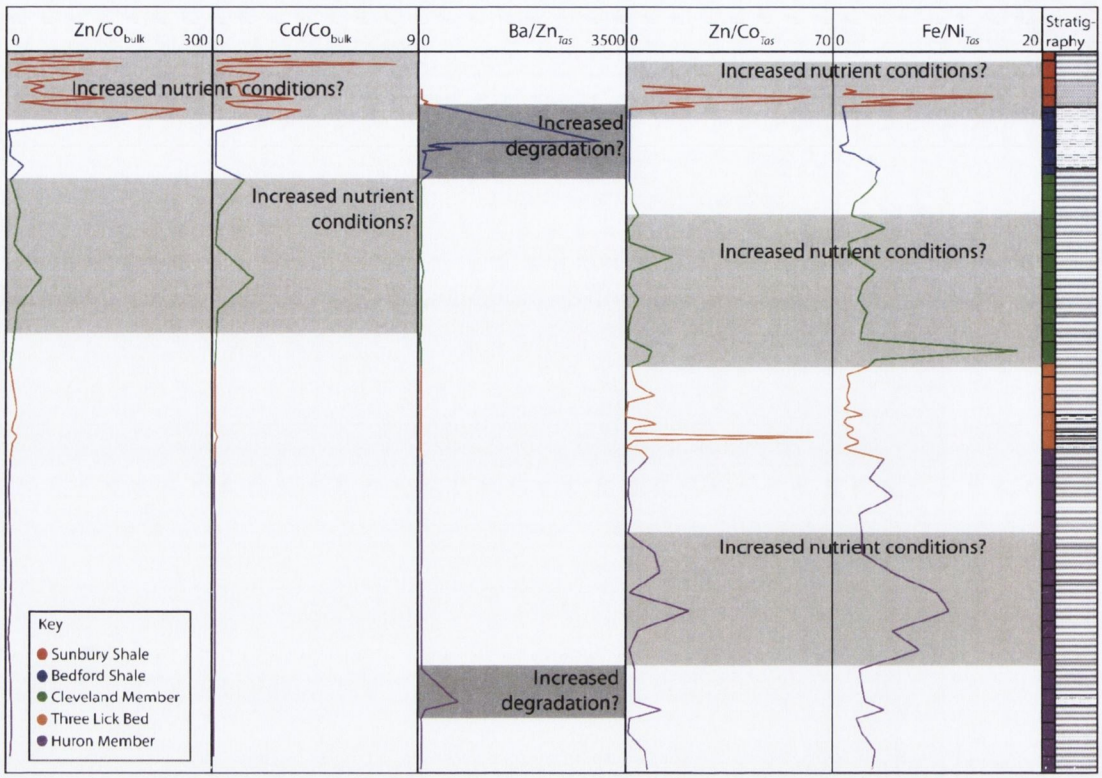

Figure 5.24. Bulk and *Tasmanites* trace element ratios discussed as proxies for nutrient conditions. The bulk data was extracted from Perkins *et al.*(2008).

Chapter 6

Conclusions

- Stable (N) isotope ratios have been determined for the first time from a single Palaeozoic palynomorph taxon (*Tasmanites* spp.).
- No single cause for the observed stratigraphic trends in $\delta^{15}N$ has been conclusively identified but it is suggested that a combination of changes in marine oxygen and nutrient levels, together with changes in palaeogeography, resulted in the recorded trends.
- Stable (N) isotope ratios of the enigmatic Late Devonian alga, *Protosalvinia*, are similar in all of the North American samples investigated, but are markedly different from *Tasmanites* spp. in the same samples, and *Protosalvinia* specimens extracted from a higher latitude Late Devonian age Brazilian sample.
- The miospore *Retusotriletes loboziakii* Rooney, Clayton and Goodhue 2013 has been erected for dispersed spores produced by the enigmatic Late Devonian alga, *Protosalvinia* spp.
- Miospores recorded from the *Protosalvinia* Zone in Kentucky are assigned to the VCo Miospore Biozone.
- Treatment with HCl, hot and cold HF and a combination of NaClO, sodium-citrate solution, sodium-bicarbonate solution and sodium-dithionite (clay mineralogy treatrment method), led to no discernable change in $\delta^{15}N_{Tas}$ and proved to be the most effective chemical treatment for the removal of unwanted material and the extraction of clean *Tasmanites* spp. specimens and *Protosalvinia* spores.
- The trace element composition of a single Palaeozoic palynomorph taxon (*Tasmanites* spp.) was successfully determined using modern laser ablation techniques, possibly recording changes in nutrient and oxic conditions within the Upper Devonian Kentucky shales.

Chapter 7

Further Research

Further investigation of extracted sedimentary N components, such as palynomorphs, will help to elucidate the relationship between nitrogen isotopes, climate change, nutrient dynamics and palaeogeography in greater detail. Studies of other sedimentary basins and stratigraphic intervals containing sufficient numbers of marine and/or terrestrial palynomorphs is clearly needed. Investigation of the stable isotope signal of terrestrial palynomorphs may help to further constrain some of the hypothesised changes within the marine environment in terms of their palaeogeographical extent. Future nitrogen isotope studies may include the routine analysis of sedimentary N fractions, such as for palynomorphs, alongside bulk samples, in order to interpret palaeoenvironments with increased precision.

Increased sampling resolution and further palynological work to assess the stratigraphic position of the Cleveland Member may resolve some of the questions raised with regard to climate changes within this stratigraphic interval. Investigation of the stable N isotope signature of a transect from the shoreline to deep marine sediments, following a formation (or equivalent formations), would aid in the reconstruction of the N cycle within the Appalachian Basin and help to interpret the isotopic variation recorded through the stratigraphy in greater detail. The cause of the large isotopic difference observed between the *Protosalvinia* thalli collected from North America and Brazil can only be determined by analysis of *Protosalvinia* thalli and *Tasmanites* spp. extracted from other high latitude palaeobasins. Further analysis and verification of the trace element ratios obtained from marine palynomorphs is required before any definitive conclusions can be made from the trace element data already obtained.

REFERENCES

Ackmann R.G., Addison R.F. and Hooper S.N. 1970. *Halosphaera virides*: fatty acid composition and taxonomical relationships. *Journal of the Fisheries Resources Board Canada*, **27**: 251–255

Ader, M., Cartigny, P., Boudou, J.P., Oh, J.H., Petit, E. and Javoy, M. 2006. Nitrogen isotopic evolution of carbonaceous matter during metamorphism: Methodology and preliminary results. *Chemical Geology*, **232**(3): 152-169

Algeo, T.J. 2004. Can marine anoxic events draw down the trace element inventory of seawater? *Geology*, **32**(12): 1057-1060

Algeo, T.J. and Scheckler, S.E. 1998. Terrestrial-marine teleconnections in the Devonian: links between the evolution of land plants, weathering processes, and marine anoxic events. *Philosophical Transactions of the Royal Society of London. Series B: Biological Sciences*, **353**(1365): 113-130

Algeo, T. J. and Scheckler, S. E. 2010. Land plant evolution and weathering rate changes in the Devonian. *Journal of Earth Science*, **21**: 75-78

Algeo, T. J., Berner, R.A., Maynard, J.B. and Scheckler, S.E., 1995. Late Devonian oceanic anoxic events and biotic crises: "Rooted" in the evolution of vascular land plants. *GSA Today*, **5**(3): 45

Altabet, M.A. and Curry, W.B. 1989. Testing models of past ocean chemistry using foraminifera $^{15}N/^{14}N$. *Global Biogeochemical Cycles*, **3**(2): 107-119

Altabet, M.A. and Francois, R. 1994. Sedimentary nitrogen isotopic ratio as a recorder for surface ocean nitrate utilization. *Global Biogeochemical Cycles*, **8**(1): 103-116

Altabet, M. A., Deuser, W. G., Honjo, S. and Stienen, C. 1991. Seasonal and depth-related changes in the source of sinking particles in the North Atlantic. *Nature*, **354**(6349), 136-139

Altabet, M.A., Francois, R., Murray, D.W. and Prell, W.L. 1995. Climate-related variations in denitrification in the Arabian Sea from sediment $^{15}N/^{14}N$ ratios. *Nature*, **373**(6514): 506-509

Altabet, M.A., Pilskaln, C., Thunell, R., Pride, C., Sigman, D., Chavez, F. and Francois, R. 1999. The nitrogen isotope biogeochemistry of sinking particles from the margin of the Eastern North Pacific. *Deep Sea Research Part I: Oceanographic Research Papers*, **46**(4): 655-679

Arnaboldi, M. and Meyers, P.A. 2006. Patterns of organic carbon and nitrogen isotopic compositions of latest Pliocene sapropels from six locations across the Mediterranean Sea. *Palaeogeography, Palaeoclimatology, Palaeoecology*, **235**(1): 149-167

Bahlmann, E., Bernasconi, S.M., Bouillon, S., Houtekamer, M., Korntheuer, M., Langenberg, F., Mayr, C., Metzke, M., Middleburg, J.J., Nagel, B., Struck, U., Voß, M. and Emeis, K.C. 2010. Performance evaluation of nitrogen isotope ratio determination in marine and lacustrine sediments: An inter-laboratory comparison. *Organic Geochemistry*, **41**(1): 3-12

Barker, C.E. and Goldstein, R.H. 1990. Fluid-inclusion technique for determining maximum temperature in calcite and its comparison to the vitrinite reflectance geothermometer. *Geology*, **18**(10): 1003-1006

Barron, L.S. and Ettensohn, F.R. 1981. *Paleoecology of the Devonian-Mississippian Black-Shale Sequence in Eastern Kentucky: With an Atlas of Some Common Fossils*. Technical Information Centre, US Department of Energy

Beaumont, V. and Robert, F. 1999. Nitrogen isotope ratios of kerogens in Precambrian cherts: a record of the evolution of atmosphere chemistry? *Precambrian Research*, **96**(1): 63-82

Becker, R.T. 1993. Analysis of ammonoid palaeobiogeography in relation to the global Hangenberg (terminal Devonian) and Lower Alum Shale (Middle Tournaisian) events. *Annales de la Société Géologique de Belgique*, **115**: 459-473

Becker, R.T. 1996. New faunal records and holostratigraphic correlation of the Hasselbachtal D/C-boundary auxiliary stratotype (Germany). *Annales de la Société géologique de Belgique*, **117**(1): 19-45

Berner, R. A. 1999. Atmospheric oxygen over Phanerozoic time. *Proceedings of the National Academy of Sciences*, **96**(20): 10955-10957

Blakey, R.C. 2011. Colorado Plateau Geosystems, Inc. Available at www.cpgeosystems.com

Bless, M. J. 1993. Comparison between Eustatic TR Cycles around the Devonian-Carboniferous boundary and the distribution of the ostracode taxon *Pseudoleperditia* gr. *venulosa*. *Annales de la Société Géologique de Belgique*, **115**: 475-81

Boalch, G. T. and Guy-Ohlson, D. 1992. *Tasmanites*, the correct name for *Pachysphaera* (Prasinophyceae, Pterospermataceae). *Taxon*, **41**(3) 529-531

Boudou, J.P., Schimmelmann, A., Ader, M., Mastalerz, M., Sebilo, M. and Gengembre, L. 2008. Organic nitrogen chemistry during low-grade metamorphism. *Geochimica et Cosmochimica Acta*, **72**(4): 1199-1221

Bradley, R., 1999. *Paleoclimatology: reconstructing climates of the Quaternary,* Academic Press, Harcourt Brace and Company, San Diego, California, 153-186

Brand, U. 1993. Global perspective of Famennian–Tournaisian oceanography: geochemical analysis of brachiopods. *Annales de la Societé Géologique de Belgique*, **115**(2): 491-496

Brand, U., Legrand-Blain, M. and Streel, M. 2004. Biochemostratigraphy of the Devonian–Carboniferous boundary global stratotype section and point, Griotte Formation, La Serre, Montagne Noire, France. *Palaeogeography, Palaeoclimatology, Palaeoecology*, **205**(3): 337-357

Brandes, J.A. and Devol, A.H. 2002. A global marine-fixed nitrogen isotopic budget: Implications for Holocene nitrogen cycling. *Global Biogeochemical Cycles*, **16**(4): 67-1

Brezinski, D.K., Cecil, C. B. and Skema, V.W. 2010. Late Devonian glacigenic and associated facies from the central Appalachian Basin, eastern United States. *Geological Society of America Bulletin*, **122**(1-2): 265-281

Brezinski, D.K., Cecil, C.B., Skema, V.W. and Kertis, C.A. 2009. Evidence for long-term climate change in Upper Devonian strata of the central Appalachians. *Palaeogeography, Palaeoclimatology, Palaeoecology*, **284**(3): 315-325

Brezinski, D.K., Cecil, C.B., Skema, V.W. and Stamm, R. 2008. Late Devonian glacial deposits from the eastern United States signal an end of the mid-Paleozoic warm period. *Palaeogeography, Palaeoclimatology, Palaeoecology*, **268**(3): 143-151

Bruland, K.W. and Lohan, M.C. 2006. The control of trace metals in seawater. In *The Oceans and Marine Geochemistry, Treatise on Geochemistry*, Vol. 6. ed. H. Elderfield. Elsevier, 23-44

Buggisch, W. and Joachimski, M. M. 2006. Carbon isotope stratigraphy of the Devonian of Central and Southern Europe. *Palaeogeography, Palaeoclimatology, Palaeoecology*, **240**(1): 68-88

Butterfield, N.J. 2009. Oxygen, animals and oceanic ventilation: an alternative view. *Geobiology*, **7**(1): 1-7

Butterfield, N.J. 2011. Animals and the invention of the Phanerozoic Earth system. *Trends in Ecology & Evolution*, **26**(2): 81-87

Calvert, S.E., Nielsen, B. and Fontugne, M.R. 1992. Evidence from nitrogen isotope ratios for enhanced productivity during formation of eastern Mediterranean sapropel. *Nature*, **359**: 223-225

Caplan, M.L. and Bustin, R.M. 1999. Devonian–Carboniferous Hangenberg mass extinction event, widespread organic-rich mudrock and anoxia: causes and consequences. *Palaeogeography, Palaeoclimatology, Palaeoecology*, **148**(4):187-207

Caputo, M.V., and Crowell, J.C. 1985. Migration of glacial centers across Gondwana during Paleozoic Era. *Geological Society of America Bulletin*, **96**(8): 1020-1036

Carman, R., Aigars, J. and Larsen, B. 1996. Carbon and nutrient geochemistry of the surface sediments of the Gulf of Riga, Baltic Sea. *Marine Geology*, **134**(1): 57-76

Carpenter, E.J., Harvey, H.R., Fry, B. and Capone, D.G. 1997. Biogeochemical tracers of the marine cyanobacterium *Trichodesmium. Deep Sea Research Part I: Oceanographic Research Papers*, **44**(1): 27-38

Cecil, C.B., Brezinski, D.K. and DuLong, F. 1998. *Allocyclic controls on Paleozoic sedimentation in the Appalachian Basin. U.S. Geological Survey. Op. File Report.* 98–577

Chaloner, W.G. and Orbell, G. 1971. A palaeobiological definition of sporopollenin. In *Sporopollenin.* Ed. Brooks, J., Grant, P.R., Muir, M., van Gizel, P. and Shaw, G. Academic Press, London, 273-294

Chaplin, J.R. and Mason, C.E. 1979. *The Devonian-Carboniferous boundary*, in Ettensohn, F.R. and Dever, G.R., Jr., eds., *Carboniferous geology from the Appalachian Basin to the Illinois Basin through eastern Ohio and Kentucky, Guidebook for Field Trip No. 4*, IX International Congress of Carboniferous Stratigraphy and Geology: Lexington, University of Kentucky, 152–162

Chaplin, J.R. and Mason, C.E. 1985. *Berea Sandstone (Lower Mississippian) sedimentation in northeastern Kentucky, Stop 1, Rock Hill Chapel Section (Garrison Quarry)*, in Haban, S.M., ed., *Field Excursion 6, Guidebook, Carboniferous of eastern Kentucky, Sixth Gondwana Symposium*: Ohio State University Institute of Polar Studies Miscellaneous Publication **#228**, 36–50

Clayton, J.L. and Swetland, P.J. 1978. Subaerial weathering of sedimentary organic matter. *Geochimica et Cosmochimica Acta*, **42**(3): 305-312

Clayton, G.,Mason, C.E., Ettensohn, F.R., Lierman, R.T., Goodhue, R., and Rooney, A. 2010. Palynological correlation of a Late Devonian dropstone in Kentucky with diamictite-bearing sections in Maryland and Pennsylvania. In *Geological Society of America Annual Meeting*. Denver, October 2010

Clayton, G, Paterson N.W., Mason, C.E., Ettensohn, F.R., Lierman, R.T., Goodhue R., Rooney A. and Wicander, R. 2012. Palynostratigraphy and palynofacies of Late Devonian rocks in the Appalachian Basin. *A Joint Meeting of the 45th Annual Meeting of AASP – The Palynological Society and Meeting of the CIMP – Commision Internationale de la Microflore du Paléozoïque Subcommisions*. Lexington, July 2012

Codispoti, L.A. and Richards, F.A. 1976. An analysis of the horizontal regime of denitrification in the eastern tropical North Pacific. *Limnology and Oceanography*, **21**(3): 379-388

Codispoti, L. A., Brandes, J. A., Christensen, J. P., Devol, A. H., Naqvi, S. W. A., Paerl, H. W. and Yoshinari, T. 2001. The oceanic fixed nitrogen and nitrous oxide budgets: Moving targets as we enter the anthropocene?. *Scientia Marina*, **65**(S2): 85-105

Colbath, G.K. and Grenfell, H.R. 1995. Review of biological affinities of Paleozoic acid-resistant, organic-walled eukaryotic algal microfossils (including "acritarchs"). *Review of Palaeobotany and Palynology*, **86**(3): 287-314

Coleman, U. and Clayton, G. 1987. Palynostratigraphy and palynofacies of the uppermost Devonian and Lower Mississippian of eastern Kentucky (USA) and correlation with Western Europe. *Courier Forschungs Institut Senckenberg*, **98**: 75-93

Colton, G. W. 1970. The Appalachian basin—its depositional sequences and their geologic relationships. *Studies of Appalachian Geology—Central and Southern.* New York, Interscience Publishers, 5-47

Crosta, X. and Shemesh, A. 2002. Reconciling down core anticorrelation of diatom carbon and nitrogen isotopic ratios from the Southern Ocean. *Paleoceanography*, **17**(1): 10-1

Crowell, J.C. 1999. *Pre-Mesozoic ice ages: Their bearing on understanding the climate system*: Geological Society of America Memoir **192**: 106

Dalsgaard, T., Canfield, D.E., Petersen, J., Thamdrup, B., and Acuña-González, J. 2003. N_2 production by the anammox reaction in the anoxic water column of Golfo Dulce, Costa Rica. *Nature*, **422**(6932): 606-608

Dean, W.E., Gardner, J.V. and Piper, D.Z., 1997. Inorganic geochemical indicators of glacial–interglacial changes in productivity and anoxia on the California continental margin. *Geochimica et Cosmochimica Acta*, **61**: 4507– 4518

DeNiro, M.J. and Epstein, S. 1981. Influence of diet on the distribution of nitrogen isotopes in animals. *Geochimica et Cosmochimica Acta*, **45**(3): 341-351

Deutsch, C., Sarmiento, J.L., Sigman, D.M., Gruber, N. and Dunne, J.P. 2007. Spatial coupling of nitrogen inputs and losses in the ocean. *Nature*, **445**(7124): 163-167

Deutsch, C., Sigman, D.M., Thunell, R.C., Meckler, A.N. and Haug, G.H. 2004. Isotopic constraints on glacial/interglacial changes in the oceanic nitrogen budget. *Global Biogeochemical Cycles*, **18**(4), GB4012

De Witt, W. 1970. Age of the Bedford Shale, Berea Sandstone, and Sunbury Shale in the Appalachian and Michigan Basins, Pennsylvania, Ohio, and Michigan. *US Geological Survey Bulletin*, 1294-G

Díaz-Martínez, E., Vavrdová, M., Bek, J. and Isaacson, P.E. 1999. Late Devonian (Famennian) glaciation in western Gondwana: evidence from the Central Andes. A*bhandlungen-Geologischen Bundesanstalt*, **54**: 213-238

Dymond, J., Suess, E. and Lyle, M. 1992. Barium in deep-sea sediment: A geochemical proxy for paleoproductivity. *Paleoceanography*, **7**(2): 163-181

Dypvik, H. 1984. Geochemical compositions and depositional conditions of upper Jurassic and lower Cretaceous Yorkshire clays. *England Geological Magazine* **121**(5): 489–504

Eames, L.E. 1978. A palynologic interpretation of the Devonian-Mississippian boundary from northeastern Ohio, USA (abst.). *Palynology*, **2**: 218-219

Eble, C.F., Nuttall, B.C., Greb, S.F. and Bustin, R.M. 2010. *Petrography and geochemistry of the Devonian Ohio Shale from a drill core in eastern Kentucky: implications for potential CO_2 sequestration and enhanced methane production.* In 2010 Geological Society of America Denver Annual Meeting, Colorado

Elam, T.D. 1981. *Stratigraphy and paleoenvironmental aspects of the Bedford-Berea sequence and the Sunbury Shale in eastern and south-central Kentucky.* Unpublished PhD thesis, University of Kentucky

Emeis, K. C. and Weissert, H. 2009. Tethyan–Mediterranean organic carbon-rich sediments from Mesozoic black shales to sapropels. *Sedimentology*, **56**(1), 247-266

Escalona, A., Mann, P. and Jaimes, M. 2011. Miocene to recent Cariaco basin, offshore Venezuela: Structure, tectonosequences, and basin-forming mechanisms. *Marine and Petroleum Geology*, **28**(1): 177-199

Ettensohn, F. R. 1985. The Catskill delta complex and the Acadian orogeny: A model. *Geological Society of America Special Papers*, **201**: 39-50

Ettensohn, F.R. 1991. Flexural interpretation of relationships between Ordovician tectonism and stratigraphic sequences, central and southern Appalachians, USA. *Advances in Ordovician geology: Geological Survey of Canada Paper*, **90**(9): 213-224

Ettensohn, F.R., 1992. *Silurian-Devonian contact and transgressive black shales at the base of the Ohio Shale, in* Ettensohn, F.R., ed., Changing interpretations of Kentucky geology—Layer-cake, facies, flexure, and eustacy: Ohio Division of Geological Survey Miscellaneous Report No. 5, 74–76

Ettensohn, F. R. 1994. Tectonic control on formation and cyclicity of major Appalachian unconformities and associated stratigraphic sequences. *Tectonic and Eustatic Controls on Sedimentary Cycles: SEPM, Concepts in Sedimentology and Paleontology*. **4**: 217-244.

Ettensohn, F. R. 1998. Compressional tectonic controls on epicontinental black-shale deposition: Devonian-Mississippian examples from North America, In Scheiber, J., Zimmerle, W. and Sethi, P. eds., *Shales and mudstones I*, E. Schweizerbart'sche Verlagsbuchhandlung, Stuttgart. 109-128

Ettensohn, F. R. 2008. The Appalachian foreland basin in eastern United States. *Sedimentary Basins of the World*, **5**: 105-179

Ettensohn, F. R., and Barron, L. S. 1981. Depositional model for the Devonian-Mississippian black shales of North America: a paleoclimatic-paleogeographic approach. *GSA Cincinnati*, **81**: 344-361

Ettensohn, F. R. and Elam, T. D. 1985. Defining the nature and location of a Late Devonian–Early Mississippian pycnocline in eastern Kentucky. *Geological Society of America Bulletin*, **96**(10): 1313-1321

Ettensohn, F. R. and Pashin, J.C. 1997. Development of multiple unconformities during the Devonian-Carboniferous transition on parts of Laurussia. In *Proceedings of the XIII International Congress on the Carboniferous and Permian. Prace Panstwowego Instytutu Geologiczego, Warszawa, CLVII, Part* **1**: 77-86

Ettensohn, F.R., Miller, M.L., Dillman, S.B., Elam, T.D., Geller, K.L., Swager, D.R., Markowitz, G., Woock, R.D. and Barron, L.S. 1988. *Characterization and implications of the Devonian-Mississippian black-shale sequence, eastern and central Kentucky, U.S.A.: Pycnoclines, transgression, regression, and tectonism, in* McMillan, N.J., Embry, A.F., and Glass, G.J., eds., Devonian of the world, Proceedings of the Second International Symposium on the Devonian System: Canadian Society of Petroleum Geologists Memoir 14, **2**: 323–345

Ettensohn, F.R., Lierman, T.R. and Mason, C.E., with contributions by Heal S., Paterson N., Eble, C., Goodhue, R., Larsson, N., Clayton, G., Dennis, A., Anderson, E. and Wilhelm, D.B. 2009. Upper Devonian–Lower Mississippian clastic rocks in northeastern Kentucky: Evidence for Acadian alpine glaciation and models for source-rock and reservoir-rock development in the eastern United States. *American Institute of Professional Geologists*—Kentucky Section Spring Field Trip

Faure, G. 1986. *Principles of Isotope Geology*. Wiley and Sons Publishers, New York..**PAGES**

Fennel, K., Follows, M. and Falkowski, P.G. 2005. The co-evolution of the nitrogen, carbon and oxygen cycles in the Proterozoic ocean. *American Journal of Science*, **305**(6-8): 526-545

Foreman, H.P. 1959. A new occurrence of Devonian radiolaria in calcareous concretions of the Huron Member of the Ohio Shale. *Journal of Paleontology*, **33**(1): 76-80

Foreman, H.P. 1963. Upper Devonian Radiolaria from the Huron member of the Ohio shale. *Micropaleontology*, **9**(3): 267-304

Frakes, L.A., Francis, J.E. and Syktus, J.I. 1992. *Climate Modes of the Phanerozoic: the History of the Earth's Climate Over the Past 600 Million Years*. Cambridge University Press, 27-35

Freudenthal, T., Wagner, T., Wenzhöfer, F., Zabel, M. and Wefer, G. 2001. Early diagenesis of organic matter from sediments of the eastern subtropical Atlantic: Evidence from stable nitrogen and carbon isotopes. *Geochimica et Cosmochimica Acta*, **65**(11): 1795-1808

Galbraith, E.D., Kienast, M., Pedersen, T.F. and Calvert, S.E. 2004. Glacial-interglacial modulation of the marine nitrogen cycle by high-latitude O_2 supply to the global thermocline. *Paleoceanography*, **19**(4)

Galbraith, E.D., Sigman, D.M., Robinson, R.S. and Pedersen, T.F. 2008. Nitrogen in past marine environments. *Nitrogen in the Marine Environment*, **2**: 1497-1535

Galbraith, E. D., Kienast, M., Albuquerque, A. L., Altabet, M. A., Batista, F., Bianchi, D., Calvert, S.E., Contreras, S., Crosta, X., De Pol-Holz, R., Dubois, N., Etourneau, J., Francois, R., Hsu, T.C., Ivanochko, T., Jaccard, S.L., Kao, S.J., Kiefer, T., Kienast, S., Lehmann, M.F., Martinez, P., McCarthy, M., Meckler, A.N., Mix, A., Möbius, J., Pedersen, T.F., Pichevin, L., Quan, T.M., Robinson, R.S., Ryabenko, E., Schmittner, A., Schneider, R., Schneider-Mor, A., Shigemitsu, M., Sinclair, D., Somes, C., Studer, A.S., Tesdal, J.E., Thunell R. and Yang, J. Y. T. 2013. The acceleration of oceanic denitrification during deglacial warming. *Nature Geoscience*, **6**: 579-584

Ganeshram, R.S., Pedersen, T.F., Calvert, S. and François, R. 2002. Reduced nitrogen fixation in the glacial ocean inferred from changes in marine nitrogen and phosphorus inventories. *Nature*, **415**(6868): 156-159

Garrels, R.M. and Christ, C.L. 1965. *Solutions, minerals, and equilibria*: NewYork, Harper and Row: 450

Gaye-Haake, B., Lahajnar, N., Emeis, K. C., Unger, D., Rixen, T., Suthhof, A., Ramaswamy, V., Schulz, H., Paropkari, A.L., Gupha, M.V.S. and Ittekkot, V. 2005. Stable nitrogen isotopic ratios of sinking particles and sediments from the northern Indian Ocean. *Marine Chemistry*, **96**(3), 243-255

Goodhue, R. and Clayton, G. 2010. Palynomorph Darkness Index (PDI)–a new technique for assessing thermal maturity. *Palynology*, **34**(2): 147 - 156

Gray J. and Boucot A.J. 1977. Early vascular land plants: proof and conjecture. *Lethaia* **10**: 145-174

Griffith, C. 1977. *Stratigraphy and paleoenvironment of the New Albany Shale (Upper Devonian) of north-central Kentucky*. Unpublished Masters thesis, University of Wisconsin

Gruber, N. and Galloway, J.N. 2008. An Earth-system perspective of the global nitrogen cycle. *Nature*, **451**(7176): 293-296

Guy-Ohlson, D. 1988. Developmental stages in the life cycle of Mesozoic *Tasmanites*. *Botanica Marina*, **31**(5): 447-456

Guy-Ohlson, D. and Boalch, G. T. 1992. Comparative morphology of the genus *Tasmanites* (Pterospermales, Chlorophyta). *Phycologia*, **31**(6): 523-528

Hallam, A. and Cohen, J.M. 1989. The case for sea-level change as a dominant causal factor in mass extinction of marine invertebrates [and discussion]. *Philosophical Transactions of the Royal Society of London. B, Biological Sciences*, **325**(1228): 437-455

Hart, M.H. 1978. The evolution of the atmosphere of the Earth. *Icarus*, **33**(1): 23-39

Hass, W.H. 1947. Conodont zones in Upper Devonian and Lower Mississippian formations of Ohio. *Journal of Paleontology*, 131-141

Haug, G.H., Hughen, K.A., Sigman, D.M., Peterson, L.C. and Röhl, U. 2001. Southward migration of the Intertropical Convergence Zone through the Holocene. *Science*, **293**(5533): 1304-1308

Haug, G.H., Pedersen, T.F., Sigman, D.M., Calvert, S.E., Nielsen, B. and Peterson, L.C. 1998. Glacial/interglacial variations in production and nitrogen fixation in the Cariaco Basin during the last 580 kyr. *Paleoceanography*, **13**(5): 427-432

Heal, S. 2009. Palynological correlation of Mississipian (Carboniferous) stage boundaries in Western Europe and the USA. Unpublished Ph.D. thesis, University of Dublin.

Heal, S. and Clayton, G. 2008. The palynology of the Hannibal Shale (Mississippian) of northeastern Missouri, U.S.A. and correlation with Western Europe. *Palynology*, **32**: 27-37

Higgs, K.T., and Streel, M. 1994. Palynological age for the lower part of the Hangenberg Shales in Sauerland, Germany. *Annales de la Societé Géologique de Belgique*, **116**(2): 243-247

Higgs, K.T., Prestianni, C., Streel, M. and Thorez, J. 2013. High resolution miospore stratigraphy of the Upper Famennian of eastern Belgium, and correlation with the conodont zonation. *Geologica Belgica*, **16**(1-2): 84-94

Isaacson, P.E., Diaz-Martinez, E., Grader, G.W., Kalvoda, J., Babek, O. and Devuyst, F.X. 2008. Late Devonian–earliest Mississippian glaciation in Gondwanaland and its biogeographic consequences. *Palaeogeography, Palaeoclimatology, Palaeoecology*, **268**(3): 126-142

Jenkyns, H.C., Gröcke, D.R., and Hesselbo, S.P. 2001. Nitrogen isotope evidence for water mass denitrification during the early Toarcian (Jurassic) oceanic anoxic event. *Paleoceanography*, **16**(6): 593-603

Jia, Y. 2006. Nitrogen isotope fractionations during progressive metamorphism: A case study from the Paleozoic Cooma metasedimentary complex, southeastern Australia. *Geochimica et Cosmochimica Acta*, **70**(20): 5201-5214

Jickells, T.D. 1998. Nutrient biogeochemistry of the coastal zone. *Science*, **281**(5374): 217-222

Johnson, J.G., Klapper, G. and Sandberg, C.A. 1985. Devonian eustatic fluctuations in Euramerica. *Geological Society of America Bulletin*, **96**(5): 567-587

Jones, B. and Manning, D.A. 1994. Comparison of geochemical indices used for the interpretation of palaeoredox conditions in ancient mudstones. *Chemical Geology*, **111**(1): 111-129

Jordan, D.W. 1980. *Trace Fossils and Stratigraphy of Devonian Black Shale in East-Central Kentucky*: ABSTRACT. *AAPG Bulletin*, **64**(5): 729-730

Junium, C.K. and Arthur, M.A. 2007. Nitrogen cycling during the Cretaceous, Cenomanian-Turonian oceanic anoxic event II. *Geochemistry, Geophysics, Geosystems*, **8**(3)

Kaiser, S.I., Steuber, T. and Becker, R.T. 2008. Environmental change during the Late Famennian and Early Tournaisian (Late Devonian–Early Carboniferous): implications from stable isotopes and conodont biofacies in southern Europe. *Geological Journal*, **43**(2-3): 241-260

Kaiser, S. I., Becker, R. T., Steuber, T. and Aboussalam, S. Z. 2011. Climate-controlled mass extinctions, facies, and sea-level changes around the Devonian–Carboniferous boundary in the eastern Anti-Atlas (SE Morocco). *Palaeogeography, Palaeoclimatology, Palaeoecology*, **310**(3): 340-364

Kaiser, S.I., Steuber, T., Becker, R.T. and Joachimski, M.M. 2006. Geochemical evidence for major environmental change at the Devonian–Carboniferous boundary in the Carnic Alps and the Rhenish Massif.*Palaeogeography, Palaeoclimatology, Palaeoecology*, **240**(1): 146-160

Kammer, T.W. 1985. Basinal and prodeltaic communities of the Early Carboniferous Borden Formation in northern Kentucky and southern Indiana. *Palaeogeography, Palaeoclimatology, Palaeoecology*, **49**: 179–121

Karl, D., Letelier, R., Tupas, L., Dore, J., Christian, J. and Hebel, D. 1997. The role of nitrogen fixation in biogeochemical cycling in the subtropical North Pacific Ocean. *Nature*, **388**(6642): 533-538

Kaufmann, B. 2006. Calibrating the Devonian time scale: a synthesis of U–Pb ID–TIMS ages and conodont stratigraphy. *Earth-Science Reviews*, **76**(3): 175-190

Kennedy, P., Kennedy, H. and Papadimitriou, S. 2005. The effect of acidification on the determination of organic carbon, total nitrogen and their stable isotopic composition in algae and marine sediment. *Rapid Communications in Mass Spectrometry*, **19**(8): 1063-1068

Kidder, D. L. and Worsley, T. R. 2010. Phanerozoic large igneous provinces (LIPs), HEATT (haline euxinic acidic thermal transgression) episodes, and mass extinctions. *Palaeogeography, Palaeoclimatology, Palaeoecology*, **295**(1): 162-191

Kienast, S.S., Calvert, S.E. and Pedersen, T.F. 2002. Nitrogen isotope and productivity variations along the northeast Pacific margin over the last 120 kyr: Surface and subsurface paleoceanography. *Paleoceanography*, **17**(4): 1055

Kienast, M., Higginson, M.J., Mollenhauer, G., Eglinton, T.I., Chen, M.T. and Calvert, S.E. 2005. On the sedimentological origin of down-core variations of bulk sedimentary nitrogen isotope ratios. *Paleoceanography*, **20**(2): PA2009

Kling, G.W., Fry, B. and O'Brien, W.J. 1992. Stable isotopes and planktonic trophic structure in arctic lakes. *Ecology*, **73**(2): 561-566

Kuypers, M.M., van Breugel, Y., Schouten, S., Erba, E. and Damsté, J.S.S. 2004. N_2-fixing cyanobacteria supplied nutrient N for Cretaceous oceanic anoxic events. *Geology*, **32**(10): 853-856

Landing, E. 2011. Time-specific black mudstones and global hyperwarming on the Cambrian–Ordovician slope and shelf of the Laurentia palaeocontinent. *Palaeogeography, Palaeoclimatology, Palaeoecology*, **367-368**: 256-272

Lavkulich, L. M. and Wiens, J. H. 1970. Comparison of organic matter destruction by hydrogen peroxide and sodium hypochlorite and its effects on selected mineral constituents. *Soil Science Society of America Journal*, **34**(5): 755-758

Le Hérissé, A., Dorning, K. J., Mullins, G. L. and Wicander, R. 2009. Global patterns of organic-walled phytoplankton biodiversity during the late Silurian to earliest Devonian. *Palynology*, **33**(1): 25-75

Lehmann, M.F., Bernasconi, S.M., Barbieri, A. and McKenzie, J.A. 2002. Preservation of organic matter and alteration of its carbon and nitrogen isotope composition during simulated and *in situ* early sedimentary diagenesis.*Geochimica et Cosmochimica Acta*, **66**(20): 3573-3584

Leythaeuser, D. 1973. Effects of weathering on organic matter in shales. *Geochimica et Cosmochimica Acta*, **37**(1): 113-120

Libes, S.M. and Deuser, W.G. 1988. The isotope geochemistry of particulate nitrogen in the Peru upwelling area and the Gulf of Maine. *Deep Sea Research Part A. Oceanographic Research Papers*, **35**(4): 517-533

Lierman, R.T. and Mason, C.E. 2007. Upper Devonian glaciation in the Ohio Shale of east-central Kentucky. In *Geological Society of America Abstracts with Programs* **39**(2): 70

Lierman, R. T., Mason, C. E., Pashin, J. C., and Ettensohn, F. R. 1992. Cleveland Shale-through-lower Borden sequence (Devonian-Mississippian) and implicatons. *Changing interpretations of Kentucky geology—layer-cake, facies, flexure, and eustacy. Ohio Geological Survey Miscellaneous Report*, **5**: 77-88.

Lin, H.L., Peterson, L.C., Overpeck, J.T., Trumbore, S.E. and Murray, D.W. 1997. Late Quaternary climate change from $\delta^{18}O$ records of multiple species of planktonic foraminifera: High-resolution records from the Anoxic Cariaco Basin, Venezuela. *Paleoceanography*, **12**(3): 415-427

Lisiecki, L. E. and Raymo, M. E. 2007. Plio–Pleistocene climate evolution: trends and transitions in glacial cycle dynamics. *Quaternary Science Reviews*,**26**(1): 56-69

Liu, K. K., Atkinson, L., Quiñones, R. and Talaue-McManus, L. 2010. *Carbon and nutrient fluxes in continental margins: a global synthesis*. Springer.

Loboziak S., Melo J.H.G., Quadros L.P. and Streel M. 1997. Palynological evaluation of the Famennian *Protosalvinia* (*Foerstia*) Zone in the Amazon Basin, northern Brazil: a preliminary study. *Review of Palaeobotany and Palynology*, **96**: 31-45

Macko, S. A. and Estep, M. L. 1984. Microbial alteration of stable nitrogen and carbon isotopic compositions of organic matter. *Organic Geochemistry*, **6**: 787-790

Marshall, J. E. and Hemsley, A. R. 2003. A Mid Devonian seed-megaspore from East Greenland and the origin of the seed plants. *Palaeontology*, **46**(4): 647-670

Martin, J.H., Coale, K.H., Johnson, K.S., Fitzwater, S.E., Gordon, R.M., Tanner, S.J., Hunter, C.N., Elrod, V.A., Nowicki, J.L., Coley, T.L., Barber, R.T., Lindley, S., Watson, A.J., Van Scoy, K., Law, C.S., Liddicoat, M.I., Ling, R., Stanton, T., Stockel, J., Collins, C., Anderson, A., Bidigare, R., Ondrusek, M., Latasa, M., Millero, F.J., Lee, K., Yao, W., Zhang, J.K., Friedrick, G., Sakamoto, C., Chavez, F., Buck, K., Kolber, Z., Greene, R., Falkowski, P., Chisholm, S. W., Hoge, F., Swift, R., Yungel, J., Turner, S., Nightingale, P., Hatton, A., Liss, P. And Tindale, N.W. 1994. Testing the iron hypothesis in ecosystems of the equatorial Pacific Ocean. *Nature*, **371**: 8

Martin, R.E. 1995. Cyclic and secular variation in microfossil biomineralization: clues to the biogeochemical evolution of Phanerozoic oceans. *Global and Planetary Change*, **11**(1): 1-23

Martin, R.E. 1996. Secular increase in nutrient levels through the Phanerozoic: implications for productivity, biomass, and diversity of the marine biosphere. *Palaios*, **11**(3): 209-219

Marynowski, L. and Filipiak, P. 2007. Water column euxinia and wildfire evidence during deposition of the Upper Famennian Hangenberg event horizon from the Holy Cross Mountains (central Poland). *Geological Magazine*, **144**(3): 569-595

Mason, C.E. and Lierman, R.T. 1985. *Stratigraphy and depositional environments of the Sunbury and lower Borden formations (Lower Mississippian in northeastern Kentucky, STOP 4, Cave Run Lake spillway section*, in Haban, S.M., ed., *Field Excursion 6, Guidebook, Carboniferous of eastern Kentucky, Sixth Gondwana Symposium*: Ohio State University Institute of Polar Studies Miscellaneous Publication **#228**: 85–95

Mason C.E., Eble C. and O'Keefe, J. 2012. *A Joint Meeting of the 45th Annual Meeting of AASP – The Palynological Society and Meeting of the CIMP – Commision Internationale de la Microflore du Paléozoïque Subcommisions: Post-Meeting Field Trip: Devonian and Carboniferous strata of Northeastern Kentucky.* Lexington, Kentucky

Mastalerz, M., Hower, J. and Carmo, A. 1998. *In situ* FTIR and flash pyrolysis/GC-MS characterization of *Protosalvinia* (Upper Devonian, Kentucky, USA): implications for maceral classification. *Organic Geochemistry,* **28**: 57-66

Matthews, R.D. 1983. Foerstia from the Antrim Shale (Devonian) of Michigan. *Geology*, **11**(6):327-330

Maziane, N., Higgs, K.T. and Streel, M. 1999. Revision of the late Famennian miospore zonation scheme in eastern Belgium. *Journal of Micropalaeontology* **18**, 17-25

McGhee, G.R., Jr. 1996. *The Late Devonian Mass Extinction: The Frasnian-Famennian Crisis.* Columbia University Press, New York, 303

McGhee, G.R., Sheehan, P.M., Bottjer, D.J. and Droser, M. L. 2012. Ecological ranking of Phanerozoic biodiversity crises: The Serpukhovian (early Carboniferous) crisis had a greater ecological impact than the end-Ordovician. *Geology*, **40**(2): 147-150

Meckler, A.N., Ren, H., Sigman, D.M., Gruber, N., Plessen, B., Schubert, C.J. and Haug, G.H. 2011. Deglacial nitrogen isotope changes in the Gulf of Mexico: Evidence from bulk sedimentary and foraminifera-bound nitrogen in Orca Basin sediments. *Paleoceanography*, **26**(4): PA4216

Meckler, A.N., Schubert, C.J., Hochuli, P.A., Plessen, B., Birgel, D., Flower, B.P., Hinrich, K.U. and Haug, G.H. 2008. Glacial to Holocene terrigenous organic matter input to sediments from Orca Basin, Gulf of Mexico—A combined optical and biomarker approach. *Earth and Planetary Science Letters*, **272**(1): 251-263

Mehra, O.P. and Jackson, M.L. 1960. Iron oxide removal from soils and clays by a dithionite-citrate system buffered with sodium bicarbonate. In *Proceedings of the 7th national Conference on Clays*. **5**: 317-327

Melchin, M.J., Mitchell, C.E., Holmden, C. and Štorch, P. 2013. Environmental changes in the Late Ordovician–early Silurian: Review and new insights from black shales and nitrogen isotopes. *Geological Society of America Bulletin*, **125**(11-12): 1635-1670

Melo, J.H.G. and Loboziak, S. 2003. Devonian–Early Carboniferous miospore biostratigraphy of the Amazon Basin, Northern Brazil. *Review of Palaeobotany and Palynology*, **124**(3): 131-202

Melo, J.H G., Barrilari, I.M.R., Quadros, L.P., Loboziak, S. and Matsuda, N.S. 1999. Miospore-Based Correlation of the Late Devonian Curuá Group, Amazon Basin, Brazil. Petrobas, pp. 1–4

Meyer, K. M. and Kump, L. R. 2008. Oceanic euxinia in Earth history: Causes and consequences. *Annual Review of Earth and Planetary Sciences*, **36**: 251-288

Minagawa, M., and Wada, E. 1986. Nitrogen isotope ratios of red tide organisms in the East China Sea: A characterization of biological nitrogen fixation. *Marine chemistry*, **19**(3), 245-259

Möbius, J., Lahajnar, N. and Emeis, K.C. 2010. Diagenetic control of nitrogen isotope ratios in Holocene sapropels and recent sediments from the Eastern Mediterranean Sea. *Biogeosciences Discussions*, **7**(1): 1131-1165

Möbius, J., Gaye, B., Lahajnar, N., Bahlmann, E. and Emeis, K.C. 2011. Influence of diagenesis on sedimentary $\delta^{15}N$ in the Arabian Sea over the last 130 kyr. *Marine Geology*, **284**(1): 127-138

Morel, F.M.M., Milligan, A. J. and Saito, M. A. 2006. Marine Bioinorganic Chemistry: The Role of Trace Metals in the Oceanic Cycles of Major Nutrients, *in* Elderfield, H., Lolland, H.D. and Turekian, K.K. eds. *The Oceans and Marine Geochemistry*, Elsevier, **6**, 113

Myrow, P.M., Strauss, J.V., Creveling, J.R., Sicard, K.R., Ripperdan, R., Sandberg, C.A. and Hartenfels, S. 2011. A carbon isotopic and sedimentological record of the latest Devonian (Famennian) from the Western US and Germany. *Palaeogeography, Palaeoclimatology, Palaeoecology*, **306**(3): 147-159

Newton, E.T. 1875. I.—On "Tasmanite" and Australian "White Coal". *Geological Magazine (Decade II)*, **2**(08): 337-342

Niklas, K.J. 1976. Organic chemistry of *Protosalvinia* (*Foerstia*) from the Chattanooga and New Albany Shales. *Review of Palaeobotany and Palynology*, **22**: 265-279

Niklas, K.J. and Phillips T.L. 1976. Morphology of *Protosalvinia* from the upper Devonian of Ohio and Kentucky. *American Journal of Botany*, **63**: 9-29

Niklas, K. J., Phillips, T. L. and Carozzi, A. V. 1976. Morphology and Paleoecology of *Protosalvinia* from the Upper Devonian (Famennian) of the Middle Amazon Basin of Brazil. *Palaeontographica Abteilung B*, 1-30

Nuttall, B.C., Eble, C.F. and Drahovzal, J.A. 2005. Analysis of Devonian Black Shales in Kentucky for Potential Carbon Dioxide Sequestration and Enhanced Natural Gas Production. *Final report for United States Department of Energy (USDOE) contract DE-FC26-02NT41442*:71

Ohkouchi, N., Kashiyama, Y., Kuroda, J., Ogawa, N.O. and Kitazato, H. 2006. The importance of diazotrophic cyanobacteria as primary producers during Cretaceous Oceanic Anoxic Event 2. *Biogeosciences*, **3**(4): 467-478

Over, D.J. 2002. The Frasnian/Famennian boundary in central and eastern United States. *Palaeogeography, Palaeoclimatology, Palaeoecology*, **181**(1): 153-169

Over, D.J., Lazar, R., Baird, G. C., Schieber, J. and Ettensohn, F.R. 2009. *Protosalvinia* Dawson and associated conodonts of the Upper *trachytera* Zone, Famennian, Upper Devonian, in the eastern United States. *Journal of Paleontology*, **83**(1):70-79

Parkin, D.W. 1974. Trade-winds during the glacial cycles. *Proceedings of the Royal Society of London. A. Mathematical and Physical Sciences*, **337**(1608): 73-100

Pashin, J.C. and Ettensohn, F.R. 1987. An epeiric shelf-to-basin transition; Bedford-Berea Sequence, northeastern Kentucky and south-central Ohio. *American Journal of Science*, **287**(9): 893-926

Pashin, J.C. and Ettensohn, F.R. 1992a. *Lowstand deposition in a foreland basin: Bedford-Berea sequence (Upper Devonian), eastern Kentucky and West Virginia*, *in* Ettensohn, F.R., ed., Changing interpretations of Kentucky geology—Layer-cake, facies, flexure, and eustacy: Ohio Division of Geological Survey Miscellaneous Report No. **5**: 123–134

Pashin, J.C. and Ettensohn, F.R. 1992b, Paleoecology and sedimentology of the dysaerobic Bedford fauna (Late Devonian), Ohio and Kentucky, U.S.A. *Palaeogeography, Paleoclimatology, Palaeoecology*, **91**, 21–34

Pepper, J.F., De Witt, W. and Demarest, D.F. 1954. Geology of the Bedford Shale and Berea Sandstone in the Appalachian basin. *Science*, **119**(3094): 512-513

Perez-Leyton, M. 1991. Miospores du Dévonien moyen et supérieur de la coupe de Bermejo-La Angostura (sud-est de la Bolivie). *Annales de la Société Géologique de Belgique*, **113**: 373-389

Perkins, R.B., Piper, D.Z. and Mason, C.E. 2008. Trace-element budgets in the Ohio/Sunbury shales of Kentucky: Constraints on ocean circulation and primary productivity in the Devonian-Mississippian Appalachian Basin. *Palaeogeography, Palaeoclimatology, Palaeoecology*, **265**: 14–29

Polissar, P.J., Fulton, J.M., Junium, C.K., Turich, C.C. and Freeman, K.H. 2008. Measurement of 13C and 15N isotopic composition on nanomolar quantities of C and N. *Analytical chemistry*, **81**(2): 755-763

Prauss, M.L. 2007. Availability of reduced nitrogen chemospecies in photic-zone waters as the ultimate cause for fossil prasinophyte prosperity. *Palaios*, **22**(5): 489-499

Prauss, M. and Riegel, W. 1989. Evidence from phytoplankton associations for causes of black shale formation in epicontinental seas. *Neues Jahrbuch für Geologie und Paläontologie, Monatshefte*, **11**: 671-682

Price N.M. and Morel, F.M.M. 1991. Colimitation of phytoplankton growth by nickel and nitrogen. *Limnology and Oceanography*, **36**(6): 1071–1077

Provo, L.J., Kepferle, R.C. and Potter P.E. 1978. Division of black Ohio Shale in Eastern Kentucky: *American Association of Petroleum Geologists Bulletin*, **62**(9): 1703-1713

Quinlan, G. M. and Beaumont, C. 1984. Appalachian thrusting, lithospheric flexure, and the Paleozoic stratigraphy of the eastern interior of North America. *Canadian Journal of Earth Sciences*, **21**(9): 973-996

Rau, G.H., Arthur, M.A. and Dean, W.E. 1987. $^{15}N/^{14}N$ variations in Cretaceous Atlantic sedimentary sequences: implication for past changes in marine nitrogen biogeochemistry. *Earth and Planetary Science Letters*, **82**(3): 269-279

Raven, J.A., Wollenweber, B. and Handley, L.L. 1992. A comparison of ammonium and nitrate as nitrogen sources for photolithotrophs. *New Phytologist*, **121**(1): 19-32

Ren, H., Sigman, D.M., Meckler, A.N., Plessen, B., Robinson, R.S., Rosenthal, Y. and Haug, G.H. 2009. Foraminiferal isotope evidence of reduced nitrogen fixation in the ice age Atlantic Ocean. *Science*, **323**(5911): 244-248

Revill, A.T., Volkman, J.K., O'Leary, T., Summons, R.E., Boreham, C.J., Banks, M.R. and Denwer, K. 1994. Hydrocarbon biomarkers, thermal maturity, and depositional setting of tasmanite oil shales from Tasmania, Australia.*Geochimica et Cosmochimica Acta*, **58**(18): 3803-3822

Riegel, W. 2008. The Late Palaeozoic phytoplankton blackout—Artefact or evidence of global change? *Review of Palaeobotany and Palynology*, **148**(2): 73-90

Rimmer, S.M. 2004. Geochemical paleoredox indicators in Devonian–Mississippian black shales, Central Appalachian Basin (USA). *Chemical Geology* **206**(3): 373–391

Rimmer, S.M., Thompson, J.A., Goodnight, S.A. and Robl, T.L. 2004. Multiple controls on the preservation of organic matter in Devonian–Mississippian marine black shales: geochemical and petrographic evidence. *Palaeogeography, Palaeoclimatology, Palaeoecology,* **215**: 125–154

Robinson, R.S., Brunelle, B. G. and Sigman, D. M. 2004. Revisiting nutrient utilization in the glacial Antarctic: Evidence from a new method for diatom-bound N isotopic analysis. *Paleoceanography*, **19**(3): PA3001

Robinson, R.S., Kienast, M., Albuquerque, A.L., Altabet, M., Contreras, S., De Pol Holz, R., Dubois N., Francois, R., Galbraith, E., Hsu, T.C., Ivanochko, T., Jaccard, S., Kao, S.J., Kiefer, T., Kienast, S., Lehmann, M.F., Martinez, P., McCarthy, M., Möbius, J., Pedersen, T., Quan, T.M., Ryabenko, E., Schmittner, A., Schneider, R., Schneider-Mor, A., Shigemitsu, M., Sinclair, D., Somes, C., Studer, A., Thunell, R. and Yang, J.Y. 2012. A review of nitrogen isotopic alteration in marine sediments. *Paleoceanography* **27**(4): PA4203

Rooney, A., Clayton, G. and Goodhue, R. 2013. The dispersed spore *Retusotriletes loboziakii* sp. nov., affiliated with the enigmatic Late Devonian alga *Protosalvinia* Dawson 1884. *Palynology*, **37**(2): 196-201

Russell, D.J. 1985. Depositional analysis of a black shale by using gamma-ray stratigraphy: The Upper Devonian Kettle Point Formation of Ontario. *Bulletin of Canadian Petroleum Geology,* **33**: 236-253

Sachs, J.P. and Repeta, D.J. 1999. Oligotrophy and nitrogen fixation during eastern Mediterranean sapropel events. *Science*, **286**(5449): 2485-2488

Sackett, W.M., Brooks, J.M., Bernard, B.B., Schwab, C.R., Chung, H. and Parker, R.A. 1979. A carbon inventory for Orca Basin brines and sediments. *Earth and Planetary Science Letters*, **44**(1): 73-81

Sallan, L. C. and Coates, M. I. 2010. End-Devonian extinction and a bottleneck in the early evolution of modern jawed vertebrates. *Proceedings of the National Academy of Sciences*, **107**(22): 10131-10135

Saltzman, M.R. 2005. Phosphorus, nitrogen, and the redox evolution of the Paleozoic oceans. *Geology*, **33**(7): 573-576

Sandberg, C.A. and Ziegler, W. 1996. Devonian conodont biochronology in geologic time calibration. *Senckenbergiana Lethaea*, **76**(1-2): 259-265

Sandberg, C.A., Mason, C.E. and Work, D.M. 2002a. Position of the Kinderhookian–Osagean boundary in northeastern Kentucky and southern Ohio. In *Geological Society of America Abstracts with Programs,* **34**(2): 88

Sandberg, C.A., Morrow, J.R. and Ziegler, W. 2002b. Late Devonian sea-level changes, catastrophic events, and mass extinctions. In *Special Papers-Geological Society of America*, 473-488

Schieber, J. 1996. Early diagenetic silica deposition in algal cysts and spores; a source of sand in black shales? *Journal of Sedimentary Research*, **66**(1): 175-183

Schopf, J.M. and Schwietering, J.F. 1970. The *Foerstia* zone of the Ohio and Chattanooga shales.*U.S.Geological Survey Bulletin: Contributions to Stratigraphy* **1294-H**: 1-15

Schimmelmann, A., Mastalerz, M., Gao, L., Sauer, P.E. and Topalov, K. 2009. Dike intrusions into bituminous coal, Illinois Basin: H, C, N, O isotopic responses to rapid and brief heating. *Geochimica et Cosmochimica Acta*, **73**(20): 6264-6281

Schmidt, M.W.I. and Gleixner, G. 2005. Carbon and nitrogen isotope composition of bulk soils, particle-size fractions and organic material after treatment with hydrofluoric acid. *European Journal of Soil Science*, **56**(3): 407-416

Schubert, C.J. and Calvert, S.E. 2001. Nitrogen and carbon isotopic composition of marine and terrestrial organic matter in Arctic Ocean sediments: implications for nutrient utilization

and organic matter composition. *Deep Sea Research Part I: Oceanographic Research Papers*, **48**(3): 789-810

Schwietering, J.F. 1979. *Devonian shales of Ohio and their eastern and southern equivalents* (No. METC/CR-79/2). West Virginia Geological and Economic Survey, Morgantown (USA), 31-47

Scotese, C.R. 2001. PALEOMAP Project. Available at www.scotese.com

Sepkoski, Jr, J.J. 1996. Patterns of Phanerozoic extinction: a perspective from global data bases. In *Global events and event stratigraphy in the Phanerozoic* (pp. 35-51). Springer Berlin Heidelberg.

Sharp, Z. 2007. Principles of Stable Isotope Geochemistry: Pearson Prentice Hall, New Jersey. **9**: 206-216

Sigman, D.M., Altabet, M.A., Francois, R., McCorkle, D.C. and Gaillard, J.F. 1999. The isotopic composition of diatom-bound nitrogen in Southern Ocean sediments. *Paleoceanography*, **14**(2): 118-134

Sigman, D.M., DiFiore, P.J., Hain, M.P., Deutsch, C. and Karl, D.M. 2009. Sinking organic matter spreads the nitrogen isotope signal of pelagic denitrification in the North Pacific. *Geophysical research letters*, **36**(8): LO8605

Sigman, D.M., Robinson, R., Knapp, A.N., Van Geen, A., McCorkle, D.C., Brandes, J.A. and Thunell, R.C. 2003. Distinguishing between water column and sedimentary denitrification in the Santa Barbara Basin using the stable isotopes of nitrate. *Geochemistry, Geophysics, Geosystems*, **4**(5): 1040

Siokou-Frangou, I., Christaki, U., Mazzocchi, M. G., Montresor, M., Ribera d'Alcalá, M., Vaqué, D. and Zingone, A. 2010. Plankton in the open Mediterranean Sea: a review. *Biogeosciences*, **7**(5): 1543-1586

Simakov, K.V. 1993. Biochronological aspects of the Devonian-Carboniferous crisis in the regions of the former USSR. *Palaeogeography, Palaeoclimatology, Palaeoecology* **104**(1): 127-137

Somes, C. J., Schmittner, A., Galbraith, E.D., Lehmann, M.F., Altabet, M.A., Montoya, J.P., Letelier, R.M., Mix, A.C., Bourbonnais, A. and Eby, M. 2010. Simulating the global distribution of nitrogen isotopes in the ocean. *Global Biogeochemical Cycles* 24, **24**(4): GB4019

Streel, M. 1986. Miospore contribution to the upper Famennian-Strunian event stratigraphy. *Annales de la Societé Géologique de Belgique*, **109**(1): 75-92

Streel, M. 1999. Quantitative palynology of Famennian events in the Ardenne-Rhine Regions. *Abhandlungen der Geologischen Bundesanstalt*, **54**: 201-212

Streel, M. 2009. Upper Devonian miospore and conodont zone correlation in western Europe. *Geological Society, London, Special Publications*, **314**(1): 163-176

Streel, M., Brice, D. and Mistiaen, B. 2006. Strunian. *Geologica Belgica*, **9**(1-2): 105-109

Streel, M., Caputo, M.V., Loboziak, S. and Melo, J.H.G. 2000. Late Frasnian–Famennian climates based on palynomorph analyses and the question of the Late Devonian glaciations. *Earth-Science Reviews*, **52**(1): 121-173

Streel, M., Caputo, M.V., Melo, J.H.G. and Perez-Leyton, M. 2012. What do latest Famennian and Mississippian miospores from South American diamictites tell us? *Palaeobiodiversity and Palaeoenvironments*, **93**(3): 1-18

Strother, P. K. 1996. Acritarchs. *Palynology: principles and applications*, **1**: 81-106

Sunda, W.G. and Huntsman, S.A. 1995. Cobalt and zinc interreplacement in marine phytoplankton: Biological and geochemical implications. *Limnology and Oceanography*, **40**(8): 1404-1417

Swager, D.R. 1978. *Stratigraphy of the Upper Devonian-Lower Mississippian shale sequence in the eastern Kentucky outcrop belts.* Unpublished PhD thesis, University of Kentucky, 39-40

Tappan, H.N. 1980. *The paleobiology of plant protists* (Vol. 1028). San Francisco: WH Freeman, 818 – 822

Taylor W.A. and Taylor T.N. 1987. Spore wall ultrastructure of *Protosalvinia*. *American Journal of Botany* **74**: 437-443

Thamdrup, B. and Dalsgaard, T. 2002. Production of N_2 through anaerobic ammonium oxidation coupled to nitrate reduction in marine sediments. *Applied and Environmental Microbioliology* **68**(3): 1312-1318

Trapp, E., Kaufmann, B., Mezger, K., Korn, D. and Weyer, D. 2004. Numerical calibration of the Devonian-Carboniferous boundary: Two new U-Pb isotope dilution–thermal ionization mass spectrometry single-zircon ages from Hasselbachtal (Sauerland, Germany). *Geology*, **32**(10): 857-860

Tribovillard, N., Algeo, T.J., Lyons, T. and Riboulleau, A. 2006. Trace metals as paleoredox and paleoproductivity proxies: An update. *Chemical Geology*, **232**(1): 12-32

Veevers, J.T. and Powell, C.M. 1987. Late Paleozoic glacial episodes in Gondwanaland reflected in transgressive-regressive depositional sequences in Euramerica. *Geological Society of America Bulletin*, **98**(4): 475-487

Vigran, J.O., Mørk, A., Forsberg, A.W., Weiss, H.M. and Weitschat, W. 2008. *Tasmanites* algae—contributors to the Middle Triassic hydrocarbon source rocks of Svalbard and the Barents Shelf. *Polar Research*, **27**(3): 360-371

Wall, D. 1962. Evidence from recent plankton regarding the biological affinities of *Tasmanites* Newton 1875 and Leiosphaeridia Eisenack 1958. *Geological Magazine*, **99**(04): 353-362

Walliser, O. H. 1996. Global events in the Devonian and Carboniferous. In *Global events and event stratigraphy in the Phanerozoic*. Springer Berlin Heidelberg. 225-250

Wells, J.W. 1941. Crinoids and Callixylon. *American Journal of Science*, **239**(6): 454-456

Wells, J.W. 1947. Provisional paleoecological analysis of the Devonian rocks of the Columbus region. *The Ohio Journal of Science* **47**(3): 119-126

Whitfield, M. 2001. Interactions between phytoplankton and trace metals in the ocean. *Advances in Marine Biology*, **41**: 1-128

Wicander, R. and Playford, G. 2008. Upper Ordovician microphytoplankton of the Bill's Creek Shale and Stonington Formation, Upper Peninsula of Michigan, USA: biostratigraphy and paleogeographic significance. *Revue de Micropaléontologie*, **51**(1): 39-66

Wicander, R., Clayton, G., Marshall, J.E.A., Troth, I. and Racey, A. 2011. Was the latest Devonian glaciation a multiple event? New palynological evidence from Bolivia. *Palaeogeography, Palaeoclimatology, Palaeoecology*, **305**(1): 75-83

APPENDICES

APPENDIX A: SAMPLE NUMBERS

LOCALITY	MEMBER / FORMATION	FIELD NUMBER	LAB NUMBER	THESIS NUMBER
KY801N	HURON MEMBER	H3	A89	1
		H4	A90	2
	THREE LICK BED	TL1	A91	3
	CLEVELAND MEMBER	C1	A92	4
		C2	A93	5
		C3	A94	6
		C4	A95	7
		C5	A96	8
		C6	A97	9
	BEDFORD SHALE	B1	A98	10
		B2	A99	11
		B3	A100	12
		B4	A101	13
		B5	A102	14
		B6	A103	15
		B7	A104	16
		B8	A105	17
		B9	A106	18
		B10	A107	19
		B11	A108	20
		B12	A109	21
		B13	A110	22
	SUNBURY SHALE	B14	A111	23
		B15	A112	24
		B16	A113	25
		B17	A114	26

LOCALITY	MEMBER / FORMATION	FIELD NUMBER	LAB NUMBER	THESIS NUMBER
KY10E	HURON MEMBER	H18	A132	1
		H17	A133	2
		H16	A134	3
		H15	A135	4
		H14b	A136	5
		H14a	A137	6
		H12	A139	7
		H11	A140	8
		H10	A141	9
		H9	A142	10
		H8	A143	11
		H7	A144	12
		H6	A145	13
		H5	A146	14
		H4	A147	15
		H3	A148	16
		H2	A149	17
		H1	A150	18
	THREE LICK BED	TL1	A151	19
	CLEVELAND MEMBER	C11	A152	20
		C10	A153	21
		C9	A154	22
		C8	A155	23
		C7	A156	24
		C6	A157	25
		C5	A158	26
		C4	A159	27
		C3	A160	28
		C2	A161	29
		C1	A162	30

LOCALITY	MEMBER / FORMATION	FIELD NUMBER	LAB NUMBER	THESIS NUMBER
I64W	THREE LICK BED	TL1	A49	1
		TL3	A51	2
		TL4	A52	3
		TL5	A53	4
		TL6	A54	5
		TL7	A55	6
		TL8	A56	7
		TL9	A57	8
		TL10	A58	9
		TL11	A59	10
		TL12	A60	11
		TL13	A61	12
		TL14	A62	13
		TL15	A63	14
		TL16	A64	15
		TL17	A65	16
		TL18	A66	17
		TL19	A67	18
		TL20	A68	19

LOCALITY	MEMBER / FORMATION	FIELD NUMBER	LAB NUMBER	THESIS NUMBER
KY2520N	CLEVELAND MEMBER	OAR2	A2	1
		OAR3	A3	2
	BEDFORD SHALE	OAR5	A5	3
		OAR6	A6	4
		OAR7	A7	5
		OAR11	A11	6
		OAR12	A12	7
		OAR13	A13	8
		OAR14	A14	9
		OAR15	A15	10
		OAR16	A16	11
		OAR17	A17	12
		OAR19	A19	13
		OAR20	A20	14
		OAR21	A21	15
		OAR22	A22	16
		OAR23	A23	17
		OAR31	A31	18
	SUNBURY SHALE	OAR 2012_1	A238	19
		OAR 2012_2	A239	20
		OAR 2012_3	A240	21
		OAR 2012_4	A241	22
		OAR 2012_5	A242	23
		OAR 2012_6	A243	24
		OAR 2012_7	A244	25
		OAR 2012_8	A245	26
		OAR 2012_10	A246	27
		OAR 2012_11	A247	28
		OAR 2012_12	A248	29
		OAR 2012_13	A249	30
		OAR 2012_14	A250	31
		OAR 2012_15	A251	32
		OAR 2012_16	A252	33
		OAR 2012_17	A253	34
		OAR 2012_18	A254	35
		OAR 2012_19	A255	36

APPENDIX B: *TASMANITES* STABLE ISOTOPE DATA

LOCALITY	SAMPLE NUMBER	RAW $\delta^{15}N$ (‰)	CORRECTED $\delta^{15}N$ (‰)
KY801N	1	1.251	3.904
		0.799	3.537
		0.956	3.476
	2	0.906	3.716
		0.646	3.508
		1.065	3.650
	3	-0.576	3.483
		-0.427	3.601
	4	1.083	3.526
		1.109	3.798
		0.607	3.047
	5	0.473	4.287
		0.324	4.185
		0.266	4.099
	6	0.332	2.889
		0.729	3.154
		0.276	2.786
	7	0.450	2.620
		0.330	2.455
		0.524	2.670
	8	1.201	3.403
		1.508	3.631
		1.262	3.273
	9	0.729	2.520
		0.299	1.965
		0.824	2.365
	10	1.506	3.335
		1.540	3.450
		1.584	3.709
	11	0.881	2.806
		1.402	3.218
		0.923	2.849
	12	0.486	3.106
		0.576	3.517
		0.751	3.578
	13	-0.268	2.488
		0.810	3.705
		0.134	3.085

LOCALITY	SAMPLE NUMBER	RAW $\delta^{15}N$ (‰)	CORRECTED $\delta^{15}N$ (‰)
KY801N	14	0.422	3.413
		0.215	3.346
		0.318	3.323
	15	-0.973	2.654
		-0.134	3.308
		0.147	3.521
	16	0.613	3.644
		-0.050	3.116
		0.821	3.953
	17	0.435	3.553
		0.409	3.389
		1.198	3.815
	18	1.222	3.005
		0.999	3.118
		1.483	3.434
	19	0.937	3.171
		1.319	3.336
		1.258	3.099
	20	1.434	2.738
		1.815	2.962
		3.114	4.365
	21	2.424	4.128
		2.476	4.063
		2.401	3.840
	22	2.282	3.772
		2.756	4.329
		2.442	3.939
	23	2.517	4.027
		2.897	4.334
		2.875	4.356
	24	0.919	3.706
		0.646	3.360
		1.078	3.448
	25	1.985	4.449
		1.161	4.037
		1.641	4.119
	26	1.508	4.133
		1.512	4.206
		1.020	3.872

LOCALITY	SAMPLE NUMBER	RAW $\delta^{15}N$ (‰)	CORRECTED $\delta^{15}N$ (‰)
KY10E	1	0.654	3.138
		0.739	3.694
		0.657	3.244
	4	0.080	2.286
		0.179	2.448
		0.136	2.251
	5	0.466	2.656
		1.289	2.748
		-0.330	0.736
	6	0.528	2.803
		0.204	2.602
		-0.082	2.262
	7	1.652	3.949
		1.299	3.920
		1.466	3.863
	9	1.315	3.518
		0.815	3.193
		0.801	3.180
	17	1.184	3.958
		1.269	4.327
		1.067	3.759
	18	1.348	4.029
		1.431	4.239
		1.410	4.171
	20	1.629	4.341
		1.545	4.016
		1.435	4.170
	21	1.656	4.010
		1.573	4.244
		1.820	4.567
	22	1.954	3.772
		1.534	3.211
		1.498	3.743
	23	2.145	3.623
		2.548	4.179
		2.414	3.989

LOCALITY	SAMPLE NUMBER	RAW $\delta^{15}N$ (‰)	CORRECTED $\delta^{15}N$ (‰)
KY10E	24	0.257	4.256
		0.448	4.313
		0.347	4.228
	25	0.090	4.377
		0.320	4.200
		0.447	4.328
	26	-0.563	3.302
		-0.114	3.932
		-0.289	3.916
	27	0.531	5.411
		0.653	4.959
		0.576	5.420
	28	1.213	4.425
		1.060	4.706
		1.186	4.526
	29	1.192	4.523
		0.594	4.261
		1.198	4.553
	30	2.656	5.363
		1.749	5.144
		2.354	5.681

LOCALITY	SAMPLE NUMBER	RAW $\delta^{15}N$ (‰)	CORRECTED $\delta^{15}N$ (‰)
I64W	1	-1.218	0.773
	2	0.938	3.017
		1.125	3.044
		0.861	3.033
	3	0.425	2.279
		1.106	2.902
		1.677	3.630
	4	0.648	2.666
		0.962	3.203
		0.387	2.586
	5	-0.097	2.305
	6	0.620	3.218
		1.789	4.306
		0.822	3.276
	7	0.868	3.499
		1.170	3.537
		0.149	2.563
	8	0.427	3.130
		0.890	3.633
		0.055	3.077
	10	4.584	6.383
		-1.339	1.562
	11	0.809	3.607
		0.841	3.447
		0.649	3.615
	12	1.050	3.441
		1.137	3.506
		1.292	3.337
	13	1.192	3.181
		1.146	3.213
		1.197	3.212
	14	0.928	3.351
		1.343	3.941
		1.227	3.648

LOCALITY	SAMPLE NUMBER	RAW $\delta^{15}N$ (‰)	CORRECTED $\delta^{15}N$ (‰)
I64W	15	0.768	3.401
		1.141	3.547
		1.095	3.685
	16	0.087	2.935
		0.520	3.003
		0.542	2.972
	17	0.542	3.338
		0.879	3.551
		1.042	3.578
	18	1.487	3.407
		1.739	3.533
		1.184	3.187
	19	1.954	3.914
		1.774	3.659
		1.418	3.375

LOCALITY	SAMPLE NUMBER	RAW $\delta^{15}N$ (‰)	CORRECTED $\delta^{15}N$ (‰)
KY2520N	1	1.636	3.673
		1.940	4.293
		2.550	4.678
	2	1.098	3.451
		1.172	3.300
		1.709	4.087
	3	1.611	4.252
		1.995	4.720
		2.039	4.833
	4	-0.451	1.877
		0.407	2.780
		0.193	2.750
	5	-0.560	1.833
		-0.593	2.184
	6	0.674	3.225
		-0.762	1.829
	7	0.134	2.381
		-0.082	2.189
		0.123	2.870
	8	-0.503	2.492
		-0.871	2.187
		-0.860	2.328
	9	-1.289	2.033
		-0.533	2.463
		-1.003	1.955
	10	5.691	7.809
		-0.457	2.898
	11	-1.163	2.308
		-0.592	2.564
		0.390	3.590
	12	-0.107	3.567
		-0.976	2.378
		-0.920	1.846
	13	-1.371	1.499
		-2.506	-0.200
		-0.943	1.539

LOCALITY	SAMPLE NUMBER	RAW $\delta^{15}N$ (‰)	CORRECTED $\delta^{15}N$ (‰)
KY2520N	14	-0.870	1.528
		0.246	2.552
		-0.699	1.639
	15	-0.423	1.897
		0.551	2.299
	16	3.590	6.002
		0.159	2.511
		0.725	2.803
	17	-0.429	1.868
		1.420	4.250
	18	-0.506	2.392
	19	0.381	2.887
		0.697	2.972
		0.913	3.399
	20	0.751	3.164
		0.920	3.373
		1.076	3.633
	21	0.796	2.921
		0.674	2.922
		0.774	3.082
	22	0.810	2.827
		0.521	2.469
		0.208	2.352
	23	1.106	2.792
		2.506	4.118
		-0.037	1.960
	24	0.156	1.931
		0.393	1.818
		0.399	1.869
	25	4.976	7.060
		-0.448	1.393
		0.009	1.695
	26	8.619	10.325
		0.287	2.163
		0.103	2.280

LOCALITY	SAMPLE NUMBER	RAW $\delta^{15}N$ (‰)	CORRECTED $\delta^{15}N$ (‰)
KY2520N	27	0.520	2.280
		0.164	2.128
		0.226	2.052
	28	0.690	3.136
		0.843	3.294
		1.400	3.728
	29	2.598	4.469
		1.880	4.133
	30	1.848	3.799
		1.450	3.346
		2.047	4.121
	31	-1.372	2.840
		1.153	4.136
		0.132	2.813
	32	0.255	2.505
		-0.415	2.040
		-0.162	2.304
	33	-0.141	2.548
		-0.271	2.479
		0.139	2.925
	34	2.287	4.853
		0.768	3.809
		1.212	4.238
		1.190	4.376
	35	0.886	3.577
		1.355	4.069
		1.704	4.627
	36	-0.190	3.070
		-0.580	2.305

APPENDIX C: BULK STABLE ISOTOPE DATA

LOCALITY	SAMPLE NUMBER	$\delta^{15}N$ (‰)
KY801N	1	1.266
	1	1.575
	2	2.677
	2	1.622
	3	3.763
	3	4.783
	4	2.044
	4	1.842
	5	2.298
	5	2.051
	6	2.952
	6	2.662
	7	1.797
	7	1.347
	8	0.758
	8	1.141
	9	1.250
	9	1.239
	10	1.860
	10	1.147
	11	1.628
	11	1.353
	12	1.575
	12	1.236
	13	1.613
	13	1.942
	14	1.983
	14	2.305
	15	1.711
	15	2.360
	16	2.089
	16	1.829
	17	2.610
	17	2.263
	18	2.510
	18	2.672
	19	2.978
	19	3.465

LOCALITY	SAMPLE NUMBER	$\delta^{15}N$ (‰)
KY801N	20	2.878
	20	3.085
	21	1.764
	21	2.766
	22	3.657
	22	3.699
	23	3.912
	23	4.094
	24	3.939
	24	4.143
	25	4.535
	25	4.559
	26	4.443
	26	4.769

LOCALITY	SAMPLE NUMBER	$\delta^{15}N$ (‰)
KY10E	1	-0.481
	1	-0.982
	1	-0.881
	1	-0.572
	1	-1.126
	2	-0.474
	2	-0.520
	2	-0.760
	3	-0.654
	3	-1.002
	3	-1.088
	3	-1.419
	3	-1.064
	4	-0.214
	4	-0.173
	4	-0.052
	4	-0.126
	4	-0.135
	5	0.007
	5	-0.016
	5	0.160
	5	-0.030
	5	-0.155
	6	1.936
	7	1.380
	7	-0.179
	7	-0.021
	7	0.023
	7	0.156
	8	0.303
	8	0.488
	8	-0.008
	8	-0.206
	9	-0.129
	11	-0.145
	11	-0.130
	11	0.141
	11	0.505
	11	1.413

LOCALITY	SAMPLE NUMBER	$\delta^{15}N$ (‰)
KY10E	12	0.431
	12	0.559
	12	0.219
	12	0.032
	12	0.025
	13	0.533
	13	0.469
	13	0.049
	13	0.125
	13	0.447
	14	0.074
	14	0.004
	14	0.084
	14	0.231
	14	0.006
	15	0.232
	15	0.266
	15	0.432
	16	0.702
	16	0.305
	16	0.350
	16	0.659
	16	0.470
	17	0.649
	17	0.347
	17	0.381
	17	0.193
	17	0.230
	18	0.007
	18	0.079
	18	0.508
	18	0.431
	19	0.40
	19	0.497
	20	2.330
	21	1.624
	22	0.056
	23	0.647
	24	0.559
	25	0.38
	25	1.263

LOCALITY	SAMPLE NUMBER	$\delta^{15}N$ (‰)
KY10E	26	1.33
	26	1.083
	26	1.549
	26	1.181
	26	0.113
	27	1.41
	27	0.797
	27	2.901
	27	2.862
	27	2.269
	27	2.274
	28	2.08
	28	2.603
	28	3.536
	28	2.866
	28	2.309
	28	2.558
	29	2.72
	29	2.696
	29	3.556
	29	2.577
	29	2.684
	29	2.252
	30	1.824
	30	2.954
	30	3.493
	30	3.505
	30	2.794
	30	2.91

LOCALITY	SAMPLE NUMBER	$\delta^{15}N$ (‰)
KY2520N	1	3.64
	3	4.51
	3	4.12
	4	2.79
	5	3.15
	5	2.88
	6	3.00
	6	2.89
	7	3.54
	7	3.64
	8	2.87
	10	2.79
	10	2.92
	11	2.94
	12	3.33
	15	4.08
	18	5.35
	19	2.78
	19	1.18
	20	1.05
	20	1.73
	21	1.38
	21	1.30
	22	0.34
	22	1.13
	23	1.40
	23	1.45
	24	-0.67
	24	-0.64
	26	-0.39
	26	0.20
	27	-0.64
	28	3.58
	28	3.50
	29	3.72
	29	3.60
	30	3.75
	30	3.55
	31	2.36
	31	2.01
	32	0.40
	32	0.07
	33	0.27
	33	0.95
	34	2.64
	34	2.88
	36	2.09
	36	2.33

LOCALITY	SAMPLE NUMBER	$\delta^{15}N$ (‰)
I64W	1	2.46
	1	1.78
	2	0.72
	2	1.35
	3	1.12
	3	0.96
	4	1.03
	4	0.91
	5	3.06
	5	2.11
	6	0.56
	6	0.60
	7	1.01
	7	0.69
	8	0.95
	8	1.22
	10	2.45
	10	2.42
	11	1.90
	11	1.49
	12	2.62
	12	2.08
	13	2.64
	13	3.54
	14	1.85
	14	1.93
	15	1.58
	15	2.39
	16	1.95
	16	2.02
	17	1.36
	17	1.51
	18	1.41
	18	1.46
	19	3.32
	19	2.72